

UNIVERSITA' VITA-SALUTE SAN RAFFAELE

**CORSO DI DOTTORATO DI RICERCA
INTERNAZIONALE IN MEDICINA MOLECOLARE**

Curriculum in Neuroscienze e Neurologia sperimentale

**CELLULAR AND MOLECULAR DRUG
SCREENING SYSTEM FOR RETT
SYNDROME THERAPY**

DoS: Prof.ssa Nicoletta Landsberger

Second Supervisor: Prof.ssa Elisa Zanier

Tesi di DOTTORATO DI RICERCA di Irene Sormonta

Matr. 015671

Ciclo di Dottorato: XXXV

Area 05 BIO/11

Anno Accademico 2022/2023

Nicoletta Landsberger

CONSULTAZIONE TESI DI DOTTORATO

Il/la sottoscritto/I Irene Sormonta
Matricola / *registration number* 015671
Nata / *born at* Padova
Il / *on* 16/09/1993

Autore della tesi di Dottorato di ricerca dal titolo / *author of the PhD Thesis titled*
..... CELLULAR AND MOLECULAR DRUG SCREENING SYSTEM FOR RETT SYNDROME
..... THERAPY
.....

AUTORIZZA la Consultazione della tesi / *AUTHORIZES the public release of the thesis*

NON AUTORIZZA la Consultazione della tesi per ..12.. mesi / *DOES NOT AUTHORIZE the public release of the thesis for months*

A partire dalla data di conseguimento del titolo e precisamente / *from the PhD thesis date specifically*

Dal / *from* ..20../..12../..2022 Al / *to* ..20../..12../..2023

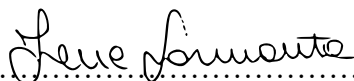
Poiché / *because*:

l'intera ricerca o parti di essa sono potenzialmente soggette a brevettabilità/ *The whole project or part of it might be subject to patentability;*

ci sono parti di tesi che sono già state sottoposte a un editore o sono in attesa di pubblicazione/ *Parts of the thesis have been or are being submitted to a publisher or are in press;*

la tesi è finanziata da enti esterni che vantano dei diritti su di esse e sulla loro pubblicazione/ *the thesis project is financed by external bodies that have rights over it and on its publication.*

È fatto divieto di riprodurre, in tutto o in parte, quanto in essa contenuto / *Copyright the contents of the thesis in whole or in part is forbidden*

Data / *Date* ..20/12/2022..... Firma / *Signature* .......

DECLARATION

This thesis has been:

- composed by myself and has not been used in any previous application for a degree.
- Throughout the text I use both 'I' and 'We' interchangeably.
- has been written according to the editing guidelines approved by the University.

Permission to use images and other material covered by copyright has been sought and obtained. For the following image/s (specify), it was not possible to obtain permission and is/are therefore included in thesis under the "fair use" exception (Italian legislative Decree no. 68/2003).

All the results presented here were obtained by myself, except for:

1) RNASeq and bioinformatic analysis (Results section 6.1, Figure 6.1, 6.2, 6.3, 6.4, 6.5, 6.6 panel D, 6.12, 8.2) were performed in collaboration with Dr. Marzia Rossato, Functional Genomic Lab, Department of Biotechnology, University of Verona, Verona, VR, Italy.

All sources of information are acknowledged by means of reference.

Abstract

Rett syndrome (RTT) is a devastating neurodevelopmental disorder caused by mutations in the X-linked *MECP2* gene, primarily acting as transcriptional repressor. Although RTT proved to be reversible in mice, no cure is yet available. Several *Mecp2*-mutant mouse models have been developed and they generally reproduce behavioral and physiological phenotypes observed in RTT patients, establishing that disease phenotypes are widely due to neuronal dysfunctions. However, their use in large drug screening programs require a great number of animals, elevated costs and time-consuming experimental approaches. To support the *in vivo* evaluation, new drug screening systems have emerged *in vitro*, usually based on the analysis of neuronal defective morphology. We previously demonstrated that the amelioration of the transcriptional profile in *Mecp2*-null neurons appears as a better indicator of functional rescue than morphological readouts. For this reason, we aimed at developing a cell-based drug screening system for RTT therapy, based on customized high-throughput 96x96 qRT-PCR arrays.

To this purpose, a longitudinal RNASeq analysis performed in differentiating *Mecp2*-null neuronal precursors cells identified consistent transcriptional defects of RTT neurons. By using different prioritization criteria and testing selected neuronal differentially expressed genes (DEGs) on 96x96 qRT-PCR cards, we established a group of reproducible DEGs which represent our quantitative probes to measure the transcriptional amelioration induced by the drugs tested. To assess whether the selected DEGs are able to reflect the efficacy of drugs *in vivo*, we analyzed the effects of the ampakine CX546, for which we previously published positive results *in vitro* and *in vivo*. The drug demonstrated to rescue 75% of our selected DEGs, though a sample size larger than expected was required to reproduce RNASeq data in qRT-PCR experiments, forcing us to reconsider its use for the screening of large drug libraries in a laboratory scale. Thus, we propose the use of our screening system as either a confirmatory approach of a previously produced selection of molecules or as a useful system to validate rationally deduced pharmacological approaches. As secondary outcome, we identified and further characterized a consistent defect in the expression of two genes, *Haus7* and *Nsdhl*, in cultured neurons and *Mecp2*-defective tissues, prompting further investigations of their role and functions in RTT pathogenesis. A comprehensive analysis of their expression across different stages and models of the disorder lay the foundation for novel possible pathogenic mechanisms of RTT and hopefully will provide new potential targets for RTT therapy.

1. Table of contents

1.	TABLE OF CONTENTS	1
2.	ACRONYMS AND ABBREVIATIONS.....	3
3.	LIST OF FIGURES AND TABLES	7
4.	INTRODUCTION	11
4.1.	RETT SYNDROME.....	11
4.1.1.	<i>Clinical features</i>	11
4.1.2.	<i>The genetics of Rett syndrome</i>	13
4.1.3.	<i>MECP2: the gene and the protein</i>	15
4.1.4.	<i>MeCP2: a multi-talented protein</i>	18
4.2.	MOUSE MODELS OF RTT.....	24
4.3.	NEUROBIOLOGICAL AND MOLECULAR ALTERATIONS IN RTT.....	29
4.4.	MOLECULAR TARGETS OF MECP2.....	33
4.5.	THERAPEUTIC APPROACHES AND CLINICAL TRIALS IN RTT.....	38
4.5.1.	<i>Treatments against MeCP2 downstream targets</i>	39
4.5.2.	<i>Treatments to restore MECP2 gene or functions</i>	42
4.6.	DRUG SCREENING SYSTEMS IN RTT	47
5.	AIM.....	51
6.	RESULTS	53
6.1.	IDENTIFICATION OF RTT-SPECIFIC NEURONAL TRANSCRIPTIONAL BIOMARKERS FOR THE DRUG SCREENING SYSTEM	53
6.1.1.	<i>Longitudinal RNASeq analyses identified differentially expressed genes of developing RTT-neurons</i>	53
6.1.2.	<i>Prioritization of DEGs permitted to select 200 genes for further validation</i>	63
6.1.3.	<i>Primary neurons are the most stable and robust cell culture to use in the screening</i>	72
6.1.4.	<i>Validation of prioritized DEGs on 96x96 IFC qRT-PCRs confirmed the reproducibility of 74 genes</i> 75	
6.2.	VALIDATION OF THE 96X96 QPCR SCREENING SYSTEM.....	81
6.3.	PRELIMINARY STUDIES ON THE POSSIBLE INVOLVEMENT OF <i>HAUS7</i> AND <i>NSDHL</i> IN RTT PATHOGENESIS.....	88

6.3.1.	<i>Haus7 is consistently downregulated in the cerebral cortex and hippocampus of Mecp2 mutant male and female mice</i>	90
6.3.2.	<i>Nsdhl is downregulated in the cerebral cortex of Mecp2 mutant mice, a possible indication of defective cholesterol homeostasis</i>	97
7.	DISCUSSION	107
8.	MATERIALS AND METHODS	117
8.1.	ANIMALS	117
8.1.1.	<i>Animal care</i>	117
8.1.2.	<i>Genotyping</i>	117
8.2.	PRIMARY CULTURES	121
8.2.1.	<i>NPCs isolation, expansion and differentiation</i>	121
8.2.2.	<i>Cortical neurons</i>	124
8.3.	GENE EXPRESSION ANALYSIS OF PRIMARY CULTURES	124
8.3.1.	<i>RNA extraction from cell cultures</i>	124
8.3.2.	<i>Quality assessment of RNA from cell cultures</i>	125
8.3.3.	<i>Library validation for the RNASeq analysis</i>	125
8.3.4.	<i>Longitudinal RNASeq analysis</i>	126
8.3.5.	<i>Delta Gene assay design, cDNA synthesis, pre-amplification and 96x96 microfluidic quantitative PCR</i>	129
8.4.	GENE EXPRESSION ANALYSIS ON MICE TISSUES	138
8.4.1.	<i>RNA purification, quality control, cDNA synthesis and quantitative RT-PCR</i>	138
8.5.	PROTEIN EXTRACTION AND WESTERN BLOT	139
8.5.1.	<i>Protein extraction and quantification</i>	139
8.5.2.	<i>Western Blot</i>	140
9.	BIBLIOGRAPHY	141
10.	APPENDICES	165
10.1.	APPENDIX I	165
10.2.	APPENDIX II	167
10.3.	APPENDIX III	170
10.4.	APPENDIX IV	175
10.5.	APPENDIX V	180
10.6.	APPENDIX VI	183

2. Acronyms and abbreviations

24-OHC	24-hydroxylated cholesterol
Amo-04	Tianeptine
Anavex-73	Blarcamesine
ApoE	Apolipoprotein E
AVV	Adeno-associated virus
BBB	Blood brain barrier
BDNF	Brain-derived neurotrophic factor
CDKL5	Cyclin-dependent kinase-like 5
cKO	Conditional knockout
CNS	Central nervous system
CREB1	cyclic AMP-responsive element binding protein
CTD	C-terminal domain
DEG	Differentially expressed gene
DIV	Day <i>in vitro</i>
DMEM/F12	Dulbecco's Modified Eagle Medium/Nutrient Mixture F-12 Ham
E/I	excitatory/inhibitory
EEG	electro-encephalogram
ER	endoplasmic reticulum
FBS	Fetal bovine serum
FC	Fold Change
Fkbp5	FKBP prolyl isomerase 5
FOXG1	Forkhead box protein G1
Fundc2	FUN14 domain containing 2
GO	Gene ontology
GPE	Glutamate-Proline-Glycine, IGF active tripeptide
Haus7	HAUS augmin like complex subunit 7
HBSS	Hank's Buffered Salt Solution
HDAC	Histone deacetylase

hEGF	human Epidermal Growth Factor
hFGF	human Fibroblast Growth Factor
HMGCR	HMG-CoA reductase
ID	Intervening domain
IFC	Integrated fluidic circuits
IGF	Insulin-like growth factor
iPSC	induced pluripotent stem cells
KI	knock-in
LFC	Log2FoldChange
MBD	Methyl-CpG-binding domain
MECP2	Methyl-CpG-binding protein 2
MeP	Mecp2 promoter
mi-RARE	MiRNA-responsive autoregulatory element
MT	microtubule
NCoR-SMRT	Nuclear receptor Co-Repressor and the Silencing Mediator of Retinoic acid and Thyroid hormone receptor
NID	NCoR/SMRT Interaction Domain
NLS	Nuclear localization signal
NPCs	Neuronal precursor cells
NSCs	Neuronal stem cells
Nsdhl	NAD(P) dependent steroid dehydrogenase-like
NTD	N-terminal domain
p-adj	false discovery rate adjusted p-value
PCA	Principal Component Analysis
PTM	Post-transcriptional modification
QC	quality control
qRT-PCR	quantitative reverse transcription polymerase chain reaction
RIN	RNA integrity number
RNASEq	RNA sequencing
RTT	Rett syndrome
SEM	Standard error mean
SQS	Squalene monooxygenase

TBS-T	Tris-buffered saline containing 0.1% Tween-20
TRD	Transcriptional repressor domain
WB	Western blot
WT	wild type
XCI	X chromosome inactivation
Xi	inactive X chromosome
γ -TuRC	γ -Tubulin ring complex

3. List of figures and tables

- Figure 4.1: Onset and progression of RTT symptoms.
- Figure 4.2: Association between most common *MECP2* mutations and different clinical severity.
- Figure 4.3: The *MECP2* gene and protein isoforms.
- Figure 4.4: The MeCP2 protein structure.
- Figure 4.5: Molecular functions of MeCP2.
- Figure 4.6: Molecular consequences of carrying a *Mecp2* Y120D allele compared to a null one.
- Figure 4.7: Schematic representation of MeCP2 functions in the brain across different developmental stages.
- Figure 4.8: Schematic overview of neuronal morphology, functionality and molecular target alterations in RTT.
- Figure 4.9: Schematic representation of available options for RTT treatment.
- Figure 4.10: Updated potential treatments for RTT therapy in clinical trials.
- Figure 6.1: Time-specific differential expression analysis allowed to identify DEGs of KO vs WT samples at each timepoint.
- Figure 6.2: PCA plots of individual sample variances according to the examined timepoints (DIV7, 14, 18).
- Figure 6.3: Enrichment analysis of GO biological processes confirmed the impact of *Mecp2* deficiency on neuronal morphology and synaptic maturation
- Figure 6.4: Differential expression analysis overtime identified a great number of DEGs with a low differential expression.
- Figure 6.5: GO enrichment analysis on DEGs overtime illustrated an impact on transcriptional maturation of RTT developing NPC-derived cultures.
- Figure 6.6: Prioritization criteria of DEGs from the bioinformatic analyses.
- Figure 6.7: Primary neurons appeared the most stable and robust cell culture to use in the screening
- Figure 6.8: Transcriptional comparison between WT and KO neurons.
- Figure 6.9: 74 reproducible and validated DEGs between WT and KO samples.

- Figure 6.10: The early treatment with ampakine CX546 ameliorates the transcriptional profile of KO treated samples.
- Figure 6.11: Ampakine CX546 rescues the expression of 75% of the DEGs tested.
- Figure 6.12: Plots representing counts for *Haus7*, *Nsdhl* and *Fundc2* at the three timepoints analyzed in the RNASeq data.
- Figure 6.13: Augmin functional domains and model of augmin binding.
- Figure 6.14: *Haus7* is consistently downregulated in the cerebral cortex and hippocampus of *Mecp2* null mice.
- Figure 6.15: *Haus7* is downregulated in the cerebral cortex and hippocampus of P40 *Mecp2* Y120D mice.
- Figure 6.16: *Haus7* is downregulated in P100 Het cerebral cortices and hippocampi.
- Figure 6.17: Cholesterol biosynthesis pathway.
- Figure 6.18: NSDHL structure and function.
- Figure 6.19: *Nsdhl* is strongly downregulated in the cerebral cortex of pre-symptomatic and symptomatic *Mecp2*-null mice.
- Figure 6.20: *Nsdhl* protein is downregulated in the cerebral cortex and hippocampus of pre-symptomatic and symptomatic *Mecp2*-null mice.
- Figure 6.21: *Nsdhl* protein is downregulated in the cerebral cortex and hippocampus of P40 *Mecp2* Y120D mice.
- Figure 6.22: *Mecp2*-null cerebral cortices of symptomatic mice exhibit a downregulation of genes involved in cholesterol synthesis.
- Figure 8.1: Schematic representation of NPCs isolation, expansion and differentiation into neurons, astrocytes and oligodendrocytes.
- Figure 8.2: Library validation for RNASeq analysis.
- Figure 8.3: RNASeq analysis pipeline.
- Figure 8.4: Schematic representation of a 96x96 IFC qPCR card developed by Fluidigm.
- Table 6.1: List of prioritized and selected DEGs to validate in the 96x96 qPCR cards.
- Table 6.2: List of 74 reproducible and validated DEGs between WT and KO samples.
- Table 6.3: List of the 51 DEGs tested in the CX546 validation.
- Table 6.4: List of the 42 significant DEGs and their percentage of expression in KO untreated and treated samples.

- Table 6.5: Not significant genes in the CX546 validation with the One-way ANOVA test.
- Table 6.6: Schematic overview of *Haus7*, *Nsdhl* and *Fundc2* expression across 4 different RNASeq experiments performed in our laboratory.
- Table 8.1: PCR reaction mix for genotyping and determination of sex.
- Table 8.2: PCR cycles for genotyping and sex determination.
- Table 8.3: Media composition for neurosphere maintenance and expansion.
- Table 8.4: List of primers of the prioritized DEGs.
- Table 8.5: primers for *Haus7* characterization study.
- Table 10.1: GO enrichment analysis at DIV7.
- Table 10.2: GO enrichment analysis at DIV14.
- Table 10.3: GO enrichment analysis in the overtime differential analysis.
- Table 10.4: Intersection of genes among the timepoints of the time-specific analysis.
- Table 10.5: DEGs belonging to cluster 1, 2, 3 of the overtime analysis.
- Table 10.6: List of the first 96 DEGs tested in the 96x96 IFC qRT-PCR and their respective primers.

4. Introduction

4.1. Rett syndrome

4.1.1. Clinical features

Rett syndrome (RTT; OMIM #312750) is a devastating neurodevelopmental disorder that primarily affects females, with an incidence of 1 to 10,000-15,000 female births alive, thus representing the second cause of severe intellectual disability in girls worldwide after Down syndrome (Gold et al., 2018). It was first described by Dr. Andreas Rett in 1966 in German medical literature, defining similar anomalous behaviors in 22 young female patients (Rett, 1966). Nonetheless, international recognition of the disorder appeared almost twenty years later, when Hagberg and colleagues detailed the same symptoms in 35 female patients in English language (Hagberg et al., 1983).

Generally, RTT patients have an apparently normal post-natal development until they reach 6-18 months of age, when the overt signs of the disorder emerge. Symptoms manifest over different stages (*Stage I to IV*) although their severity and clinical manifestations can be extremely variable (Chahrour & Zoghbi, 2007; Hagberg & Witt-Engerström, 1986; Nomura & Segawa, 2005).

- *Stage I* or “*stagnation stage*” (early infancy, first 6-18 months):

Before the dramatic regression of the disorder, subtle but visible symptoms have progressively been reported and include delay in the acquirement of expected developmental motor milestones, difficulty in posture and movements, hypotonia, deceleration of head growth and undemanding nature.

- *Stage II* or “*rapid destructive stage*” (late infancy to three-four years of age):

Stage II represents the rapid developmental regression, characterized by the sudden onset of autistic features, the loss of previously acquired communication skills and motor coordination, seizures, microcephaly and ataxia. Girls lose purposeful use of their hands and the hallmark of stereotypical hand movement starts to appear.

- *Stage III* or “*pseudo stationary stage*”:
Symptoms of patients between five to ten years of age typically stabilize although intellectual ability become severely affected. Girls can start manifesting autonomic dysfunction, including breathing abnormalities, scoliosis and osteopenia.
- *Stage IV* or “*Late motor deterioration stage*”
In this phase, most girls experience the loss of mobility and become wheelchair-bound by teenage years. Patients can also develop parkinsonism and cardiac abnormalities at later age. As girls get older, their clinical features become more static and some patients can survive up to sixty-seventy years in a severely debilitated physical condition, requiring total care (Figure 4.1).

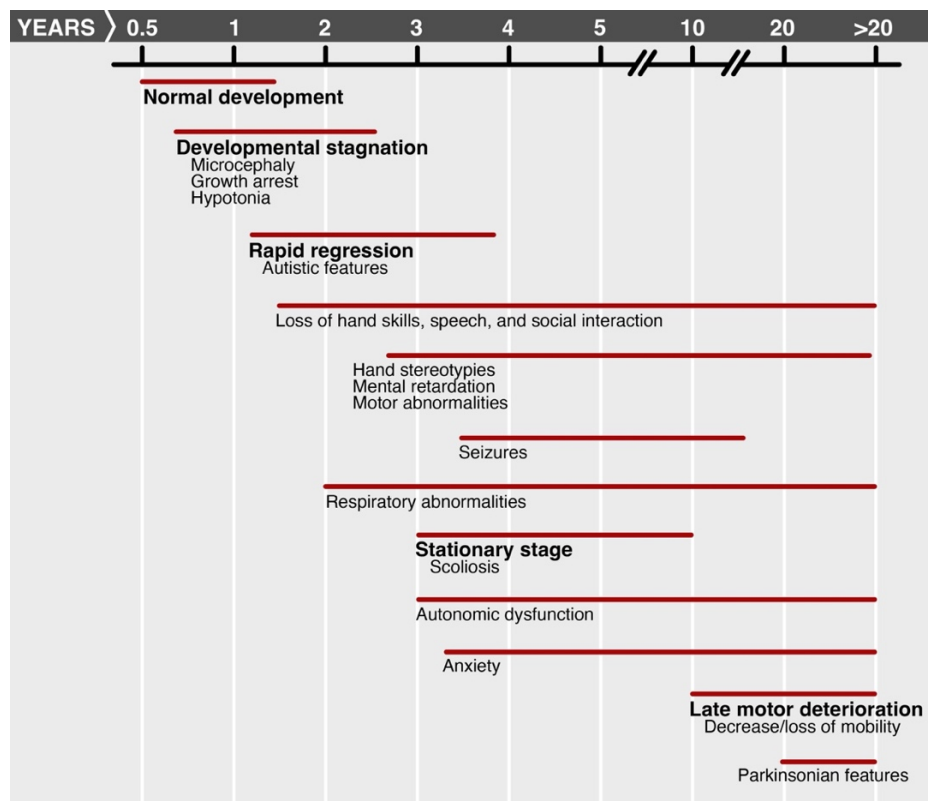


Figure 4.1: Onset and progression of RTT symptoms. After a period of apparent normal development, RTT girls enter a phase of developmental stagnation, manifesting microcephaly, hypotonia and a general arrest of their growth, followed by a rapid regression stage. In this stage, RTT patients suddenly exhibit autistic features and experience loss of previously acquired motor and communication skills, accompanied by severe mental retardation and hand stereotypies, typical of the disorder. After a stationary stage, usually characterized by the onset of autonomic dysfunctions and breathing abnormalities, the condition worsens with the occurrence of loss of mobility, requiring constant assistance and care. Modified from (Chahrour & Zoghbi, 2007). (Open access)

Given the great plethora of RTT symptoms and different grades of severity, a clear diagnosis in the early stages of the disorder has been very challenging. Internationally accepted diagnostic criteria have been refined over the years and thoroughly described by Neul and colleagues to distinguish classic and variant forms of RTT (Neul et al., 2010). Of note, the key feature required for both classic and variant RTT diagnosis is a period of rapid regression followed by recovery or stabilization. In addition, patients affected by classic RTT must exhibit four other main signs typical of the disorder, including loss of acquired spoken language, loss of fine purposeful hand skills, gait abnormalities and the presence of hand stereotypic movements. Variant RTT forms require at least 2 out of the 4 main criteria and other supportive symptoms, such as breathing problems, cardiovascular dysfunctions, growth retardation, scoliosis and diminished response to pain.

4.1.2. The genetics of Rett syndrome

The genetic basis of RTT was discovered in 1999, when Amir and colleagues identified *de novo* mutations in the X-linked gene *MECP2*, encoding the Methyl-CpG-binding protein 2 (MeCP2), as the cause of most RTT cases (Amir et al., 1999). Of note, nowadays 95% of classic RTT and over 75% of atypical RTT cases are linked to *MECP2* mutations (Gold et al., 2018).

The gene is located in the Xq28 chromosome region and most of its mutations arise *de novo* in the paternal germline, explaining respectively the vast majority of female patients and the 99% sporadic appearance (Amir et al., 1999; Trappe et al., 2001).

Although RTT is generally considered a monogenic disorder, female patients are characterized by a large phenotypic variability. As a matter of fact, due to random X chromosome inactivation (XCI), heterozygous female RTT patients are a mosaic for cells expressing either the wild type or mutant *MECP2* allele, but skewed inactivation can favor the expression of either one allele, thus affecting clinical severity and leading to great phenotypic variability (Chahrour & Zoghbi, 2007).

Beside the pattern of XCI, different *MECP2* mutations are another major source of variability of RTT symptoms and severity. Of note, since the discovery of the causative

link between RTT and *MECP2*, over 900 unique variants have been identified within the gene, with 518 being pathogenic (55.8%), mainly represented by frameshift, insertion/deletions and missense mutations (Gold et al., 2018). Loss of function mutations in *MECP2* account for the vast majority of RTT cases, with a recurrence (almost 47% of all mutations) of 8 specific missense (R106W, R133C, T158M, R306C) and nonsense (R168X, R255X, R270X, R294X) mutations distributed along the different domains of the gene (Neul et al., 2008). Interestingly, these hotspots are responsible for 60% of all RTT cases (Gold et al., 2018). As a matter of fact, each *MECP2* mutation could differentially affect protein function and can be used as an indicator of disease severity: for example, the T158M or R106W missense mutations are usually associated with a more severe RTT phenotype, while patients carrying R133C or R306C mutations often display a milder clinical manifestation (Cuddapah et al., 2014). On the contrary, nonsense mutations located before or including R270X usually lead to more severe symptoms (Figure 4.2) (Lombardi et al., 2015). Of note, most missense mutations involve the methyl binding domain (MBD, 35.9%), while the transcriptional repressor domain (TRD) is the most affected by nonsense and frameshift mutations (Bedogni et al., 2014).

Additionally, the presence of modifier genes mutations can also differentially impact RTT clinical outcomes, alleviating or enhancing patients' symptoms and eventually modulating RTT phenotype (Vashi & Justice, 2019).

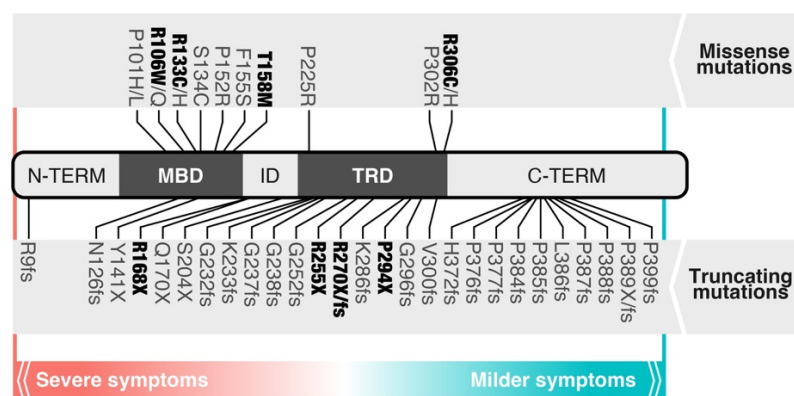


Figure 4.2: Association between most common *MECP2* mutations and different clinical severity. Missense mutations are depicted above the figure, while nonsense mutations are represented below. The 8 hotspots responsible for 60% of RTT cases are reported in bold. Patients carrying a missense mutation usually present a more severe RTT phenotype. On the contrary, truncating mutations after the R270X are often associated with milder symptoms (modified from Lombardi et al., 2015). (Open access)

On the contrary, RTT male patients represent only the 8.8% of RTT cases against over 90% of females (Krishnaraj et al., 2017) and they generally present a more severe phenotype, leading to grave neonatal encephalopathy often accompanied by infantile death within few years of life (Ip et al., 2018).

Not all patients diagnosed with RTT have a mutation in *MECP2*; in fact, 5% of classic RTT cases and almost 25% of atypical form of RTT have been linked to mutations in other genes. For example, mutations in the X-linked gene *Cyclin-dependent kinase-like 5 (CDKL5)* have for long been associated with the early-seizure onset variant of RTT, characterized by patients experiencing early refractory epilepsy and severe mental retardation. In 2013, when 25% of *CDKL5* mutated patients did not meet the accepted diagnostic criteria for the early-onset seizure RTT variant, Fehr and colleagues linked mutations in this gene to an independent disorder called *CDKL5 Deficiency Disorder (CDD)* (Fehr et al., 2013). Another gene linked to atypical forms of RTT is the *Forkhead box protein G1 gene (FOXP1)*, a brain specific transcriptional factor essential for early brain development, which is generally associated with the congenital form of RTT (Ariani et al., 2008).

Nonetheless, given that the vast majority of classic and atypical RTT patients bear *de novo* mutations in *MECP2*, this still remains the elected gene to study RTT.

4.1.3. MECP2: the gene and the protein

Before the identification of the causative link between *MECP2* mutations and RTT, *MECP2* protein had already been characterized; the protein was described as a nuclear protein able to bind DNA containing at least one symmetrically methylated 5'CpG-dinucleotide (Lewis et al., 1992).

The *MECP2* gene spans ~ 76kb in the long arm of the X-chromosome (Xq28) and consists of four different exons and three introns. Due to alternative splicing, the gene is transcribed and spliced into two different isoforms: *MECP2-e1* and *MECP2-e2*. These two transcripts generate two protein isoforms which differ only for their N-terminal regions (Mnatzakanian et al., 2004). *MECP2-e1* is the longer isoform, with 21 unique N-

terminal aminoacidic residues and is translated by splicing exon 1, 3 and 4. MeCP2-e2 has only 9 unique N-terminal amino acids and it is encoded from exon 2 (Figure 4.3) (Tillotson & Bird, 2019).

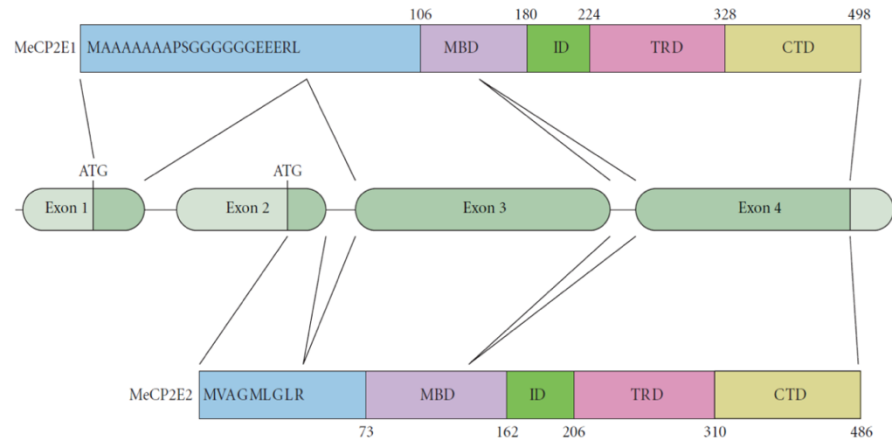


Figure 4.3: The MECP2 gene and protein isoforms. Schematic representation of MECP2 gene structure and the respective protein isoforms encoded from the gene, MeCP2-e1 and MeCP2-e2 (Zachariah & Rastegar, 2012). (Open access)

In addition, *MECP2* transcript has a large and highly conserved 3'-UTR containing four polyadenylation sites with different binding sites for proteins and miRNAs, which impact transcript stability and translation (Tillotson & Bird, 2019). Therefore, post-transcriptional regulation, such as alternative splicing and different polyadenylations at the 3'-UTR, and post-translational modifications (PTMs) of the protein are responsible for the poor correlation between *MECP2* gene transcription and MeCP2 protein levels in human and mouse tissues.

MeCP2 protein is ubiquitously expressed, with great levels in lungs, spleen and brain, where it is most abundant. Of note, the most abundant isoform in the mouse and human brains is the e1 isoform, which is ten-times more expressed than the e2 isoform (Chahrour & Zoghbi, 2007). Given that the specific deletion of the e1 isoform results in RTT-like neurologic defects in mice, while the lack of isoform e2 does not recapitulate neurological symptoms (Itoh et al., 2012; Yasui et al., 2014) e1 represents the most relevant isoform studied in the context of RTT. MeCP2 expression in brain starts during embryogenesis,

when its levels are quite low, and progressively increase during neuronal maturation (Bedogni et al., 2016; M. D. Shahbazian et al., 2002), reaching a plateau at 10 years in humans (M. D. Shahbazian et al., 2002) and 5 weeks in mice (Wood et al., 2016). In the mature brain, the protein is more expressed in cortex and cerebellum rather than in the olfactory bulb, striatum, hippocampus, thalamus or brain stem (Zachariah et al., 2012). In mature neurons, MeCP2 levels reach 16 million molecules per neuronal nuclei, 10-30 times more than the levels detected in glial cells (i.e., astrocytes, oligodendrocytes and microglia), where it is still modestly expressed (Ballas et al., 2009; Maezawa & Jin, 2010), highlighting its crucial role for neuronal function (M. D. Shahbazian et al., 2002; Skene et al., 2010; Zachariah et al., 2012).

The protein structure is highly conserved and the human and mouse aminoacidic sequences are 95% identical. In details, MeCP2_e2 consists of 486 residues, while MeCP2_e1 measures 498 amino acids; both primary structures consist of 5 different functional domains (Figure 4.4) (Bedogni et al., 2014; Gulmez Karaca et al., 2019)

- the N-terminal domain (NTD, 1-90 aa in the e1 isoform);
- the methyl-CpG-binding domain (MBD, 91-174 aa);
- the intervening domain (ID, 175-218 aa);
- the transcriptional repressor domain (TRD, 219-322 aa), containing a nuclear localization signal (NLS) relevant for its nuclear localization;
- the C-terminal domain (CTD α and β , 323-498 aa)

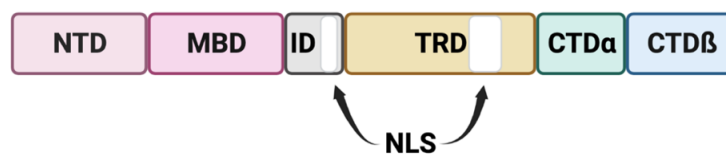


Figure 4.4: The MeCP2 protein structure. Schematic illustration of MeCP2 protein structure, with its structural and functional domains. The protein is composed of a N-terminal domain (NTD), the methyl-CpG-binding domain (MBD), an intervening domain (ID) and a transcriptional repressor domain (TRD), both containing nuclear localization signals (NLS) and a C-terminal domain (CTD).

The different domains have been assigned to elucidate MeCP2 multiple functions, through direct DNA binding (MBD), interaction with protein partners or by recruiting other factors (Guy et al., 2011). Given the interaction with methylated DNA and its ability to modulate chromatin compaction, most of the studies on MeCP2 structure focused on the two main functional domains, the MBD and the TRD. Among its domains, the MBD is the only one that has a definite secondary structure, while the majority of MeCP2 protein (around 60%) is unstructured, thus conferring the ability to interact with different partners and contributing to the multifunctional versatility that characterizes the methyl binding protein (Adams et al., 2007). The importance of the other domains has emerged subsequently over the years (Adkins & Georgel, 2011). For example, the CTD facilitates MeCP2 binding to naked DNA and mediates MeCP2 interaction with splicing factors (Chahrour & Zoghbi, 2007), while the ID enhances the affinity of the MBD for DNA and offers an independent site of interaction with a dsDNA molecule (Claveria-Gimeno et al., 2017).

4.1.4. MeCP2: a multi-talented protein

Although in the last 30 years several studies have been investigating the role of MeCP2, its functions still remain to be fully unraveled.

MeCP2 and transcriptional regulation

Its primary function is related to repression of transcription. The MBD is able to bind to methylated DNA, with a preferential association to methylated cytosines belonging to mCpG or mCpA dinucleotides (the latter mostly in the trinucleotide mCAC form), inducing chromatin compaction and promoting transcriptional repression (Connelly et al., 2020; Kinde et al., 2015; Lewis et al., 1992; Nan et al., 1996). Intriguingly, its ability to bind mCpA appears to be quite relevant for RTT pathogenesis, since these methylated dinucleotides accumulate throughout development and are abundant in post mitotic neurons, where MeCP2 reaches its greatest levels of expression (Gabel et al., 2015; Guo et al., 2014; Kinde et al., 2015). In this regard, mice harboring a mutated *Mecp2* MBD, which cannot interact with mCA but maintains its ability to bind to mCG, develop RTT-

like phenotypes, typical of the *Mecp2*-null model (Tillotson et al., 2021). Nonetheless, a recent study published by the same laboratory highlighted that in brain cell nuclei *Mecp2* is not preferentially bound to mCA repeat blocks, giving a new prospective model to MeCP2 function (Chhatbar et al., 2022).

In parallel, the TRD is able to recruit corepressors and histone deacetylase (HDAC)-containing complexes, leading to chromatin compaction and transcriptional repression. In detail, the TRD interacts with the HDAC-containing corepressor complexes Sin3A (Nan et al., 1998), c-Ski (Sloan-Kettering Institute) (Kokura et al., 2001) and the Nuclear receptor Co-Repressor and the Silencing Mediator of Retinoic acid and Thyroid hormone receptor (the NCoR-SMRT complex) (Lyst et al., 2013). More specifically, MeCP2 directly interacts with two subunits contained in the NCoR-SMRT complex, the TBL1 (transducing β -like protein 1) and TBLR1 (TBL-related protein 1), through the NCoR-SMRT interaction domain (NID), located within its TRD, inducing chromatin remodeling by removing acetyl groups from histone lysine residues (Lyst et al., 2013). In addition, MeCP2 is able to repress transcription in a HDAC-independent manner by recruiting the DNA methyltransferase DNMT1 and SUV39H1 (an H3K9 histone methyltransferase), thus reinforcing the compaction of chromatin (Fuks et al., 2003).

Of note, in mature neurons, MeCP2 is also able to induce gene silencing by direct control of global chromatin architecture. Indeed, given its great levels of expression in neurons, MeCP2 can replace histone H1, binding to mCpGs via the MBD and stabilizing DNA through its CTD, mimicking H1 association and inducing chromatin compaction (Chandler et al., 1999; Nan et al., 1997; Skene et al., 2010). In line with these results, Skene and colleagues demonstrated that H1 levels are halved in wild type mouse brain and almost doubled in *Mecp2*-null brains as a possible result of compensatory mechanisms, reaching levels typical of most cell types (Skene et al., 2010).

In recent years, a function as transcriptional activator has also been proposed for MeCP2, suggesting that its transcriptional regulatory role depends on its interacting protein partners. As a matter of fact, MeCP2 proved to be able to bind the cyclic AMP-responsive element binding protein (CREB1) which recruits and activates RNA polymerase II at transcription starting sites, promoting the expression of target genes (Chahrour et al., 2008). This activity could be originated by the ability of MeCP2 to bind 5-hydroxymethylcytosine (5hmC)-containing DNA, which is often associated with gene

activation and it is enriched in genes that are actively expressed in neurons (Mellén et al., 2012). Nonetheless, this interaction still remains controversial and appear weaker than the one between MeCP2 MBD and 5mCs (Mellén et al., 2012), leading to speculate that MeCP2 can act as a transcriptional repressor when it binds to 5mCpG- or 5mCpA-containing DNA but it might function as an activator when interacting with DNA containing 5hmC (Lyst & Bird, 2015).

Intriguingly, considering its ability to bind RNA *in vitro* (Jeffery & Nakielny, 2004), MeCP2 proved to modulate gene expression also at a post-transcriptional level, regulating miRNA processing and alternative splicing.

MeCP2 and miRNA processing

The interplay between MeCP2 and miRNA processing is relevant for RTT since miRNAs are abundant in the nervous system and modulate the expression of genes involved in developmental processes such as neurogenesis, cell fate determination, synaptic plasticity and brain maturation (Ip et al., 2018; Krol et al., 2010). Proves of the link between MeCP2 and miRNAs have been reported in several RTT studies, where the levels of many miRNAs were found dysregulated *in vivo* in *Mecp2*-null mice, in *Mecp2*-deficient neuronal cultures and in iPSC-derived neuronal cultures of RTT patients (Ip et al., 2018). In detail, MeCP2 represses the transcription of primary miRNAs (pri-miRNAs), both directly, by interacting with the mCpG-containing gene promoter regions through the MBD, and indirectly, by binding to the microprocessor protein DiGeorge syndrome critical region 8 (DGCR8) via the CTD, preventing its interaction with another member of the microprocessor complex, DROSHA, and thus regulating gene expression at a post-transcriptional level (Ip et al., 2018). As a consequence, the loss of MeCP2 leads to an increased pri-miRNA transcription, which in turn results in a subsequent increase in mature miRNA levels and gene silencing. In particular, MeCP2 deficiency is linked to an increase in miR-137, miR-15a and miR-134, associated with impaired dendritic maturation (Gao et al., 2015; Smrt et al., 2010).

MeCP2 and RNA splicing

As mentioned above, contributing to the broad spectrum of MeCP2 functions and RTT phenotypes, MeCP2 is reported to regulate alternative splicing, thus indirectly modulating gene expression. This effect is mediated by its ability to interact with the Y-box transcription factor 1 (YB1), a conserved RNA-binding protein involved in RNA splicing (Young et al., 2005), as well as the spliceosome-associated protein PRPF3, the pre-mRNA processing factor 3 (Long et al., 2011), and the splicing factors MATR3, SFPQ, and SFRS1 (Yasui et al., 2014). Evidence of these interactions can be found in *Mecp2*-null cortical neurons, where the loss of *Mecp2* led to widespread alterations of mRNA alternative splicing, such as intron retention and exon skipping (Cheng et al., 2017; Osenberg et al., 2018). However, a recent study using a machine-learning approach on high-quality transcriptomic data questioned the role of MeCP2 as a regulator of RNA splicing, by demonstrating that widely different levels of the protein induced minimal effects on alternative splicing in different systems of *Mecp2*-null neurons and brains and their respective WT controls (Chhatbar et al., 2020).

MeCP2 and protein synthesis

Another evidence of the role of MeCP2 in finely modulating gene expression is related to protein synthesis regulation through the AKT/m-TOR pathway, which is crucial for synaptic organization and whose alteration was already related to other neurodevelopmental disorders (Sharma & Mehan, 2021). Indeed, it was demonstrated that phosphorylation of ribosomal protein S6 (rpS6), an important target of mTOR pathway, is severely impaired in pre-symptomatic (P28) and symptomatic (P60) *Mecp2*-null brains (Ricciardi et al., 2011).

All in all, given its ability to modulate gene expression at a transcriptional and post-transcriptional level, both directly and indirectly intervening in gene silencing and chromatin remodeling, MeCP2 can be globally considered a master regulator of gene expression. These functions can be summarized in Figure 4.5.

MeCP2 and centrosomal functions

Beside MeCP2 nuclear functions, recent studies conducted in our laboratory have discovered a role of MeCP2 in centrosome-related functions. Indeed, it was proved that MeCP2 and its Tyr-120 phospho-isoform are enriched at the centrosome of both dividing and post-mitotic cells and its loss causes impaired spindle geometry, prolonged mitosis, and defects in microtubule nucleation (Bergo et al., 2015). Interestingly, considering that primary cilium, a protruding organelle which functions as “sensory antenna” of most differentiated cells including neurons, originate from the centrosome and that dysfunctions in their assembly or signaling lead to disorders called “ciliopathies” which share many clinical features with RTT, our laboratory decided to further investigate the centrosomal role of MeCP2 studying the link between MeCP2 and primary cilia (Frasca et al., 2020). Intriguingly, Frasca and colleagues demonstrated that the loss of MeCP2 affects ciliogenesis in cultured neurons, RTT fibroblasts and in the mouse brain, with consequent impairment of the cilium-related Sonic Hedgehog pathway, fundamental for neurodevelopment and brain functioning (Figure 4.5).

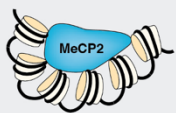

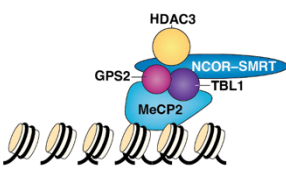
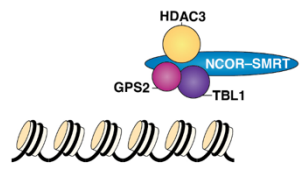
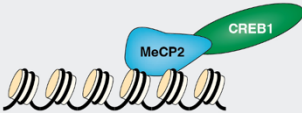

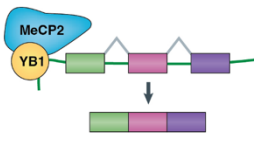
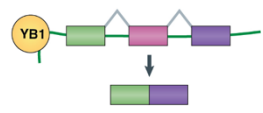
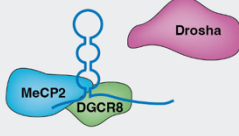
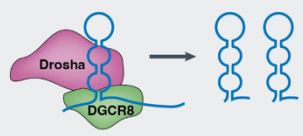
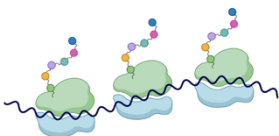
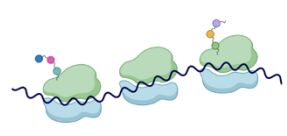
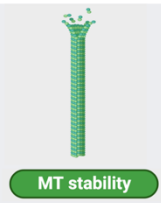
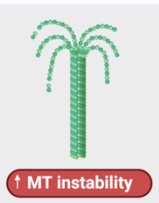
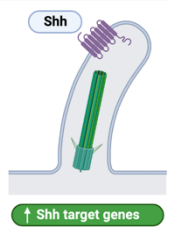
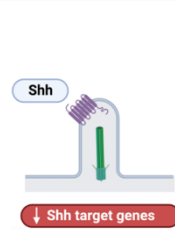
	Wild type	Null
Chromatin compaction model		
Repressor model		
Activator model		
Alternative splicing model		
miRNA processing model		
Protein synthesis		
Microtubule (MT) stability		
Ciliogenesis		

Figure 4.5: Molecular functions of MeCP2. The figure represents the proposed functions for MeCP2 in the “wild type” column and the consequences of its loss in the “null” column on the right. Modified from (Bergo et al., 2015; Frasca et al., 2020; Lyst & Bird, 2015). License number 5431460168063.

4.2. Mouse models of RTT

Since the discovery of the causative link between *MECP2* mutations and RTT, many mouse models have been developed in order to investigate the molecular mechanisms of RTT pathogenesis and design new possible therapies. Several approaches have been used to impair *Mecp2* expression and/or protein functions; indeed, full knockout, conditional knock-out, or knock-in mutant alleles have been generated in mice.

The first models developed shortly after the identification of *MECP2* as the causative gene of RTT were two *Mecp2*-knockout mouse lines, which still remain the most commonly used models to study the disorder: the *Mecp2*^{tm1.1Bird} mouse line, developed by Dr. Adrian Bird laboratory (Guy et al., 2001), and the *Mecp2*^{tm1.1Jae} strain, originated from Dr. Jaenisch and colleagues (Chen et al., 2001). The *Mecp2*^{tm1.1Bird} mouse model completely lacks of *Mecp2* protein product by deleting exons 3 and 4, thus removing most of the coding portion with the exception of the NTD. It was obtained by inserting two loxP sites flanking *Mecp2* exons 3 and 4 and crossing the *Mecp2*^{lox/lox} line with a germline-deleting Cre driver (Guy et al., 2001). The *Mecp2*^{tm1.1Jae} line expresses is characterized by exon 3 deletion, that removes the majority of the MBD and therefore expresses a small and C-terminal portion of *Mecp2* (Chen et al., 2001).

Both strains share similar phenotypes and well recapitulate RTT symptoms. Nonetheless, although RTT mainly affects females, hemizygous *Mecp2*-null male mice have still been predominantly used in the majority of RTT studies since they present an earlier manifestation of pathological phenotypes and more consistent symptoms. In particular, similarly to RTT patients, *Mecp2*-null hemizygous male mice of both knockout models appear normal at birth until three-four weeks of age, when they start experiencing a rapid regression and manifesting neurological symptoms, motor defects, abnormal gait, hind limb clasping, tremors and breathing irregularities (Chen et al., 2001; Guy et al., 2001). These phenotypical features progressively get worse, severely shortening their expected lifespan, which rarely reaches more than three months of age (Vashi & Justice, 2019). On the contrary, even though heterozygous female *Mecp2*-mutant mice represent the most clinically relevant model to study RTT, they display milder phenotypes and a slower disease progression: first evident symptoms become overt after three/four months

of age and their lifespan reaches at least 10 months (Lombardi et al., 2015). In particular, they develop uncoordinated gait, breathing difficulties, hindlimb clasping and hypoactivity. In addition, they might present deviations in phenotypic manifestations due to skewed XCI, making it more challenging to study disease progression and pathogenesis (Vashi & Justice, 2019). Importantly, while the *Mecp2*-mutant females are fertile, the knock-out males are sterile; thus, the heterozygous females are necessary for colony maintenance. Of relevance, the *Mecp2*^{tm1.1Bird} strain is produced in a C57BL/6 background, which bears some significant issues in terms of poor maternal care, low number of pups per litter and frequent events of litter cannibalism, thus limiting their use for pre-clinical studies. To overcome this limitation, our laboratory transferred the *Mecp2*^{tm1.1Bird} strain on an outbred CD1 genetic background, which in addition to recapitulating RTT-like phenotypes displayed by the BL/6 strain at the behavioral and molecular levels, produces large litters, with very low frequency of cannibalism, therefore facilitating and speeding up our studies (Cobolli Gigli et al., 2016).

However, *Mecp2*-null mice might not always well mimic the human pathology at the molecular level, since most RTT patients bear missense or late frameshift/stop codon mutations which do not cause the complete absence of the protein as the knockout strains. Thus, to recapitulate clinically relevant and common RTT mutations correlating them with the severity of symptoms and study their variable molecular consequences, several mouse models with missense or early truncating point mutations in *Mecp2* have been engineered. For instance, the *Mecp2*^{T308X} and *Mecp2*^{R168X} mouse models bear truncating mutations which falls in different domains of the protein, thus correlating with diverse degree of RTT severity. In particular, the *Mecp2*^{T308X} mutation maintains the MBD and the TRD while it deletes the CTD, resulting in hemizygous mice manifesting milder symptoms, with a delayed onset of the disease (around 6 weeks of age) and a lifespan of almost 1 year (M. Shahbazian et al., 2002). On the contrary, the *Mecp2*^{R168X} mouse model retains the MBD, while the TRD, NLS and the CTD are eliminated. These mice appear normal until four weeks of age when they start manifesting RTT like symptoms, such as hind limb clasping, spontaneous tremors and progressive motor impairment, leading to death in about 12 weeks (Brendel et al., 2011).

Similarly, other knock-in mice were generated to better characterize *Mecp2* functions and the molecular consequences of clinical RTT mutations. Of note, Brown and

colleagues dissected the molecular and behavioral phenotypes of the most common mutations observed in RTT patients, represented by the T158M, R306C and R133C mutations, respectively associated with severe, intermediate and milder clinical severity. The T158M and the R133C are located in the MBD, and the two transgenic mouse lines bearing these mutations display compromised *Mecp2* stability and weaker DNA binding. On the other hand, the R306C is detected in the NCoR/SMRT Interaction Domain (NID), instrumental to better characterize the relevance of recruiting the NCoR/SMRT complex. Indeed, the R306C mutation does not impact *Mecp2* stability but prevent the interaction of *Mecp2* with the NCoR/SMRT co-repressor complexes (Brown et al., 2016).

Another relevant knock-in model is represented by the *Mecp2*^{Y120D} mouse line, recently generated in our laboratory and mimicking the mutation found in a Japanese RTT girl (Gandaglia et al., 2019). Phenotypically, these mice develop a severe RTT-like behavior, reproducing the phenotype displayed by *Mecp2*-null mice, even though they diverge at the molecular level. This mutation is localized in the MBD of the protein and by changing its conformation impacts on MeCP2 interaction with chromatin. More specifically, *Mecp2* Y120D is characterized by decreased affinity for DNA that in turns negatively affects the recruitment of corepressors on heterochromatin, thus globally leading to more opened and transcriptionally active chromatin structure compared to the knockout mouse model. Indeed, and unexpectedly, a more condensed and closed chromatin structure was revealed in the *Mecp2* null brain, probably due to compensatory mechanisms (Figure 6). Of relevance, these data suggest that different *MeCP2* mutations might have diverse molecular consequences particularly on gene transcription; if verified, this hypothesis suggests that molecular mechanisms involved in RTT pathogenesis might vary in function of the genetic lesion and that precision medicine might be indicated for the disease.

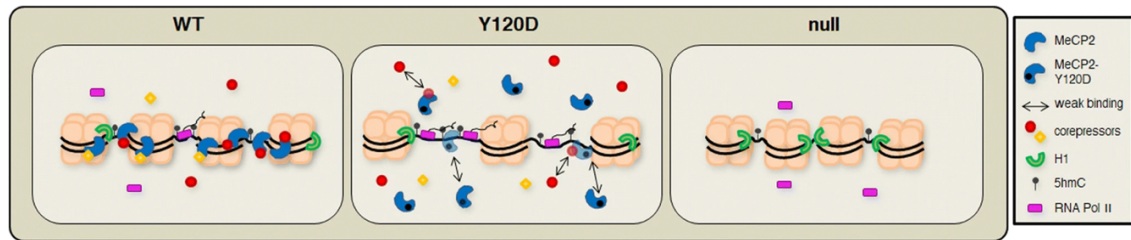


Figure 4.6: Molecular consequences of carrying a *Mecp2* Y120D allele compared to a null one. Schematic representation of chromatin structure in the brain of wild-type (WT panel), *Mecp2* Y120D (Y120D) and *Mecp2*-null (null) mouse models. The full absence of *Mecp2* might activate compensatory mechanisms that result in a more compact and less transcriptionally active chromatin structure (null panel). On the contrary, the Y120D mutation produces an hypomorphic protein unable to induce the *Mecp2*-null compensatory mechanisms but instead weakening *Mecp2* interaction with DNA, leading to a more accessible and more transcriptionally active chromatin structure (Y120D panel) (Gandaglia et al., 2019). (Open access)

To investigate the role of *Mecp2* in specific tissues, brain regions or cell types, and its contribution to RTT pathogenesis, different conditional knockout (cKO) models have been generated by crossing *Mecp2*-floxed mice with transgenic mice carrying a tissue or cell type-specific Cre recombinase, thus achieving spatial or temporal deletion of the gene. Initially, the contribution of *Mecp2* to RTT pathogenesis in the central nervous system (CNS) was assessed both in the Bird and the Jaenisch strains by selectively deleting *Mecp2* from embryonic day 12 (E12) using Nestin-Cre transgenic mice, which causes 90% recombination only in neural and glial cells of the brain (Chen et al., 2001; Guy et al., 2001). The resulting phenotype of both lines was almost identical to the *Mecp2*-null mouse, demonstrating that the primary contribution to the RTT phenotype is related to the lack of *Mecp2* in the CNS rather than in peripheral tissues. To support these findings and investigate the peripheral contribution of *Mecp2* to RTT phenotypes, the gene was selectively removed from peripheral tissues. In particular, while Conti et al., inactivated it from skeletal muscles with no evident phenotypes, Ross et al., generated mice in which normal levels of *Mecp2* were maintained exclusively in the nervous system leading to mild and specific peripheral consequences such as hypoactivity and bone abnormalities (Ross et al., 2016).

In addition, to investigate the role of *Mecp2* among different CNS cells types, *Mecp2*-floxed mice were crossed with glial-specific GFAP-Cre transgene animals, obtaining specific deletion of *Mecp2* in astrocytes. Even though selective loss of *Mecp2* from

astrocytes led to relatively milder phenotypic consequences, such as decreased body weight, hindlimb clasping, and irregular breathing, the re-expression of the protein in astrocytes was associated with an evident improvement of mice locomotion, anxiety levels, respiratory abnormalities and lifespan, proving glial cells contribution to RTT pathogenesis (Lioy et al., 2011).

Moreover, given that most of RTT studies involved germline ablation, the relevance of *Mecp2* in postnatal stages was investigated by crossing *Mecp2*-floxed mice with animals expressing a tamoxifen-inducible Cre recombinase and a modified estrogen receptor (CreER) to delete the gene at later age. When *Mecp2* was removed at P60, mice developed behavioral deficits, hind-limb clasping and impaired learning and memory similar to germline null mice and died prematurely after 13 weeks from gene removal, proving that *Mecp2* is not only essential during CNS development, but it is also required for maintaining mature neuronal networks (McGraw et al., 2011).

Of relevance, considering the lack of neurodegeneration in RTT patients, the possibility to re-express *Mecp2* and thereby restore full function and reverse RTT have been firstly investigated by Guy and colleagues in 2007 (Guy et al., 2007). More specifically, a *Mecp2* mouse line with a STOP cassette flanked by *loxP* sites was crossed with mice expressing CreER, allowing *Mecp2* silencing until the injection of tamoxifen and the consequent removal of the cassette. Intriguingly, sudden re-expression of *Mecp2* by acute tamoxifen injection caused either rapid death or total phenotypic restoration of the null mice, a possible indication that the sudden ignition of *Mecp2* that has activated compensatory mechanisms to support the absence of the protein, might lead to a devastating “molecular short-circuiting”. On the contrary, gradual and repeated administrations of tamoxifen after the onset of RTT symptoms (even at late stages of the disease) reversed neurological phenotypes and normalized the lifespan of both adult hemizygous male mice and heterozygous females, indicating that neurons are not permanently damaged. Remarkably, these results represent a milestone for RTT studies and paved the way for pursuing a cure for symptom reversal.

4.3. Neurobiological and molecular alterations in RTT

Considering that the primary contribution to RTT pathogenesis is related to MeCP2 deficiency in the CNS, many studies investigated neuroanatomical changes and neurophysiological abnormalities caused by MeCP2 deficiency.

At the anatomical level, studies on post-mortem tissues and MRI analyses revealed global cortical thinning and reduction in grey and white matter volumes, with most prominent effects in the prefrontal, posterior frontal, and anterior temporal regions, resulting in 12-24% weight and volume reduction of the brain (Armstrong, 2005; Chahrour & Zoghbi, 2007). In addition, since no sign of neurodegeneration was detected and the rate of brain growth abnormally decelerated two months after birth, reduced brain size in RTT patients has been linked to delayed brain development (Armstrong, 2005; Tarquinio et al., 2012). At the cellular level, histological analyses on post-mortem tissues of RTT patients revealed that cortical and subcortical regions of the brain present decreased neuronal cell size and increased cell density (Bauman et al., 1995), with reduced dendritic complexity in hippocampal pyramidal neurons and in frontal and motor cortices. These morphological defects were also associated with decreased number of synapses and spine density detected in RTT patient brains (Armstrong et al., 1995; Chapleau et al., 2009).

These phenotypes are well-reproduced by different *Mecp2* mutant lines. Indeed, mouse models of RTT exhibited global decline in brain size and decreased thickness of the cerebral cortex starting from 4 weeks of age (Chen et al., 2001; Fukuda et al., 2005). Accordingly, *Mecp2* mutant neurons appeared smaller and more densely packed, with decreased dendritic arborization and spine density in several brain areas, such as hippocampal CA1 and motor and somatosensory cortex (Baj et al., 2014; Belichenko et al., 2009; Chao et al., 2007; Chen et al., 2001; Fukuda et al., 2005). Interestingly, *Mecp2*-null male mice displayed thinner somatosensory cortex already at P10 and the decrement progressed over time (Moroto et al., 2013). These evidences suggested that, similarly to RTT patients, the reduction of brain volume could be promoted by decreased complexity and size of neurons (Gulmez Karaca et al., 2019). Nonetheless, the analysis of neuronal morphology in different *Mecp2* mutant models along neurodevelopment highlighted an

intrinsic variability across different ages, cell types and *Mecp2* mutations (Belichenko et al., 2009; Guy et al., 2011; I. T. Wang et al., 2013), suggesting that the use of dendritic morphology as a measurable readout to test the therapeutic potential of treatments for RTT should be carefully evaluated.

In addition, since impairments in synaptic formation and maturation are expected to affect brain connectivity and plasticity, many studies analyzed the impact of *MECP2* mutations on neuronal spontaneous activity and transmission. Several clinical researches reported altered somatosensory evoked potentials and abnormal electro-encephalograms (EEG) suggesting overall altered cortical excitability in the RTT brain, which however varied among patients, also depending on the stage of the disease (Chahrour & Zoghbi, 2007; Glaze, 2005; Moser et al., 2007). On the same line, *Mecp2* mutant mice exhibited decreased spontaneous activity in pyramidal cortical neurons due to excitatory/inhibitory (E/I) imbalance, with reduced spontaneous excitatory synaptic input and increased inhibition (Dani et al., 2005). Reduced cortical excitability was already present after 2 weeks of age, and worsened at 5 weeks, when mice start to manifest the first symptoms. At a molecular level, these findings were corroborated by decreased number of functional glutamatergic synapses, with almost 40% reduction in VGlut1-PSD95 puncta (Chao et al., 2007). On the contrary, a shift towards hyperexcitation was detected in acute slices of CA3 hippocampal region from symptomatic *Mecp2*-null mice, leading to a hyperactive hippocampal network (Calfa et al., 2015). Decreased expression of GABA-1 receptors and increased number of GluA1 subunits supported the imbalance toward excitatory outputs (Calfa et al., 2015; Medrihan et al., 2008). Nonetheless, as for morphological defects, impaired neuronal activity changes according to the brain region and neuronal circuit, contributing to the great variability of RTT features.

Overall, these data indicate that MeCP2 is required for the maintenance of brain circuits, activity-dependent plasticity and neuronal morphology throughout neuronal maturation and adulthood.

In addition to this, several evidences and retrospective analyses of RTT patients established that already during the usually defined pre-symptomatic stage, RTT girls display hypotonia, limited social interaction, decreased interest in the surrounding environment, jerkiness of limb movements and delayed acquirement of speech milestones, suggesting a possible pre-natal role of MeCP2 already at early stages of

neuronal development and differentiation (Dolce et al., 2013; Einspieler et al., 2005; Fehr et al., 2011; Marschik et al., 2013; Nomura, 2005). Alterations during the “pre-symptomatic phase” have also been identified in *Mecp2*-null mice; indeed, increased ultrasonic vocalization was measured already during the first post-natal week of life (Picker et al., 2006). In accordance with its pre-natal role, MeCP2 expression in humans was already detected after three months of gestation in multiple brainstem nuclei and in the cerebral cortex and it increased progressively over the next 10 years (M. D. Shahbazian et al., 2002). Similarly, traces of *Mecp2* expression were revealed in the marginal zone of developing mice brain at E10.5, and progressively increased along time and different brain areas, starting from the deeper layers up to the superficial parts of the brain (M. D. Shahbazian et al., 2002). More recent studies demonstrated that human neuronal progenitor cells (NPCs) derived from induced pluripotent stem cells (iPSCs) as well as mouse neuronal stem cells (NSCs) and mouse NPCs exhibited low but detectable levels of MeCP2 (Kim et al., 2011; Okabe et al., 2010). Our laboratory contributed to these findings, demonstrating that *Mecp2* can be already detected in the mouse neocortex already at E10, suggesting that the protein is involved in the regulation of all stages of neurodevelopment and adult brain functions (Bedogni et al., 2016). Accordingly, a role for MeCP2 in promoting NPC differentiation towards neurons has been proposed (Andoh-Noda et al., 2015; Squillaro et al., 2012; Tsujimura et al., 2009). In addition, neurons derived from RTT iPSCs displayed the aforementioned morphological and functional defects found in mature neurons (Nageshappa et al., 2016). At the molecular level, these phenotypes might be driven by the transcriptional defects induced by MeCP2 deficiency. Indeed, our laboratory demonstrated that in the absence of *Mecp2*, the embryonic cortex featured an upregulation of transcripts typically expressed by neuronal progenitors and the downregulation of genes associated with more mature neuronal phenotypes (Bedogni et al., 2016; Cobolli Gigli et al., 2018). All in all, these transcriptional derangements might trigger in RTT neurons typical morphological and synaptic spine defects which in turn would impact neuronal spontaneous activity and responsiveness. A summary of MeCP2 functions throughout neuronal development is summarized in Figure 4.7.

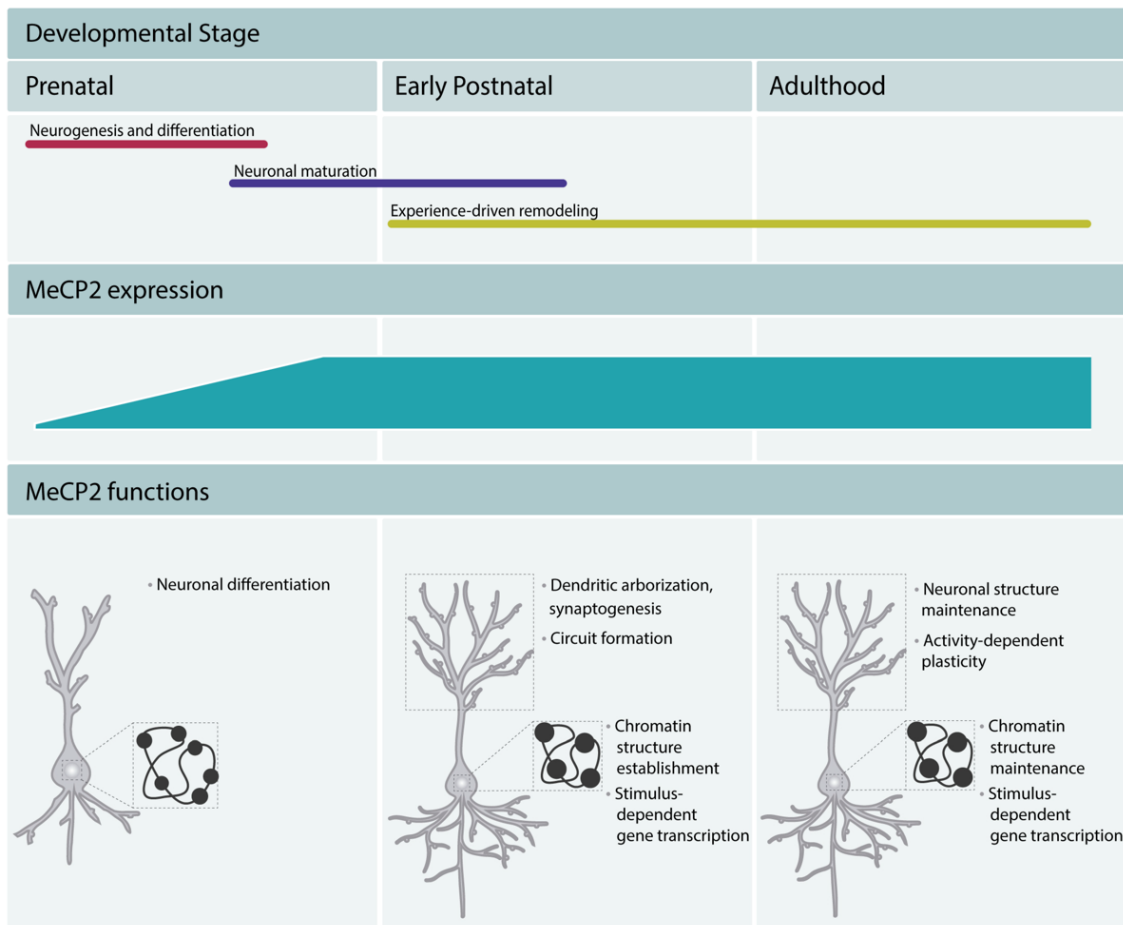


Figure 4.7: Schematic representation of MeCP2 functions in the brain across different developmental stages. During the prenatal and post-natal stages, MeCP2 affects neuronal differentiation, neuronal maturation and circuit formation. It participates to the establishment of proper chromatin structure and gene transcription in response to external stimuli. During adulthood, MeCP2 is fundamental for the maintenance of brain circuits and activity-dependent plasticity (Gulmez Karaca et al., 2019) (Open access)

Eventually, since MeCP2 is primarily expressed in neuronal cells, most of RTT studies investigated the consequences of its deficiency in neurons. However, in light of its expression in astrocytes and that astrocytes lacking *Mecp2* did not well support neuronal growth (Ballas et al., 2009), more recent works posed their attention on the role of astrocytes in RTT, which represent the most abundant glial cell type in the CNS and control dendritic outgrowth, synapsis formation, organization and plasticity (Barres, 2008). *Mecp2*-null astrocytes co-cultured with WT neurons induced neuronal morphological impairment, with neurons appearing more immature and with fewer dendritic branches (Ballas et al., 2009; Maezawa et al., 2009). Similarly, RTT astrocytes

differentiated from human iPSCs and their conditional medium failed to support WT mouse neurons, which also displayed decreased postsynaptic excitatory currents (Williams et al., 2014). Of note, Lioy and colleagues demonstrated that selective reactivation of *Mecp2* in astrocytes improved locomotor and respiratory impairments of *Mecp2*-null mice, prolonging their lifespan, and ameliorating morphological and synaptic defects of RTT neurons, therefore highlighting the importance of non-cell autonomous mechanisms mediated by RTT astrocytes (Lioy et al., 2011). On the same line during my PhD activity, I contributed to this field proving that *Mecp2*-null astrocytes exhibit themselves morphological defects according to the brain region and the age examined, which worsen along disease progression, with a prominent effect in the motor and somatosensory cortices (Albizzati et al., 2022). Given the importance of astrocytes in regulating brain metabolism and the increased oxidative stress found both in RTT patients and mouse models leading to hypersensitivity to hypoxia (De Felice et al., 2012; Grosser et al., 2012; Müller, 2019; Neul et al., 2020), the possible role of RTT astrocytes in supporting aberrant brain metabolism was also investigated. Interestingly, RTT astrocytes featured greater number of mitochondria and increased expression of proteins involved in mitochondrial respiratory chain, accompanied by lower activity of complex I and II (Bebensee et al., 2017; Dave et al., 2019).

4.4. Molecular targets of MeCP2

Considering MeCP2 role as an epigenetic and transcriptional regulator, many transcriptional studies have been conducted over the years to identify possible molecular biomarkers for early diagnosis of disorder, the design of new therapeutic approaches and the quantitative response to the novel treatments. However, the comparison of results obtained across different RTT transcriptional profiles have not led to concordant lists of deregulated genes (DEGs); as a matter of fact, very few common DEGs have been identified. One of the confounding factors might have been the difference in nature, age and stage of the samples analyzed. In fact, transcriptomic analyses have been conducted either in tissues or cell cultures and the nature of tissues analyzed varied among the

experiments, as well as the stages of the progression of the pathology and the models of the disorder (Krishnaraj et al., 2019; Marano et al., 2021). Moreover, as previously described, the type of *MECP2* mutation might also impact the molecular consequences and the transcriptional profiles (Marballi & MacDonald, 2021). Another confounding factor might be related to the heterogeneous cell populations of the mature whole-brain. Indeed, since MeCP2 is differentially expressed across cell types and its effects on transcription vary among different cell populations, the transcriptional effects of *Mecp2* deficiency were probably diluted when the whole brain or a highly heterogeneous tissue were analyzed (Kriaucionis et al., 2006; Krishnaraj et al., 2019; Nuber et al., 2005; Tudor et al., 2002). Additionally, since MeCP2 finely tunes gene expression producing subtle differences in a large group of genes, sensitivity of technical procedures and how transcriptome data are analyzed might have impacted on the lists of DEGs identified across different transcriptional profiles (Krishnaraj et al., 2019; Marano et al., 2021; Marballi & MacDonald, 2021). Eventually, most of the studies conducted in male *Mecp2*-null mice were performed when animals were highly symptomatic, thus making it more difficult to distinguish direct MeCP2 targets versus secondary transcriptional alternations due to disease progression, phenotypes and, possibly, compensatory mechanisms (Marballi & MacDonald, 2021). Among the only few genes concordantly deregulated across three or more studies, interleukin-1 receptor-associated kinase (*Irak1*), Brain-derived neurotrophic factor (*Bdnf*), Ephrin A5 (*Efna5*), fatty acid binding protein 7 (*Fabp7*), FKBP prolyl isomerase 5 (*Fkbp5*), NAD(P) dependent steroid dehydrogenase-like (*Nsdhl*), serum/glucocorticoid regulated kinase 1 (*Sgk1*), Plag1 like zinc finger 1 (*Plagl1*), fibroblast growth factor 11 (*Fgf11*) and homer scaffold protein 2 (*Homer2*) were reported (Krishnaraj et al., 2019). Thus, besides identifying specific gene lists, the focus has also been posed on the identification of common molecular pathways and biological networks altered across different RTT samples. More relevant results are highlighted below.

Neurodevelopment and synaptic plasticity

Given MeCP2 role in regulating neuronal maturation and activity-dependent synaptic plasticity, it is not surprising that DEGs involved in synaptic function and transmission, neuronal migration, learning and behavior modulation, and dendrite development were

identified in several transcriptional analyses of *Mecp2* mutant mouse neocortex (Bedogni et al., 2016), cerebellum (Jordan et al., 2007), in neuronal cells of *Mecp2*-null motor cortex, cerebellum and corpus ceruleus (Ehrhart et al., 2016; Sugino et al., 2014), and in neuronal nuclei extracted from *Mecp2* mutant male and female mice (Johnson et al., 2017). The targets identified included several immediate early and late response genes and genes involved in ionic channels and glutamatergic receptors. Interestingly, RNASeq profiles of cultured RTT astrocytes highlighted the presence of DEGs enriched in neuronal support and function (Yasui et al., 2013) and glutamate receptor signaling (Delépine et al., 2015). Of note, *BDNF* is one of the few genes whose expression has been found consistently downregulated in both RTT patients and mouse models (Abuhatzira et al., 2007; Deng et al., 2007; Klein et al., 2007), given the impaired neuronal activity and plasticity caused by MeCP2 deficiency. The involvement of BDNF in RTT pathogenesis has been supported by conditional knockout mice for *Bdnf*, which exhibited many RTT-like symptoms, and *Bdnf* overexpression in *Mecp2*-null mice that ameliorated lifespan and motor activity (Chang et al., 2006; Ehinger et al., 2020).

Lipid metabolism

Altered expression of genes involved in lipid metabolism was also detected in RTT patient brains and plasma (Buchovecky et al., 2013; Lekman et al., 1991, 1999; Segatto et al., 2014) and in *Mecp2*-null mice (Bedogni et al., 2014; Buchovecky et al., 2013; Lopez et al., 2017; Luoni et al., 2020; Pacheco et al., 2017), especially involving cholesterol metabolism. Cholesterol is one of the most abundant lipids in brain; it is present in lipid rafts embedded in the membrane of neuronal cells and functions as signaling molecule and energy source for synaptogenesis, neurogenesis, neuronal activity and regulation of several ion channels, and transporters (Hussain et al., 2019). Several genes involved in the CNS cholesterol synthesis were found downregulated in *Mecp2*-null brains, including farnesyl diphosphate farnesyltransferase (*Fdft1*), the squalene monooxygenase (*Sqs*) and NAD(P) dependent steroid dehydrogenase-like (*Nsdhl*) (Lopez et al., 2017; Luoni et al., 2020).

Immuno-response and inflammation

Many DEGs belonging to the NF- κ B, TNF, and TLR signaling pathways were also found associated with RTT and *Mecp2* mutations. The NF- κ B transcription factor controls the expression of many genes involved in immune response and inflammation, but also dendritic complexity and axon outgrowth (Gutierrez & Davies, 2011). Overexpression of genes belonging to the NF- κ B pathway were found both in *Mecp2*-null brains (Kishi et al., 2016) and RTT patient blood lymphomonocytes (O'Driscoll et al., 2015), including Calcium/Calmodulin Dependent Protein Kinase II Delta (*Camk2d*), regulating synaptic plasticity, and tumor necrosis factor (*Tnf*), a pro-inflammatory cytokine involved in immune-response. Further, *Irak1*, a kinase involved in the activation of the NF- κ B pathway, mediating the expression of pro-inflammatory cytokines, was found consistently upregulated in several *Mecp2* mutant neuronal transcriptional profiles (Jordan et al., 2007; Kishi et al., 2016; Urdinguio et al., 2008) and in *Mecp2* mutant astrocytes (Delépine et al., 2015). Genes enriched in TNF signaling pathway also appeared upregulated in *Mecp2*-null embryonic cortical neurons (Vacca et al., 2016) and microglia (Cronk et al., 2015). The importance of this pathway and its involvement in RTT pathogenesis was confirmed by overexpressing *Irak1* in cortical neurons, thus causing the reduction of dendritic complexity, and by knocking down *Nfkb1* which, by reducing NF- κ B signal, ameliorated the dendritic phenotype and extended the life span of *Mecp2*-null mice (Kishi et al., 2016).

Mitochondrial function

Mitochondrial dysfunctions have been identified in brains of both *Mecp2*-null models (Belichenko et al., 2009; Kriaucionis et al., 2006) and RTT patients (Gibson et al., 2010), causing the extensively reported oxidative stress in RTT (De Felice et al., 2012; Filosa et al., 2015; Signorini et al., 2011). Expression of genes enriched in mitochondrial function were found dysregulated in RTT patient brain and blood (Gibson et al., 2010; Pecorelli et al., 2013) and mouse neuronal cells (Kriaucionis et al., 2006), and can be responsible for the aforementioned mitochondrial alterations. In particular, downregulation of cytochrome c oxidase subunit 1 (*MTCOI*) and increased expression of the ubiquinol-cytochrome c reductase core protein 1 (*Uqcrc1*) genes were both detected in RTT (Gibson

et al., 2010; Kriaucionis et al., 2006; Pecorelli et al., 2013). Notably, *Uqcrc1* upregulation positively correlated with increased mitochondrial respiratory activity and severity of *Mecp2*-null mice symptoms (Kriaucionis et al., 2006).

In order to validate gene expression results, proteomic studies have also been performed; however, these analyses detected minimal changes and weak correlations with transcriptional profiles (Marballi & MacDonald, 2021). Only Pacheco and colleagues integrated transcriptomic and proteomic datasets derived from the same *Mecp2* mutant cortical samples (Pacheco et al., 2017): among the significant DEGs and proteins detected in the study, only 35 gene-protein hits were identified. These genes are involved in metabolic pathways, protein stability and calcium-mediated processes. Notably, only one of these hits, the FKBP prolyl isomerase 5 (*fkbp5*), able to modulate glucocorticoid sensitivity and associated with stress and mood disorders in humans, was found consistently deregulated across three or more transcriptomic studies (Ben-Shachar et al., 2009; Krishnaraj et al., 2019; Zhao et al., 2013).

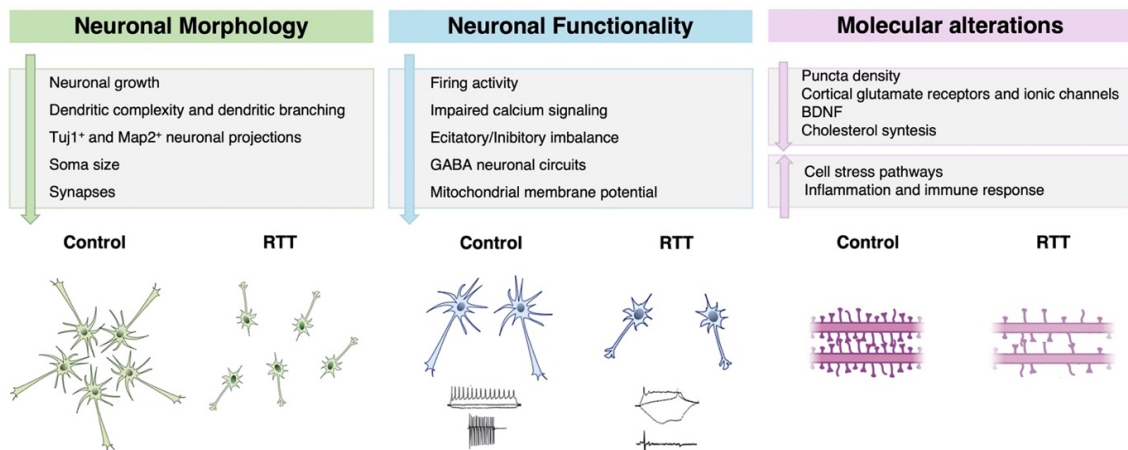


Figure 4.8: Schematic overview of neuronal morphology, functionality and molecular target alterations in RTT. RTT neurons appear more immature, with dendritic atrophy and decreased soma size. They have reduced synaptic puncta density and spontaneous activity and functionality. They present a downregulation in markers of mature and active neurons and of cholesterol synthesis and an upregulation of oxidative stress and immune response pathways.

4.5. Therapeutic approaches and clinical trials in RTT

Although RTT proved to be reversible at least in mice (Guy et al., 2007), to date no cure exists and available treatments are mainly symptomatic, addressed at ameliorating secondary phenotypes and improving patients' quality of life. Given the social impact and the severity of the pathology, researchers have rushed over the past twenty years to discover novel potential treatments for the disorder and so far, more than 60 clinical trials have been proposed (Gomathi et al., 2020; Panayotis et al., 2022).

As represented in Figure 4.9, potential treatments for RTT can be mainly ascribed to two main categories (Vashi & Justice, 2019):

- therapies addressing *MECP2* downstream targets;
- treatments aiming at restoring *MECP2* gene and related functions.



Figure 4.9: Schematic representation of available options for RTT treatment. Potential therapies can be divided into treatments targeting directly *MECP2* mutations or its downstream targets (Vashi & Justice, 2019). (Open access)

4.5.1. Treatments against MeCP2 downstream targets

Pharmacological therapies against MeCP2 downstream pathways are directed towards the molecular pathways and biological networks affected by MeCP2 and are usually based on clinical observations found in other diseases (Neul et al., 2022). In general, these pharmacological strategies belong to drugs targeting either neurotransmitter signaling, growth factors pathways and RTT metabolic defects. Unfortunately, these trials have often produced modest or null effects. Several reasons might justify these negative results, including the lack of blinded investigations in the pre-clinical studies, the fact that no sufficient attention was given to a good correspondence between the age and length of treatment in mice and humans and, eventually, the necessity to include in the pre-clinical studies also the heterozygous female mice and possibly a knock-in mutation of *Mecp2*.

One example is represented by desipramine, a noradrenaline uptake inhibitor, which appeared promising in ameliorating breathing abnormalities and apneas in *Mecp2* mutant mice (Roux et al., 2012b; Zanella et al., 2008) but no clinical amelioration was identified in a phase II clinical trial (NCT00990691) (Mancini et al., 2018). In line with desipramine, another drug acting on neurotransmitter signaling, sarizotan, a 5-HT1a agonist and a dopamine D2-like partial agonist, proved effective in reducing apneas in *Mecp2* mutant mice but, once moved into clinical trials, it showed no efficacy in a recently completed phase III clinical trial (NCT02790034) (Leonard et al., 2022). Other molecules targeting neurotransmitter signaling are still currently being evaluated. As a matter of fact, promising results in pre-clinical studies were demonstrated by low doses of ketamine, an NMDA receptor agonist, tested in *Mecp2*-null mice, which exhibited an increase in cortical activity and a decreased synaptic excitability in the brainstem after treatment, thus modulating the excitatory/inhibitory imbalance typical of RTT (Kron et al., 2012; Patrizi et al., 2016). Additionally, ketamine administration ameliorated motor defects and breathing abnormalities of *Mecp2*-null mice. Given these promising results, safety and viability of ketamine are being evaluated in a new randomized, double-blind, placebo-controlled phase II trial (NCT03633058) (Vashi & Justice, 2019). The Sigma-1 receptor agonist, blarcamesine or Anavex 2-73, able to reduce protein misfolding and to decrease cellular stress, improving the function of mitochondria, proved to ameliorate neurologic impairments in RTT mice (Kaufmann et al., 2019) thus leading to an active

phase III double-blind, randomized, placebo-controlled, safety and efficacy study called EXCELLENCE (NCT04304482), which is currently recruiting (Leonard et al., 2022). Finally, tianeptine, also called Amo-04, a repurposed antidepressant which modulates glutamate signaling, demonstrated to be effective *in vivo* by ameliorating motor coordination and visual function of *Mecp2*-null mice. Since the drug has been already proved safe in clinic, the authorization for moving directly into a phase II clinical trial is currently pending (https://www.amo-pharma.com/amo_04.htm).

Another possible treatment for RTT is based on the modulation of growth factors signaling. The first growth factor pathway to be targeted belonged to BDNF. Nonetheless, even though BDNF appeared one of the few genes downregulated both in RTT patients and mouse models (Abuhatzira et al., 2007; Deng et al., 2007; Klein et al., 2007), its direct administration would have not been practicable since it is not able to cross the blood-brain barrier (BBB) (Vashi & Justice, 2019). To overcome this problem, the use of fingolimod (FTY720), a sphingosine-1 phosphate receptor agonist, was proposed since it appeared to modestly increase BDNF levels and BDNF-dependent downstream targets and activity-related proteins, such as c-Fos and pERK1/2 (Deogracias et al., 2012; Patnaik et al., 2020), improving morphological defects of developing *Mecp2*-null cortical neurons (Patnaik et al., 2020). These ameliorations correlated with increased motor coordination of *Mecp2* mutant animals (Deogracias et al., 2012). Given these encouraging results and its previous clinical use for the treatment of multiple sclerosis, a phase II trial (NCT02061137) started to assess safety and efficacy of FTY720 in children with RTT (Naegelin et al., 2021). After one year of administration, fingolimod proved safe in RTT girls but no evidence of increased BDNF levels in serum and cerebrospinal fluid (CSF) nor changes in deep gray matter volumes or in clinical scoring were detected (Naegelin et al., 2021). On the contrary, a promising treatment is represented by the administration of insulin-like growth factor-1 (IGF1). IGF1 is involved in neuronal maturation, axonal outgrowth, and synapse formation, by stimulating the same downstream pathways as BDNF (D'Ercole et al., 1996; O'Kusky et al., 2000; Zheng & Quirion, 2004). IGF1 is transcriptionally regulated by *MECP2* (Itoh et al., 2007) and is able to cross the BBB, especially in its tri-peptide form, which maintains the same neurotrophic effects of the full-length protein (Tropea et al., 2006). Thus, both the full-length human recombinant IGF1 (Castro et al., 2014) and the N-terminal active tripeptide of IGF1 (Glutamate-

Proline-Glycine, GPE) (Tropea et al., 2009) were daily administered to *Mecp2*-null mice starting at the pre-symptomatic stages, P28 and P15 respectively, and were able to partially restore many RTT phenotypes. In particular, the treatments improved locomotor activity, breathing abnormalities and cardiac function of *Mecp2*-null mice; at the neuroanatomical levels, they ameliorated the brain weight of treated animals and increased PSD-95 density, the number of spines and cortical excitatory synaptic transmission (Castro et al., 2014; Tropea et al., 2009). In addition, since mecasermin, a human recombinant IGF1, was already approved for the long-term treatment of growth failure in children, two open-label clinical trials were initially carried out in RTT girls to assess its safety, tolerability, pharmacokinetics and preliminary efficacy (Khwaja et al., 2014; Pini et al., 2016). In these trials, the drug demonstrated to ameliorate apneas, anxiety, stability of disease severity and social and cognitive ability of RTT girls. RNA extracted from serum of patients treated with mecasermin in the Khawaja trial was then sequenced in order to identify possible molecular targets measuring the efficacy of the drug and its correlation with breathing amelioration (Shovlin et al., 2022). This study identified two subclasses of patients according to the severity of breathing abnormalities and their corresponding transcriptome profiles. In fact, patients with severe breathing abnormalities, called responders, and patients with low indices of apnea, called mecasermin study reference group, before IGF1 treatment presented differentially expressed genes which progressively decreased at the subsequent timepoints after mecasermin administration, correlating with the amelioration of the apnea index manifested by the responder group (Shovlin et al., 2022). These promising clinical observations were followed by a randomized placebo-controlled phase II trial (based on mecasermin) opened to a larger group of patients. Nonetheless, this study failed to replicate the previous amelioration in the apnea index, probably because the severity of the breathing problems at the beginning of the trial was not high enough to demonstrate treatment efficacy (O'Leary et al., 2018). On the contrary, significant ameliorations in stereotypic behavior and social communication were still detected, keeping open the possibility to use IGF1 for the treatment of RTT. In parallel, a new synthetic analog of the GPE, trofinetide, was synthesized and its safety and tolerability were tested in a multicenter, double-blind, placebo-controlled phase II trial (NCT02715115), demonstrating to be well tolerated and improving several core symptoms of RTT, such

as stereotypic movements, mood dysfunction/disruptive behavior, and ambulation (Glaze et al., 2019; Glaze et al., 2017). These encouraging observations led to an on-going randomized double-blind placebo-controlled phase III confirmatory LAVENDER trial (NCT04181723) to evaluate trofinetide efficacy and safety in RTT girls and women (5–20 years of age) and the possible ameliorations in communication, ambulation, and use of hands (Neul et al., 2022).

Eventually, since RTT patients manifest altered lipid and cholesterol homeostasis, drugs properly modulating metabolism might represent another therapeutic target. Indeed, higher levels of total brain cholesterol was found in symptomatic *Mecp2*-null mice together with decreased biosynthesis and turnover, suggesting defective cholesterol biosynthesis in the RTT brain (Buchovecky et al., 2013). On the contrary, higher levels of cholesterol and triglycerides were present in the serum of *Mecp2*-null mice; the use of Fluvastatin was tempted to balance cholesterol levels and homeostasis. The treatment improved motor activity of *Mecp2*-null mice and prolonged their lifespan (Buchovecky et al., 2013), thus leading to a still on-going open label trial testing the efficacy and safety of statins in RTT girls (NCT02563860) (Leonard et al., 2022).

4.5.2. Treatments to restore MECP2 gene or functions

The most difficult yet efficient strategy to treat RTT is probably represented by direct restoration of *MECP2* gene or functions. Since the reversal of RTT symptoms after *Mecp2* re-expression in mice (Guy et al., 2007), two main approaches have been proposed: gene therapy and inactive X chromosome reactivation.

Gene therapy has been widely studied for multiple genetic disorders and can be intended either as the re-introduction of new gene copies to compensate the absence of the mutated protein (gene replacement) or as the editing of the specific endogenous gene or its transcript (genome or RNA editing).

To develop novel therapies based on efficient gene replacement strategies, several types of viruses have been deeply investigated over the last decade. Lentivirus and retrovirus vectors were the first used in pre-clinical studies since they bare the advantage of carrying larger DNA payload (Bulcha et al., 2021). Nonetheless, their application was

soon reduced given that the integration of their genetic material into the host genome increases the risk of insertional mutagenesis and carcinogenesis (Hacein-Bey-Abina et al., 2008; McCormack & Rabbitts, 2004). Novel gene replacement strategies have then emerged, based on adeno-associated viruses (AVVs), especially for neurological disorders, since they can efficiently infect post-mitotic neurons and provide stable long-term expression of the transgene integrated in the genome of the host (Li & Samulski, 2020). However, due to their small packaging size, they can incorporate small DNA products, which range from less than 4.7 kb for single stranded and approximately to 2.3 kb in the more efficacious self-complementary (sc) packaging approaches (Lykken et al., 2018). Another limitation is represented by their systemic administration: only the serotype 9 (AAV9) can cross the BBB and the doses required to efficiently transduce the CNS after systemic injection often lead to liver toxicity (Li & Samulski, 2020). Several strategies to avoid off-target toxicity and increase tissue-specific tropism have been engineered, including cell-type specific promoters (de Leeuw et al., 2014; Gray et al., 2011) and microRNA target sites as autoregulatory elements (Hordeaux et al., 2020). Two independent studies have initially evaluated the use of recombinant AAV vectors as a possible gene replacement strategy for *MECP2* (Gadalla et al., 2013; Garg et al., 2013). Gadalla and colleagues demonstrated the efficacy of direct brain injection of single stranded AAV9-*MECP2* in neonatal *Mecp2*-null mice, prolonging their lifespan and delaying the onset of behavioral defects of mutant animals. Conversely, systemic administration of scAAV9-MeP-*MECP2* in juvenile mice displayed liver toxicity and low levels of transduction in the brain (2-4%), despite the presence of a truncated *MECP2* specific promoter (Gadalla et al., 2013). Similarly, Garg et al. reported that systemic administration in 10 month-of-age heterozygous females of an scAAV9 virus containing *MECP2_e1* cDNA under control of a fragment of its own promoter ameliorated behavioral defects and prolonged mice lifespan (Garg et al., 2013). Accordingly, Matagne and colleagues developed a scAAV9-MCO expressing a codon-optimized *Mecp2* which was able to improve survival, weight gain and apneas, and delay the occurrence of behavioral deficits after systemic administration in P30 early symptomatic *Mecp2*-deficient mice, even though the brain transduction efficiency still remained quite low as for previous studies (5-20%) (Matagne et al., 2017). These studies posed attention on several aspects of gene replacement strategy for RTT, demonstrating that optimizing

the viral construct could induce beneficial effects in ameliorating RTT-like phenotypes but it was not sufficient to rescue these defects to a wild-type level; in addition, the systemic administration still triggered liver toxic side effects mediated by MeCP2-overexpression and produced low brain transduction efficiency. Thus, to increase the efficiency of transduction in the CNS and better control peripheral MeCP2 expression, a new scAAV9 vector was engineered by using a small part of the promoter of *MECP2* (*MeP426*), a modified 3' UTR incorporating its conserved polyadenylation signal (pA), and a panel of miRNA-binding sites specific to endogenous miRNAs able to interact with the *MECP2* 3'UTR and thus regulating the possible deleterious overexpression of MeCP2 (Gadalla et al., 2017). Systemic delivery of this vector in P30 *Mecp2*-null mice did not induce liver toxicity but instead improved lifespan and body weight of mutant animals. Similar results were obtained after *intra cisterna magna* administration of the same vector in juvenile *Mecp2*-null mice (Sinnott et al., 2017). Subsequently, the AAV-PHP.B, a novel generation of synthetic vector, was engineered carrying a specific insertion of 7 amino-acids in the capsid protein enabling higher permeabilization of the BBB in adult mice and more efficient transduction of neural cells (Morabito et al., 2017). This vector was used to incorporate an instable *Mecp2_e1* (*iMecp2*) transgene cassette lacking a long 3'-UTR sequence which limits the overexpression of *Mecp2* within the cells. This AAV-PHP.B vector was systemically injected in P30 *Mecp2*-null mice, showing to increase CNS transduction and robustly ameliorate RTT-like behavioral phenotypes with no hepatotoxic effects, even though it induced a strong immune response that severely affected the lifespan of treated animals (Luoni et al., 2020). To overcome this issue, chronic immunosuppression with cyclosporine A ameliorated the general health conditions and prolonged mice lifespan up to nine months. Unfortunately, the brain tropism of this vector is restricted to C57Bl/6J mice since the LY6A receptor mediating its BBB transport is not expressed in non-human primates (Hordeaux et al., 2018). To further control MeCP2 expression and insert new regulatory elements in the developed scAAV9 vectors, different strategies based on reducing the packaging of the transgene to *MeCP2* essential domains have been recently developed. To this purpose, Bird's laboratory designed a novel viral vector containing a minimal-*MECP2* only expressing the MBD and the N-CoR domain, inducing an amelioration of RTT-like phenotypes and survival after direct injection in the brain of neonatal *Mecp2*-null mice (Tillotson et al.,

2017). Sinnett and colleagues incorporated new regulatory elements in this vector by inserting a 3' UTR carrying targets of microRNAs, called mi-RARE (MiRNA-responsive autoregulatory element) which would block miniMeCP2 overexpression in any transduced cell by a negative feedback mechanism (Sinnett et al., 2021), improving safety without compromising efficacy. The study revealed that after direct injection in juvenile *Mecp2*-null mice, the percentage of transduced brain cells reached 40%, against the 8% identified in WT animals, extending mutant mice survival and delaying onset of gait abnormalities. These encouraging results in RTT mice and the positive data obtained after a six-month toxicology study in non-human primates prompted the approval by Health Canada of TSHA-102, the first gene therapy phase I clinical trial for RTT. TSHA-102 contains the miniMECP2 transgene under the control of its neuronal promoter MeP426 and the miRARE elements, packaged into scAAV9 vectors (<https://tayshagtx.com/pipeline/#tab-id-2-active>).

In addition, since its ground-breaking application in gene therapy, CRISPR/Cas9 have been widely investigated as a genome editing approach for several genetic disorders, including RTT. This novel strategy would guarantee the expression of the endogenous healthy protein, thus avoiding overexpression side effects observed with the replacement strategy. Recent proof of concept studies showed the success of this novel approach in human iPSC-derived TT neurons to correct the T158M and R270X point mutations (Croci et al., 2020; Le et al., 2019); however, the capacity to transduce two vectors carrying CRISPR/Cas9 and gRNA respectively into the same cell and the possibility of off-target modifications still remain to be investigated.

The reactivation of the inactive X chromosome (Xi) appears another interesting and yet less explored approach to treat RTT, given the lack of complete understanding of the molecular mechanisms and key factors regulating XCI. Reactivation of the entire Xi was originally obtained *in vitro* using a small-molecule inhibitor of DNA methylation and an antisense oligonucleotide against *Xist* (Carrette et al., 2018). However, the pharmacological inhibition of XCI-inducing factors still represents the elective strategy to modulate Xi reactivation. Indeed, Przanowski and colleagues demonstrated that pharmacological inhibition of ACVR1 (activin A receptor type I) and PDPK1 (pyruvate dehydrogenase kinase 1) can reactivate Xi-linked MECP2 in female mouse fibroblasts, human iPSC-derived RTT neurons and in cerebral cortical neurons of P30 adult female

mice bearing an Xi-linked *Mecp2-Gfp* reporter, after direct brain injection every two days for three weeks (Przanowski et al., 2018). These small-inhibitor molecules hamper the recruitment of transcriptional activators to Xist promoter thus decreasing Xist expression. Interestingly, the Xi reactivation did not increase the total expression levels of X-linked genes, probably due to the presence of compensatory mechanisms (Bhatnagar et al., 2014). Another class of pharmacological inhibitors of XCI-inducing factors is represented by JAK/STAT pathway inhibitors, identified in a small-molecule screen (Lee et al., 2020). These compounds reactivated *MeCP2* from Xi *in vitro* in different cell types, including mouse fibroblasts and primary cortical neurons. Nonetheless, further studies are required to test mechanisms, safety and efficacy in *Mecp2* mutant mouse models and identify possible novel hit compounds to implement this therapeutic strategy.

For convenience, proposed novel treatments for RTT which are currently being tested in clinical trials or are under evaluation by FDA or for clinical trials are reported in Figure 4.10.

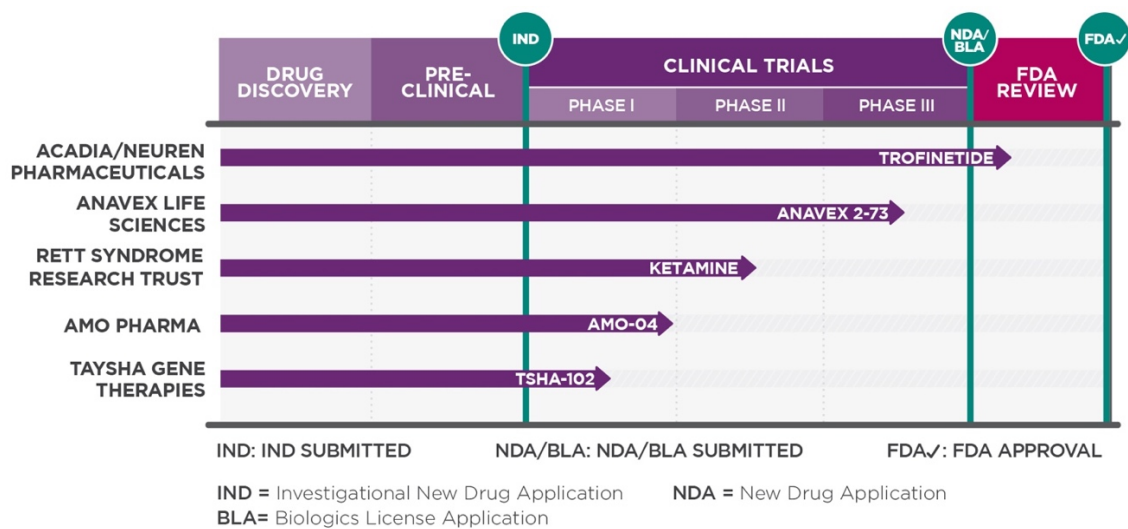


Figure 4.10: Updated potential treatments for RTT therapy in clinical trials. To date, only Trofinetide and Anavex 2-73 have been evaluated in phase III clinical trials. Ketamine is currently being evaluated in a phase II trial, while Tsha-102 is the first gene therapy approach to move into clinic and whose safety will be assessed. Amo-04 (tianeptine) is currently waiting for directly moving into phase II. Modified from (<https://research.rettysndrome.org/>).

4.6. Drug screening systems in RTT

RTT severity and incidence underline the social emergency of finding effective treatments. Over the years, RTT mouse models have been considered the golden standard in evaluating the potential therapeutic effects of new possible treatments for the disorder, since they robustly model many RTT phenotypes. As a matter of fact, animal-based drug screenings for RTT therapy are routinely used to evaluate drug efficacy as a first step towards clinical trials. However, this approach requires a large number of animals and is extremely expensive and time-consuming. A paradigmatic example is represented by the SCOUT program that, by combining technical expertise of bio-tech and pharma companies with academic knowledge, initiated a drug screening program in 2013 aimed at aggressively accelerating compound testing in standardized pre-clinical studies (<https://www.rettsyndrome.org/research/for-researchers/scout-program/>). It was based on the use of heterozygous female mice, considered a better model of RTT. In detail, the PsychoGenics company provided a screening platform to screen libraries of potential drugs using advanced bioinformatic tools and artificial intelligence to establish the dose with a greater probability of success in RTT heterozygous females (<https://www.psychogenics.com/cube-technology/#smartcube>). This platform led to the identification of few compounds that were then directly tested *in vivo* with standardized behavioral evaluations. Nonetheless, in almost 10 years only 33 compounds were tested on Rett heterozygous female mice between 8-12 weeks of age. Among these, 5 compounds passed the first level of evaluation and made it to the second phase where breathing and visual responses and molecular analysis were measured. At the end of the process, three compounds successfully moved from the Scout Program to clinic, which include the already mentioned:

- Sarizotan, which unfortunately showed no amelioration of RTT phenotypes in a phase III clinical trial;
- Anavex 2-73 or blarcamesine, which proved safe in a phase II clinical trial and is currently recruiting in the EXCELLENCE phase III trial;

- Amo-04 (tianeptine), a repurposed antidepressant drug, whose authorization for moving into a phase II clinical trial is currently pending (https://www.amo-pharma.com/amo_04.htm).

Besides these positive results, this screening system indicates how the animal-based testing is time-consuming, highlighting the need to quickly pre-select drug before moving to *in vivo* studies. For this reason, research has been focusing on finding new approaches of *in vitro* drug screening to support and accelerate the *in vivo* evaluation. *In vitro* assessments are usually carried out on neuronal-based cell models, such as primary neurons, patients-derived induced pluripotent stem cells (iPSCs) and neuronal precursor cells (NPCs), which are able to recapitulate key features of RTT pathology and offer large, fast, scalable and relatively inexpensive drug screening systems. In addition, these cell systems allow to investigate the early phases of RTT pathogenesis, thus helping to dissect pathways affected as primary result of *MECP2* deficiency, which might have greater therapeutic value. Generally, these *in vitro* evaluations are based on the ability of drugs to rescue morphological defects typical of RTT neurons. Dendritic branching and synaptic puncta density have been considered for long the elective quantitative biomarkers to preliminary assess drug efficacy in RTT (Bittolo et al., 2016; Frasca et al., 2020; Marchetto et al., 2010; Nerli et al., 2020; Patnaik et al., 2020; Tang et al., 2019; Tropea et al., 2009; Trujillo et al., 2021). Nonetheless, the use of morphological analyses alone should be cautioned, since it is intrinsically variable according to *Mecp2* mutations, brain region and developmental stage (Belichenko et al., 2009; Guy et al., 2011; Wang et al., 2013). Thus, in most of these studies, morphological rescue has been corroborated by the evaluation of neuronal responsiveness after treatment. However, morphological and functional analyses remain difficult to scale up since they would require high-throughput automated equipment which would not be easily accessible in every-day laboratory procedures. Additionally, our group has recently suggested that transcriptional rescue of genes typically deregulated in *Mecp2*-null neurons might ensure a better chance of functional restoration than morphological analysis (Scaramuzza et al., 2021). In this study a novel model of RTT, which consists of neurons differentiated from mouse *Mecp2*-null neural-precursor cells (NPCs) able to reflect transcriptional, morphological and functional phenotypes typical of RTT neurons, was optimized. Based on the hypothesis

that neuronal activity modulates the expression of genes fundamental for the establishment of proper neuronal maturity (Spitzer, 2006), our group tested whether the administration of a positive modulator of AMPA receptors, the ampakine CX546, could improve neuronal development and possibly rescue transcriptional and morphological impairments. Intriguingly, an early treatment of NPC-derived *Mecp2*-null neurons with CX546 was able to ameliorate the expression of many deregulated genes, and to rescue typical functional and morphological phenotypes. Conversely, a late treatment rescued dendritic arborization of NPC-derived RTT neurons without, however, recovering transcriptional and functional defects. The validity of this study was confirmed by proving that early exposure (from P3 to P9) of *Mecp2*-null mice to CX546 delayed the progression of the disorder, significantly prolonging their lifespan, ameliorating their general condition, and improving their motor and cognitive functions, even 30 days after the last treatment (Scaramuzza et al., 2021).

Overall, this evidence points to the importance of developing novel approaches of drug screening for RTT, in order to select drugs with a better chance of success in animal-based studies, therefore accelerating pre-clinical evaluations and their movement towards clinical trials.

5. Aim

Rett syndrome (RTT) is a devastating neurodevelopmental disorder, caused by loss-of-function mutations in the *MECP2* gene and representing the second cause of severe intellectual disability in girls worldwide. Although research has proved that RTT is reversible in mice, no cure for RTT is yet available, thus finding an effective treatment has become a real social emergency. In the last two decades many mouse models of the disorder have been developed, able to reproduce behavioral, physiological, and cellular phenotypes observed in patients. These models are considered the most valuable step to evaluate drug efficacy before clinical trials. Nonetheless, their exploitation in large programs of drug screenings is limited by the great number of animals required, elevated costs and the length of studies. RTT research is thus looking for efficient novel approaches of drug screening useful to pre-select candidates' molecules to be tested in animals. Our laboratory has recently proposed that the amelioration of the transcriptional deregulations typical of RTT neurons ensure a better functional restoration compared to morphological rescue, suggesting that transcriptional analysis might represent a better quantitative readout to measure drug efficacy.

Based on this evidence, the main aim of my PhD project consisted in developing and testing the efficacy of a new and fast platform for *in vitro* screening of drugs on *Mecp2*-null neurons, based on a customized high-throughput transcriptional array.

The development of this new drug screening system consists of three main objectives: i) identifying consistent transcriptional defects, using a longitudinal bulk RNASeq analysis of *Mecp2*-null neurons derived from differentiating neuronal precursor cells; ii) validating and selecting reproducible differentially expressed genes, which would represent our quantitative probes to measure drug efficacy, therefore forming our customized Array card; iii) assessing hit confirmation by evaluating the ability to rescue RTT-specific transcriptional defects of at least one molecule whose efficacy in mouse models of RTT was already established.

As secondary outcome, the transcriptional profile of cultured RTT neurons might have led to the identification of novel deregulated genes/pathways whose characterization might contribute to a better comprehension of RTT pathogenesis and/or its treatment.

6. Results

6.1. Identification of RTT-specific neuronal transcriptional biomarkers for the drug screening system

6.1.1. Longitudinal RNASeq analyses identified differentially expressed genes of developing RTT-neurons

As thoroughly described in section 4.3, beside its crucial role in maintaining neuronal structure and ensuring a proper activity-dependent plasticity, recent preclinical and clinical evidences demonstrated that MeCP2 is involved in all stages of neurodevelopment, including embryonic and early post-natal neurogenesis and neuronal maturation. As a matter of fact, MeCP2 is already detectable in neural stem cells (NSCs), neuronal precursor cells (NPCs) and in human iPSC-derived NPCs, even though in a much lower quantity with the respect to mature neurons, contributing to the early evidences of MeCP2 involvement in neurodevelopment (Kim et al., 2011; Li et al., 2013; Okabe et al., 2010). Our laboratory supported these findings, detecting the presence of *Mecp2* already in the embryonic mouse neocortices and demonstrating that *Mecp2*-null neurons exhibit a delayed transcriptional maturation, decreased neuronal responsiveness to stimuli and defective morphology already during corticogenesis (Bedogni et al., 2016). To further dissect early mechanisms of neuronal maturation of *Mecp2*-null developing neurons during corticogenesis, a cellular system of neurons, astrocytes and oligodendrocytes differentiated from NPCs, permitting to follow cells during neuronal development in a more physiological environment compared to primary neurons was optimized and proved to well-recapitulate transcriptional, morphological and functional phenotypes typical of RTT neurons, with no effect on the relative frequency of distinct cell populations in *Mecp2*-null samples compared to wild types (see Method section, 8.2.1) (Scaramuzza et al., 2021). Prompted by these results, we decided to use NPC-derived cultures as the elective cell system for the screening and for identifying a solid

and reproducible group of RTT-specific neuronal genes to use as quantitative probe in our customized cards.

To characterize the transcriptional consequences of *Mecp2* deficiency in developing neurons and identify consistent and robust RTT neuronal transcriptional defects that might become valid biomarkers for the screening, we performed a longitudinal RNASeq analysis on 7 WT and *Mecp2*-null (KO) longitudinal NPC-derived cultures at DIV7, DIV14 and DIV18 of neuronal maturation, for a total of 42 samples. Of note, only samples that permitted to obtain all the three timepoints starting from the same original culture were sequenced, as described in the methods section.

Two different types of bioinformatic analyses were performed:

1. time-specific analysis of differentially expressed genes (DEGs) between WT and *Mecp2*-null cultures;
2. identification of DEGs that are consistently and significantly differentially expressed overtime.

6.1.1.1. Time-specific analysis allowed to set DIV14 as the elective timepoint to perform the screening

With the purpose of developing the proposed molecular drug screening system on customized cards, and considering that the ability of a drug to ameliorate the RTT-specific neuronal transcriptional biomarkers will be evaluated at a specific timepoint of neuronal maturation, a time-specific analysis was performed at DIV7, 14 and 18 in order to identify DEGs between *Mecp2*-null and WT samples at each timepoint and establish the most suitable one to perform the screening.

Time-specific differential expression analysis provided a list of DEGs of KO vs WT cultures at each timepoint examined, as reported in Figure 6.1.

Time	Padj < 0.1	Padj < 0.1 & LFC > 1	Padj < 0.1 & LFC > 1	Padj < 0.1 & LFC < -1	Padj < 0.05	Padj < 0.05 & LFC > 1	Padj < 0.05 & LFC > 1	Padj < 0.05 & LFC < -1
DIV7	256	33	3	30	102	24	1	23
DIV14	1469	133	9	124	805	129	8	121
DIV18	160	18	6	12	65	9	2	7

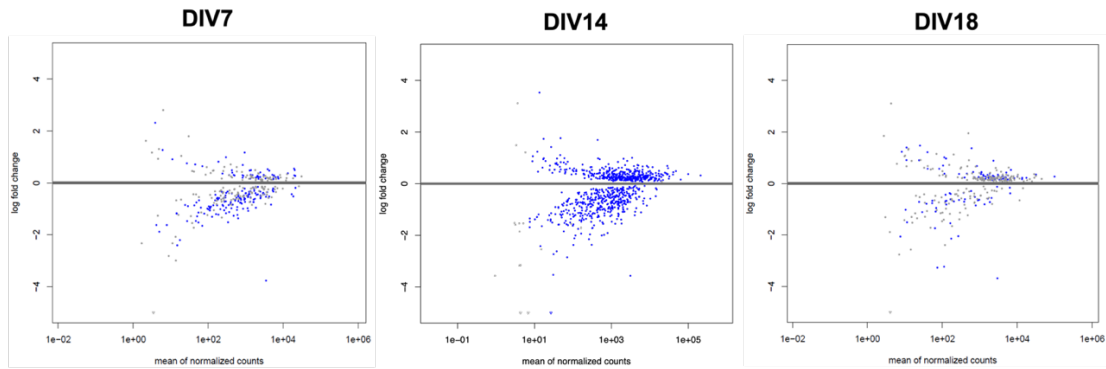


Figure 6.1: Time-specific differential expression analysis allowed to identify DEGs of KO vs WT samples at each timepoint. Above: Summary table of the number of DEGs for each timepoint considered. DEGs were divided according to their false discovery rate adjusted p-value (in green $p\text{-adj} < 0.1$, in blue $p\text{-adj} < 0.05$) and Log2 Fold Change (LFC) > 1 or < -1 . Below: MA plots of the LFC of all genes for the three different timepoints. Blue dots indicate DEGs with a $p\text{-adj} < 0.1$ by *apeglm* shrinkage.

Interestingly, the greatest number of DEGs was present at DIV14, considering either the significance alone (false discovery rate adjusted p-value, $p\text{-adj}$) or in combination with the amplitude of the differential expression (Log2FoldChange, LFC) (Figure 6.1). This result could be related to the fact that at DIV14 neurons have become more mature and functionally active compared to DIV7, exacerbating the delayed transcriptional maturation defects and thus permitting to statistically detect transcriptional changes typical of RTT neurons. Unexpectedly, the lowest number of DEGs was observed at DIV18; we hypothesize that this could be due to the increasing percentage of astrocytes within the culture with respect to neurons, reaching almost 80% at the late timepoint (Scaramuzza et al., 2021). Indeed, it is well known that MeCP2 plays a fundamental role in neurons, where its great percentage of expression (16 million molecules per neuronal nuclei) impacts the transcription of a great number of genes (Maezawa et al., 2009). On the contrary, in possible accordance with its reduced levels of expression in astrocytes (10-30 times less compared to neurons) and the consequent modest impact on glial

transcription, MeCP2 transcriptional effects in astrocytes still remains poorly understood. Of note, the differences between the two biological conditions (KO vs WT) were also quite low in amplitude, with a prevalence of significant downregulated genes with respect to the ones with an LFC > 1 (Figure 6.1). These findings are in perfect accordance with previous studies that profiled gene expression in *Mecp2*-null neurons and tissues and the role of *Mecp2* as a fine transcriptional regulator of a great number of genes (Bedogni et al., 2014; Gandaglia et al., 2019; Li et al., 2013; Riedmann & Fondufe-Mittendorf, 2016). Further, these results underline the difficulties in conducting transcriptional analyses on RTT heterogeneous samples (Bedogni et al., 2016).

We then used Principal Component Analysis (PCA) plots of individual sample variance in the DESeq2 model, to identify the timepoint which better represented the segregation between WT and KO samples. As depicted in Figure 6.2 (A), the best PCA segregation was obtained at DIV14, where WT and KO samples were mainly divided along the first principal component (PC1), responsible for the greatest variance among samples. The effect became even more evident when performing the PCA only on significant DEGs ($p\text{-adj} < 0.05$) (Figure 6.2, B).

In addition, given the high heterogeneity of NPC-derived cultures, PCA was also used to evaluate the possible presence of batch effects related to cell preparation, in order to avoid any possible confounding source impacting the analysis. Fortunately, no batch effect was detected at any timepoint (data not shown).

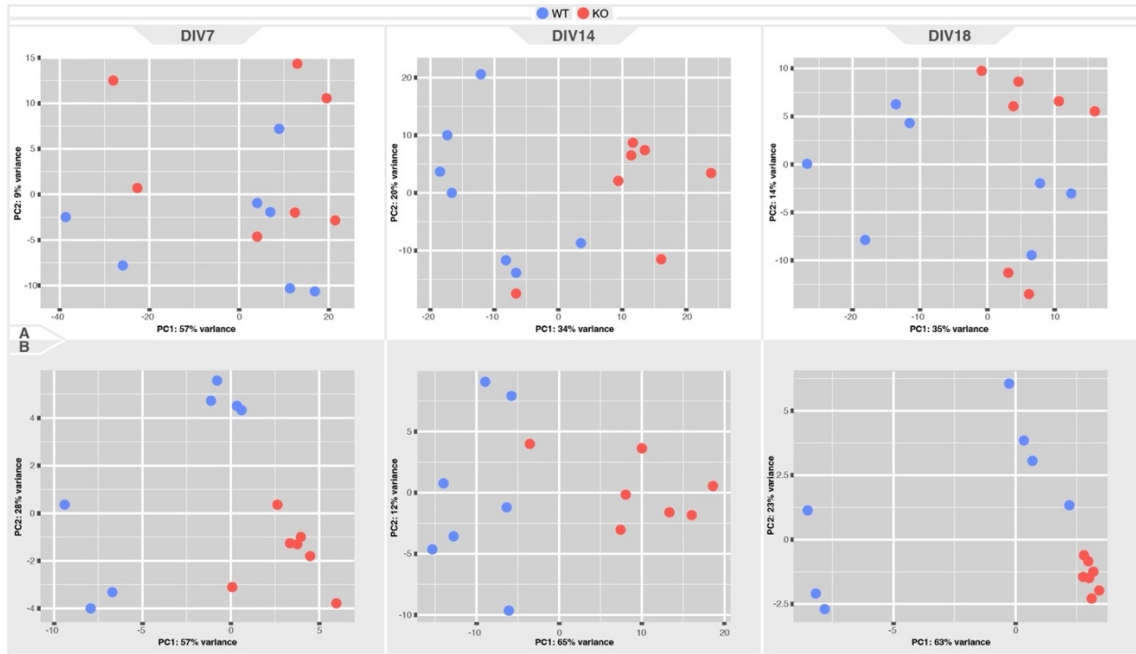
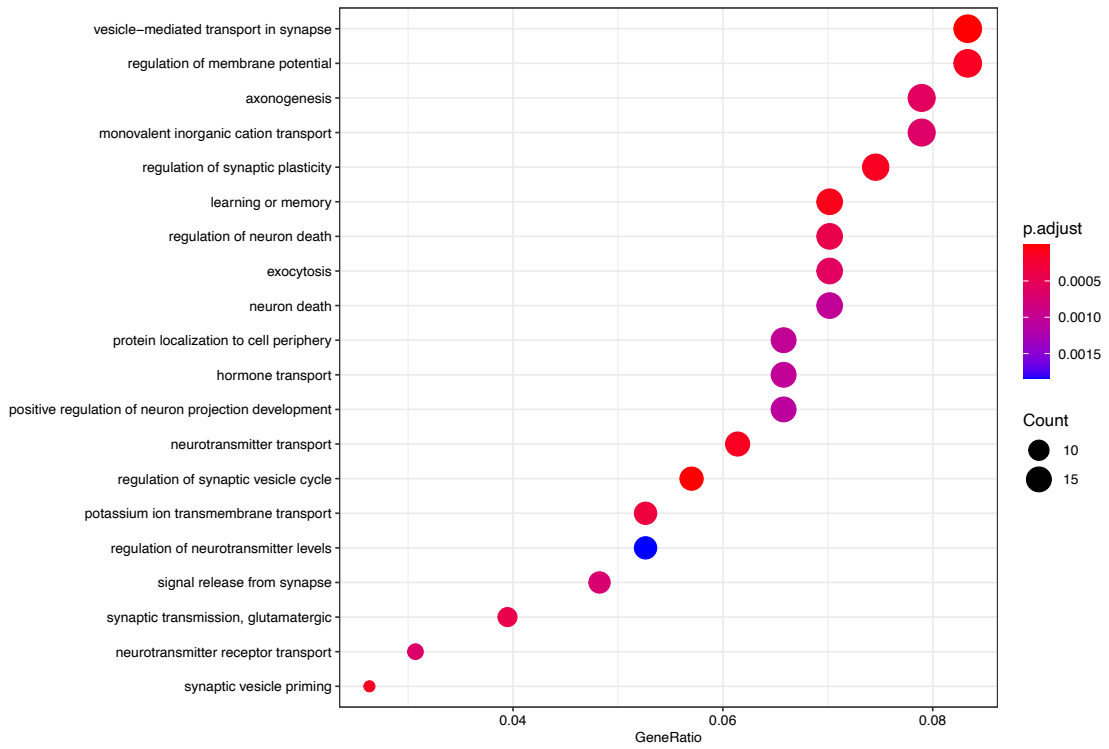


Figure 6.2: PCA plots of individual sample variances according to the examined timepoints (DIV7, 14, 18). Individual sample variances between WT and KO samples are displayed as PCA plots. (A) represents PCA plots of all the sequenced transcripts, while (B) depicts WT and KO segregation only considering significant DEGs ($p\text{-adj} < 0.05$). The percentage of total variation represented by each component is reported on the axes. Each dot represents a sample. Sample size of each biological group: $n=7$. Considering both the overall transcripts (A) and the significant DEGs (B), DIV14 displayed the best PCA segregation between WT and KO samples.

To reveal whether the identified DEGs might be connected with typical phenotypes of *Mecp2* deficient neurons, Gene Ontology (GO) analysis on DEGs with $p\text{-adj} < 0.1$ was performed to determine the biological processes mostly affected and their relevance for RTT. Of note, no enrichment was reported at DIV18, further highlighting possible technical problems associated with cell composition within the cultures. The top 20 biological processes enriched at DIV7 and DIV14 are depicted in Figure 6.3, while the whole list of GO enriched categories is reported in Appendix I and II. In detail, a total of 73 significant biological processes was identified in the GO analysis performed at DIV7 (Appendix I). According to the well-known role of MeCP2 in neuronal development and maturation, most of the enriched categories at DIV7 are related to the acquisition of proper neuronal morphology, and the regulation of transport and release of neurotransmitter across the membrane. Enrichment analysis also highlighted the expected impact of *Mecp2* deficiency on synaptic plasticity, signal release and

transmission across synapses. The number of significant categories doubled to 149 biological processes at DIV14 (Appendix II), in which most of the significant DEGs impinge on pathways linked to synapse transport and organization, regulation of neurotransmitters and membrane potential, cell junctions and channel activity. All these processes have already been found as mainly involved in RTT, therefore well validating our study (Bedogni et al., 2014; Ehrhart et al., 2019; Nectoux et al., 2010; Pacheco et al., 2017; Shovlin & Tropea, 2018).

DIV7



DIV14

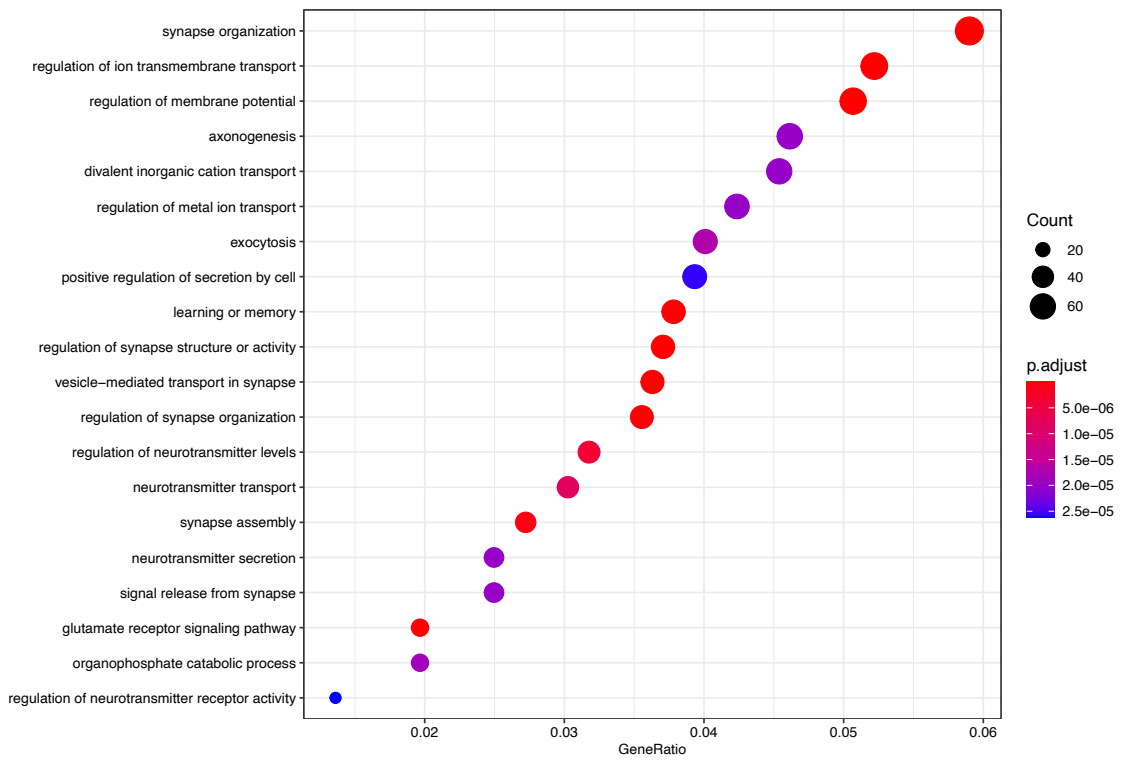


Figure 6.3: Enrichment analysis of GO biological processes confirmed the impact of Mecp2 deficiency on neuronal morphology and synaptic maturation. Figures represent Gene Ontology (GO) analyses of DIV7 and DIV14, performed with clusterProfiler. The plots show the top 20 enriched biological processes obtained from DEGs with a p-adj cut-off < 0.1. The function simplify was used to remove redundancy of enriched GO terms. Color intensity indicates the value of the p-adj related to that biological process (red < p-adj; blue: > p-adj), while the dimension of the dots represents the number of genes counted for each biological process (the greater the size, the greater the count).

Overall, among the time-specific analysis, DIV14 appeared the most suitable timepoint to perform the screening, since it displays the best PCA segregation between WT and *Mecp2*-null samples and the greatest number of DEGs and biological processes mainly related to pathways relevant for the disorder.

6.1.1.2. Differential expression analysis overtime highlighted impaired transcriptional maturation of RTT developing neurons

As mentioned in the previous section, the first objective of this study was to identify solid and reproducible biomarkers useful to represent a gene signature typical of RTT neurons. To this purpose, we also performed a differential expression analysis overtime, to highlight consistently deregulated genes along the process of neuronal maturation between WT and KO samples. The analysis identified a great number of DEGs even with a stringent p-adj cut-off of 0.01, as depicted in Figure 6.4 (A). Moreover, Principal Component Analysis (PCA) performed on DEGs with a p-adj < 0.05 highlighted the segregation between WT and KO samples along the PC1 (Figure 6.4, B). However, as for the previous analysis, the differences between the two biological conditions were low in amplitude, as illustrated in the heatmaps below (Figure 6.4, panel C), making it necessary to resize the scale to ± 2 .

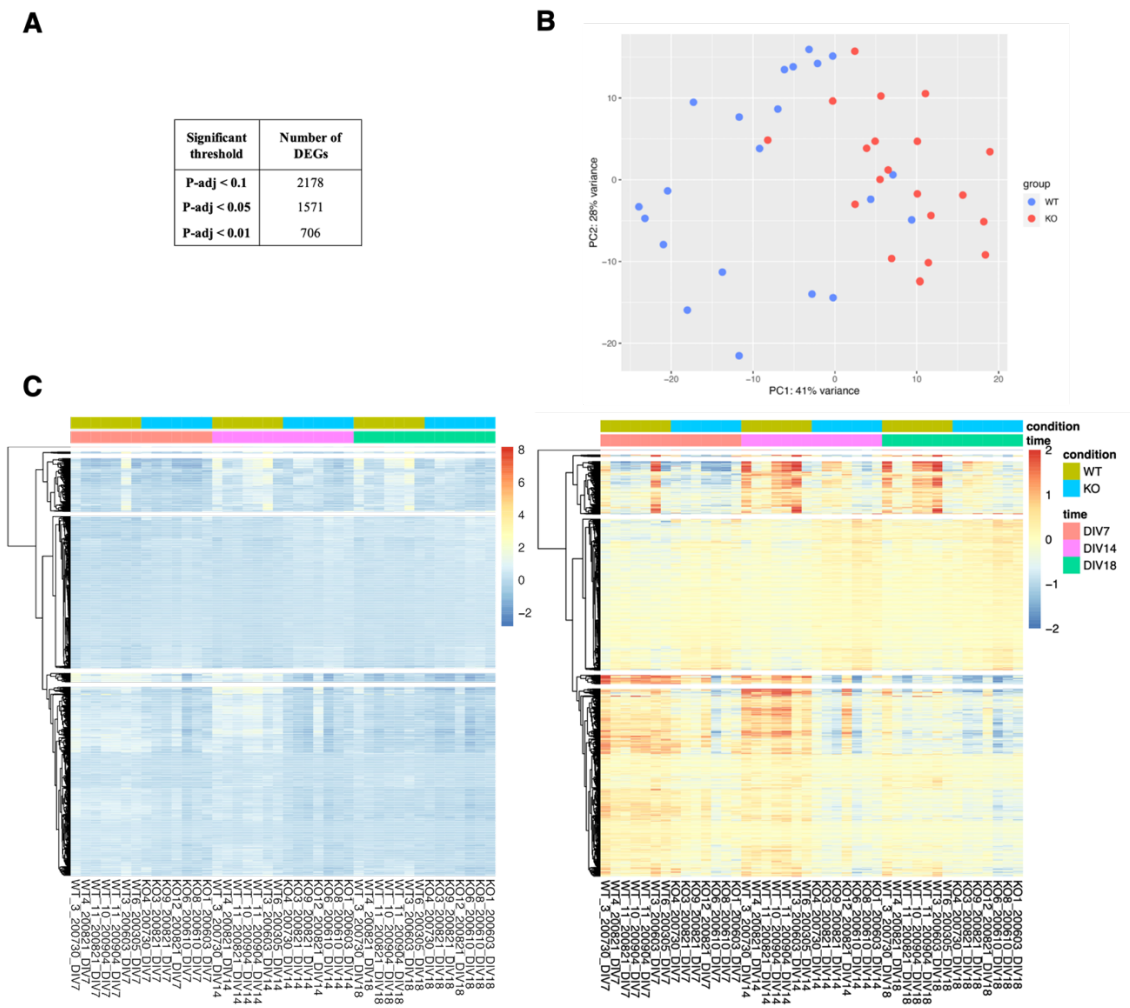


Figure 6.4: Differential expression analysis overtime identified a great number of DEGs with a low differential expression. (A) Summary table of the number of DEGs for each threshold considered: DEGs were divided according to their p -adj cut-off values into three groups (p -adj < 0.1, p -adj < 0.05 and p -adj < 0.01). (B) PCA plot performed on DEGs with a p -adj < 0.05 confirmed a segregation between WT and KO samples. (C) The heatmaps show the 1571 deregulated genes selected according to their statistical significance (p -adj < 0.05), separating samples based on the genotype (first bar “condition”, WT in green and KO in blue) and the timepoint (second bar “time”, DIV7 in orange, DIV14 in pink and DIV18 in green). Scale bar had to be set to ± 2 (heatmap on the right) to appreciate the differential expression between WT and KO longitudinal samples.

GO analysis was performed to categorize the enriched biological processes related to DEGs with a p -adj < 0.05. A total of 174 biological processes were identified (listed in Appendix III). The 20 most enriched categories are illustrated in Figure 6.5 and comprehend pathways involved in neuronal differentiation and morphology, synaptic assembly, regulation of membrane potential and transport, and synaptic transmission and

plasticity. These enrichments further corroborated previous results highlighting the impact of *Mecp2* deficiency on synaptic maturation and transmission, and thus validating also our overtime analysis (Bedogni et al., 2016; Ehrhart et al., 2019; Nectoux et al., 2010; Pacheco et al., 2017; Shovlin & Tropea, 2018).

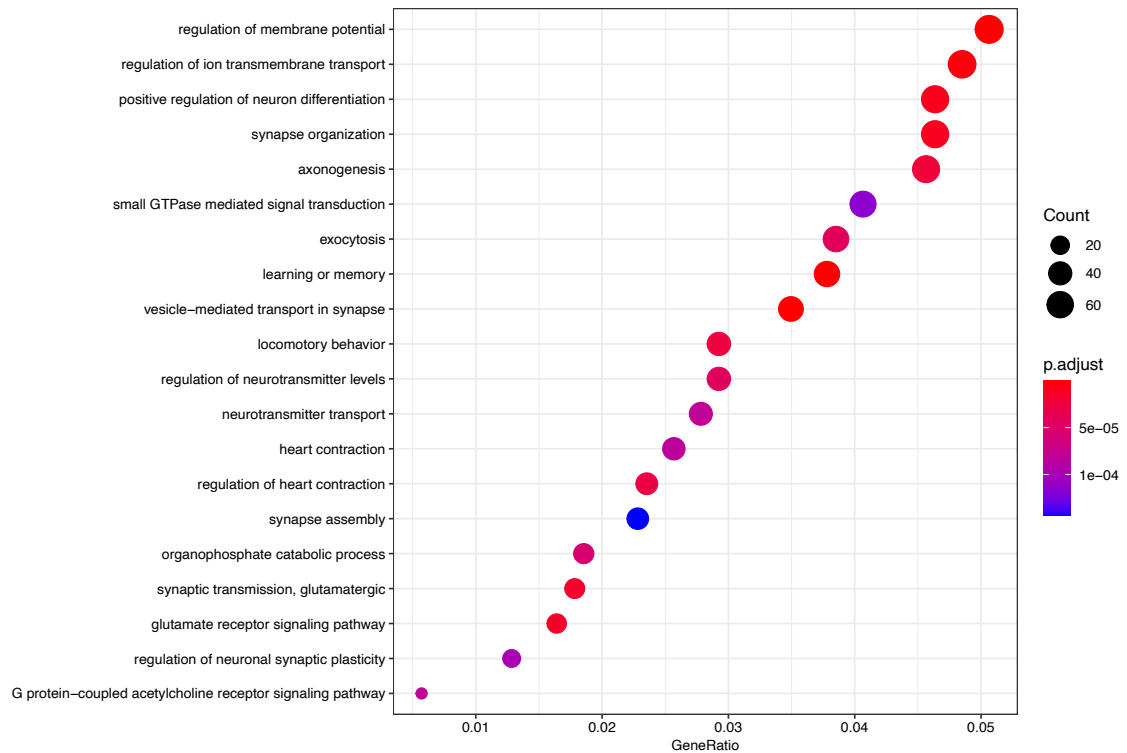


Figure 6.5: GO enrichment analysis on DEGs overtime illustrated an impact on transcriptional maturation of RTT developing NPC-derived cultures. The graph represents GO enrichment analysis of DEGs overtime, performed with clusterProfiler. The plots show the top 20 enriched biological processes obtained from DEGs with a *p*-adj cut-off < 0.05. The function simplify was used to remove redundancy of enriched GO terms. Color intensity indicates the value of the *p*-adj related to that biological process (red < *p*-adj; blue: > *p*-adj), while the dimension of the dots represents the number of genes counted for each biological process (the greater the size, the greater the count).

6.1.2. Prioritization of DEGs permitted to select 200 genes for further validation

Once obtained the DEGs from the time-specific and overtime bioinformatic analyses, these genes had to be progressively prioritized in order to screen their reproducibility on 96x96 qPCR microfluidic cards and, eventually, their value to measure drug efficacy.

We applied several cut-off factors in order to proceed with the ranking. The prioritization criteria are described in the following section and further summarized in Figure 6.6 (panel A):

1. In the time-specific analysis, we applied a p-adj cut-off < 0.1 and firstly focused on those DEGs in common in at least two timepoints. Of note, 16 genes were in common among the three timepoints, 124 were significantly deregulated both at DIV7 and 14, while 62 were in common between DIV14 and 18 (Figure 6.6, panel C, full list provided in Appendix IV). These genes were further prioritized according to their fold change (FC) of expression, preferring those with an $LFC > |0.5|$ at DIV14, to increase the possibility of their detection by qRT-PCR.
2. In the overtime analysis, considering the great number of genes and the low amplitude of FC, DEGs were ranked according to the p-adj < 0.05 , selecting only those genes with an $LFC > |0.3|$. In addition to these genes, DEGs also included in the clusters reported in Figure 6.6 panel D were examined. Gene clusters include DEGs that share the same trend of expression overtime; cluster 1, 2 and 3 were selected according to the biological relevance of the trend. For example, group 1 include genes that are longitudinally overexpressed in the KO samples; on the contrary, the second cluster contains defective DEGs in mutant cultures, while group 3 consists of genes whose expression does not increase along neuronal maturation compared to the WT. Full list is provided in Appendix V. Among these genes, only those that answered the significance and FC amplitude requirements were included in the list. Significant DEGs present in the overtime GO analysis belonging to biological processes relevant for RTT were also considered.
3. Priority was given to common DEGs derived from points 1 and 2.
4. DEGs were further prioritized including genes with a strong relevance in biological processes defective in patients and mouse models of RTT or other

neurodevelopmental disorders. In particular, we mainly focused on neuronal genes or genes that can be expressed both by neurons and glia and are linked to neurogenesis and neural differentiation, axon and dendrite morphogenesis, neurotransmission, channel activity, synaptic organization, learning and memory.

5. Furthermore, priority was also given to those genes included in the SFARI and SPARK Gene databases (www.gene.sfari.org), containing genes implicated in autism susceptibility in murine models and in human samples, in the geneset previously produced in our laboratory from E15.5 *Mecp2*-null mice cortices (Bedogni et al., 2016), in the list produced by Pacheco and colleagues (Pacheco et al., 2017), and in the one provided by Sanfeliu et al. (Sanfeliu et al., 2019), who identified a subset of genes affected consistently across 38 transcriptomic datasets of RTT.

In parallel, given the selection of DIV14 as the elective timepoint to perform the screening, other DEGs significantly deregulated at this timepoint with a $p\text{-adj} < 0.1$ and an $LFC > |0.5|$ were further prioritized and selected according to their involvement in biological processes important for RTT and their presence in relevant GO categories and in the datasets reported in point 5 (Figure 6.6, panel B).

A total of 200 prioritized DEGs was obtained and progressively validated in several qPCR microfluidic experiments, as thoroughly described in the following sections. The list of all the genes tested is provided in Table 6.1.

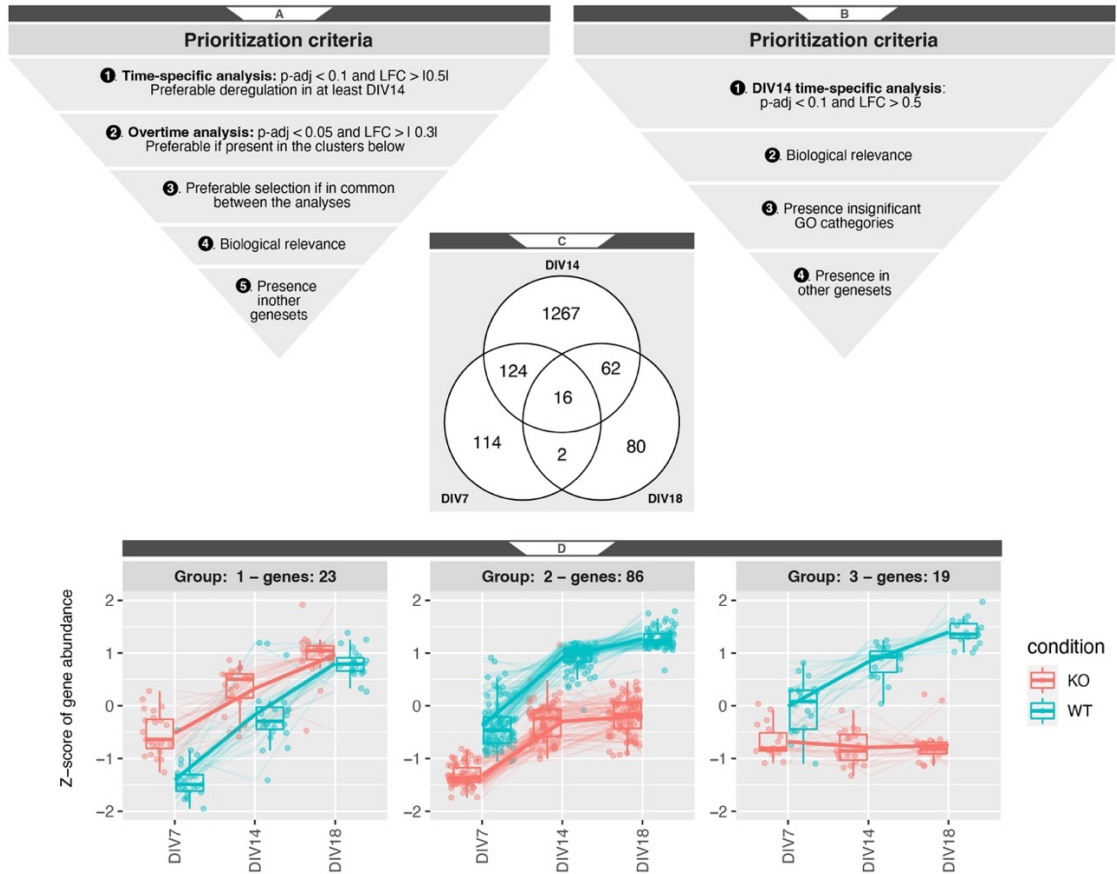


Figure 6.6: Prioritization criteria of DEGs from the bioinformatic analyses. (A) Schematic representation of the prioritization criteria applied for the selection of DEGs. (B) Sets of common DEGs between the three time-specific analysis, DIV7, 14 and 18. (C) Comparison between WT and KO DEGs belonging to three different clusters of expression overtime: group 1 includes DEGs overexpressed in the KO samples compared to the WT; group 2 consists of genes downregulated in the KO overtime; group 3 represents DEGs which are not progressively expressed along culture maturation in the KO samples.

List of selected DEGs	DIV14		Biological function	Datasets
	LFC	p-adj		
<i>Rbfox3</i>	-1,9829	1,08E-04	Nervous system development	
<i>Cpne4</i>	-1,9145	0,0118	Nervous system development	
<i>Rasgrp1</i>	-1,5483	0,0026	nervous system development	
<i>Sstr3</i>	-1,5211	0,0056	nervous system development	
<i>Wnt7b</i>	-1,2996	0,0015	nervous system development	Pacheco et al., 2017, Sanfelieu et al., 2019
<i>L1cam</i>	-1,2618	0,0314	Nervous system development	Sanfelieu et al., 2019
<i>Pmepa1</i>	-1,2300	0,0040	Nervous system development	
<i>Wif1</i>	-1,1919	0,0179	Nervous system development	
<i>Gng4</i>	-1,1553	0,0374	Nervous system development	
<i>Dok4</i>	-1,0083	0,0010	Nervous system development	
<i>Pcdha11</i>	-0,9469	0,0089	nervous system development	
<i>Kalrn</i>	-0,9277	0,0135	nervous system development	
<i>Scrt1</i>	-0,9195	0,0074	nervous system development	
<i>Hecw2</i>	-0,8042	0,0252	nervous system development	
<i>Efna3</i>	-0,8027	0,0030	nervous system development	
<i>Nexmif</i>	-0,7794	0,0088	nervous system development	SFARI
<i>Camk2n1</i>	-0,7388	0,0253	Nervous system development	
<i>Plcb1</i>	-0,6869	0,0347	nervous system development	Sanfelieu et al., 2019
<i>Plxna2</i>	-0,6061	0,0299	Nervous system development	Sanfelieu et al., 2019
<i>Slitrk1</i>	-0,5841	0,0253	nervous system development	
<i>Gap43</i>	-0,4663	0,0352	Nervous system development	Pacheco et al., 2017, Sanfelieu et al., 2019
<i>Fgf14</i>	-1,61E-05	0,0108	Nervous system development	
<i>St8sia2</i>	-1,38E-05	0,0685	Nervous system development	SFARI
<i>Ccn3</i>	-9,84E-06	2,59E-05	Nervous system development	
<i>Mdga1</i>	-9,40E-06	0,0758	Nervous system development	
<i>Nkd2</i>	-8,61E-06	0,1174	Nervous system development	
<i>Rbfox1</i>	-6,37E-06	0,0063	Nervous system development	SFARI
<i>Bhlhe22</i>	-6,17E-06	0,0013	Nervous system development	
<i>Junb</i>	-5,59E-06	0,0997	Nervous system development	Pacheco et al., 2017, Sanfelieu et al., 2019
<i>Ntf3</i>	-3,30E-06	0,0699	Nervous system development	
<i>Bdnf</i>	-3,89E-08	0,9657	Nervous system development	Chahrour et al., 2008

<i>Fgf2</i>	0,4502	0,0666	nervous system development	
<i>Daam2</i>	0,5980	0,0033	Nervous system development	
<i>Mitf</i>	0,6176	0,0118	Nervous system development	
<i>Prtg</i>	0,8425	0,0021	nervous system development	
<i>Klhl1</i>	-2,4224	0,0010	microtubule cytoskeleton organization	
<i>Ccsap</i>	-1,2402	0,0074	microtubule cytoskeleton organization	
<i>Kank3</i>	-1,1600	0,0040	microtubule cytoskeleton organization	
<i>Tubb3</i>	-1,0881	0,0116	microtubule cytoskeleton organization	
<i>Epha3</i>	-1,0751	0,0061	microtubule cytoskeleton organization	
<i>Wipf3</i>	-1,0457	0,0346	microtubule cytoskeleton organization	Pacheco et al., 2017
<i>Ankfn1</i>	-1,0088	0,0553	microtubule cytoskeleton organization	
<i>Myo5b</i>	-0,9785	0,0318	microtubule cytoskeleton organization	
<i>Kifc2</i>	-0,5223	0,0627	microtubule cytoskeleton organization	
<i>Pdxdp</i>	-0,4976	0,0175	microtubule cytoskeleton organization	
<i>Hap1</i>	-0,4847	0,0206	microtubule cytoskeleton organization	
<i>Arhgap4</i>	-1,34E-05	0,0444	microtubule cytoskeleton organization	
<i>Tbcel</i>	0,4078	0,0035	microtubule cytoskeleton organization	
<i>Fgd6</i>	0,4161	0,0188	microtubule cytoskeleton organization	
<i>Stard13</i>	0,6076	0,0021	microtubule cytoskeleton organization	
<i>Zmym6</i>	0,6797	0,0073	microtubule cytoskeleton organization	
<i>Dock6</i>	1,0022	0,0040	microtubule cytoskeleton organization	
<i>Vstm2l</i>	-1,5721	0,0083	neuron projection morphogenesis	
<i>Cpne6</i>	-1,5579	0,0252	neuron projection morphogenesis	
<i>Rap1gap2</i>	-1,5520	7,26E-06	neuron projection morphogenesis	Sanfelieu et al., 2019
<i>Lamb1</i>	-1,2519	0,0074	neuron projection morphogenesis	
<i>Nyap2</i>	-1,2416	0,0164	neuron projection morphogenesis	
<i>Camk2b</i>	-1,2252	0,0095	neuron projection morphogenesis	Bedogni et al., 2016
<i>Psd</i>	-1,1978	0,0075	neuron projection morphogenesis	
<i>Ptk2b</i>	-1,1400	0,0118	neuron projection morphogenesis	Sanfelieu et al., 2019
<i>Shank1</i>	-0,9150	0,0466	neuron projection morphogenesis	Pacheco et al., 2017, SFARI
<i>Atp8a2</i>	-0,7295	0,0489	neuron projection morphogenesis	
<i>Haus7</i>	-0,6734	1,64E-07	neuron projection morphogenesis	
<i>Ntng1</i>	-0,6295	0,0347	neuron projection morphogenesis	Sanfelieu et al., 2019, SFARI

<i>Vash2</i>	-0,5481	0,0010	neuron projection morphogenesis	
<i>Auts2</i>	-0,5285	0,0417	neuron projection morphogenesis	Pacheco et al., 2017, SFARI, SPARK
<i>Vip</i>	-6,2486	0,0000	Ion transmembrane transport	
<i>Kcng2</i>	-3,5308	0,0000	Ion transmembrane transport	
<i>Slc30a3</i>	-2,7297	0,0011	Ion transmembrane transport	
<i>Slco1c1</i>	-1,9653	0,0013	Ion transmembrane transport	Pacheco et al., 2017, Sanfelieu et al., 2019
<i>Stc1</i>	-1,5755	0,0006	Ion transmembrane transport	Sanfelieu et al., 2019
<i>Trpm2</i>	-1,4401	0,0009	Ion transmembrane transport	
<i>Stac2</i>	-1,1853	0,0152	Ion transmembrane transport	
<i>Ryr2</i>	-1,1469	0,0243	Ion transmembrane transport	Sanfelieu et al., 2019
<i>Kcnp1</i>	-1,1094	0,0027	Ion transmembrane transport	
<i>Dpp10</i>	-1,0848	0,0016	Ion transmembrane transport	
<i>Kcnq2</i>	-1,0172	0,0053	Ion transmembrane transport	SFARI
<i>Scn3b</i>	-0,8256	0,0051	Ion transmembrane transport	Pacheco et al., 2017, Sanfelieu et al., 2019
<i>Cacna1e</i>	-0,8239	0,0414	Ion transmembrane transport	Bedogni et al., 2016
<i>Orai2</i>	-0,7404	0,0069	Ion transmembrane transport	
<i>Unc80</i>	-0,7007	0,0317	Ion transmembrane transport	
<i>Dpp6</i>	-0,6627	0,0086	Ion transmembrane transport	SFARI
<i>Cacna1c</i>	-0,6086	0,0396	Ion transmembrane transport	Bedogni et al., 2016, SFARI, SPARK
<i>Slc8a3</i>	-0,5799	0,0087	Ion transmembrane transport	Bedogni et al., 2016
<i>Kcnh2</i>	-0,5605	0,0272	Ion transmembrane transport	Bedogni et al., 2016
<i>Cacna1g</i>	-9,05E-06	0,0253	Ion transmembrane transport	Sanfelieu et al., 2019, SFARI
<i>Gla2</i>	-5,62E-06	0,0164	Ion transmembrane transport	SFARI
<i>Grin1</i>	-4,33E-06	0,1102	Ion transmembrane transport	Bedogni et al., 2016, SFARI
<i>Cacna1i</i>	-3,92E-06	0,0989	Ion transmembrane transport	Bedogni et al., 2016
<i>Atp1a1</i>	0,3701	0,0007	Ion transmembrane transport	
<i>Trpc3</i>	0,9640	0,0084	Ion transmembrane transport	
<i>Lgi2</i>	-1,4798	0,0142	synapse assembly and organization	
<i>Camkv</i>	-1,4733	0,0345	synapse assembly and organization	Bedogni et al., 2016
<i>Syndig1</i>	-1,3982	0,0118	synapse assembly and organization	
<i>Pcdhgc4</i>	-1,0965	0,0254	synapse assembly and organization	
<i>Pnck</i>	-1,0346	0,0095	synapse assembly and organization	

<i>Dlgap3</i>	-0,9331	0,0138	synapse assembly and organization	Pacheco et al., 2017
<i>Cbln1</i>	-0,7569	0,0138	synapse assembly and organization	
<i>Add2</i>	-0,6941	0,0044	synapse assembly and organization	
<i>Lhfpl4</i>	-0,5159	0,0074	synapse assembly and organization	
<i>Sv2c</i>	-2,3697	2,59E-05	synaptic transmission and plasticity	
<i>Gsg1l</i>	-1,8486	8,26E-09	synaptic transmission and plasticity	
<i>Grm4</i>	-1,7136	2,59E-05	synaptic transmission and plasticity	Bedogni et al., 2016
<i>Oxtr</i>	-1,5816	0,0260	synaptic transmission and plasticity	SFARI
<i>Chrm2</i>	-1,4438	0,0253	synaptic transmission and plasticity	
<i>Gabrg3</i>	-1,4138	0,0141	synaptic transmission and plasticity	
<i>Rgs14</i>	-1,4067	0,0346	synaptic transmission and plasticity	
<i>Neur11b</i>	-1,3388	0,0080	synaptic transmission and plasticity	Pacheco et al., 2017
<i>Ly6h</i>	-1,2820	0,0006	synaptic transmission and plasticity	
<i>Jph4</i>	-1,2629	0,0007	synaptic transmission and plasticity	Pacheco et al., 2017
<i>Chrm3</i>	-1,2569	0,0354	synaptic transmission and plasticity	
<i>Lgr5</i>	-1,2250	0,0108	synaptic transmission and plasticity	
<i>Gad1</i>	-1,0862	0,0198	synaptic transmission and plasticity	Bedogni et al., 2016, Sanfelieu et al., 2019
<i>Gabbr2</i>	-1,0504	0,0273	synaptic transmission and plasticity	Bedogni et al., 2016
<i>Plppr4</i>	-0,9801	0,0158	synaptic transmission and plasticity	
<i>Gabrb3</i>	-0,9749	0,0048	synaptic transmission and plasticity	SFARI
<i>Hpcal4</i>	-0,9055	0,0066	synaptic transmission and plasticity	Pacheco et al., 2017, Sanfelieu et al., 2019
<i>Cnih2</i>	-0,8609	0,0194	synaptic transmission and plasticity	Pacheco et al., 2017
<i>Cabyr</i>	-0,8085	4,06E-05	synaptic transmission and plasticity	
<i>Nptxr</i>	-0,7895	0,0254	synaptic transmission and plasticity	
<i>Gabra3</i>	-0,7577	0,0036	synaptic transmission and plasticity	Bedogni et al., 2016, Sanfelieu et al., 2019
<i>Syn1</i>	-0,7252	0,0468	synaptic transmission and plasticity	SFARI
<i>Gng2</i>	-0,6938	0,0283	synaptic transmission and plasticity	
<i>Slc12a5</i>	-0,6358	0,0726	synaptic transmission and plasticity	
<i>Shisa7</i>	-0,5589	0,0076	synaptic transmission and plasticity	
<i>Insyn1</i>	-0,5256	0,0032	synaptic transmission and plasticity	

<i>Ncdn</i>	-0,5063	0,0290	synaptic transmission and plasticity	
<i>Grm5</i>	-0,4765	0,0551	synaptic transmission and plasticity	Bedogni et al., 2016, SFARI
<i>Neur11a</i>	-9,29E-06	0,0035	synaptic transmission and plasticity	
<i>Cckbr</i>	-9,21E-06	0,0006	synaptic transmission and plasticity	
<i>Fos</i>	-5,09E-06	0,0232	synaptic transmission and plasticity	Pacheco et al., 2017, Sanfeliu et al., 2019
<i>Npas4</i>	-2,55E-06	0,4333	synaptic transmission and plasticity	
<i>Nptx2</i>	7,26E-07	0,0948	synaptic transmission and plasticity	
<i>Sorcs1</i>	0,5540	0,0506	synaptic transmission and plasticity	
<i>Caly</i>	-1,6133	0,0057	synaptic vesicle-mediated transport, exo- and endocytosis	
<i>Mal2</i>	-1,4722	0,0072	synaptic vesicle-mediated transport, exo- and endocytosis	
<i>Snap25</i>	-1,3911	0,0016	synaptic vesicle-mediated transport, exo- and endocytosis	Sanfeliu et al., 2019
<i>Sncb</i>	-1,2728	0,0283	synaptic vesicle-mediated transport, exo- and endocytosis	Bedogni et al., 2016
<i>Lin7a</i>	-1,2507	0,0021	synaptic vesicle-mediated transport, exo- and endocytosis	
<i>Synpr</i>	-1,0893	0,0112	synaptic vesicle-mediated transport, exo- and endocytosis	
<i>Rab3c</i>	-1,0154	0,0155	synaptic vesicle-mediated transport, exo- and endocytosis	
<i>Dnajc6</i>	-0,9707	0,0005	synaptic vesicle-mediated transport, exo- and endocytosis	
<i>Cplx1</i>	-0,9249	0,0304	synaptic vesicle-mediated transport, exo- and endocytosis	
<i>Napb</i>	-0,8637	0,0098	synaptic vesicle-mediated transport, exo- and endocytosis	
<i>Rin1</i>	-0,8358	0,0108	synaptic vesicle-mediated transport, exo- and endocytosis	
<i>Nsg1</i>	-0,8019	0,0019	synaptic vesicle-mediated transport, exo- and endocytosis	
<i>Slc29a4</i>	-0,5516	0,0069	synaptic vesicle-mediated transport, exo- and endocytosis	
<i>Stxbp1</i>	-1,21E-05	0,0646	synaptic vesicle-mediated transport, exo- and endocytosis	SFARI, SPARK
<i>Syt1</i>	-6,56E-06	0,0880	synaptic vesicle-mediated transport, exo- and endocytosis	
<i>Itsn1</i>	0,3905	0,0282	synaptic vesicle-mediated transport, exo- and endocytosis	
<i>Ston1</i>	0,4980	0,0028	synaptic vesicle-mediated transport, exo- and endocytosis	
<i>Oprl1</i>	-0,6485	0,0028	signal transduction	
<i>Rgs10</i>	-0,4830	0,0428	signal transduction	

<i>Arhgdig</i>	-1,35E-05	0,0421	signal transduction	Pacheco et al., 2017, Sanfelieu et al., 2019
<i>Gpr21</i>	-1,6061	0,0011	Metabolic processes	Bedogni et al., 2016
<i>Necab3</i>	-1,1964	0,0378	Metabolic processes	Ben-Shachar et al., 2009, Sanfelieu et al., 2019
<i>Pgm21l</i>	-0,9878	0,0293	Metabolic processes	Pacheco et al., 2017, Sanfelieu et al., 2019
<i>Plppr3</i>	-0,9151	0,0119	Metabolic processes	
<i>Abca8a</i>	-0,6856	0,0368	Metabolic processes	
<i>Arhgap33</i>	-0,6600	0,0163	Metabolic processes	Pacheco et al., 2017, Sanfelieu et al., 2019
<i>Nsdhl</i>	-0,4322	0,0060	Metabolic processes	Pacheco et al., 2017
<i>Vldlr</i>	-1,63E-05	0,0745	Metabolic processes	
<i>Gipr</i>	-5,96E-06	0,0030	Metabolic processes	
<i>Pitpnc1</i>	0,4637	0,0052	Metabolic processes	
<i>Cyp27a1</i>	1,6923	0,0053	Metabolic processes	
<i>Gdap1</i>	-0,7399	0,0092	Mitochondria	
<i>Pdp2</i>	0,3771	0,0279	Mitochondria	
<i>Fundc2</i>	0,4640	0,0025	Mitochondria	
<i>Spock3</i>	-2,1167	0,0063	Extracellular matrix and cell-cell adhesion	
<i>Ajap1</i>	-1,4097	0,0074	Extracellular matrix and cell-cell adhesion	
<i>Icam5</i>	-1,2784	0,0176	Extracellular matrix and cell-cell adhesion	
<i>Col6a2</i>	-1,2322	0,0317	Extracellular matrix and cell-cell adhesion	
<i>Mmp24</i>	-1,0455	0,0030	Extracellular matrix and cell-cell adhesion	
<i>Cobll1</i>	0,4925	0,0018	Extracellular matrix and cell-cell adhesion	
<i>Nxph3</i>	0,5306	0,0520	Extracellular matrix and cell-cell adhesion	Pacheco et al., 2017
<i>Rnase4</i>	-1,1856	0,0220	Transcription regulation	
<i>Ralyl</i>	-1,1274	0,0033	Transcription regulation	
<i>Klf8</i>	-0,7690	0,0018	Transcription regulation	
<i>Basp1</i>	-0,7181	0,0057	Transcription regulation	
<i>Mef2c</i>	-0,6095	0,0473	Transcription regulation	Sanfelieu et al., 2019, SFARI
<i>Asxl3</i>	-0,5166	0,0399	Transcription regulation	SPARK
<i>Pcbp3</i>	-0,5078	0,0333	Transcription regulation	Sanfelieu et al., 2019
<i>Bcl6</i>	0,3712	0,0177	Transcription regulation	
<i>Epas1</i>	0,6399	0,0032	Transcription regulation	
<i>Cntnap3</i>	-2,6208	0,0002	Other	Sanfelieu et al., 2019
<i>Pcdhgb8</i>	-2,0061	0,0175	Other	

<i>Sphkap</i>	-1,5453	0,0203	Other	
<i>Mpped1</i>	-1,4384	0,0177	Other	
<i>Adarb2</i>	-1,2177	0,0036	Other	
<i>Zdhc22</i>	-1,0839	0,0150	Other	
<i>Fbxo41</i>	-0,9851	0,0203	Other	
<i>Ical1</i>	-0,9415	0,0001	Other	
<i>Pnma2</i>	-0,9067	0,0129	Other	
<i>Clqtnf4</i>	-0,8147	0,0220	Other	
<i>Tbc1d9</i>	-0,7737	0,0073	Other	
<i>Eef1a2</i>	-0,0002	0,0929	Other	SFARI
<i>Serpine1</i>	-3,48E-06	0,0623	Other	
<i>Lamp5</i>	-2,98E-06	0,0767	Other	
<i>Sepsecs</i>	0,3601	0,0158	Other	
<i>Arhgef37</i>	0,6174	0,0098	Other	

Table 6.1: List of prioritized and selected DEGs to validate in the 96x96 qPCR cards. DEGs are divided and colored according to their principal biological function. LFC and *p*-adj of each gene at DIV14 is provided. Their presence in one of the reference databases is also reported in the “Datasets” column. For each biological function, genes are ranked according to their LFC (lowest to greatest).

6.1.3. Primary neurons are the most stable and robust cell culture to use in the screening

As mentioned in the previous sections, NPC-derived cultures seemed to bare many advantages for cell and pharmacological manipulations (Gorba & Conti, 2013), since they allow neuronal maturation in a more physiological environment than primary neurons thanks to the presence of astrocytes, they allow to focus on early stages of neuronal maturation which can be synchronously followed among different samples and can be expanded in several batches and cryopreserved, reducing the number of mice required for the analyses. Nonetheless, the production of 42 longitudinal NPC-derived samples and the RNASeq bioinformatic analysis highlighted difficulties in the analysis of data deriving from a mixed population of cells and characterized by low amplitude of differential expressions typical of *Mecp2*-null samples. Given these unexpected evidences and considering also that we mostly prioritized neuronal DEGs or genes mainly expressed

by neurons, we decided to test the reproducibility of a first group of 96 prioritized genes on a 96x96 IFC qRT-PCR Array card (Fluidigm) by comparing their expression in primary and NPC-derived neurons, in order to detect any possible masking effect given by the great percentage of astrocytes. As a matter of fact, even though both these cell cultures are originated at E15.5 corresponding to the peak of corticogenesis, according to the protocol used for their production, we can obtain either primary cortical neurons, which are virtually devoid of astrocytes, or NPCs which are able to differentiate into neurons, astrocytes, and oligodendrocytes in the presence of fetal bovine serum (FBS) (Magri *et al.*, 2013). The list of the first group of 96 selected DEGs and their respective pairs of primers are reported in Appendix VI. Primers were designed and synthesized as described in the Method section (Table 8.4). 8 WT vs 8 KO samples were produced and tested for each culture condition at DIV14, for a total of 32 samples, analyzed in triplicates.

Obtained results are depicted in Figure 6.7. In details, NPC-derived neurons confirmed the reproducibility of only 3 genes (*Fundc2*, *Haus7* and *Nsdhl*, Figure 6.7, panel A: *Fundc2* percentage of KO expression with respect to WT = 144.78% with p-value = 0.0026, *Haus7*: KO = 78.05%, with p-value = 0.035, *Nsdhl*: KO = 62.91%, with p-value 1,003E-06), while 4 other genes exhibited a tendency to deregulation (*Cobll*, *Pitpnc1*, *Ston1*, *Zmym6*, $0.05 < \text{p-value} < 0.1$). The overall trend of expression of these 7 genes was in line with RNASeq data. In addition, even if the small number of confirmed DEGs did not permit to identify if they insist on specific biological functions, we observed that they are involved in extracellular matrix homeostasis (*Cobll*), metabolic processes (*Nsdhl* and *Pitpnc1*) and regulation of endocytosis at the synaptic level (*Ston1*), which are typical astrocytic functions, possibly indicating that their expression largely derive from the glial population within the culture.

On the contrary, primary neurons appeared more stable, confirming the reproducibility of 19 significant DEGs, with other 6 almost reaching a significant p-value of 0.05 (Figure 6.7 panel B). Globally, these genes also exhibited a greater amplitude of deregulation compared to NPC-derived cultures and their deregulation was in line with transcriptomic results. Concerning their biological functions, reproducible DEGs in primary neurons are mainly involved in neuronal development and morphogenesis, neuronal transmission and synapsis function and maturation, as depicted in Figure 6.7 panel B. Of note, *Fundc2*, a

mitochondrial PIP3-binding protein, *Haus7*, involved in microtubule polarization and synaptic formation, and *Nsdhl*, enzyme implicated in the synthesis of cholesterol, appeared deregulated also in primary neurons, with a 35% downregulation of *Haus7* (KO percentage of expression with respect to WT = 65.69%, p-value=3.81E-07), almost 25% reduction of *Nsdhl* (KO = 78.41%, p-value=0.00077), and a 40% upregulation of *Fundc2* in KO primary neurons (KO= 140,06%, p-value=0.00024), thus exhibiting also a great amplitude of deregulation with respect to the usual ones detected in RTT qRT-PCR experiments. Functions of these genes will be further dissected in section 6.3. The other 4 DEGs detected in the NPC-derived cultures (*Cobll*, *Pitpnc1*, *Ston1*, *Zmym6*) are no longer differentially expressed in primary neurons, reinforcing our hypothesis that astrocytes might have mainly contributed to their deregulation.

The higher number of validated DEGs and their relevance in neuronal processes relevant for RTT suggested the use of primary neurons as the elective cellular system for the screening system, since they appeared more robust and appropriate for typical RTT phenotypes compared to NPC-derived cultures.

Nonetheless, the number of significant DEGs in primary neurons still remained lower than expected (25% of the total genes tested); thus, given the amplitude of deregulation and the standard deviation obtained for each gene, using G*Power we estimated the suitable sample size to reach significant results. Therefore, in the subsequent 96x96 qRT-PCR experiments we increased the sample size to 10 samples per biological group, as described in the following paragraph.

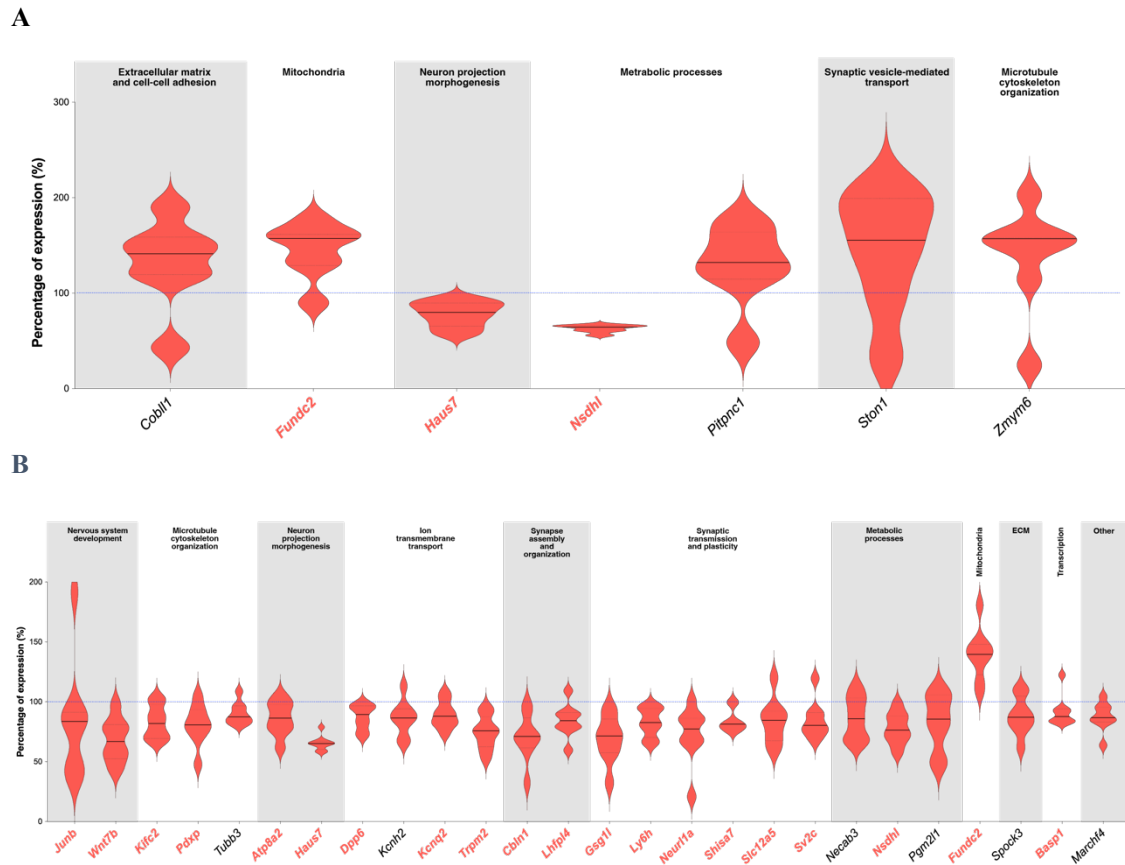


Figure 6.7: Primary neurons appeared the most stable and robust cell culture to use in the screening. (A) NPC-derived cultures and (B) neuronal samples validation. (A) Violin plots representing the expression values of validated DEGs in KO NPC-derived cultures with respect to WT (blue dotted line set to 100%). (B) Violin plots showing the expression levels of KO neuronal samples compared to WT (set to 100%, blue dotted line). D'Agostino-Pearson test was used to test normality distribution among genes. Unpaired Student's t-test or Mann-Whitney was used to compare KO and WT samples, accordingly to the normal distribution of data. Genes with p -value < 0.05 are in red. Genes with a p -value between 0.05 and 0.1 are indicated in black. Deregulated genes are divided according to their biological function, indicated above. Sample size $n = 8$ for each biological group.

6.1.4. Validation of prioritized DEGs on 96x96 IFC qRT-PCRs confirmed the reproducibility of 74 genes

Once established the most stable cellular system to use in the screening, we proceeded testing among the 201 prioritized genes (Table 6.1) which ones exhibited a reproducible and solid differential expression with the microfluidic approach, to identify the ones to use in our customized array card. This was obtained running 3 subsequent 96x96 IFC

qRT-PCR experiments; each of these cards contained 10 WT vs 10 KO neuronal samples. To reduce the possibility that litter specific phenotypes might affect the result, samples derived from 4 different cell preparations, containing at least 2 KO samples coupled with at least 2 WT littermates. Each plate contained at least three housekeeping genes (*Actb*, *Gapdh*, *Hprt*, *Ppia*, *Rpl13*) and *Mecp2*, used to confirm the genotype of the cells. The expression of KO samples was normalized to the average expression of the WT samples belonging to the same original batch of cell production, to minimize any batch effect possibly confounding the analysis.

Among the 201 DEGs tested, 61 confirmed the reproducibility in 96x96 qRT-PCRs, with 13 showing a tendency to deregulation ($0.05 < p\text{-value} < 0.1$), for a total of 74 genes. PCA performed on these DEGs allowed to visualize the segregation of WT and KO samples in two distinct populations (Figure 6.8), confirming the differential expression of these reproducible DEGs among the two groups. Of note, considering the low amplitude of differential expression of *Mecp2*-null samples and the results obtained with the PCA and given the fact that the underlying process of drug selection with our transcriptional platform is based on the identification of drugs which better reduce the differences in the whole transcriptional profile rather than focusing on the expression of single DEGs, we decided to use all the 74 genes as quantitative biomarkers. The reproducible DEGs identified and their deregulation is shown in Figure 6.9; genes have been organized according to their biological function as indicated above the plots. Of note, most of these genes belonged to biological processes involved in neuronal development and transmission, synapsis organization and plasticity, neuronal morphogenesis and cytoskeleton organization. On the contrary, very few deregulated genes were linked to metabolic homeostasis and extracellular matrix functions, leading us to speculate that the main contribution to the differential expression of these genes in the RNASeq analysis originated from astrocytes in NPC cultures. In addition, significant DEGs are mostly downregulated when compared to WT samples, corroborating previous results obtained from our RNASeq and other transcriptomic analyses (Bedogni et al., 2014; Gandaglia et al., 2019; Li et al., 2013; Riedmann & Fondufe-Mittendorf, 2016). Interestingly, *Haus7*, *Fundc2* and *Nsdhl* still remained significantly and highly deregulated (*Haus7*: percentage of KO expression with respect to WT = 64.04%, p-value

= 0.000049, *Fundc2*: KO = 133.44%, p-value = 0.0000036, *Nsdhl*: KO = 72.50%, p-value = 0.0011). All values are reported in Table 6.2.

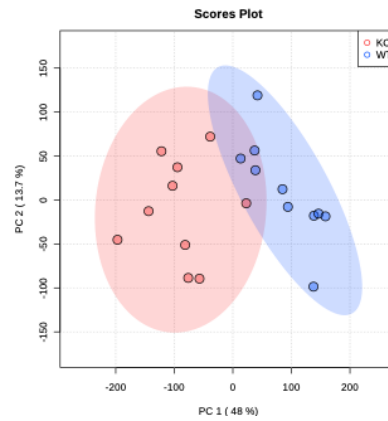


Figure 6.8: Transcriptional comparison between WT and KO neurons. The differential expression of the significant deregulated genes was used to perform the principal component analysis (PCA). The analysis allowed to visualize the segregation between the two biological conditions: KO samples are colored in red, while WT neurons are in blue. Each dot represents a single sample deriving from four different preparations. Each preparation is composed by at least 2 embryos per genotype, for a total of 10 samples per group.

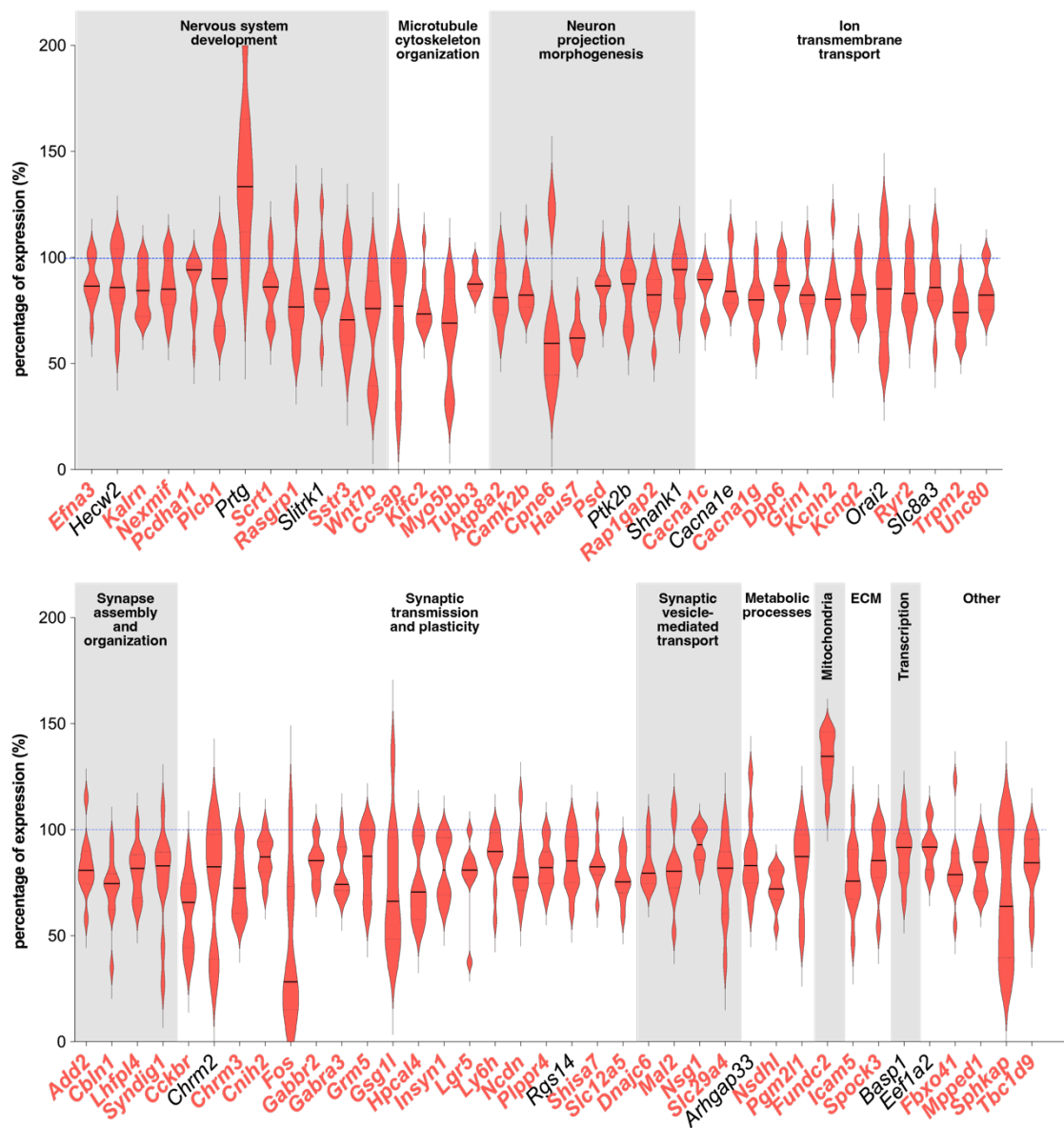


Figure 6.9: 74 reproducible and validated DEGs between WT and KO samples. Violin plots represent DEGs validated using 96x96 IFC qRT-PCR cards. D'Agostino and Pearson test was used to test normality of data distribution. Unpaired Student's t-test or Mann-Whitney test were used to compare KO and WT samples, according to the normal distribution of data. Genes with p -value < 0.05 are in red. Genes with a p -value between 0.05 and 0.1 are indicated in black. Deregulated genes are divided according to their biological functions, indicated above. Only reproducible genes are depicted in figure. Sample size $n = 10$ for each biological group.

Gene	Average KO (%)	p-value WT vs KO	Biological function
<i>Sstr3</i>	75,463	0,00552	nervous system development
<i>Kalrn</i>	84,446	0,00909	nervous system development
<i>Wnt7b</i>	69,665	0,01046	nervous system development
<i>Efna3</i>	87,850	0,01308	nervous system development
<i>Rasgrp1</i>	79,684	0,01919	nervous system development
<i>Nexmif</i>	86,704	0,02053	nervous system development
<i>Pcdha11</i>	85,643	0,02932	nervous system development
<i>Sert1</i>	85,207	0,03772	nervous system development
<i>Prtg</i>	141,104	0,03775	nervous system development
<i>Plcb1</i>	87,340	0,04920	nervous system development
<i>Slitrk1</i>	87,940	0,06261	nervous system development
<i>Hecw2</i>	88,288	0,06941	nervous system development
<i>Kifc2</i>	78,299	0,00290	microtubule cytoskeleton organization
<i>Tubb3</i>	88,944	0,00387	microtubule cytoskeleton organization
<i>Myo5b</i>	64,041	0,00736	microtubule cytoskeleton organization
<i>Ccsap</i>	72,526	0,02633	microtubule cytoskeleton organization
<i>Haus7</i>	64,036	4,87E-05	neuron projection morphogenesis
<i>Atp8a2</i>	83,093	0,00144	neuron projection morphogenesis
<i>Camk2b</i>	84,535	0,00390	neuron projection morphogenesis
<i>Psd</i>	86,269	0,00524	neuron projection morphogenesis
<i>Cpne6</i>	66,993	0,02359	neuron projection morphogenesis
<i>Rap1gap2</i>	81,169	0,03172	neuron projection morphogenesis
<i>Ptk2b</i>	83,755	0,06132	neuron projection morphogenesis
<i>Shank1</i>	91,512	0,08590	neuron projection morphogenesis
<i>Trpm2</i>	74,021	2,18E-05	Ion transmembrane transport
<i>Kcnq2</i>	83,698	0,00171	Ion transmembrane transport
<i>Unc80</i>	83,767	0,00172	Ion transmembrane transport
<i>Cacna1c</i>	85,325	0,00384	Ion transmembrane transport
<i>Cacna1g</i>	79,341	0,00415	Ion transmembrane transport
<i>Grin1</i>	86,424	0,00725	Ion transmembrane transport
<i>Kcnh2</i>	80,201	0,01033	Ion transmembrane transport
<i>Dpp6</i>	87,603	0,01428	Ion transmembrane transport
<i>Ryr2</i>	85,800	0,01786	Ion transmembrane transport
<i>Orai2</i>	83,928	0,07404	Ion transmembrane transport
<i>Cacna1e</i>	88,821	0,08090	Ion transmembrane transport
<i>Slc8a3</i>	88,387	0,09540	Ion transmembrane transport
<i>Cbln1</i>	71,618	3,77E-04	synapse assembly and organization
<i>Lhfp14</i>	80,386	4,13E-04	synapse assembly and organization
<i>Add2</i>	82,737	0,00944	synapse assembly and organization

<i>Syndig1</i>	76,375	0,03497	synapse assembly and organization
<i>Cckbr</i>	61,213	1,60E-05	synaptic transmission and plasticity
<i>Plppr4</i>	82,824	1,75E-04	synaptic transmission and plasticity
<i>Gabbr2</i>	85,053	1,87E-04	synaptic transmission and plasticity
<i>Gabra3</i>	80,577	3,61E-04	synaptic transmission and plasticity
<i>Slc12a5</i>	76,999	4,78E-04	synaptic transmission and plasticity
<i>Fos</i>	43,584	5,24E-04	synaptic transmission and plasticity
<i>Hpcal4</i>	73,902	0,00189	synaptic transmission and plasticity
<i>Shisa7</i>	84,307	0,00261	synaptic transmission and plasticity
<i>Ncdn</i>	81,425	0,00557	synaptic transmission and plasticity
<i>Cnih2</i>	86,988	0,00663	synaptic transmission and plasticity
<i>Insyn1</i>	81,926	0,01150	synaptic transmission and plasticity
<i>Chrm3</i>	74,597	0,01221	synaptic transmission and plasticity
<i>Gsg11</i>	72,945	0,02009	synaptic transmission and plasticity
<i>Grm5</i>	84,978	0,02184	synaptic transmission and plasticity
<i>Ly6h</i>	87,093	0,02603	synaptic transmission and plasticity
<i>Lgr5</i>	78,151	0,02660	synaptic transmission and plasticity
<i>Rgs14</i>	85,147	0,08776	synaptic transmission and plasticity
<i>Chrm2</i>	74,508	0,08989	synaptic transmission and plasticity
<i>Dnajc6</i>	82,953	0,00177	synaptic vesicle-mediated transport, exo- and endocytosis
<i>Slc29a4</i>	77,117	0,00841	synaptic vesicle-mediated transport, exo- and endocytosis
<i>Nsg1</i>	92,750	0,02758	synaptic vesicle-mediated transport, exo- and endocytosis
<i>Mal2</i>	81,480	0,04391	synaptic vesicle-mediated transport, exo- and endocytosis
<i>Nsdhl</i>	72,506	1,08E-04	Metabolic processes
<i>Pgm2l1</i>	83,352	0,03037	Metabolic processes
<i>Arhgap33</i>	86,898	0,06155	Metabolic processes
<i>Fundc2</i>	133,446	3,63E-06	Mitochondria
<i>Icam5</i>	78,468	0,00792	Extracellular matrix and cell-cell adhesion
<i>Spock3</i>	85,399	0,01927	Extracellular matrix and cell-cell adhesion
<i>Baspl</i>	90,045	0,05357	Transcriptional regulation
<i>Mpped1</i>	82,538	5,96E-04	Other
<i>Fbxo41</i>	81,776	0,00890	Other
<i>Tbc1d9</i>	83,298	0,01131	Other
<i>Sphkap</i>	67,668	0,03346	Other
<i>Eef1a2</i>	91,618	0,05202	Other

Table 6.2: List of 74 reproducible and validated DEGs between WT and KO samples. The Table summarizes percentages of KO expression and their respective *p*-values of the 74 reproducible DEGs depicted in Figure 6.9. Genes are organized according to their biological function. For each function, genes are ranked based on their *p*-values.

To summarize the results obtained in this section, the longitudinal RNASeq analyses allowed the identification of DEGs characterizing KO maturing neurons. Prioritization of these genes led to the selection of 201 DEGs consistently deregulated among two different types of bioinformatic analyses. Data were validated using the high-throughput 96x96 IFC dynamic array cards (Fluidigm) leading to the identification in *Mecp2*-null neurons of 74 mis-regulated genes, that might represent the transcriptional signature characterizing KO neurons and, therefore, could be used on a customized 96x96 qRT-PCR Array cards whose efficacy to evaluate drug efficacy will be tested.

6.2. Validation of the 96x96 qPCR screening system

We next wanted to verify whether these reproducible DEGs could actually be effective quantitative probes able to reflect the efficacy of drugs in pre-clinical studies. To this purpose, we initiated by testing the ability of the ampakine CX546 to rescue the expression of the selected and validated genes.

The Ampakine CX546 is a positive modulator of AMPA receptors able to bind the Gria1 and Gria2 subunits reducing desensitization and delaying channel closure (Nagarajan et al., 2001). It was initially chosen by our laboratory for its ability to promote axonal and dendritic outgrowth of *in vitro* differentiating SVZ neurons (Schitine et al., 2012) and to successfully restore normal breathing in *Mecp2*-null mice by increasing BDNF expression (Ogier et al., 2007). Based on these results and the hypothesis that neuronal activity modulates the expression of genes essential for the establishment of proper neuronal maturity (Spitzer, 2006), our laboratory decided to test whether the modulation of activity with CX546 during early neuronal maturation in RTT could rescue transcriptional and morphological impairments, leading to a more physiological cell development. To this purpose, the efficacy of an early and late treatment of CX546 was evaluated both *in vitro* and *in vivo* (Scaramuzza et al., 2021). Interestingly, an early treatment of CX546 *in vitro* (DIV3-6) was able to ameliorate transcriptional defects of NPC-derived RTT neurons, which was accompanied by

morphological and functional restorations. On the contrary, a late treatment (DIV7-10) produced lighter beneficial effects, rescuing only the morphological defects. Importantly, early exposure of KO mice to CX546 (P3-P9) delayed the progression of the disorder, significantly prolonging life span and ameliorating their behavioral scoring, and improved their motor and cognitive functions, even one month after the treatment (Scaramuzza et al., 2021). Thus, given these promising results obtained *in vitro* and *in vivo*, we decided to test whether selected DEGs represent valid quantitative probes to measure the potential success of drugs in pre-clinical studies. In details, we wanted to test whether the benefic effects of an early treatment with CX546 can rescue a great number of genes in our transcriptional system, possibly permitting to bring the transcriptional profile of the KO samples closer to the WT ones.

To this purpose, 10 WT vs 10 KO untreated and treated samples were produced, for a total of 30 samples, tested in triplicates. Each group derived from 4 different cell preparations containing at least 2 KO samples coupled with at least 2 WT littermates. KO primary neurons were exposed to 10 μ M of CX546 at DIV1 and DIV3; the drug was then washed out and cells were collected at DIV14 for transcriptional evaluation. So far, the effect of the drug has been evaluated on 51 out of 74 validated DEGs on two subsequent 96x96 qPCR experiments. The list of these genes is reported in Table 6.3 below.

Gene	Biological function
<i>Prtg</i>	nervous system development
<i>Sstr3</i>	nervous system development
<i>Rasgrp1</i>	nervous system development
<i>Slitrk1</i>	nervous system development
<i>Wnt7b</i>	nervous system development
<i>Ccsap</i>	microtubule cytoskeleton organization
<i>Myo5b</i>	microtubule cytoskeleton organization
<i>Kifc2</i>	microtubule cytoskeleton organization
<i>Tubb3</i>	microtubule cytoskeleton organization
<i>Atp8a2</i>	neuron projection morphogenesis
<i>Camk2b</i>	neuron projection morphogenesis
<i>Cpne6</i>	neuron projection morphogenesis
<i>Psd</i>	neuron projection morphogenesis

<i>Ptk2b</i>	neuron projection morphogenesis
<i>Rap1gap2</i>	neuron projection morphogenesis
<i>Haus7</i>	neuron projection morphogenesis
<i>Shank1</i>	neuron projection morphogenesis
<i>Cacna1g</i>	Ion transmembrane transport
<i>Kcnh2</i>	Ion transmembrane transport
<i>Kcnq2</i>	Ion transmembrane transport
<i>Grin1</i>	Ion transmembrane transport
<i>Trpm2</i>	Ion transmembrane transport
<i>Ryr2</i>	Ion transmembrane transport
<i>Dpp6</i>	Ion transmembrane transport
<i>Lhfp14</i>	synapse assembly and organization
<i>Syndig1</i>	synapse assembly and organization
<i>Cbln1</i>	synapse assembly and organization
<i>Cckbr</i>	synaptic transmission and plasticity
<i>Chrm2</i>	synaptic transmission and plasticity
<i>Chrm3</i>	synaptic transmission and plasticity
<i>Cnih2</i>	synaptic transmission and plasticity
<i>Fos</i>	synaptic transmission and plasticity
<i>Gabra3</i>	synaptic transmission and plasticity
<i>Grm5</i>	synaptic transmission and plasticity
<i>Gsg11</i>	synaptic transmission and plasticity
<i>Lgr5</i>	synaptic transmission and plasticity
<i>Ly6h</i>	synaptic transmission and plasticity
<i>Rgs14</i>	synaptic transmission and plasticity
<i>Shisa7</i>	synaptic transmission and plasticity
<i>Slc12a5</i>	synaptic transmission and plasticity
<i>Mal2</i>	synaptic vesicle-mediated transport, exo- and endocytosis
<i>Nsg1</i>	synaptic vesicle-mediated transport, exo- and endocytosis
<i>Nsdhl</i>	Metabolic processes
<i>Pgm2l1</i>	Metabolic processes
<i>Funde2</i>	Mitochondria
<i>Icam5</i>	Extracellular matrix and cell-cell adhesion
<i>Spock3</i>	Extracellular matrix and cell-cell adhesion
<i>Baspl</i>	Transcriptional regulation
<i>Eef1a2</i>	Other
<i>Mpped1</i>	Other
<i>Sphkap</i>	Other

Table 6.3: List of the 51 DEGs tested.

The set of these 51 genes was first analyzed by PCA to highlight whether CX546 was able to produce any transcriptional rescue. The segregation between WT and KO untreated samples was confirmed by PCA, as depicted in Figure 6.10 panel A. On the contrary, the distance from the WT samples was minimized by the exposure to an early treatment with CX546 producing a complete overlapping profile between the two groups (Figure 1.10, panel B).

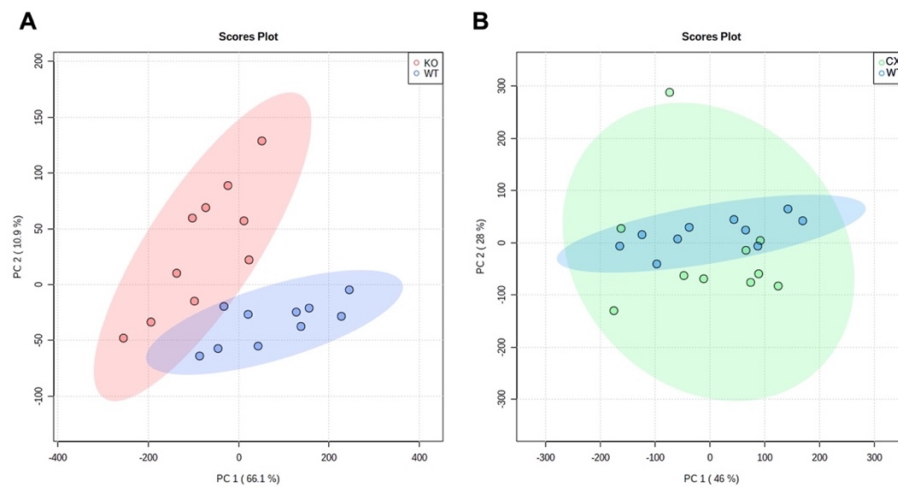


Figure 6.10: The early treatment with ampakine CX546 ameliorates the transcriptional profile of KO treated samples. Both PCAs were performed considering the 51 genes tested. Two different clusters are depicted in each PCA: (A) represents KO untreated (in red) and WT (in blue), while (B) illustrates KO treated (in green) and WT (in blue). Each dot represents a single sample deriving from four different preparations. Each preparation is composed by at least 2 embryos per genotype, for a total of 10 samples per group. The distance from the WT samples was minimized by the exposure to an early treatment with CX546 producing a complete overlapping profile between the two groups.

In line with the PCA data, the detailed analysis of the transcriptional profile is depicted in Table 6.4 and Figure 6.11 below. Of note, 42 of these genes confirmed the significant deregulation between WT and KO untreated samples with the more stringent one-way ANOVA test. Among these genes, 75% DEGs (32 out of 42) were ameliorated by the early exposure to CX546, measured either with the loss of significant deregulation between WT and KO treated samples alone or in combination with the significant deregulation between KO untreated and treated groups, indicated with the * in the Table. Genes which were not ameliorated by the exposure to CX546 and their respective

biological functions are reported in grey in Table 6.4 below. Only the 32 genes rescued by the early treatment with CX546 and their respective biological functions are illustrated in Figure 6.11.

Gene	Average KO (%)	Average KO treated (%)	Biological function
<i>Prtg</i>	219.383	187.057	nervous system development
<i>Sstr3</i>	60.319	\$ 93.337	nervous system development
<i>Rasgrp1</i>	81.645	77.524	nervous system development
<i>Ccsap</i>	72.526	\$ 98.159	microtubule cytoskeleton organization
<i>Myo5b</i>	64.041	* 117.780	microtubule cytoskeleton organization
<i>Kifc2</i>	82.191	\$ 98.449	microtubule cytoskeleton organization
<i>Tubb3</i>	88.944	** 104.389	microtubule cytoskeleton organization
<i>Atp8a2</i>	72.837	* 94.986	neuron projection morphogenesis
<i>Camk2b</i>	68.677	\$ 94.055	neuron projection morphogenesis
<i>Cpne6</i>	66.993	\$ 97.196	neuron projection morphogenesis
<i>Psd</i>	86.269	\$ 100.144	neuron projection morphogenesis
<i>Ptk2b</i>	66.328	\$ 96.102	neuron projection morphogenesis
<i>Rap1gap2</i>	62.652	\$ 95.972	neuron projection morphogenesis
<i>Haus7</i>	63.387	54.586	neuron projection morphogenesis
<i>Kcnh2</i>	71.064	\$ 96.474	Ion transmembrane transport
<i>Kcnq2</i>	84.044	* 98.284	Ion transmembrane transport
<i>Trpm2</i>	78.410	* 96.457	Ion transmembrane transport
<i>Ryr2</i>	72.535	\$ 100.964	Ion transmembrane transport
<i>Dpp6</i>	87.603	87.729	Ion transmembrane transport
<i>Lhfp14</i>	83.204	* 101.061	synapse assembly and organization
<i>Syndig1</i>	76.375	* 102.581	synapse assembly and organization
<i>Cbln1</i>	73.794	69.868	synapse assembly and organization
<i>Cckbr</i>	58.377	82.641	synaptic transmission and plasticity
<i>Chrm3</i>	74.597	\$ 97.585	synaptic transmission and plasticity
<i>Gabra3</i>	68.268	* 90.502	synaptic transmission and plasticity
<i>Shisa7</i>	82.896	* 97.427	synaptic transmission and plasticity
<i>Slc12a5</i>	81.886	* 101.064	synaptic transmission and plasticity
<i>Grm5</i>	75.192	\$ 102.375	synaptic transmission and plasticity
<i>Cnih2</i>	86.988	88.239	synaptic transmission and plasticity
<i>Gsg11</i>	75.773	78.575	synaptic transmission and plasticity
<i>Ly6h</i>	85.440	86.049	synaptic transmission and plasticity
<i>Mal2</i>	81.480	\$ 101.743	synaptic vesicle-mediated transport, exo- and endocytosis
<i>Nsg1</i>	92.750	\$ 100.190	synaptic vesicle-mediated transport, exo- and endocytosis

<i>Nsdhl</i>	74.886	69.995	Metabolic processes
<i>Pgm2l1</i>	83.352	79.988	Metabolic processes
<i>Fundc2</i>	136.910	**** 107.218	Mitochondria
<i>Icam5</i>	72.555	* 96.022	Extracellular matrix and cell-cell adhesion
<i>Spock3</i>	85.399	80.855	Extracellular matrix and cell-cell adhesion
<i>Baspl</i>	83.775	94.054	Transcriptional regulation
<i>Eef1a2</i>	72.923	96.885	Other
<i>Mpped1</i>	67.798	* 91.988	Other
<i>Sphkap</i>	67.668	96.064	Other

Table 6.4: List of the 42 significant DEGs and their percentage of expression in KO untreated and treated sample with respect to WT. One-way ANOVA followed by Tukey's multiple comparison test was used to compare WT, KO untreated and treated samples. All the genes listed above are significantly deregulated between WT and KO untreated samples. Significance between untreated and treated KO is indicated with * (p*-value < 0.05; ***p*-value < 0.01, ****p*-value < 0.001, *****p*-value < 0.0001); the tendency to deregulation is reported with \$ (0.05 < *p*-value < 0.1). DEGs which were not rescued by the exposure to CX546 are reported in grey.**

Of note, the 9 genes which were not found significantly deregulated with the one-way ANOVA test in the basal condition between WT and KO untreated samples are reported in Table 6.5. Nonetheless, we hypothesized that the lack of significance could be related to the strictness of the ANOVA test and the great standard deviation of those genes, since they still remained statistically deregulated with the unpaired Student t-test.

Genes (not significant WT vs KO – ANOVA)	Average KO (%)	Average KO treated (%)	Biological function
<i>Slitrk1</i>	87.940	90.079	nervous system development
<i>Wnt7b</i>	64.175	90.597	nervous system development
<i>Shank1</i>	91.512	94.286	neuron projection morphogenesis
<i>Caena1g</i>	69.796	100.475	Ion transmembrane transport
<i>Grin1</i>	76.678	101.648	Ion transmembrane transport
<i>Chrm2</i>	74.508	102.219	synaptic transmission and plasticity
<i>Fos</i>	43.584	88.141	synaptic transmission and plasticity
<i>Lgr5</i>	78.151	85.217	synaptic transmission and plasticity
<i>Rgs14</i>	74.148	96.807	synaptic transmission and plasticity

Table 6.5: Nine genes were not found significantly deregulated in the basal condition between WT and KO untreated samples with the One-way ANOVA test.

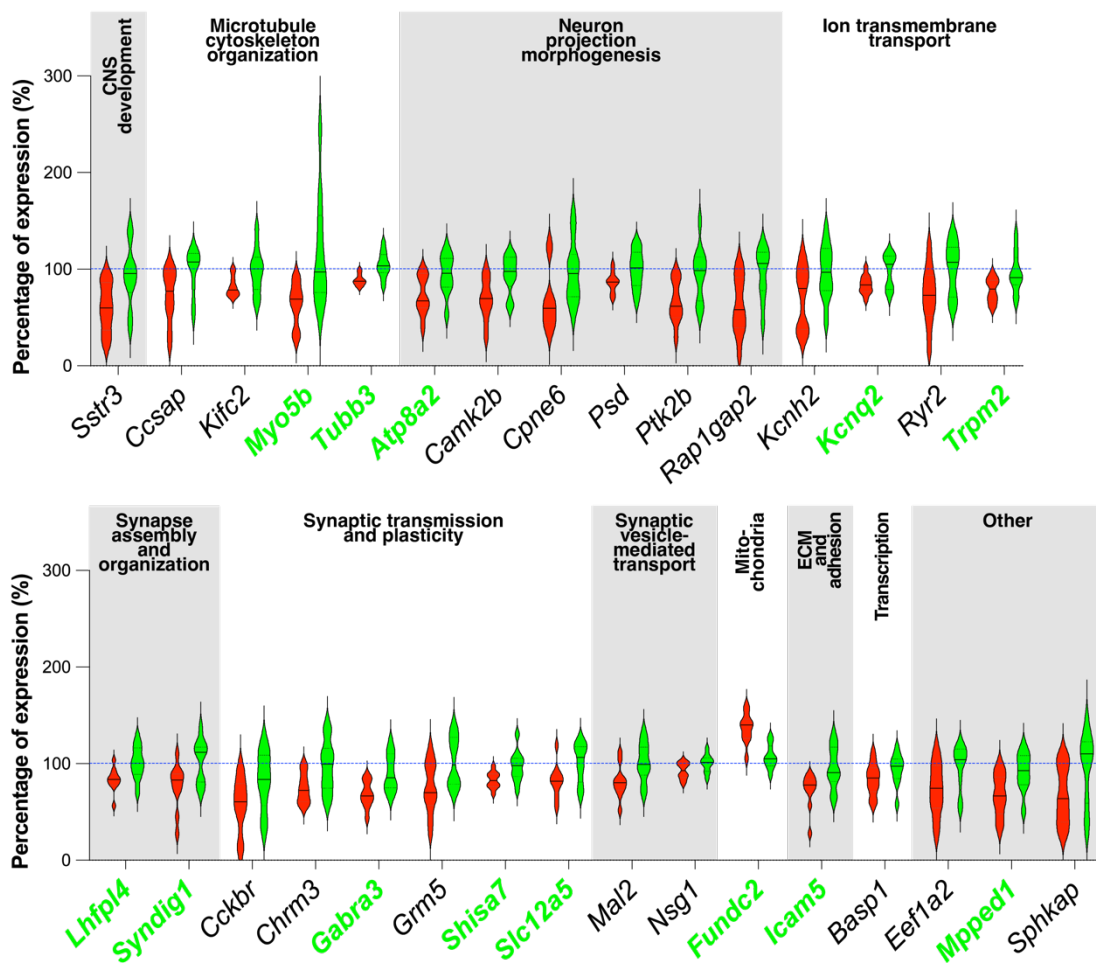


Figure 6.11: Ampakine CX546 rescues the expression of 75% of the DEGs tested: Violin plots represent the expression values of validated DEGs in KO untreated (in red) and treated (in green) neurons with respect to WT (blue dotted line set to 100%). One-way ANOVA followed by Tukey's multiple comparison test was used to compare WT, KO untreated and treated samples. Genes which no longer exhibit a significant difference between WT and KO treated samples are depicted in figure. Genes in green display also a significant deregulation between the KO untreated and treated samples (p -value < 0.05).

As expected, most of the DEGs ameliorated by the treatment belongs to biological processes involved in modulation of neuronal activity (ion transport, synapse assembly and organization, synapse transmission and plasticity and synaptic vesicle-mediated transport, exo- and endocytosis). Interestingly, the categories of other genes mostly impacted by the early exposure to CX546 impinge on processes related to the

development of proper neuronal morphology (microtubule cytoskeleton organization and neuronal projection morphogenesis), corroborating the link between neuronal activity, transcriptional regulation and neuronal morphology described by Spitzer and colleagues (Scaramuzza et al., 2021; Spitzer, 2006).

Overall, given the results obtained we concluded that the DEGs validated and selected using the 96x96 IFC dynamic array cards (Fluidigm) could be used as quantitative probes to select drugs with a higher chance of success in pre-clinical studies.

6.3. Preliminary studies on the possible involvement of *Haus7* and *Nsdhl* in RTT pathogenesis

As mentioned in the previous section, along our studies, we came across three genes, *Haus7*, *Nsdhl* and *Fundc2*, that were consistently and significantly deregulated between WT and KO samples.

Already in the RNASeq data, *Haus7* and *Nsdhl* were among the most significantly downregulated genes across all the three timepoint analyzed in the time-specific analyses (DIV7-14-18) and, respectively, the second and the third most significant DEGs in the overtime analysis, with *Mecp2* being the first one (Figure 6.12). On the other hand, *Fundc2* appeared among the 15 most upregulated genes in the overtime analysis and one of the few highly upregulated DEGs in common between DIV14 and 18 (Figure 6.12).

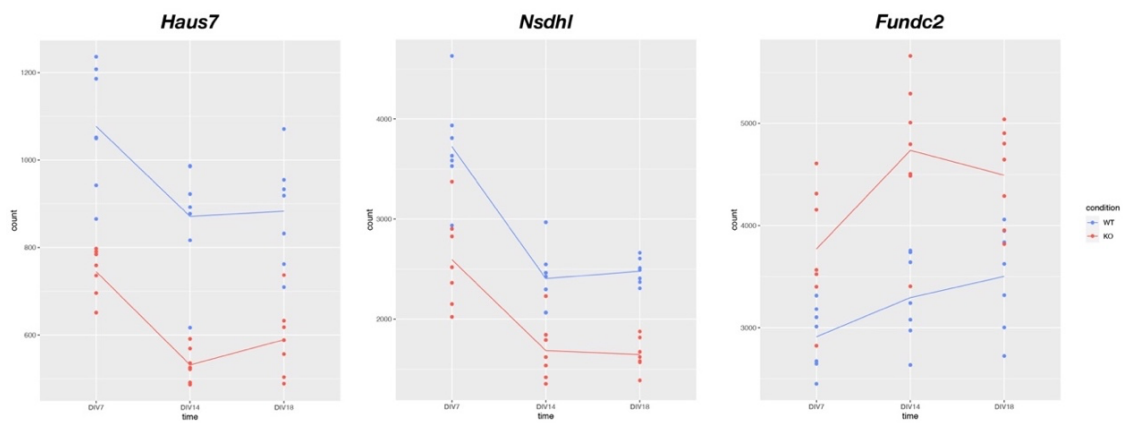


Figure 6.12: Plots representing counts for *Haus7*, *Nsdhl* and *Fundc2* at the three timepoints analyzed in the RNASeq data. Blue dots represent WT samples, while red dots indicate counts obtained from each KO replicate. Sample size for each biological group $n=7$.

Their significant deregulation in KO samples was further confirmed in each 96x96 RT-qPCR experiment, both in NPC-derived cultures and primary neurons. Notably, the amplitude of deregulation was consistent between the RNAseq and microfluidic analysis.

Thus, to gain further insight on their consistent deregulation in *Mecp2*-null samples, we first investigated whether their expression was altered in other RNASeq data obtained in our laboratory. As reported in Table 6.6, *Haus7* was downregulated in all the *in vitro* and *ex vivo* transcriptomic analyses performed in our laboratory, while *Nsdhl* was consistently downregulated in cerebral cortices and hippocampi of P60 *Mecp2*-null mice. On the contrary, *Fundc2* upregulation was not confirmed in our *ex vivo* analyses.

Samples	Timepoint	Comparison	<i>Haus7</i>		<i>Nsdhl</i>		<i>Fundc2</i>	
			Log2FC	p-adj	Log2FC	p-adj	Log2FC	p-adj
NPC-derived neurons	DIV7	WT vs <i>Mecp2</i> KO	-0,49102	0,00024	-0,44073	0,02423	0,26876	ns
	DIV14		-0,67335	0,00000	-0,43221	0,00601	0,46403	0,00245
	DIV18		-0,52151	0,00180	-0,56220	0,00000	0,28146	0,09659
Primary cortical neurons	DIV7	WT vs <i>Mecp2</i> KO	-0,57315	0,00011	–	–	–	–
Mouse cortex	P60	WT vs <i>Mecp2</i> KO	-0,64774	0,00077	-0,49309	2,025E-06	–	–
Mouse hippocampus	P60	WT vs <i>Mecp2</i> KO	-0,54740	0,00225	-0,39916	0,00081	0,01307	ns

Table 6.6: Schematic overview of *Haus7*, *Nsdhl* and *Fundc2* expression across 4 different RNASeq experiments performed in our laboratory. *Haus7* appeared consistently and significantly downregulated in all our datasets examined, spanning from in vitro cultures of NPC-derived and primary neurons, to ex vivo cortical and hippocampal tissues of P60 symptomatic mice. *Nsdhl* also confirmed its downregulation in cortices and hippocampi of adult mice at P60, with consistent Log2FC across the analyses. On the contrary, *Fundc2* did not appear upregulated in any dataset obtained from ex vivo tissues. (“ns”: not significant; “–”: not detected).

These preliminary data and the specific functions associated with these genes prompted a study aimed at evaluating *Haus7* and *Nsdhl* deregulation in *Mecp2*-mutant mice during different stages of the disorder and among different brain areas. Interesting results will bring us to investigate if these genes can be ascribed as modifiers of the RTT pathology. To this purpose, by modulating their expression in *Mecp2* null neurons, we will investigate if and to what extent they impact on typical phenotypes of RTT neurons.

6.3.1. *Haus7* is consistently downregulated in the cerebral cortex and hippocampus of *Mecp2* mutant male and female mice

HAUS7, also known as UIP1 and UCHL5IP, is one of the eight subunits composing the HAUS augmin-like protein complex which plays an important role in a non-centrosomal microtubule (MT) nucleation pathway, thus regulating MT branching, mitotic spindle integrity and cell polarity.

The augmin complex was originally identified in *Drosophila melanogaster* (Goshima et al., 2008) and then subsequently discovered in plants (Ho et al., 2011; Hotta et al., 2012) and human cells (Hutchins et al., 2010; Lawo et al., 2009; Uehara et al., 2009), where it appears highly conserved (Gabel et al., 2022; Zupa et al., 2022).

Cryo-electron microscopy, mass spectroscopy and different computational approaches were used to predict and define augmin functional elements, which are represented by two stable hetero-tetramers (Figure 6.13, panel A): tetramer TII containing HAUS2, 6, 7 and 8 mediating MT-binding, and tetramer TIII consisting of HAUS1, 3, 4 and 5, which is able to bind to the γ -Tubulin ring complex (γ -TuRC) via the adaptor protein NEDD1 (neural precursor cell expressed developmentally down-regulated protein 1), allowing the nucleation of 20-30° angled daughter MTs starting from a pre-existing filament to maintain spindle polarity (Figure 6.13, panel B) (Zupa et al., 2022). Given its ability to bind both MTs and γ -TuRC, augmin complex determines both the site of MT branching and the orientation of the branched microtubule. In addition, the angles defined by the complex spanning from 0-30° (Kamasaki et al., 2013; Petry et al., 2013) rapidly increases the MT density of the spindle, which would progressively tend to decrease with increasing distance from the central organizer due to the geometry of radial arrays. More specifically, the highly flexible HAUS8 N-terminus is fundamental to the initial interaction with the MT, and the binding affinity is then ten-time increased and stabilized by the presence of HAUS6 and 7 (Hsia et al., 2014). Tetramer TIII then forms a predominantly rigid structure to position γ -TuRC at a specific distance and orientation with respect to the pre-existing MT (Zupa et al., 2022).

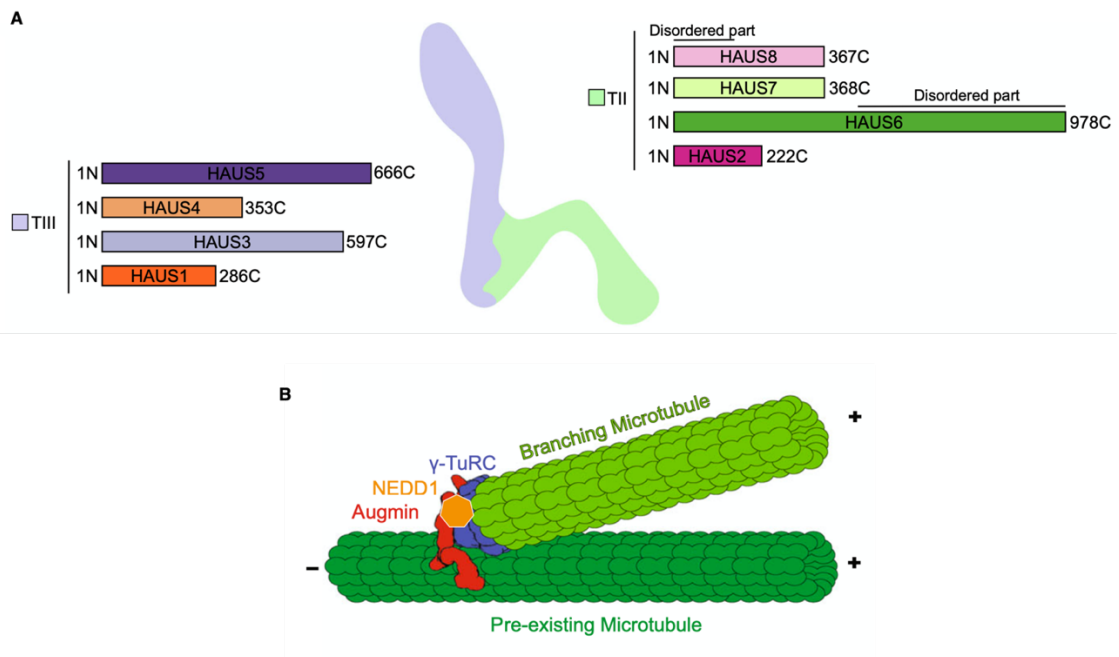


Figure 6.13: Augmin functional domains (panel A) (Zupa et al., 2022) and model of augmin binding to NEDD1 and γ -TuRC in microtubule branching (panel B) (Gabel et al., 2022) (Open access)

Given its structure and interacting partners, the augmin complex appears to be primarily involved in the correct assembly of non-centrosomal mitotic spindle of cells during mitosis and meiosis and in regulating MT branching in non-dividing cells, like neurons, where it participates at organizing microtubule networks and establishing axonal microtubule polarity.

In detail, Goshima and colleagues demonstrated that in dividing cells augmin complex is located in metaphase bipolar spindle of both S2 and HeLa cells where it is required for the non-centrosomal MT generation taking place within the metaphase spindle. In the study, a new model for augmin-dependent MT nucleation was proposed: during the early prometaphase γ -TuRC generates MTs from centrosome and chromosomes, building the first set of mitotic MTs and providing the nucleating material, and then the augmin- γ -TuRC complex becomes essential in the subsequent amplification and/or maintenance of MTs, rapidly increasing spindle density and facilitating kinetochore-fiber and bipolar spindle formations (Goshima et al., 2008). Of note, the depletion of any of the augmin-complex subunits led to increased monopolar spindle, delayed conversion from monopolar to bipolar spindle, whose MT density appeared reduced, and chromosome

misalignment, without diminishing MT nucleation at centrosomes, where astral MTs appeared much longer compared to controls (Goshima et al., 2008; Lawo et al., 2009). These results were later confirmed in Haus7-knockdown mouse meiotic oocyte maturation (Y. P. Wang et al., 2013), while HAUS8 KO RPE1 cultures additionally presented an arrest in G1 mitotic phase (McKinley & Cheeseman, 2017).

In neurons, the augmin-complex appears involved in neuronal migration, polarization and development through local regulation of the MT cytoskeleton, both in axons and dendrites (Cunha-Ferreira et al., 2018; Sánchez-Huertas & Lüders, 2015). The complex, in fact, localizes in MT clusters along axon and dendrites of neurons, already starting from early stages of neuronal development. In particular, the augmin-complex proved to be necessary in axonal outgrowth and polarization, in dendritic branching and in the maintenance of MT density in dendrites (Cunha-Ferreira et al., 2018). In addition, depleting Haus6 in E14.5 mice impaired migration and delayed neuronal development, with neurons remaining in the sub-ventricular and intermediate zones of the cortex (Cunha-Ferreira et al., 2018).

Notably, the HAUS7 subunit of the augmin-complex was localized at the excitatory pre-synaptic boutons of mature hippocampal neurons, where it appeared fundamental for the maintenance of axon polarity, oriented MT nucleation and the transport of cargos in the pre-synaptic boutons (Qu et al., 2019). As a matter of fact, neuronal activity was able to increase MT nucleation mediated by the augmin complex and these newly formed MTs at excitatory pre-synapses were required for interbouton synaptic vesicle motility and storage and the consequent neurotransmitter release, suggesting an activity-dependent role of the augmin-complex at the synapsis and its possible impact on neuronal synaptic plasticity (Qu et al., 2019).

Of note, all these evidences appear relevant in the context of RTT, where impaired MT dynamics and stability have also been reported. As a matter of fact, beside its role in gene expression and chromatin compaction, MeCP2 was found to colocalize with γ -tubulin at the centrosome of both proliferating cells and primary cortical neurons (Bergo et al., 2015). The importance of this novel localization was suggested by the identification of several MT phenotypes in MeCP2 deficient dividing cells, such as a significant rise of the percentage of monopolar spindle with respect to bipolar ones and induced abnormal spindle orientation, with prolonged and/or aberrant mitosis and delayed MT nucleation,

thus suggesting a role of MeCP2 in MT initiation from centrosomes (Bergo et al., 2015). In addition, given the impact of MeCP2 on MT nucleation and that in mature neurons primary cilia are made of MTs originating from the centrosome migrated towards the cell surface, our laboratory demonstrated that MeCP2 deficiency also significantly reduced ciliogenesis in different cells types, including cortical neurons, RTT fibroblasts, and the *Mecp2*-null brain (Frasca et al., 2020). Furthermore, it is well established that neurons depend on MT-mediated transport of cargos at the synapses for synaptic development, structure and function; MT impairments in RTT mice proved to significantly reduce BDNF-vesicle transport to synapsis, indicating a possible impact of MT instability on neurotransmitter release and neuronal synaptic plasticity (Roux et al., 2012a).

Thus, although the majority of MeCP2-associated defects, such as impaired neuronal morphology, synaptic structure and reduced responsiveness to external stimuli, might be at first caused by the transcriptional defects induced by MeCP2 deficiency, MT instability might participate in the observed phenotypes, thereby offering a possible therapeutic target.

All these evidences have led us to investigate the possible causative link between MeCP2 and HAUS7 and the role of the latter in RTT pathogenesis.

Levels of *Haus7* transcript were first longitudinally analyzed in *Mecp2*-null mice at four different timepoints: P7 and P24, generally defined as pre-symptomatic stages, P40, corresponding to a mild symptomatic phase and P60, a fully symptomatic age. The analysis was performed in cerebral cortex and hippocampus, given their major implication in RTT pathogenesis (Figure 6.14). Surprisingly, *Haus7* appeared strongly downregulated at each timepoint examined, with a prominent effect in the hippocampus, where it reaches a 50% reduction both at the early timepoint (P7, KO percentage of expression with respect to WT: 48.63%) and in the highly symptomatic stage (P60, KO: 50.27%), while the amplitude of deregulation in the cerebral cortex appeared consistent along time (P7: 61.23%, P24: 62.20%, P40: 83.57%, P60: 69.24%).

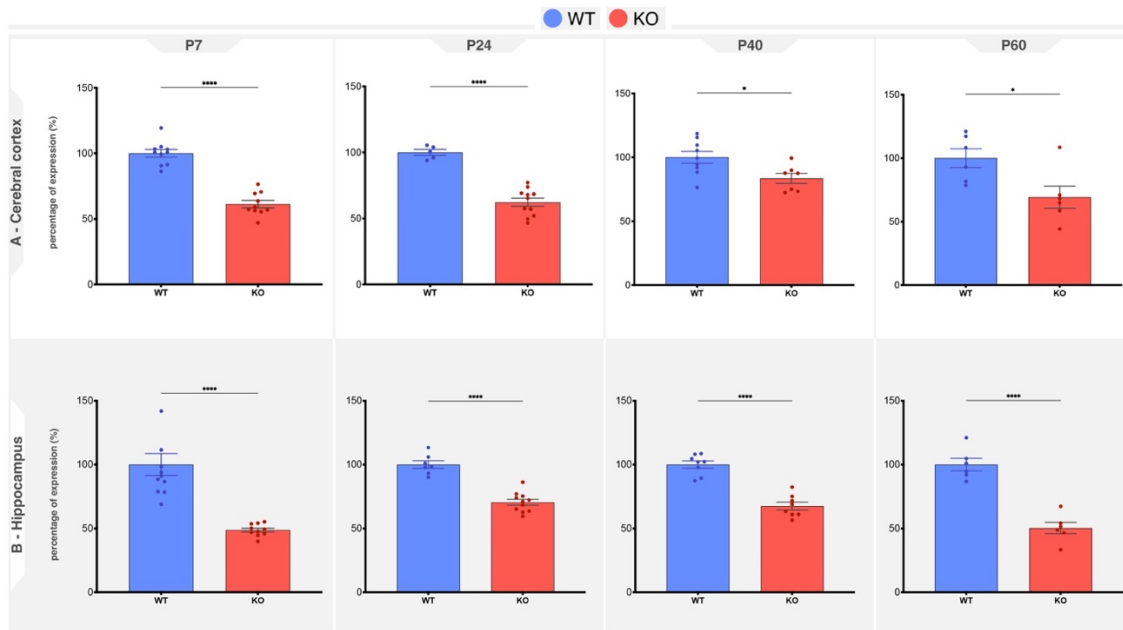


Figure 6.14: *Haus7* is consistently downregulated in the cerebral cortex and hippocampus of *Mecp2* null mice. Bar graphs (mean \pm SEM) represent percentages of *Haus7* expression in the cerebral cortex (panel A) and hippocampus (panel B) of P7, P24, P40 and P60 KO mice (in red) with respect to their WT littermates (in blue, normalized at 100%). D'Agostino-Pearson test was used to test normality distribution. Unpaired Student's *t*-test was used to compare KO and WT samples, according to the normal distribution of data. Significance between WT and KO is indicated with * (**p*-value < 0.05; ***p*-value < 0.01, ****p*-value < 0.001, *****p*-value < 0.0001). Sample size for each biological group is *n*=10 for P7, 8 for P24 and P40 and *n*=6 for P60.

Prompted by these results, we moved to investigate its expression in male symptomatic mice from another mouse model of the disease, the *Mecp2* Y120D, described in section 4.2, and mimicking a mutation found in a RTT patient. These mice reproduce the phenotypes of *Mecp2*-null animals but they diverge at the molecular level, exhibiting a more open and transcriptionally active chromatin (Gandaglia et al., 2019). *Haus7* expression was evaluated at P40 of knock-in hemizygous male mice (KI), when they typically start to exhibit the first evident signs of the pathology. Results are depicted in Figure 6.15 below. Notably, *Haus7* consistent downregulation was confirmed both in the cerebral cortex and hippocampus of KI symptomatic mice, with percentage of KI expression with respect to WT littermates of 68.43% for the cerebral cortex and of 69.21% for the hippocampus, suggesting that its downregulation might be independent from the type of *Mecp2* mutation.

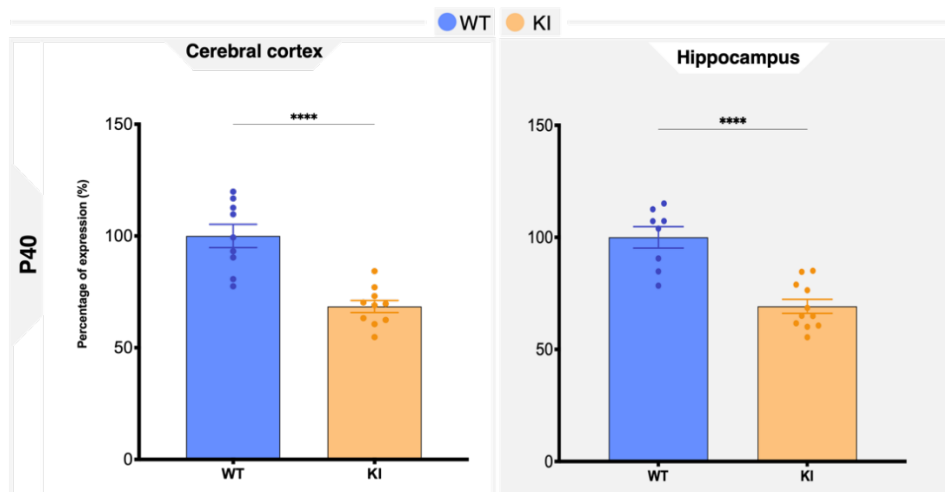


Figure 6.15: *Haus7* is downregulated in the cerebral cortex and hippocampus of P40 *Mecp2* Y120D mice. Bar graphs (mean \pm SEM) represent percentages of *Haus7* expression in the cerebral cortex (on the left) and hippocampus (on the right) of P40 KI male mice (in orange) with respect to their WT littermates (in blue, normalized at 100%). D'Agostino-Pearson test was used to test normality distribution. Unpaired Student's t-test was used to compare KI and WT samples, according to the normal distribution of data. Significance between WT and KI is indicated with * (**p-value < 0.01, ****p-value < 0.0001). Sample size is n=8 for WT mice and n=11 for KI animals.

Given that RTT primarily affects females, we decided to test *Haus7* expression also in female *Mecp2*-mutant mice, which represent the most clinically relevant model to study RTT, even though they display a milder phenotype and a slower disease progression due to a mosaic expression of the mutant or WT alleles, making it more challenging to study disease pathogenesis. *Haus7* expression was investigated in the cerebral cortex and hippocampus of P100 heterozygous female (Het), when only few signs of the pathology are present. Intriguingly, we confirmed a strong and consistent downregulation in the cerebral cortex of pre-symptomatic females (percentage of Het expression: 64.12%) (Figure 6.16). A mild but yet significant decrease was also detected in the hippocampus, where the reduction reaches only 10% with respect to their WT littermates (percentage of Het expression: 89.71%).

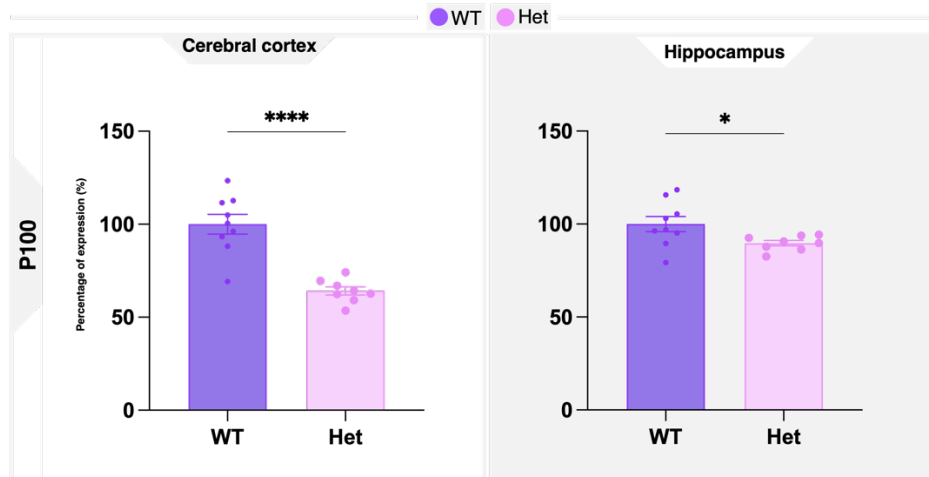


Figure 6.16: Haus7 is downregulated in P100 Het cerebral cortices and hippocampi. Bar graphs (mean \pm SEM) represent percentages of Haus7 expression in the cerebral cortex (on the left) and hippocampus (on the right) of P100 heterozygous female mice (in pink) with respect to their WT littermates (in purple, normalized at 100%). D'Agostino-Pearson test was used to test normality distribution. Unpaired Student's *t*-test was used to compare Het and WT samples, according to the normal distribution of data. Significance between WT and Het is indicated with * (**p*-value < 0.05; ***p*-value < 0.01, ****p*-value < 0.001, *****p*-value < 0.0001). Sample size for each biological group is *n*=9 for WT and 8 for Het.

Many attempts have been made to characterize Haus7 protein expression but all of the tested antibodies against the murine protein (Santa Cruz sc-393259 and Abcam ab192616) failed to produce a clear signal unequivocally corresponding to the protein target, making it difficult to establish a possible correspondent deregulation between the protein and the transcript (data not shown). In the future we will establish the specificity of the observed signals by specifically knocking down Haus7 expression.

6.3.2. Nsdhl is downregulated in the cerebral cortex of Mecp2 mutant mice, a possible indication of defective cholesterol homeostasis

In the CNS, cholesterol is a crucial structural component of cellular membranes and myelin sheaths, it regulates membrane fluidity, facilitates ion channel function, neurotransmitter transport and vesicle exocytosis, and modulates synapse and dendrite

formation, axon guidance and synaptic transmission (Allen et al., 2007; Tracey et al., 2018; van Deijk et al., 2017). Since circulating cholesterol cannot cross the blood brain barrier (BBB), its biosynthesis and homeostasis are tightly and finely regulated within the brain by a complex interplay between different cell types, starting from early embryonic development (Zhang & Liu, 2015). NPCs and developing neurons actively synthesize cholesterol, whose rate of production progressively decreases along neuronal maturation (Genaro-Mattos et al., 2019). Mature neurons, in fact, mostly rely on exogenous cholesterol synthesized by astrocytes, which support neuronal maturation throughout childhood and neuronal maintenance throughout adulthood (van Deijk et al., 2017). Astrocytes secrete cholesterol through ABC transporters (ABCA1 and ABCG1) in apolipoprotein particles (apoE and apoJ), which are subsequently up taken by mature neurons via lipoprotein receptors (LRP1) (Zhang & Liu, 2015). Excess cholesterol in neurons is either converted by neuron-specific cytochrome CYP46A1 into its 24-hydroxylated derivate (24-OHC), which is able to cross lipophilic membranes, including the BBB (Lund et al., 2003; Meaney et al., 2002), or it can be directly secreted via ABC transporters or converted in its esterified form (1% of the total cholesterol) forming lipid droplets and subsequently stored within the cell (Zhang & Liu, 2015). The resource-intensive process of cholesterol biosynthesis requires the action of more than 20 different enzymes and it can be divided into the early stage, where the acetyl-CoA is progressively converted into lanosterol, and the post-lanosterol stage, aiming at oxidizing methyl groups for carbon removal and leading to cholesterol synthesis (Figure 6.17) (Qian et al., 2022).

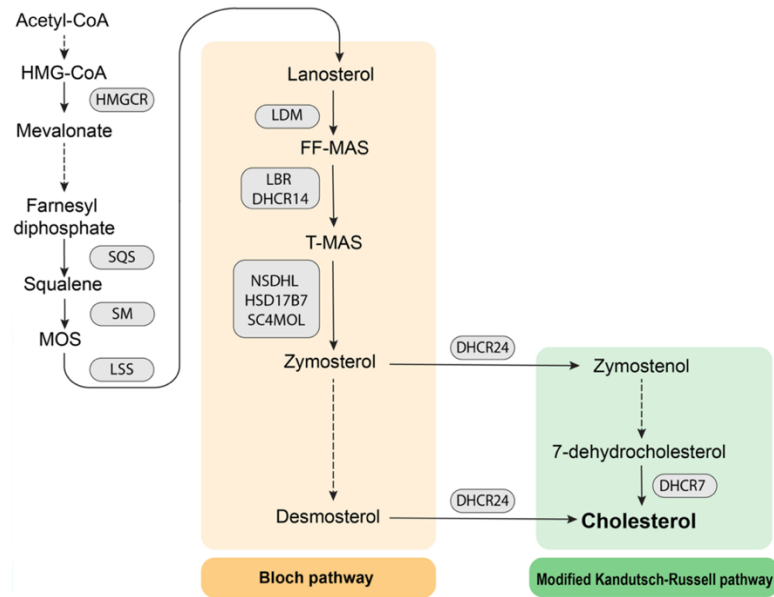


Figure 6.17: Cholesterol biosynthesis pathway. The process consists of two main stages: the early one starts from the conversion of Acetyl-CoA into mevalonate, thanks to the action of HMG-CoA reductase (HMGCR), which represents the rate-limiting and irreversible step of cholesterol biosynthesis. Downstream the early stage, squalene synthase (SQS) leads to the production of squalene, the first step specific to sterol biosynthesis, followed by the conversion to lanosterol. The post-lanosterol process can follow two different pathways, the Bloch and the Kandutsch-Russell, which both lead to the synthesis of cholesterol. Modified from (Qian et al., 2022) (Open access).

NSDHL, also named NAD(P)H steroid dehydrogenase-like, is an X-linked gene which encodes for a sterol-4- α -carboxylate 3-dehydrogenase, representing one of the key enzymes implicated in post-lanosterol synthesis of cholesterol. *NSDHL* localizes on the membrane of the endoplasmic reticulum (ER), the main site of cholesterol biosynthesis, and accumulates on the surface of lipid droplets (LDs) (Caldas & Herman, 2003). In particular, it is bound to the ER membrane through a single short transmembrane region, with both the N- and C-terminal domains extruding into the cytoplasm (Figure 6.18, panel A) (Kim et al., 2021). The N- and C-terminal domains represent respectively the NAD⁺ coenzyme-binding domain and substrate-binding domain: the interaction of NAD⁺ induces a conformational change allowing the binding of 4-methyl, 4-carboxy zymosterone, a cholesterol precursor, catalyzing the NAD⁺-dependent oxidative decarboxylation of the C4 methyl groups (Figure 6.18, panel B) (Caldas & Herman, 2003; Kim et al., 2021; Liu et al., 1999; Mo et al., 2002; Penning, 1997).

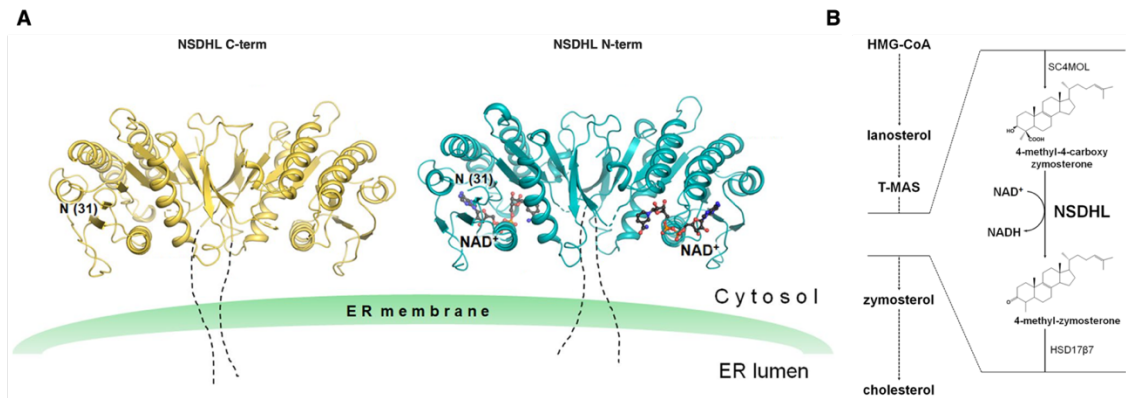


Figure 6.18: NSDHL structure and function. NSDHL is located in the ER membrane, with the N-terminal NAD^+ coenzyme domain and the C-terminal substrate-binding domain extruding into the cytosol (A), where it decarboxylates 4-methyl, 4-carboxy zymosterone into its 4-methyl derivative (B). Modified from (Kim et al., 2021). (License number 5431840718087)

Nsdhl is already present at the E6.5 embryonic stage, where the protein is uniformly and ubiquitously expressed in all cell types, and progressively increases along development in the neural tube and the embryonic liver compared to other tissues (Cunningham et al., 2009; Laubner et al., 2003). In the developing mouse brain, differentiating neurons of the cortical plate and the hippocampus are characterized by the greatest expression of Nsdhl, which stabilizes at P2 and reaches a most pronounced expression in the cerebral cortex and hippocampal CA1 and CA3 regions of WT adult mice compared to other brain areas (Cunningham et al., 2009). The intracellular distribution and the density of Nsdhl staining were visibly different between P2 and adult mouse brains: the P2 Nsdhl signal is stronger and present in both neuronal dendrites and cell bodies, while in the adult brain the signal appeared fainter and restricted to neuronal somas, which is consistent with the decreasing rate of cholesterol synthesis in mature neurons (Cunningham et al., 2009).

CNS is particularly susceptible to alterations in cholesterol homeostasis and its perturbations have been associated with a variety of human CNS disorders, ranging from neurodegenerative diseases (Petrov et al., 2016) to autism (Björkhem et al., 2010; Tierney et al., 2006). Among these pathologies, mutations in *NSDHL* have been linked to neurodevelopmental disorders, including CK syndrome (OMIM: 300831). CK syndrome is an X-linked recessive disorder caused by hypomorphic mutations in *NSDHL* gene which primarily affects males. Affected patients display a long-term survival but exhibit

mild to severe cognitive impairment, microcephaly, cerebral cortical malformations, seizures, facial dysmorphisms, mild skeletal abnormalities (scoliosis), loss of speech and significant behavior problems (aggression, attention deficit hyperactivity disorder, and irritability) (du Souich et al., 2009; du Souich et al., 1993; McLarren et al., 2010). Notably many of these features are shared with RTT patients. Few studies have been conducted to elucidate the molecular consequences of CK syndrome. At the molecular level, CK patients have normal plasma cholesterol, steroid hormone levels and lipoprotein profiles but display accumulation of 4-methyl and 4,4-dimethyl sterol intermediates, lathosterol and desmosterol, which are unable to fulfill the role of cholesterol within the cells (McLarren et al., 2010).

Alterations in cholesterol homeostasis have been also reported in RTT patients and mouse models. A recent comprehensive LC-MS/MS lipidomic analysis revealed a normal lipidomic profile in RTT patients' plasma but decreased CSF levels of cholesterol, phospholipids and sphingomyelins compared to their age-matched controls (Zandl-Lang et al., 2022). A decreased rate of cholesterol synthesis was identified in the developing brains of *Mecp2*-null mice (Buchovecky et al., 2013; Lopez et al., 2017), where also perturbations of genes involved in cholesterol metabolism were identified, which included *Hmgcr*, *Sqs* and *Nsdhl* (Lopez et al., 2017; Luoni et al., 2020; Pacheco et al., 2017).

These results prompted us to further elucidate the possible connection between MeCP2 and NSDHL and its possible contribution to RTT pathogenesis.

Initially, we analyzed *Nsdhl* expression in *Mecp2*-null cerebral cortices of pre-symptomatic (P20) and early symptomatic mice (P40), to confirm previous results and address if the defect could be observed also at ages in which symptoms are not overt. Interestingly, we detected a strong and consistent downregulation of the gene at both timepoints examined, with a 40% reduction in pre-symptomatic mice (percentage of KO expression with respect to WT littermates: 58.01%) which almost reaches 50% at the subsequent timepoint, when symptoms start to manifest (percentage of KO expression: 53.74%) (Figure 6.19).

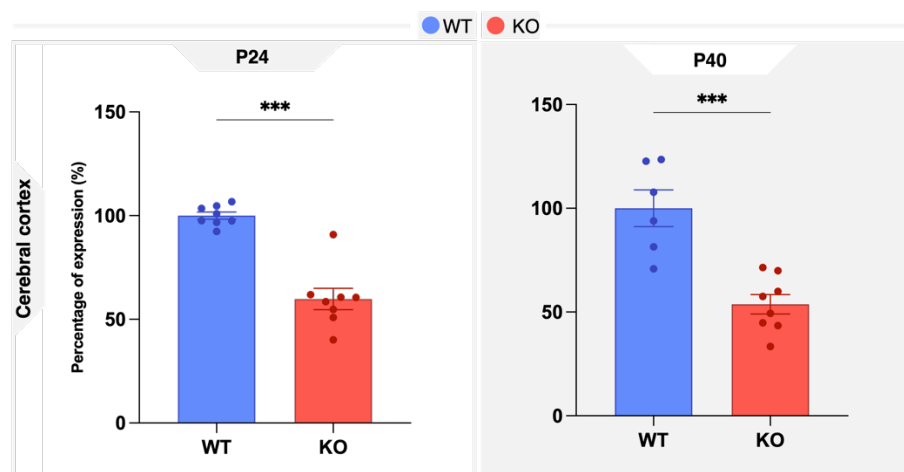


Figure 6.19: *Nsdhl* is strongly downregulated in the cerebral cortex of pre-symptomatic and symptomatic *Mecp2*-null mice. Bar graphs (mean \pm SEM) represent percentages of *Nsdhl* expression in the cerebral cortices of P24 (on the left) and P40 (on the right) KO mice (in red) with respect to their WT littermates (in blue, normalized at 100%). D'Agostino-Pearson test was used to test normality distribution. Mann-Whitney and Unpaired Student's *t*-test tests were used to compare KO and WT samples respectively at P24 and P40, according to the normal distribution of data. Significance between WT and KO is indicated with * (***p*-value < 0.001, ****p*-value < 0.0001). Sample size for each biological group is *n*=8.

We then proceeded investigating *Nsdhl* protein expression in the contralateral tissues of the cerebral cortices previously examined and in *Mecp2*-null hippocampi at the same timepoints, to determine whether its downregulation was confirmed at the protein level and if it was restricted to cerebral cortices or extended to other brain areas, such as hippocampus. A strong downregulation of the protein was confirmed in the cerebral cortex of pre-symptomatic *Mecp2*-null mice at P24 (percentage of KO expression: 68.87%) (Figure 1.20, panel A), which was corroborated also in the symptomatic stage (percentage of KO expression at P40: 56.92%). Hippocampi also exhibited a significant downregulation of *Nsdhl*, even though a greater standard deviation reduced statistical significance (percentage of KO expression at P24: 63.50%; % of KO at P40: 75.93%) (Figure 6.20, panel B).

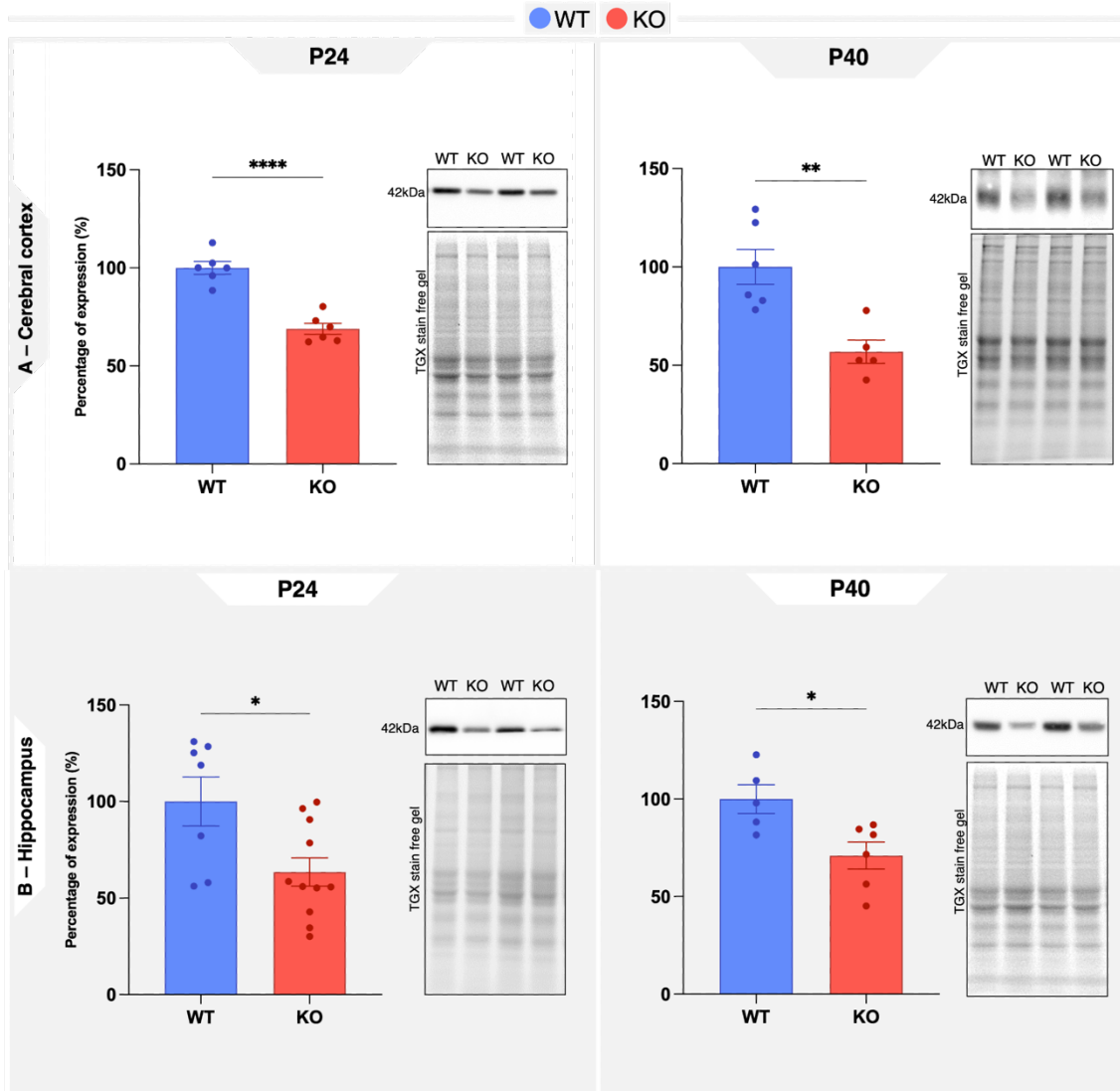


Figure 6.20: *Nsdhl* protein is downregulated in the cerebral cortex and hippocampus of pre-symptomatic and symptomatic *Mecp2*-null mice. Bar graphs (mean \pm SEM) represent percentages of *Nsdhl* protein expression in the cerebral cortex (panel A) and hippocampus (panel B) of P24 and P40 KO mice (in red) with respect to their WT littermates (in blue, normalized at 100%). Quantification of *Nsdhl* for each biological group was normalized on the total protein content; the KI ratio was expressed as percentage with respect to the normalized *Nsdhl* expression of the WT group. Next to each graph a representative image of *Nsdhl* signals (MW = 42kDa) is reported above the corresponding lanes of a 10% TGX stain free gel. Shapiro-Wilk test was used to test normality distribution. Unpaired Student's *t*-test was used to compare KO and WT samples, according to the normal distribution of data. Significance between WT and KO is indicated with * (**p*-value < 0.05; ***p*-value < 0.01, ****p*-value < 0.001, *****p*-value < 0.0001).

To further validate *Nsdhl* downregulation, we analyzed whether the protein was also differentially expressed in the Y120D knock-in mouse model of the disorder mimicking a RTT patient's mutation. Lysates of cerebral cortices and hippocampi of symptomatic hemizygous knock-in mice (P40) were used to perform this validation (Figure 6.21). *Nsdhl* appeared consistently downregulated in Y120D hemizygous male mice at P40, reaching almost a 40% reduction in both the areas examined (KI percentage in the cerebral cortex: 63.17%, KI percentage in the hippocampus: 62.17%).

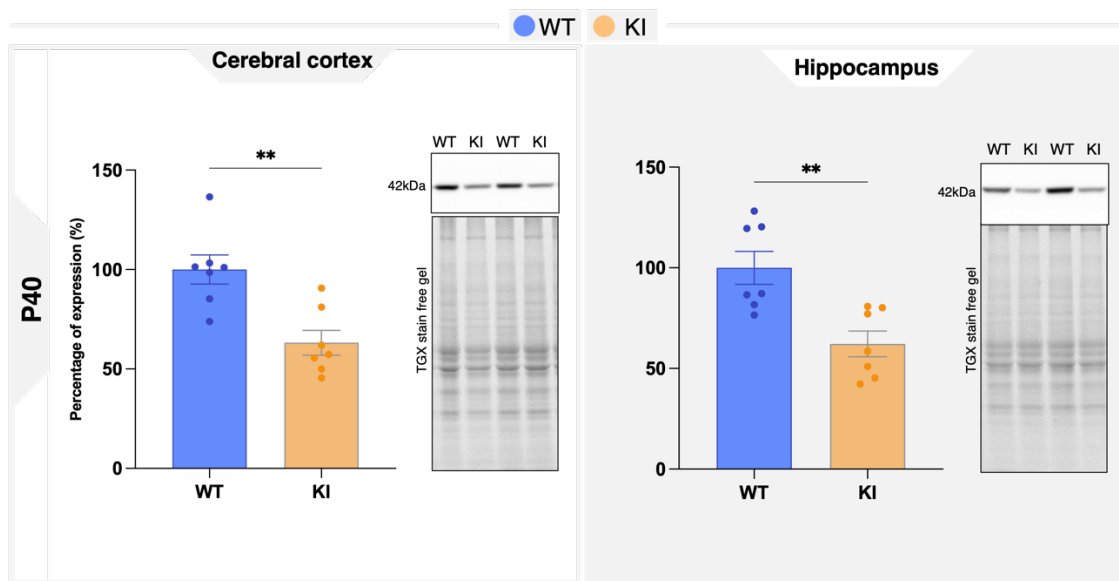


Figure 6.21: *Nsdhl* protein is downregulated in the cerebral cortex and hippocampus of P40 *Mecp2* Y120D mice. Bar graphs (mean ± SEM) represent percentages of *Nsdhl* protein expression in the cerebral cortex (on the left) and hippocampus (on the right) of P40 KI male mice (in orange) with respect to their WT littermates (in blue, normalized at 100%). Quantification of *Nsdhl* for each biological group was performed on the total protein content; the KI ratio was then expressed as percentage with respect to the normalized *Nsdhl* expression of the WT group. Next to each graph a representative image of *Nsdhl* signals (MW = 42kDa) is reported above the corresponding lanes of a 10% TGX stain free gel. Shapiro-Wilk test was used to test normality distribution. Unpaired Student's *t*-test was used to compare KI and WT samples. Significance between WT and KI is indicated with * (***p*-value < 0.01). *n* = 7 for each biological group.

Prompted by these results, we investigated whether *Nsdhl* consistent downregulation could be an indicator of other alterations related to cholesterol homeostasis in RTT. To this purpose, we analyzed the expression of genes related to cholesterol biosynthesis and

metabolism in the cerebral cortex of early symptomatic *Mecp2*-null mice at P40, including genes involved in cholesterol synthesis (*Hmgcr*, *Mvk*, *Sqs*, *Cyp51* and *Nsdhl*), transport (*ApoE*), efflux (*Abca1* and *Abcg1*), metabolism in neurons (*Cyp46a1*) and astrocytes (*Lcat*) and in the transcriptional regulation of proteins regulating cholesterol homeostasis (*Srebf2*) (Figure 6.22). Besides *Nsdhl*, significant downregulations were detected in genes involved in cholesterol synthesis, such as *Sqs* and *Cyp51* (respectively with a percentage of expression in KO samples of 63.03% and 58.22%) and a tendency to deregulation for *Hmgcr* and *Mvk* (respective percentage of KO expression: 74.06% and 78.01%). Interestingly, a strong decrease was identified for *Lcat* (Lecithin–cholesterol acyltransferase) expression (percentage of KO expression: 47.54%), which is mainly expressed by astrocytes and converts free cholesterol into cholesteryl ester (Petrov et al., 2016). The downregulation of an astrocytic-specific gene is in line with the essential role of astrocyte in regulating cholesterol homeostasis in the adult brain and suggest to further dissect astrocytic contribution to cholesterol alterations in RTT. Overall, these deregulations pave the way to a thorough characterizations of cholesterol homeostasis in our *Mecp2*-null model of the disorder.

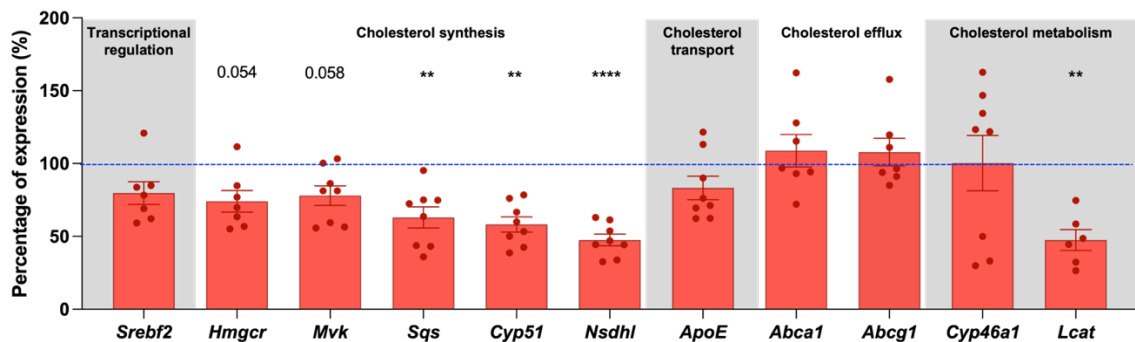


Figure 6.22: *Mecp2*-null cerebral cortices of symptomatic mice exhibit a downregulation of genes involved in cholesterol synthesis. Bar graphs (mean \pm SEM) represent the expression of genes involved in cholesterol homeostasis in cerebral cortices of *Mecp2*-null mice at P40. D'Agostino and Pearson test was used to test normality of data distribution. Unpaired Student's *t*-test or Mann-Whitney test were used to compare KO and WT samples, according to the normal distribution of data. Genes are divided based on their biological functions, indicated above. Significance between WT and KO is indicated with * (**p*-value < 0.05; ***p*-value < 0.01, ****p*-value < 0.001, *****p*-value < 0.0001). Sample size *n* = 8 for each biological group.

7. Discussion

Mutations in the *MECP2* gene, a master regulator of gene expression, cause several neurodevelopmental disorders, among which Rett syndrome (RTT) represents the first cause of severe intellectual disability in girls worldwide (Gold *et al*, 2018). To date no cure for RTT is available, and our restricted understanding of the pathology limits rational experimental therapies. However, research demonstrated that RTT is reversible in mice, proving that the disorder can be treated (Guy *et al*, 2007). Since this groundbreaking discovery, many efforts have been posed in finding new potential treatments for RTT. Preclinical studies largely benefit from the use of mouse models of *Mecp2*, which mimic a broad spectrum of neuronal phenotypes manifested by RTT patients. Nonetheless, their exploitation in large-scale drug screening systems is limited by the great number of animals required, time-consuming experimental approaches and elevated costs. To support and accelerate *in vivo* evaluation of drugs, many *in vitro* systems have been developed, mainly exploiting the capacity of rescuing dendritic arborization, spine morphology or density to quantitatively measure drug efficacy (Bittolo *et al*, 2016; Frasca *et al*, 2020; Marchetto *et al*, 2010; Nerli *et al*, 2020; Patnaik *et al*, 2020; Tang *et al*, 2019; Tropea *et al*, 2009; Trujillo *et al*, 2021). However, our laboratory has recently proposed that transcriptional amelioration might ensure a better chance of neuronal functional restoration compared to morphological readouts (Scaramuzza *et al*, 2021). Thus, my PhD project aimed at investigating whether the development of a new, reproducible, versatile cellular drug screening system assessing the capacity of drugs to ameliorate transcriptional defects of *Mecp2*-null neurons in a customized high-throughput 96x96 microfluidic RT-qPCR array card, could represent an efficient approach for drug discovery in RTT.

To this purpose, we started using a cellular model recently optimized by our laboratory based on neurons differentiated from neuronal precursor cells (NPCs), that we proved to well mimic morphological, functional and transcriptional defects typical of RTT primary neurons (Scaramuzza *et al.*, 2021). NPCs have recently gained much promise as powerful system for modelling a neuropathological condition. Indeed, they are able to self-renew and can be cryopreserved thus permitting to reduce the number of animals required for

experiments. Further, their differentiation can be synchronously induced, generating cells whose maturation appears quite homogeneous and that allows studying early mechanisms of neuronal maturation (Goffredo *et al*, 2008; Gorba & Conti, 2013; Haase *et al*, 2021; Haggarty *et al*, 2016). These features might be particularly relevant for RTT because our laboratory has largely contributed to prove MeCP2 involvement in early stages of neuronal and brain development (Bedogni *et al*, 2016; Bedogni *et al*, 2014; Cobolli Gigli *et al*, 2018); further, they might permit the identification of early molecular mechanisms of RTT pathogenesis that have a higher chance to represent primary results of MeCP2 deficiency. Eventually, NPCs are able to differentiate into neurons, astrocytes and oligodendrocytes, therefore making these cultures closer to the *in vivo* physiological conditions than primary neurons. Nonetheless, these cells usually appear more immature compared to corresponding primary cultures and the presence of different cell types makes molecular analyses more challenging, according to the relative percentage of cells within the culture (Goffredo *et al.*, 2008; Gorba & Conti, 2013; Haase *et al.*, 2021; Haggarty *et al.*, 2016).

This cellular system was used to longitudinally identify transcriptional alterations of *Mecp2*-null (KO) neurons using a bulk RNASeq analysis at three different timepoints along neuronal maturation, with the purpose of selecting a group of solid deregulated genes to use as quantitative probes to measure drug efficacy. To the best of our knowledge, a longitudinal transcriptomic analysis on differentiating neuronal cells is new in the context of RTT or other neurodevelopmental disorders, and was only previously performed to study glioma and multiple sclerosis progressions (Absinta *et al*, 2021; Wang *et al*, 2017). Further, few studies focused on dissecting transcriptional deregulations in early stages of RTT neuronal maturation. In particular, a pioneering study conducted by our laboratory analyzed the transcriptional consequences of *Mecp2* loss in mouse embryonic cortices (Bedogni *et al.*, 2016), while two other studies were carried out in either primary or iPSC-derived neurons (Landucci *et al*, 2018; Vacca *et al*, 2016). Our results obtained performing both a time-specific or overtime analysis of differentially expressed genes (DEGs) corroborated previous studies, demonstrating an enrichment in pathways related to neuronal maturation and differentiation, neuronal activity, neurotransmitter release, transport across the membrane (Bedogni *et al.*, 2016; Vacca *et al.*, 2016), cytoskeleton dynamics and microtubules (Landucci *et al.*, 2018). The same

processes can be found in other transcriptomic data obtained from different adult mice brain areas or patient post-mortem tissues (Bedogni *et al.*, 2014; Ehrhart *et al.*, 2019; Nectoux *et al.*, 2010; Pacheco *et al.*, 2017; Shovlin & Tropea, 2018), thus further validating our results. The number of DEGs in our time-specific analyses and the relevance of the categories enriched in gene ontology (GO) led us to select DIV14 as the suitable timepoint to perform the screening.

Obtained lists of DEGs were crossed between themselves and with other RTT datasets in order to search for consistent results and render the process of gene selection unbiased, contrary to previous studies on drug efficacy evaluation (Patnaik *et al.*, 2020; Scaramuzza *et al.*, 2021; Yuan *et al.*, 2020). By including genes belonging to the main affected pathways, we aimed at representing a solid gene signature typical of *Mecp2*-null neurons. The intent was also to exploit these genes to further dissect RTT pathogenesis and offer to the scientific community new possible targets for RTT therapy, as it was performed in a previous study (Gogliotti *et al.*, 2018).

However, the application of NPC-derived KO cells in our transcriptomic analyses highlighted some technical difficulties. Differences between wild type (WT) and KO samples appeared quite low in amplitude, a result that is probably caused by the fact that *Mecp2* functions as a fine regulator of a great number of genes (Bedogni *et al.*, 2014; Gandaglia *et al.*, 2019; Li *et al.*, 2013; Riedmann & Fondufe-Mittendorf, 2016). Although this result was expected, the progressively increasing percentage of astrocytes probably masked the number of neuronal DEGs detectable at the latest timepoint (DIV18), further amplifying this technical difficulty. In addition, astrocytes express reduced levels of *Mecp2* with respect to neurons (10-30 times less); as a consequence, *Mecp2* deficiency might modestly impact on glial transcription, a feature that might have further constrained the identification of DEGs (Maizawa *et al.*, 2009). We believe that these features limited the possibility to characterize the *Mecp2*-null neuronal transcriptional profile over time along cell maturation, and compare it with the WT transcriptional phenotype. This analysis would have allowed us to identify which genes and when they are activated/silenced along physiological neuronal development and in KO cells, in order to establish whether mutant samples undergo a delay or a blockage of neuronal differentiation and to discover druggable pathways for the treatment of RTT.

Additionally, the great percentage of astrocytes with respect to neurons questioned the use of NPC-derived cultures in our drug screening system, since qPCR analysis would not be able to detect such a little differential expression in neurons that are under-represented within the culture. For this reason, the previously sequenced NPC-derived samples were also used to validate a first group of prioritized DEGs in a customized 96x96 microfluidic RT-qPCR array card and compare results with those derived from primary cortical neurons in the same array. As suspected, the qPCR experiment confirmed differential expression of much less genes in NPC-derived cells with respect to primary neurons, leading us to abandon the use of NPC-derived cultures. Through few cycles of validation, we confirmed the reproducibility of 74 neuronal DEGs which will represent the quantitative probes in our customized array card.

Validation experiments disclosed a further limitation of the system when applied to *Mecp2*-deficient samples. Given the low amplitude of differential expression between WT and KO samples and the standard deviation obtained for each gene, the sample size had to be increased to 10 for each biological group, thus, permitting to load on the card a maximum of 9 experimental groups. Considering that the production of 10 independent treated samples for each drug is time-consuming and really expensive, this result obviously poses unexpected limits to the proposed approach, making it quite difficult to use it for the screening of large libraries of drugs in a laboratory scale. As a consequence, this system can be proposed as a novel confirmatory approach to validate possible drugs which already appeared promising in other *in vitro* assays. To confirm our hypothesis, we have initiated a collaboration with the University of Trieste to validate five of their lead compounds selected from a morphological screening (unpublished data). The two best candidates able to rescue the greatest number of DEGs in our transcriptional platform will be administrated to our *Mecp2*-null mouse model, therefore testing the efficacy of passing molecules through a second step of selection. Conversely, we believe that our transcriptional card can still be proposed as a drug screening platform for RTT therapy to companies which probably detain the economic and technical resources to produce such a great number of treated samples for each drug. Moreover, our customized platform might be further simplified to develop a new preliminary screening system which can be analyzed with ordinary RT-qPCR experiments. In this case, only few DEGs will be selected, focusing only on those belonging to specific pathways and among these on the

most solid and consistent ones. This targeted approach will permit to further reduce costs and render our system more versatile and accessible.

To confirm that the 74 reproducible DEGs could be effective quantitative probes able to reflect the efficacy of drugs in pre-clinical studies, we proceeded by testing the ability of an early treatment of CX546 to ameliorate DEG expression; treatment was selected considering our already published positive *in vitro* and *in vivo* results (Scaramuzza *et al.*, 2021). So far, DEG validation has been carried out in 51 out of 74 reproducible genes, demonstrating that the drug is able to rescue the expression of 75% of the tested DEGs, thus leading the previously separated WT and KO transcriptional signatures to converge after treatment in a PCA analysis. These promising results further validate DEG selection, reinforcing their use as quantitative probes to select drugs with a higher chance of success in pre-clinical studies. Notably, as results of two main technical obstacles we faced over the past year, the effect of CX546 still has to be tested in the remaining 23 genes. Initially, the Biomark instrument required to perform the 96x96 RT-qPCR and whose use was granted to our lab by the INGM Institute broke down, severely delaying our experiments for several months. Subsequently, we and other Italian laboratories have come across significant difficulties in producing primary neurons caused by trophic factors deficiency in the commercial culture media, which have taken several time-consuming experiments to identify and solve.

Besides these technical problems, our preliminary data encourage us to continue the study and conclude the setting of this novel transcriptional platform. To this purpose, we plan to finish the validation of the selected DEGs with the ampakine CX546 and eventually compare its transcriptional effects with those induced by trofinetide and lovastatin. Trofinetide is the synthetic analog of the IGF active tripeptide and represents the latest promising therapy for RTT syndrome that after having proved its efficacy in *in vitro* and *in vivo* pre-clinical studies and passed a phase III clinical trial for the treatment of Rett syndrome (Castro *et al.*, 2014; Khwaja *et al.*, 2014; Neul *et al.*, 2022; O'Leary *et al.*, 2018; Pini *et al.*, 2016; Shovlin *et al.*, 2022; Tropea *et al.*, 2009; Tropea *et al.*, 2006). On the contrary, lovastatin only appeared effective in animal-based studies, while no sign of clinical improvement was detected once moved into clinics (Buchovecky *et al.*, 2013; Villani *et al.*, 2016). These treatments will be used as proof of concept to assess whether transcriptional effects on selected DEGs positively correlate with their clinical efficacy,

therefore confirming the validity of our reproducible genes as quantitative markers able to represent the potential success of a drug.

As stated, the secondary objective of this project was to identify novel pathways and related deregulated genes to better dissect RTT pathogenesis and propose novel therapeutic targets for its treatment. To this purpose we started investigating the implications of two genes, *Haus7* and *Nsdhl*, chosen for their respective functions and consistent deregulations across our time-specific and overtime transcriptomic data and several gene expression analyses in NPC-derived and primary cortical neurons.

HAUS7 codes for a member of the HAUS/augmin complex formed by eight subunits (Goshima *et al*, 2008; Uehara *et al*, 2009) and regulating non-centrosomal microtubule (MT) nucleation in post-mitotic neurons. Its disruption impairs neurite formation, axonal polarization and trafficking, therefore revealing its involvement in proper neuronal maturation and migration (Cunha-Ferreira *et al*, 2018; Sánchez-Huertas & Lüders, 2015). Interestingly, augmin depletion led to decreased levels of acetylated γ -tubulin, a defect that has often been reported in *MECP2* deficient human and mouse neurons and astrocytes, thus appearing as an interesting pharmacological target to reverse cellular and synaptic RTT impairments to several groups, including our laboratory (Delépine *et al*, 2016; Frasca *et al.*, 2020; Gold *et al*, 2015; Landucci *et al.*, 2018). In addition, augmin complex participates in increasing MT nucleation induced by neuronal activity in pre-synaptic boutons, providing dynamic tracks for bidirectional synaptic vesicles transport (Qu *et al*, 2019). Notably, a MT dependent defect in vesicular trafficking of BDNF was reported in *Mecp2*-null hippocampal neurons and the phenotype was normalized by restoration of MT acetylation (Xu *et al*, 2014). These evidences prompt the interest of further characterizing *Haus7* functions in WT mouse neurons, and investigating whether its downregulation participates to the pathogenic mechanisms of RTT.

To confirm *Haus7* deficiency in RTT tissues, we evaluated its expression in *Mecp2*-mutant brains, determining at which stage of RTT severity its impairment becomes evident and whether it is consistent across different models of the disorder. *Haus7* appeared strongly and consistently downregulated in *Mecp2*-null cortices and hippocampi, from early stages of brain development (P7; a stage that is generally

considered asymptomatic) to the highly symptomatic P60. These data were confirmed at P40 in a second mouse model of RTT, the *Mecp2* Y120D, which mimics a patient mutation, thus suggesting that *Haus7* deficiency is independent from the type of *Mecp2* mutation. We then tested whether its disruption persists in the mosaic condition typical of heterozygous females. Importantly, we confirmed a strong downregulation in the cerebral cortex of early symptomatic females, while just a mild reduction was detected in the hippocampus. Many efforts have been made to characterize and quantify the corresponding protein expression, but we failed to obtain measurable *Haus7* signals in western blot analyses, posing an unexpected limitation to our study. To overcome this issue, we will establish the specificity of the observed signals by specifically knocking down *Haus7* expression in cortical neurons which will represent our elective cell model, in accordance with transcriptional data. Considering that no report has ever analyzed the specific role of *Haus7* on neuronal maturation and activity, we will also analyze the consequences of *Haus7* depletion in WT cortical neurons, focusing on dendritic arborization, spine development and synaptic function. We hypothesize that its downregulation will mimic typical defects of RTT neurons.

In parallel, to gain more insight on *Haus7* regulation and functions we will describe its temporal and spatial expression in WT mouse brains and define its subcellular localization in resting and stimulated WT neurons. Attention will be mainly posed on the post-synaptic compartment, where *Haus7* expression and functions remained fully uncharacterized. Further, we will address if the observed *Haus7* deficiency is neuronal specific or at least limited to the central nervous system. To this purpose *Haus7* mRNA levels will be compared in WT and KO astrocytes and fibroblasts. The translational value of this studies will require to assess *HAUS7* deficiency in human RTT samples and to investigate whether RTT neurons benefit from restoring *Haus7* expression via virus infection *in vitro* and *in vivo*.

The second gene we found consistently deregulated was the *NAD(P)H steroid dehydrogenase-like gene (Nsdhl)*, encoding for one of the enzymes involved in regulating cholesterol synthesis. CNS cholesterol is the results of a complex interplay between different neural cell types and plays a crucial role in neuronal maturation, synaptogenesis and synaptic transmission (Allen *et al*, 2007; Tracey *et al*, 2018; van Deijk *et al*, 2017),

which all appear impaired in RTT. As for *Mecp2*, *Nsdhl* expression increases along neuronal development and stabilizes in the adult brain, with a marked expression in the cerebral cortex and hippocampus. Hypomorphic mutations in *NSDHL* are linked to CK syndrome, a neurodevelopmental disorder which share many features with RTT, including microcephaly, mental retardation, seizures, loss of speech and autistic-like features (du Souich *et al.*, 2009; du Souich *et al.*, 1993; McLarren *et al.*, 2010). The molecular consequences of *Nsdhl* deficiency in CK syndrome have been poorly investigated, but impairments in cholesterol synthesis and accumulation of methylated sterol intermediates seem to have a crucial role in causing the typical signs of the disorder (McLarren *et al.*, 2010). Disruptions in cholesterol homeostasis have also been reported in RTT human and mouse samples. Indeed, decreased cholesterol levels were detected in RTT patients' CSF (Zandl-Lang *et al.*, 2022) and a reduced rate of cholesterol synthesis was identified in the developing brain of *Mecp2*-null mice, accompanied by downregulations of genes regulating the biosynthetic process (Lopez *et al.*, 2017; Luoni *et al.*, 2020; Pacheco *et al.*, 2017). These findings prompted us to investigate the link between MeCP2 and NSDHL and establish its possible implications in RTT pathogenesis.

We first confirmed *Nsdhl* downregulation in *Mecp2*-null cerebral cortices of pre-symptomatic and symptomatic mice. These results were reinforced by *Nsdhl* protein level disruptions found in the cerebral cortex and hippocampus of mice lacking *Mecp2* at the same timepoints and in the Y120D *Mecp2*-mutant brains of symptomatic mice, with a prominent downregulation in the cerebral cortex. Decreased expression of other genes involved in cholesterol synthesis in the cerebral cortex of symptomatic *Mecp2*-null mice (*Hgmc1*, *Mvk*, *Sqs* and *Cyp51*) lays the foundation for future studies elucidating cholesterol homeostasis in RTT brains.

In this regard, given cell heterogeneity of tissues and the complex interplay of different cell types in CNS cholesterol synthesis, *ex vivo* approaches would not completely elucidate the role and the possible defects of different cell types underlying cholesterol dysregulation. To this purpose, we will first investigate *Nsdhl* expression in either primary cortical astrocytes or neurons, to dissect their contribution to its downregulation. We will also analyze the expression of genes involved in cholesterol synthesis, metabolism and transport in the same culture systems, to identify possible additional impairments involving other key elements of cholesterol homeostasis. Particular attention

will be posed on astrocyte-enriched genes, such as *Srebp1*, *Scap*, *ApoE*, *Abca1*, *Abcd1*, *Ldlr*, *Lxr*, given astrocytes' essential role in providing cholesterol to neuronal cells (Petrov *et al.*, 2016; Zhang & Liu, 2015).

In parallel, CNS cholesterol levels will be also assessed to establish whether gene expression deregulations reflect an altered functional biosynthetic pathway. An anticipated limitation for this analysis could be represented by the contribution of different types of cholesterol in the brain. As a matter of fact, cholesterol in myelin sheaths constitutes the 70% of total CNS cholesterol, with a very low turnover in the human adult brain (half-time of 5 years), followed by the one found in the plasma membrane of neurons (10%) and glial cells (20%), characterized by a relatively faster turnover rates of approximately 10 months (Petrov *et al.*, 2016). Beside the structural component, the cholesterol secreted by astrocytes represents the remaining and limited part. Another factor to consider would be the cellular contribution to cholesterol synthesis and the stage of development in which cholesterol levels will be assessed. Indeed, during neuronal development, neurons, astrocytes and oligodendrocytes actively produce cholesterol, while mature brains mainly rely on cholesterol secreted by astrocytes (Zhang & Liu, 2015). Thus, to dissect the cellular contribution to cholesterol synthesis and assess its possible defective levels, we will preliminarily quantify either total cholesterol levels in *Mecp2*-null primary cortical neurons or measure the secreted one in the conditional medium of cortical primary astrocytes (ACM). These analyses will be performed in collaboration with Professor Elena Chiricozzi at the University of Milan using thin layer chromatography (TLC). If indications of disrupted cholesterol levels will be detected, we will evaluate the effects of cholesterol supplementation on *Mecp2*-defective cellular models as proof of concept for the contribution of cholesterol impairments to RTT pathogenesis. Given cholesterol role in synaptogenesis and neuronal maturation, we will evaluate amelioration of defective synaptic puncta density in RTT cultured neurons.

In conclusion, our preliminary investigation on *Haus7* and *Nsdhl* provided promising insights on potential novel mechanisms underlying RTT pathogenesis, representing a solid starting point to establish a more comprehensive link between RTT and MT dynamics and cholesterol homeostasis and hopefully offer new potential avenues for the treatment of RTT.

8. Materials and methods

8.1. Animals

8.1.1. Animal care

Mice were housed in the animal facility of the San Raffaele Scientific Institute in groups of five in Tecniplast cages, in a temperature- and humidity-controlled environment (21 ± 2 °C) and a 12-hour light/dark cycle, with food and water *ad libitum*. Two different mouse line were used in this study: the *Mecp2* null mouse strain developed by Guy and colleagues (Guy et al., 2001) and the *Mecp2* knock-in Y120D mouse line generated in our laboratory and characterized by Gandaglia et al. (Gandaglia et al., 2019). The *Mecp2*^{tm1.1Bird} mouse strain was originally purchased from the Jackson Laboratories and then backcrossed and maintained on a CD1 background (Cobolli Gigli et al., 2016), which well recapitulate the typical phenotype of C57BL/6 mice, with the advantage of having a larger progeny and minor risk of litter cannibalization.

All procedures were conducted in accordance with the European Community Council Directive 2010/663/UE for care and use of experimental animals and the protocols were authorized by the Italian Minister for Scientific Research (decrees No. 1172/2020-PR and 175/2015-PR) and by the San Raffaele Scientific Institutional Animal Care and Use Committee.

8.1.2. Genotyping

Genotype of mice and mouse embryos was performed by Polymerase Chain Reaction (PCR) protocol on genomic DNA purified from ear biopsies of P10 mice or paws/tails in case of embryos.

DNA extraction from mice biopsies:

Genotyping of mice was performed at P10 following an over-night (O/N) protocol. Tail Lysis Buffer (Tris 100mM pH=8, EDTA 10mM pH=8, SDS 0.5%, NaCl 100mM) and Proteinase K (0.5 mg/mL, Genespin, #STS-OK500) were used to dissociate each sample and maintained O/N at 55° C. The day after, samples were centrifuged (13,000rpm, 10 minutes) to remove any debris left. Then,

1:1 of 100% isopropanol (SIGMA, 33539) was added to the supernatants to induce DNA precipitation (13,000rpm, 10 minutes, room temperature RT). Supernatants were removed and DNA pellets were washed with 500µL of 70% ethanol (EtOH) and centrifuged at 13,000rpm for 5 minutes. EtOH was eliminated, pellets were dried at RT and resuspended in 200µL of TE (Tris 10mM, EDAT 1mM, pH=8) for DNA quantification, performed with a spectrophotometer (Nanodrop 1000, ThermoFisher)

DNA extraction from embryonic paw biopsies:

Tissues were dissociated with “Phire animal tissue direct PCR kit” (Thermo Scientific F140WH) to rapidly extract DNA from samples used in primary cultures. In detail, each sample (mouse paw or tail) was incubated with a 20 µL mix (19.5µL Dilution Buffer + 0.5µL DNA Release Additive provided with the “Phire animal tissue direct PCR kit”) for 3 minutes at RT. Then, the reaction was stopped at 98°C for 2 minutes and supernatant was diluted with 10µL of the Dilution buffer and directly used for DNA quantification. For embryonic samples, both genotyping and sex PCRs were conducted.

PCR and gel electrophoresis:

PCR products were resolved by electrophoresis run in 2% agarose gel (110V, 40 minutes run in TAE 1X buffer). The reaction mix for one sample (Final volume = 20µL) for PCR amplification is the following (Table 8.1):

<i>Mecp2</i> null protocol			
Reagents	Initial concentration	Final concentration	Final volume
Xtra RTL GL Reaction Buffer (Genespin, #XSTS-T5XRTL)	5X	1X	4 μ L
dNTPs (Promega, #U120A, U121A, U122A, U123A)	10mM	10 μ M	0.4 μ L
Common primer	10 μ M	0.25 μ M	0.5 μ L
Reverse primer (WT allele)	10 μ M	0.25 μ M	0.5 μ L
Reverse primer (null allele)	10 μ M	0.25 μ M	0.5 μ L
XtraTaq Pol RTL (Genespin, #XSTS-T5XRTL)	5U/ μ L	0.125U/ μ L	0.5 μ L
H ₂ O	–	–	12.6 μ L
gDNA	100ng	5ng/ μ L	1 μ L

<i>Mecp2</i> Y120D protocol			
Reagents	Initial concentration	Final concentration	Final volume
Xtra RTL GL Reaction Buffer (Genespin, #XSTS-T5XRTL)	5X	1X	4 μ L
dNTPs (Promega, #U120A, U121A, U122A, U123A)	10mM	10 μ M	0.4 μ L
Forward primer	10 μ M	0.25 μ M	0.5 μ L
Reverse primer	10 μ M	0.25 μ M	0.5 μ L
Reverse primer (mutant allele)	10 μ M	0.25 μ M	0.5 μ L
XtraTaq Pol RTL (Genespin, #XSTS-T5XRTL)	5U/ μ L	0.125U/ μ L	0.5 μ L
H ₂ O	–	–	12.6 μ L
gDNA	100ng	5ng/ μ L	1 μ L

Sex protocol			
Reagents	Initial concentration	Final concentration	Final volume
Xtra RTL GL Reaction Buffer (Genespin, #XSTS-T5XRTL)	5X	1X	4 μ L
dNTPs (Promega, #U120A, U121A, U122A, U123A)	10mM	10 μ M	0.4 μ L
Forward primer	100 μ M	0.625 μ M	0.125 μ L
Forward primer	100 μ M	0.625 μ M	0.125 μ L
XtraTaq Pol RTL (Genespin, #XSTS-T5XRTL)	5U/ μ L	0.125U/ μ L	0.5 μ L
H ₂ O	–	–	13.85 μ L
gDNA	100ng	5ng/ μ L	1 μ L

Table 8.1: PCR reaction mix for genotyping *Mecp2* null and *Mecp2* Y120D mice and for the determination of sex.

Negative control (19 μ L reaction mix + 1 μ L H₂O) and positive controls (19 μ L reaction mix + 1 μ L DNA of a heterozygous, WT and mutant mice) were always included.

The primers used for the genotyping are the following:

- For *Mecp2* null mice: common forward 5'–AAATTGGGTTACACCGCTGA–3', WT reverse 5'–CTGTATCCTTGGGTCAAGCTG–3', mutant reverse 5'–CCACCTAGCCTGCCTGTACT–3'.
- For *Mecp2* Y120D: common forward 5'–CAGGGCCTCAGAGACAAGC–3'; common reverse 5'–GCAGATCGGCCAGACTTCC–3'; reverse for the KI allele 5'–GGGTAAATTGATATCCAATTGGGATCC–3'.
- For sex determination: the animal sex was determined by using primers recognizing the male gene *Jarid1*; forward 5'–CCAGGATCTGACGACTTTCTACC–3', reverse 5'–TTCTCCGCAATGGGTCTGATT–3'.

The PCR cycles used for the experiments are reported in Table 8.2.:

Step	<i>Mecp2</i> null	<i>Mecp2</i> Y120D	Sex
Heat lid	110°C	110°C	110°C
Denaturation	94.0°C (5 min)	95.0°C (2 min)	95.0°C (2 min)
Start loop	35X	35X	35X
Denaturation	94.0°C (30sec)	95.0°C (30sec)	95.0°C (30sec)
Annealing	60.0°C (30 sec)	60.0°C (30 sec)	59.0°C (30 sec)
Extension	72.0°C (1 min)	72.0°C (45 sec)	72.0°C (30 sec)
Close loop	–	–	–
Final extension	72.0°C (5 min)	72.0°C (5 min)	72.0°C (5 min)
Hold	4°C (∞)	4°C (∞)	4°C (∞)

Table 8.2: PCR cycles for genotyping and sex determination.

PCR products were resolved by electrophoresis run in 2% agarose gel and the resulting products are:

- For *Mecp2* null strain: WT mice present a band of 465 bp, while *Mecp2* KO mice present a band of 240 bp. Heterozygous mice exhibit both bands, one for each allele.
- For *Mecp2* Y120D: A 300-bp fragment is common for WT and knock-in animals, while a 550-bp fragment is specific for the mutated one.
- For sex determination: the amplification of *Jarid1* produces a fragment of 113bp only in males.

8.2. Primary cultures

Time-pregnant females were generated by crossing overnight WT CD1 males with *Mecp2*^{+/-} heterozygous CD1 females; the day of vaginal plug was considered E0.5. Timed-gestation female mice were sacrificed by dislocation and E15.5 mouse embryos were collected for primary cultures. Embryos were individually dissected under a microscope and immersed in ice-cold Hank's Buffered Salt Solution (HBSS, Sigma H6648). Meninges were removed, and cerebral cortex was rapidly dissected and maintained in cold HBSS until tissue dissociation.

8.2.1. NPCs isolation, expansion and differentiation

The procedure to generate neuronal precursor cell (NPC) culture was first described by Gritti and colleagues (Gritti et al., 1996) and then further optimized in our laboratory (Cobolli Gigli et al., 2018; Scaramuzza et al., 2021). Briefly, once isolated, the neocortex was washed and then incubated at 37° C for 10 minutes with Papaine (Sigma P4762, 9U/mL) and DNase (0,1 mg/ml, Roche, 11284932001) in a stabilizing solution of HBSS containing EDTA pH=8 0.5mM, L-cystein 5mM, to induce enzymatic digestion. Tissues were centrifuged at 1,300 rpm for 5 minutes and after supernatant removal, cortices were

added with Dulbecco's Modified Eagle Medium/Nutrient Mixture F-12 Ham (DMEM/F12 Sigma, D8437) to dilute any enzyme residual and centrifuged again at 1,000 rpm for 10 minutes. Digested tissues were then mechanically dissociated by pipetting in complete medium (Table 8.3) supplemented with 20ng/ml human Epidermal Growth Factor (hEGF, ThermoFisher PHG0311) and 10ng/ml human Fibroblast Growth Factor b (hFGFb, ThermoFisher PHG0021) in which they spontaneously expand to form cell aggregates called neurospheres. Spontaneously formed neurospheres were collected after three to five days of free-floating culture and dissociated to single cell before plating on matrigel-coated plastic multiwells or expanded and passaged to reform neurospheres. The total number of viable cells was assessed at each passage by Trypan Blue (Automated Cell Counter, Biorad).

To progressively induce differentiation, cells were grown in complete medium supplemented with hEGF and hFGFb until adhesion on Matrigel-coated plates to select for undifferentiated progenitors, followed by one day of culture in the same medium containing only hFGFb to promote the expansion of neuronal precursors (NPCs). Culture medium was then replaced with the complete medium containing 2% of Fetal Bovine Serum (FBS) (ThermoFisher 10500064). DIV0 corresponded to the day of serum addition. The presence of FBS drives their differentiation into neurons, astrocytes and oligodendrocytes (Figure 8.1). Our laboratory previously characterized these cultures and demonstrated that the absence of *Mecp2* does not impact their cell fate commitment but in turn impairs their transcriptional maturation, reproducing the transcriptional defects typical of RTT neurons (Scaramuzza et al., 2021). Their delayed transcriptional profile is accompanied by a reduced spontaneous electrical activity and a neuronal defective morphology, overall mimicking the RTT neuronal phenotype.

Given the possibility to follow neuronal early maturation and differentiation overtime, these cells were selected for the longitudinal RNASeq analysis.

Complete medium		
Reagent	Initial concentration	Final concentration
DMEM/F12 (Sigma D8437)	-	-
Glucose (50X)	30,0%	0,66%
Pen/Strep (Sigma P0781)	100X	1X
Hormon Mix	10X	1X
Heparin (500X) (Sigma H3149)	2mg/mL	4µg/mL

Hormon Mix		
Reagent	Initial concentration	Final concentration (10X)
DMEM/F12 (Sigma D8437)	-	-
Glucose (50X)	30,0%	0,66%
Insulin (Sigma I9278)	10mg/mL	250µg/mL
Putrescin (Sigma P5780)	1,3 mg/mL	97µg/mL
Apotransferrin (Sigma T2252)	8mg/mL	1mg/mL
Sodium Selenite (Sigma S5261)	3mM	0,3µM
Progesterone (Sigma P8783)	2mM	0,2µM

Table 8.3: Media composition for neurosphere maintenance and expansion.

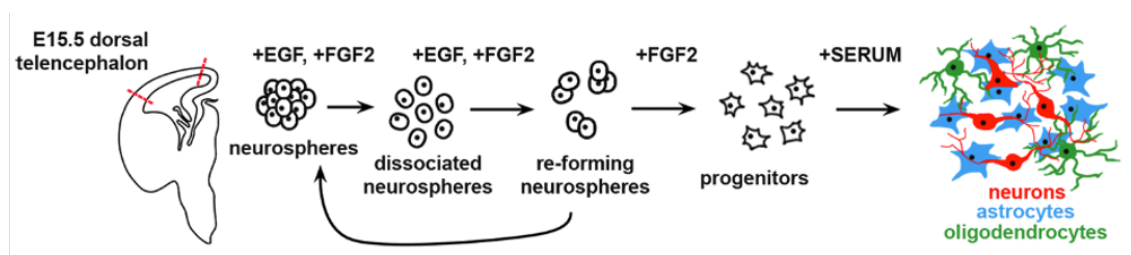


Figure 8.1: Schematic representation of NPCs isolation, expansion and differentiation into neurons, astrocytes and oligodendrocytes (Scaramuzza et al., 2021) Open access.

8.2.2. Cortical neurons

Once embryos were dissected and neocortex isolated, tissues were washed in HBSS, incubated with 0.25% trypsin/EDTA (Sigma 25200-056) for 10 min at 37°C and the digestion was blocked with 10% FBS in Dulbecco's Modified Eagle's Medium (DMEM) High Glucose with pyruvate (ThermoFisher, 41966029). Then, cortices were accurately washed and mechanically dissociated by pipetting in neuron culture medium (Neurobasal Plus medium, Penicillin/Streptomycin 1%, B27 Plus 2%, GlutaMax 0.75%). Cell count was performed with an automated cell counter by using Trypan blue (Automated Cell Counter, Biorad). Depending on experimental needs, neurons were seeded on poly-D-lysine (0.1 mg/mL)-coated plates, poly-D-lysine-coated glass coverslips (Neuvitro). Primary neurons were used for the gene expression analysis on 96x96 IFC RT-qPCR cards (Fluidigm).

8.3. Gene expression analysis of primary cultures

8.3.1. RNA extraction from cell cultures

After a rapid wash in D-PBS (Sigma D8537) to remove any cell debris, total RNA was extracted from primary cultures using Purezol (1mL/10cm², BioRad, 7326890). Samples were either conserved in Purezol at -80°C or immediately processed to isolate RNA, as follows. Samples were incubated for 5 minutes at RT and 100% chloroform (Sigma, 372978) was added 1:5 (200 µL/1 mL Purezol).

Then, samples were manually inverted to gently mix the phenol:chloroform mixture and following 2 minutes of incubation at RT they were centrifuged (13,000 g, 15 minutes, 4°C) to separate aqueous and organic phases. The upper aqueous phase containing RNA was collected and RNA was precipitated with 100% isopropanol 1:2 (500 µL /1 mL Purezol) in the presence of 10 µg/sample of glycogen, an inert co-precipitant agent to increase pellet visualization, and stored at -20 °C. The day after, RNA was centrifuged

(13,000 g, 15 minutes, 4 °C), pellets were washed in 70% EtOH (500µL/sample) (7,500 g, 5 minutes, 4 °C). To remove genomic DNA, DNase (Sigma AMPD1) was directly added to dried pellets (20 µL of a mix composed of: 17 µL H₂O RNase-free + 2 µL supplied DNase buffer + 1 µL DNase amplification grade) and incubated at 37°C for 15 minutes in a dry bath. RNA was then purified by adding 80 µL Purezol/sample, following the exact protocol and proportions of the volumes mentioned above, until pellet precipitation in 100% isopropanol and wash in 70% EtOH the next day. At this step, RNA was completely dried at RT, resuspended in 10 µL H₂O RNase-free and stored at – 80°C until analysis.

8.3.2. Quality assessment of RNA from cell cultures

Integrity of the total RNA extracted from samples was assessed using Agilent 2100 Bioanalyzer and the RNA 600 Nano Reagent.

Bioanalyzer uses microfluidics/capillary electrophoresis to analyze nucleic acids by comparing the fluorescence of the sample, to which an RNA-specific dye has been added, with that of a standard. High quality total RNA presents two distinct bands for 28S and 18S subunits, with a ratio of 2:1, respectively, in the electropherograms. Agilent 2100 Bioanalyzer software (Expert 2100 software) uses an algorithm to calculate the RNA Integrity Number (RIN), that ranges from 0 (totally degraded RNA) to 10 (completely intact RNA).

8.3.3. Library validation for the RNASeq analysis

To establish the most suitable starting input of RNA extracted from our NPC-derived cultures, a library validation was performed on six NPC-derived samples with a RIN>9 before proceeding with the longitudinal RNASeq analysis.

The 150bp paired-end protocol was tested using two different starting inputs of total mRNA (standard input of 500ng and low input of 200ng). First, mRNA was polyA-selected, fragmented and randomly primed for reverse transcription. Double-stranded

cDNA was 3' A-tailed for adaptor ligation and ligated fragments were PCR amplified for cluster generation. Next, final QC library analysis was assessed by evaluating the size distribution and concentration of cDNA fragments. Since the total insert size to be sequenced is 300bp (150bp for each read) and the adaptor length is 60bp for each end, size-selection was required to choose fragments with an average size of 420bp (fragment length) (Figure 8.2). Quality and size of libraries were assessed by capillary electrophoretic analysis with the Agilent 4200 Tape station (Agilent) and quantified by real-time PCR against a standard curve with the KAPA Library Quantification Kit (KapaBiosystems, Wilmington, MA, USA). The post-size selection QC and quantification of libraries confirmed their high-quality and suitable molarity to perform the sequencing, even with the lower starting input of 200ng, proving the validity of our RNA extracting method and subsequent concentrations.

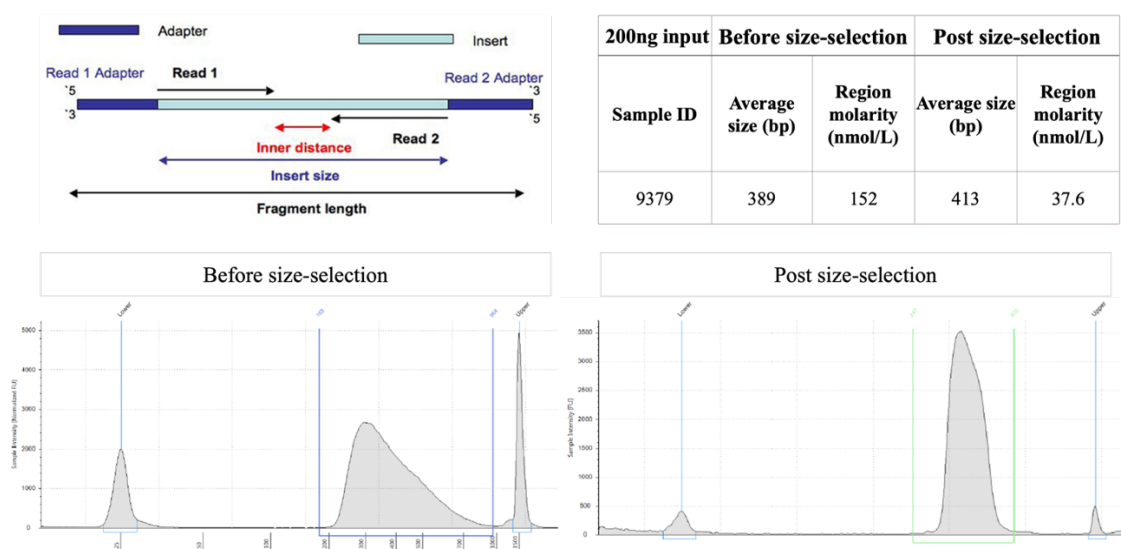


Figure 8.2: Library validation for RNASeq analysis. (A) Schematic representation of the insert size and fragment length. (B) Table indicating the average size of fragments for one of the samples tested for a low input of RNA of 200ng, before and after size-selection, with their respective distribution graphs below.

8.3.4. Longitudinal RNASeq analysis

Longitudinal RNASeq analysis was performed in collaboration with the Functional Genomic Lab, Department of Biotechnology, at the University of Verona. The analysis

was conducted at DIV7, 14 and 18 on 7 *Mecp2* wild-type (WT) and null (KO) longitudinal NPC-derived cultures (for a total of 42) and only from those samples that permitted to obtain all the three timepoints (DIV7, 14 and 18) from the same original culture. Only samples with a RIN > 9 were sequenced and used for the analysis. The analysis was performed as follows:

- 1) RNA quality control was performed on 42 RNA samples. RNA purity was measured using a NanoDrop Spectrophotometer, while RNA integrity was assessed using the RNA 6000 Nano Kit on a Bioanalyzer (Agilent Technologies). All samples showed an RNA integrity number (RIN) >9. RNA samples were quantified using the Qubit RNA BR Assay Kit (Thermo Fisher Scientific).
- 2) Library generation: RNAseq libraries were generated using the TruSeq stranded mRNA kit (Illumina) from 200ng of RNA samples, after poly(A) capture and according to manufacturer's instructions. Prior to sequencing, libraries were size selected using automated electrophoresis (BluePippin instrument) to obtain an insert size of around 300bp.
- 3) Library quality control: Quality and size of RNAseq libraries were assessed by capillary electrophoretic analysis with the Agilent 4200 Tape station (Agilent). Libraries were quantified by real-time PCR against a standard curve with the KAPA Library Quantification Kit (KapaBiosystems, Wilmington, MA, USA).
- 4) Sequencing: Libraries were pooled at equimolar concentration and sequenced on a NovaSeq6000 (Illumina) analyzing >50 million fragments in 50PE mode for each sample.
- 5) Quality control and filtering of the sequencing data (Figure 8.3): Quality of reads was assessed using FastQC software (<http://www.bioinformatics.babraham.ac.uk/projects/fastqc/>). Starting from raw FASTQ files, reads with more than 10% of undetermined bases or more than 50 bases with a quality score <7 were discarded (script: filter_reads.py). Reads are then clipped from adapter sequences using Scythe software (<https://github.com/vsbuffalo/scythe>), and low-quality ends (Q score <20 on a 15-nt window) were trimmed with Sickle (<https://github.com/vsbuffalo/sickle>) (script: trimFastq.sh). Filtered reads were aligned to the Human reference genome

GRCh38 (Ensembl release 99) using STAR (v2.7.6a) with default parameters and --quantMode TranscriptomeSAM option that output alignments translated into transcript coordinates. Mapping rate was >98% on average. After reads mapping, the distribution of reads across known gene features, such as exons (CDS, 5'UTR, 3'UTR), introns and intergenic regions was verified using the script read_distribution.py provided by RSeQC package (v3.0.1).

- 6) Transcriptome quantification and differential expression analysis (Figure 8.3): Read counts on genes were quantified using RSEM (v.1.3.3). Genes-level abundance, estimated counts and gene length obtained with RSEM were summarized into a matrix using the R package tximport (v1.12.3) and subsequently the differential expression analysis was performed with DESeq2(v1.24.0). To generate more accurate Log2 FoldChange estimates, the shrinkage of the Log2 FoldChange was performed applying the apeglm method.
- 7) Gene Ontology (GO) enrichment analysis was performed using clusterProfiler, an R Package for comparing biological themes among gene clusters (Bioconductor version: Release (3.12)). The function simplify has been used to remove redundancy of enriched GO terms. Differentially expressed genes (DEGs) with an FDR adjusted p-value (p-adj) <0.1 were included in the analysis. P-adj <0.05 or 0.1 was used as a threshold and GO terms fulfilling this condition were defined as significantly enriched.

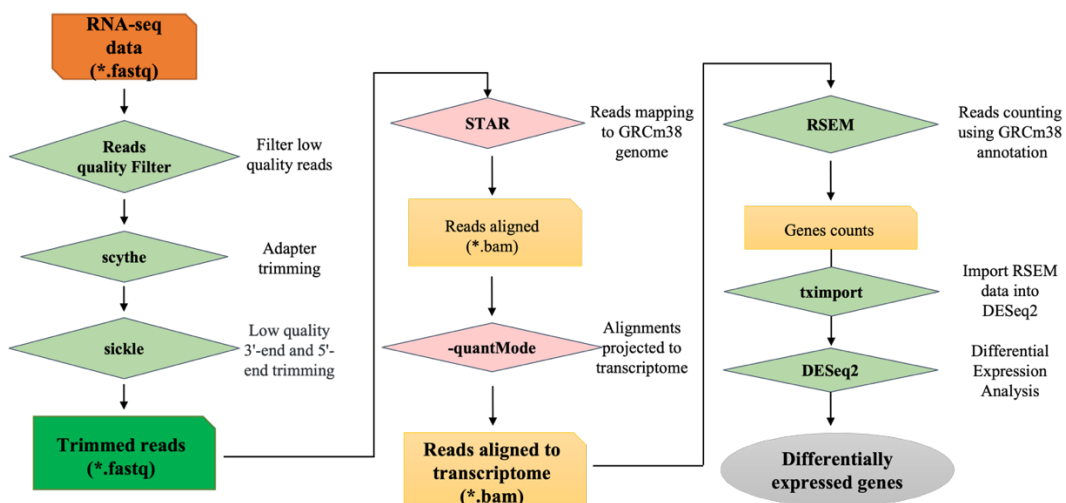


Figure 8.3: RNASeq analysis pipeline.

8.3.5. Delta Gene assay design, cDNA synthesis, pre-amplification and 96x96 microfluidic quantitative PCR

For the validation of DEGs selected from the RNASeq and the development of the screening system, we took advantage of the high-throughput 96x96 integrated fluid circuits (IFC) quantitative RT-PCR (qPCR) protocol developed by Fluidigm for gene expression.

Firstly, primers for the DEGs prioritized were designed by Fluidigm and tested *in silico* using their online tool (<https://d3.fluidigm.com>). 207 pairs of primers (including five housekeeping genes and *Mecp2*) were progressively designed according to the prioritization of DEGs from the RNASeq analysis. The full list of DEGs used and the respective pairs of primers tested are reported in Table 8.4 below.

Gene	Biological function	Forward primer (5'-3')	Reverse primer (5'-3')
<i>Bdnf</i>	Nervous system development	TCCAAAGGCCAACTGAAGCA	CTGCAGCCTTCCTTGGTGTA
<i>Bhlhe22</i>	Nervous system development	GCTCCTCGCCAAGAACTACA	CTTGGTTGAGGTAGCGACTAA
<i>Camk2n1</i>	Nervous system development	CAGATCGGCCCGGAGCAA	TGTCTTTGGGGCAGTTAGACA
<i>Ccn3</i>	Nervous system development	CATCGTTCGGCCTTGTGAAC	GATTTCTTGGTGCGGAGACAC
<i>Cpne4</i>	Nervous system development	AGAGTTCACCTCCACCTTCAA	ACTTGGGGTTGATGCATTCC
<i>Daam2</i>	Nervous system development	AGAGGAACCAAGTTGTAGAAGACC	ATCGATGAAGCGGGTCACAA
<i>Dok4</i>	Nervous system development	CTCGCACCTTCACTTGTGAC	CCGTGATCCCAGACATTCCA
<i>Efna3</i>	nervous system development	TTCCATGCCGGCCAAGAATA	CGAACACCTTCATCCTCAGACA
<i>Fgf14</i>	Nervous system development	TCGATGGAACCAAGGATGACA	ACTCCCTGGATGGCAACAA
<i>Fgf2</i>	nervous system development	TCTCCTGCGCATCCATCC	GCACACACTCCCTTGATAGACA
<i>Gap43</i>	Nervous system development	TCCAACGGAGACTGCAGAAA	TCCTGTGCGGGCACTTCC
<i>Gng4</i>	Nervous system development	TGGAGCAGCTGAAGATGGAA	GCACGTGGGCTTCACAGTA
<i>Hecw2</i>	nervous system development	CTTCAGGAAGCCTGCACTCTA	CATCCCTTCTTGAGCCCAAC
<i>Junb</i>	Nervous system development	TTTTCGGGTCAGGGATCAGAC	TTGCTGTTGGGGACGATCAA
<i>Kalrn</i>	nervous system development	GACTCTCAGGACACACGAA	CTTCTACATGCTCGGTCACA
<i>L1cam</i>	Nervous system development	TCTCTGAGACTGTGGTCACAC	TGTTGGTCTCATTCCCTTCCC
<i>Mdga1</i>	Nervous system development	GCATCCCAGACAAGGCTATCA	ACCACCAGAGTTTCGTTTCCACA
<i>Mitf</i>	Nervous system development	CCAGCCAACCTTCCCAACATA	GCCAATGCTCTTGCTTCAGAC
<i>Nexmif</i>	nervous system development	GCCTCAGCCAATGGAGACAA	CGAATGACTTCATTGCCACTTCC

<i>Nkd2</i>	Nervous system development	GGGTCCACTGAGACTTAGCAA	TGGCGGTTGTCTTCTTCCA
<i>Ntf3</i>	Nervous system development	CCGAGCACTGACTTCAGAAAAC	TTCTCGACAAGGCACACACA
<i>Pcdha11</i>	nervous system development	TGGCCACGGATAAAGGAACA	GGGGAGTTGTCATTGGTGTCTA
<i>Plcb1</i>	nervous system development	AGAAGGCCGCATTCTCTTA	AAGCCTCTAGTGCAGTTTCAAC
<i>Plxna2</i>	Nervous system development	ACTGGAAGCGCTTAACACA	AGGAGGTCTGCTTAGGAACCA
<i>Pmepal1</i>	Nervous system development	GCCAGCGCTCTTTGTTC	ATGACCACGATTGCACGAAC
<i>Prtg</i>	nervous system development	ATAGAACAGCCCTGCCTACA	ACGTCGTAGATCTGCAACAC
<i>Rasgrp1</i>	nervous system development	TCAGCCGAGCTGCTACAAA	CTTCAGGCAAACCTCTGGAGAA
<i>Rbfox1</i>	Nervous system development	AGAAGACTGTCAACCCCTACAC	GCATAGAAGTCGGGGCTGTA
<i>Rbfox3</i>	Nervous system development	ACCAATAAGAAGCCTGGGAACC	TCAGGGCCATAGACTGTTCTTA
<i>Scrt1</i>	nervous system development	AGACCTCGACAGCTCTAC	CCCACGTAGTCACTGAGGTA
<i>Slitrk1</i>	nervous system development	ATCCCAGGCTCAGGCTTAAA	CGTTGGAAAGCTTAGGCTTCA
<i>Sstr3</i>	nervous system development	AGCTCTTCATGCTAGGGCTAC	AGACGGCACATGAGAGATCC
<i>St8sia2</i>	Nervous system development	GCCTCATCCAAATGGAGACAC	TCCTTCTCCGCATCCAAGAA
<i>Wif1</i>	Nervous system development	AGTGTCCGGATGGGTTCTAC	CACACAGACCACCGTTCATAC
<i>Wnt7b</i>	nervous system development	CGCCTCATGAACCTTCACAA	CTGACACACCGTGACACTTAC
<i>Ankfn1</i>	microtubule cytoskeleton organization	ATCGCCAGAGATGCACAGAA	TTCCGAGCAGCCTTCTTCA
<i>Arhgap4</i>	microtubule cytoskeleton organization	GGGCTACAACCTGAGTATGAC	CTGAAGCTCCAGGCAATGAA
<i>Ccsap</i>	microtubule cytoskeleton organization	GGAAGCCAGAAGACACACAAC	AGCCAGCTTCCTTTTCTCCA
<i>Dock6</i>	microtubule cytoskeleton organization	TACTGGTGAAGTGCCTGTCA	TCTTCTTCTCCCGCACATCA
<i>Epha3</i>	microtubule cytoskeleton organization	AAGGAGTTGGATGCCACCAATA	CCGCTGCAAACCTTCTCCAAA
<i>Fgd6</i>	microtubule cytoskeleton organization	TGAAGCTGTCTCGGAAAGTCA	ACTGCATGGGTGTGGTGTGA
<i>Hap1</i>	microtubule cytoskeleton organization	CAGATGCTGGCCTCAGAGAA	TGCTCCATAATCCTGCATGTA
<i>Kank3</i>	microtubule cytoskeleton organization	ATTGCACTGGAGGCTGAACA	AGTGGGAGACCCTGTGGAA
<i>Kifc2</i>	microtubule cytoskeleton organization	CTGGACTGGGTCTTCTCTCAA	CTGGAGGCAGGACAACACA
<i>Klh11</i>	microtubule cytoskeleton organization	AAGGTGGCACACAGCTACA	GCTCTTCACTGGAAGGAGTA
<i>Myo5b</i>	microtubule cytoskeleton organization	CTGCCAGCCTTCTGAATTTAA	TGTTTCTCCATGGGCTGTA
<i>Pdyp</i>	microtubule cytoskeleton organization	CGCTCAGCGACGGAAG	ATGCACTGGAACATGTAAGGG
<i>Stard13</i>	microtubule cytoskeleton organization	TGCCTCAGAGCATCCAACAA	TCACTCTGACTTGCAGAAAA

<i>Tbcel</i>	microtubule cytoskeleton organization	TCTGTGCTCACGTGTCAGAA	CTCCAGCTGAGGAACATTGAC
<i>Tubb3</i>	microtubule cytoskeleton organization	GCGCATCAGCGTATACTACA	AGGTTCCAAGTCCACCAGAA
<i>Wipf3</i>	microtubule cytoskeleton organization	GCGGAAAGTCACCCAGATCAA	CCTCCCTCTTTGCTGGTTCC
<i>Zmym6</i>	microtubule cytoskeleton organization	GCGGTTCTCAGGGATTGACA	GCTTCCCCATCTTTCCCCAAA
<i>Atp8a2</i>	neuron projection morphogenesis	GAACAGACATTCGGGATCCTCA	ATGCAGTCGGACAATGACA
<i>Auts2</i>	neuron projection morphogenesis	TGGCACGACCTTCCACTTTA	ATGAGGTGGTGCCCAAAA
<i>Camk2b</i>	neuron projection morphogenesis	GCCTGCTGAAGCATTCCAA	GATCGAAGACCAGGTAGTGAA
<i>Cpne6</i>	neuron projection morphogenesis	TTGTGCAGCTGTGACATCC	CGATGAAGTCGTGCTTTCCA
<i>Haus7</i>	neuron projection morphogenesis	CCCCATCATCCAAGCTGTCTA	GGTGTCTGCAATCTCCATGAC
<i>Lamb1</i>	neuron projection morphogenesis	CTGAGCTGTTGCTTGAGGAA	TTCACCATGTCTGCAGTGAC
<i>Ntng1</i>	neuron projection morphogenesis	CGCCGTTGGGAAATATTTGTA	AAACACGAAGTGGCATGCA
<i>Nyap2</i>	neuron projection morphogenesis	TGCTGCGGAAGTCATCCA	GCTGTGGCTTCGAACTTCA
<i>Psd</i>	neuron projection morphogenesis	CTATACCGACTCGATGGCTTCA	CCAGCCACCAATTTGCTGAA
<i>Ptk2b</i>	neuron projection morphogenesis	TGGAGAGCCTGAAAGAAGACA	CGTAGCGTTGCATGTAGTCA
<i>Rap1gap2</i>	neuron projection morphogenesis	ATGATGCAGTGGGGCTGAAA	ATCATGCTCATCATAGGACACAATCA
<i>Shank1</i>	neuron projection morphogenesis	AGTGCCAGCATGGAGAAAA	CTGCAGCCAAGATCTCATCCA
<i>Vash2</i>	neuron projection morphogenesis	ATGGTAGGCGCCATCAGAAA	GGATCGTCATGGACAACCTGTA
<i>Vstm2l</i>	neuron projection morphogenesis	GACTGGACTGACAAGCAGAC	TATTTGGTGGCGTCCTTCC
<i>Atp1a1</i>	Ion transmembrane transport	AAGCTGACACCAGGAGAA	ATTCTGGACAGAGCGAACCA
<i>Cacna1c</i>	Ion transmembrane transport	AGATGCACAAGACCTGCTACA	TCTCCAAAGCACAAGGGGAA
<i>Cacna1e</i>	Ion transmembrane transport	ACTGACCTGGCTACGTTTA	CATGATGACAGCCACGAACA
<i>Cacna1g</i>	Ion transmembrane transport	TCTGCTGTGCCTTCTTCATCA	CTCACCTGACACACGAAGAA
<i>Cacna1i</i>	Ion transmembrane transport	TCTTTGTTGGGCGAGATGACA	TTCCAGCTGCTACGCAAGTA
<i>Dpp10</i>	Ion transmembrane transport	CTCGGTTTACTGGAGCACTGTA	CACTGATGGGTTTCGCTTGAC
<i>Dpp6</i>	Ion transmembrane transport	GTGCATAACACCACGGACAA	GGTCGTTGATAGCCTTCTGAAC
<i>Gtra2</i>	Ion transmembrane transport	GAGACGACAGAAGAGGCAGAA	CCCATCCCATAGCCACTGAA
<i>Grin1</i>	Ion transmembrane transport	GATGGCAAGTTTGGCACACA	AGCAGCTCTCCCATCATTCC
<i>Kcng2</i>	Ion transmembrane transport	GCTCTTCGCCTACGTCTCC	CCGTCTCCAGCACGAACA

<i>Kcnh2</i>	Ion transmembrane transport	GTCTCTCCCAACACCAACTCA	TGCCGAAGATGCTGGCATA
<i>Kcni1</i>	Ion transmembrane transport	ACCCAGACAGGCTCTGTAAA	TTCATGGACTGTCCCTCTCA
<i>Kcnq2</i>	Ion transmembrane transport	ACTTTGAGAAAACGGCGGAAC	CGGTGCGTGAGAGGTTAGTA
<i>Orai2</i>	Ion transmembrane transport	ACCTCAGCCCTCCTGTCT	GGCTGAGGGTACTGGTACTTG
<i>Ryr2</i>	Ion transmembrane transport	TGGAGGACATGCATCCAACA	TCCTATGCCTGACAAGAACTCC
<i>Scn3b</i>	Ion transmembrane transport	CGAAGAGGCAGCTCAGGAA	CGGGTACCACAGAGTTCTCC
<i>Slc30a3</i>	Ion transmembrane transport	GCCCTGACGCTTACTTACCA	CTTCAGCCAGGACAGCTTCA
<i>Slc8a3</i>	Ion transmembrane transport	TGGGTGAACACCCCAAATA	AATGGGTCCCCACAACCAA
<i>Slco1c1</i>	Ion transmembrane transport	TCTAGGTGGCATACTGGATA	GGTGTAGATACCCAGAGCAAA
<i>Stac2</i>	Ion transmembrane transport	CAGCCTGTGCCATGAACAA	TAGCGCAGCGTCTCATAAAC
<i>Stc1</i>	Ion transmembrane transport	TCCTTCTGTACAGTGCTGCTA	CCCATTGGCGATGCACTTTAA
<i>Trpc3</i>	Ion transmembrane transport	GTGAAGACCACCCAGTTCAC	CTTGCACTCAGACCACATCA
<i>Trpm2</i>	Ion transmembrane transport	TGAGAAGGATGTGGCTCTCA	TCCATCCACGACGTTGTAAC
<i>Unc80</i>	Ion transmembrane transport	TCGCAGGAGCATTCAACCTA	TCTGGCTGAGCCTCAATGAA
<i>Vip</i>	Ion transmembrane transport	GCAGAAAATGGCACACCCTA	CTGCTGTAATCGCTGGTGAA
<i>Add2</i>	synapse assembly and organization	ACCTGCGACAGGACTTCAA	CTTCCAGCTCCTCCCTGAAA
<i>Camkv</i>	synapse assembly and organization	TTGTGACCCGCAAGGAATAC	TGGTCCAGGATCCAGTCAAAA
<i>Cbln1</i>	synapse assembly and organization	CGTGGTGAAAGTCTACAACAGAC	CGGCGAAGGCTGAAAATCAC
<i>Dlgap3</i>	synapse assembly and organization	TCAAGCCAACAGCTGGAAA	CGCGAGGGCTTCTTTGGTA
<i>Lgi2</i>	synapse assembly and organization	TGGAGTGGGACCACATAGAAA	CACAAAGACCTGGTCGTCAA
<i>Lhfp14</i>	synapse assembly and organization	GGAGGAGCTCAAACAGGAGAA	TGAGCAACAGGGCATGGTA
<i>Pcdhgc4</i>	synapse assembly and organization	GAAGTCACCCAGTGCACCTA	CTTGAGAGAAAACGCCAGTCA
<i>Pnck</i>	synapse assembly and organization	AAGAAACAGACGGAGGACATCA	GCCAGCATCACCTCAGAGAA
<i>Syndig1</i>	synapse assembly and organization	CTGTCTATGACGTGGAGGAA	CTGTGTGCTGGAGTAGTCA
<i>Cabyr</i>	synaptic transmission and plasticity	GGGGCAAAGAGGAAGCTCTA	GTACAACAAGTCTGGGCTTTGAA
<i>Cckbr</i>	synaptic transmission and plasticity	CCAGTGAACGTGTCCAACAA	CATAGGCCACCGCCATAAC

<i>Chrm2</i>	synaptic transmission and plasticity	TTCTCCACACCCAGGTCTCC	CACAGCTCGGAGTCCTCA
<i>Chrm3</i>	synaptic transmission and plasticity	CCGAGCCAAACGAACAACAA	CAGGAGCCACAGGACAAA
<i>Cnih2</i>	synaptic transmission and plasticity	CCTGGGCCTCAACATCCC	ACATGACCTCAGAGCCATCC
<i>Fos</i>	synaptic transmission and plasticity	ATGGGCTCTCTGTCAACAC	GCTGTCACCGTGGGGATAAA
<i>Gabbr2</i>	synaptic transmission and plasticity	TTGGCCAGTTTGACCAGAAC	CTGGTACTTGCTGCCAAACA
<i>Gabra3</i>	synaptic transmission and plasticity	AACAAGCTGCTCAGACTGGTA	ATGGGGCATTACAGCGTGTA
<i>Gabrb3</i>	synaptic transmission and plasticity	GATACCCACTGGATGAGCAAAAC	CGCCACGCCAGTAAAATTCA
<i>Gabrg3</i>	synaptic transmission and plasticity	CCCAACCAGCTCCTCAGAA	GCTGGCACTCTGCATTGATA
<i>Gad1</i>	synaptic transmission and plasticity	CACAGAGACCGACTTCTCCA	TTTGCTCCTCCCCGTTCTTA
<i>Gng2</i>	synaptic transmission and plasticity	CAGCTGAAGATGGAAGCCAAC	TTGGCATGTGCCTCACAGTA
<i>Grm4</i>	synaptic transmission and plasticity	TCAAGAAGGGAAGCCACATCAA	ACCTTCCCCTCCTGTTGTA
<i>Grm5</i>	synaptic transmission and plasticity	TGCAGTGAACCGTGTGAGAA	AAGGTGTGCAGGTCCAACAA
<i>Gsg1l</i>	synaptic transmission and plasticity	ATAGACGGGCTGAAGCTCAA	ATCATGTGTGCGACCATTCC
<i>Hpcal4</i>	synaptic transmission and plasticity	GCTGGAGATGCTGGAGATCA	GTGAGCCCATCCTGGTTCA
<i>Insyn1</i>	synaptic transmission and plasticity	GGGCAACTTGAAGGCATCC	AGCTTGTCGATCTGACTCAC
<i>Jph4</i>	synaptic transmission and plasticity	GCTGATAGCCCAGGATCTACA	TGTCAGAACCTCCTGAGTCC
<i>Lgr5</i>	synaptic transmission and plasticity	CTCCAACCTCAGCGTCTTCA	ATGTAGGAGACTGGCGGGTA
<i>Ly6h</i>	synaptic transmission and plasticity	TGCCAGCCCACCGATAC	TAACGAAGTCGCAGGAGGAA
<i>Ncdn</i>	synaptic transmission and plasticity	TCCTCAACCTGGTGGTCAC	TGACGTGTCAGGGTGTTC
<i>Neurl1a</i>	synaptic transmission and plasticity	AGCTGCACCTGAGTCACAA	GCCACCCCGTTCAGTCA
<i>Neurl1b</i>	synaptic transmission and plasticity	AGTCGTCCTCAGCATCAGAA	GGAGAAGGCTGGGGACAC
<i>Npas4</i>	synaptic transmission and plasticity	GCCCAAGCTTCTTCTCAACA	TGCTTGCTTGAAGTCTCAC
<i>Nptx2</i>	synaptic transmission and plasticity	AAGACAGAGAGCACGCTGAA	GCATCTGGTGACTTGAATGCA

<i>Nptxr</i>	synaptic transmission and plasticity	TGCGAGACCGCATCGA	GGTGGGCATGGCTGGA
<i>Oxtr</i>	synaptic transmission and plasticity	GACGTCAATGCGCCCAAA	GGAAGAGATGGCCCGTGAA
<i>Plppr4</i>	synaptic transmission and plasticity	CGGAGGCTGCAACTTCAAC	TGTGGAGCACAGTCCAAACA
<i>Rgs14</i>	synaptic transmission and plasticity	GCCTCTCTGCTGACATTA	ACGGTGCAATCCTGATCCA
<i>Shisa7</i>	synaptic transmission and plasticity	GTCTATGAGGCTGCTGTGAA	GCTTCAGGTAGGCTTCATCCA
<i>Slc12a5</i>	synaptic transmission and plasticity	ACCTTTGCTGGGGCTATGTA	AAGATGGCCATAGCTGGGAA
<i>Sorcs1</i>	synaptic transmission and plasticity	TCCATCCGAAGCAAGAAGAC	CCAAACTCAGCAGAGCTGTA
<i>Sv2c</i>	synaptic transmission and plasticity	TGGATGATTGGCGGCATCTA	TAGGCTGAACCCATGCTGAA
<i>Syn1</i>	synaptic transmission and plasticity	CAAGGACGGAAGGGATCACA	GATGAGCTGCTTGTCTTCATCC
<i>Caly</i>	synaptic vesicle-mediated transport, exo- and endocytosis	GCTTGCAGTCACTCAGAGGAA	CACAGCCCAGAAGTGCCATA
<i>Cplx1</i>	synaptic vesicle-mediated transport, exo- and endocytosis	GGTCATGCGGCAGGGTATAA	CTTCCGAGTTGGCCTCCA
<i>Dnajc6</i>	synaptic vesicle-mediated transport, exo- and endocytosis	TTTCTGCAGCCCACGAGAA	AATGTCGGGCTGGATGTCA
<i>Itsn1</i>	synaptic vesicle-mediated transport, exo- and endocytosis	CCCTGTCATGAAACAGCAACC	GCATGCTAGCAATCCCTCCTA
<i>Lin7a</i>	synaptic vesicle-mediated transport, exo- and endocytosis	GGACCAGCTGCTATCAGTGAA	TCTGACCACCAGCTTCACAC
<i>Mal2</i>	synaptic vesicle-mediated transport, exo- and endocytosis	GGTGACTCAGATTGATGCCAAC	ACGCTCCGAAGTAGAAGACAA
<i>Napb</i>	synaptic vesicle-mediated transport, exo- and endocytosis	GGAACAGAACAGTGAAGCGTAC	AGCCACTGATCCAAACGTGATA
<i>Nsg1</i>	synaptic vesicle-mediated transport, exo- and endocytosis	GAGTTCACCGTCAGCATCAC	AAGACGACACAGGTGAGGAA
<i>Rab3c</i>	synaptic vesicle-mediated transport, exo- and endocytosis	GGCCATGGGCTTCATTTAA	CCTGGGCATTATCCAAGAGTA
<i>Rin1</i>	synaptic vesicle-mediated transport, exo- and endocytosis	GCCTGCAAGCTGCTATACAC	CAGCAGAGGCAGGAACTCA
<i>Slc29a4</i>	synaptic vesicle-mediated transport, exo- and endocytosis	ATGATCCTGGCAGCTGGAAA	CCGACATGTAGGACACAGTCA

<i>Snap25</i>	synaptic vesicle-mediated transport, exo- and endocytosis	CGCCAGATCGACAGGATCA	CACGTTGGTTGGCTTCATCA
<i>Sncb</i>	synaptic vesicle-mediated transport, exo- and endocytosis	TTGAGCCTCTGATGGAACCA	CTCTGGCTCGTATTCTGGTA
<i>Ston1</i>	synaptic vesicle-mediated transport, exo- and endocytosis	AGACCGGCTTCCGGATAAAA	CCTGGTCTGACCCAAGTTCTA
<i>Stxbp1</i>	synaptic vesicle-mediated transport, exo- and endocytosis	ACGATGGACCCCGATCATT	GCGGGTAGAGATGTATGGTA
<i>Synpr</i>	synaptic vesicle-mediated transport, exo- and endocytosis	CCAGAACAAGTACCGCGAAA	CCACCAGCCACAAGAATGAA
<i>Syt1</i>	synaptic vesicle-mediated transport, exo- and endocytosis	ACCGGAAAACCCTCAATCCA	CAGTGTCTTGCCACCTAATTCC
<i>Arhgdig</i>	signal transduction	GCTCCAGGGCCTATCATCA	ATGCCCTCCTTCAGGACAAA
<i>Opr11</i>	signal transduction	AATCTGGCACTGGCTGATACC	AAATGGCCAGAAGCCCAGAA
<i>Rgs10</i>	signal transduction	CCACACCCTCTGATGTTCCA	AGACTTCAAGAAGCGGCTGTA
<i>Abca8a</i>	Metabolic processes	ACCAGGCTTCGCTTCTTGAA	GCAGAAGTCCAATCCCCAAAAC
<i>Arhgap33</i>	Metabolic processes	CGCTAACACCAGCATGCA	CCACCGACTCCAGTTCATA
<i>Cyp27a1</i>	Metabolic processes	GCCCACATGCCTCTGCTAA	ATCCGGGAGTTTGTGGGAAC
<i>Gipr</i>	Metabolic processes	AGATGTTGGAGACCACAGAACC	CGTGTAGTTCACGAGGCATA
<i>Gpr21</i>	Metabolic processes	GCATTGCAAGGCTTTCGGTTA	AGCAGGAGTTGTAATGAGTCTCC
<i>Necab3</i>	Metabolic processes	CTCACTGCCATGGACACTACA	GCAGCAGAAATCGTGTGACAA
<i>Nsdhl</i>	Metabolic processes	TCATTGGCACCAAGACTGTCA	AACACTGGCACTGCTGGTTA
<i>Pgm2l1</i>	Metabolic processes	GCTTGTGTGGGCTATGACA	CTGCAGCTGTGAGTTTAGCAA
<i>Pitpnc1</i>	Metabolic processes	CTGCCGAAATTCTCCATCCA	GGTCTTGGCTTCACTGTCA
<i>Plppr3</i>	Metabolic processes	CTGGTGGCTGCAACTTCAA	ACAGGCCAAACACGTGTAC
<i>Vldlr</i>	Metabolic processes	ACTGCAGAGACTGGAGTGAC	GGGAACAGCCACCATTATTGAC
<i>Fundc2</i>	Mitochondria	GTTGGAAAATTGGCTGCAACA	ACTGCTCTTTGGCTTCTTCA
<i>Gdap1</i>	Mitochondria	CTGTGAGGCCACTCAGATCA	CTTCCTTCATCGGGCATTAAACC
<i>Pdp2</i>	Mitochondria	TTCGGGGATGTCCAGCTAAA	TTGAGGGCCTCCGTATCAAAA
<i>Ajap1</i>	Extracellular matrix and cell-cell adhesion	GACCGGGGAGTACAAGTCC	CCACAGGGATGAGATGCCTA
<i>Cobll1</i>	Extracellular matrix and cell-cell adhesion	CCCTGGCTCAGACTGATGAA	CATGCTGTCTGGAGCAATCC
<i>Col6a2</i>	Extracellular matrix and cell-cell adhesion	GGAGATCCTGGAGACAAAGGAA	CCTCCCTTGCCTCCTTCA
<i>Icam5</i>	Extracellular matrix and cell-cell adhesion	AAGCAGGGAGACCCAGGAA	GGGCTTCTGGCTCACTCAAAA

<i>Mmp24</i>	Extracellular matrix and cell-cell adhesion	AAGGGCCTTCATCAGCAA	CGCTCAGTTTCTGGTTGTCAAA
<i>Nxph3</i>	Extracellular matrix and cell-cell adhesion	TAGTGCAGGGCAGCCTCTA	CCCTCATGGTCATCGTGTCA
<i>Spock3</i>	Extracellular matrix and cell-cell adhesion	GCACTTGGAAATCCAGGAAAACC	GCGGCTGCATTTTCGTCTTTA
<i>Asx3</i>	Transcription regulation	CAGTGCAAAGCAAGCTGGTA	CTTTTCTGCTGCTGCCTCAA
<i>Basp1</i>	Transcription regulation	CGCCACAGGCACCCAAA	TTGGCCTTCTCGTCGTTTCC
<i>Bcl6</i>	Transcription regulation	GGGGAAACCCAGTCAGAGTA	CTCAGAGAAACGGCAGTCAC
<i>Epas1</i>	Transcription regulation	AAGCTTTTCGCCATGGACAC	CAAGGTCTCCAAATCCAGTTTCC
<i>Klf8</i>	Transcription regulation	AAAGCTACCCGAGAATCCA	TCCGAGCGAGCAAATTTCCA
<i>Mef2c</i>	Transcription regulation	TGATGGGCGGAGATCTGACA	GCAGGCTGGTGAGTTCC
<i>Pcbp3</i>	Transcription regulation	AAGGTGGCCTGAACGTAAC	CTTCCCGATGATGCTTCCAA
<i>Raly1</i>	Transcription regulation	TGGTTACGTATTTGACTACGATTACTACA	GAGGTACACGGCCATGGTAA
<i>Rnase4</i>	Transcription regulation	ACTGCAGAGAGACAGGGAAC	AGGCAATGACAACTCGCCTA
<i>Adarb2</i>	Other	CCACAAAACACTGGCAGGAA	TTGGTCCCAGAGGACAGAAC
<i>Arhgef37</i>	Other	TCCAGGATGTGAACGGCAATA	TCAGCTGCTCCACTTTGGTA
<i>C1qtnf4</i>	Other	CTCACCGAGCAGGATAGCC	GCCTAGGAAGCCCAGCAA
<i>Cntnap3</i>	Other	TCAACCCTTGAGAGCATCA	CTACCCTTAGCAGACACGGAAA
<i>Eef1a2</i>	Other	CAACATGCTGGAGCCTTCCAC	CCGCTTGCAATTCCTTCCCTTAC
<i>Fbxo41</i>	Other	AAGCAGGACCTGGTGCATAA	CTGCCGTCTCCTTCAGGAA
<i>Ical1</i>	Other	ATCAAAGCGACGGGAAAGAA	TGTCTCCTGGATGGAGTGAA
<i>Lamp5</i>	Other	GCACATCCAGCCCTTTGATA	CAACTGCTCTTGCTCATCCA
<i>Marchf4</i>	Other	TCTGCCGCATCTGTTTCCA	TGAGACATGGCTGGTGTGTAC
<i>Mpped1</i>	Other	ACGTCTTTGGCCACATCCA	ACACCGACGCGTTCACATA
<i>Pcdhgb8</i>	Other	GTGAGTGTGCTGAGGAGAA	GGTCTCTGGGCTTGAGAGAAA
<i>Pnma2</i>	Other	CTTGGCTCCTGGTTCTTGAAA	CAACTCTGGGGAGTCACACA
<i>Sepsecs</i>	Other	AGGCTCTAGCCTCTTGAACAAA	GCAACTGGCCACTGAATGAA
<i>Serpine1</i>	Other	CAGACAATGGAAGGGCAACA	GAGGTCCACTTCAGTCTCCA
<i>Sphkap</i>	Other	ATCCAGATGTGGCCAGAAA	CTACTTCCCCACTGGTCTCAA
<i>Tbc1d9</i>	Other	CAAGGATTTGCCAAGCTGAA	GGGTCTTCACTGAACATGTTGTAC
<i>Zdhhc22</i>	Other	GCTCCTGCCCACTTCAATCA	GGTAGAGCATGAGGATGACGAA
<i>Meep2</i>	–	GGCCGATCTGCTGGAAAGTA	GGTCCAAGGAGGTGTCTCC
<i>Actb</i>	Housekeeping gene	CCCTAAGGCCAACCGTGAAG	AGCCTGGATGGCTACGTACA
<i>Gapdh</i>	Housekeeping gene	CAAGGTCATCCCAGAGCTGAA	CAGATCCACGACGGACACA
<i>Hprt</i>	Housekeeping gene	CAGTACAGCCCCAAAATGGTTA	AGTCTGGCCTGTATCCAACA
<i>Ppia</i>	Housekeeping gene	CTTTGCAGACGCCACTGT	GCCGTGATGTGAAGAACA
<i>Rpl13</i>	Housekeeping gene	TGAGATTGGCCGACTCCCTA	AGAACGGCCGAGCGGAAA

Table 8.4: List of the 207 DEGs tested in the 96x96 IFC qRT-PCR experiments for validation and their respective pairs of primers. Housekeeping genes are included in the list.

For the qPCR experiments, 200ng of RNA extracted from primary cultures were reverse-transcribed using the Reverse Transcription Master Mix (Fluidigm PN 100-6297) following manufacturer's instructions. A mixture of random primers and oligo dT was used for priming. The cDNA prepared using the Reverse Transcription Master Mix was then pre-amplified using the Preamp Master Mix (Fluidigm PN 100-5580). 50ng of cDNA were then pre-amplified using a 0.2X pool of 96 genes for each 96x96 qPCR IFC chip. 12 cycles of amplification were set for multiplex sequence-specific amplification of targets. The reaction products were then cleaned up using 4U/ μ L Exonuclease I (ThermoFisher EN0581) following manufacture's procedure. Pre-amplified cDNA was then 5-fold diluted using a DNA suspension buffer (10 mM Tris, pH 8.0, 0.1 mM EDTA) and analyzed on 96x96 IFC qRT-PCR cards using the Biomark HD (Fluidigm) according to Fluidigm's instructions (Figure 8.4).

Baseline correction was set on Linear (Derivative), Ct Threshold Method was set on Auto (global) and Ct calculations were then processed in Excel (Microsoft). To normalize Ct, the stability of five housekeeping genes (HK) was analyzed using NormFinder (Excel add-in). The five HK used in the experiments were *Actb*, *Gapdh*, *Hprt*, *Ppia* and *Rpl13*. When the output stability values were below 0.3, the best combination of two HK was used as normalizer by calculating their average Ct values. Excel and Prism were used to analyze the transcriptional data. Metaboanalyst was used to perform PCAs.

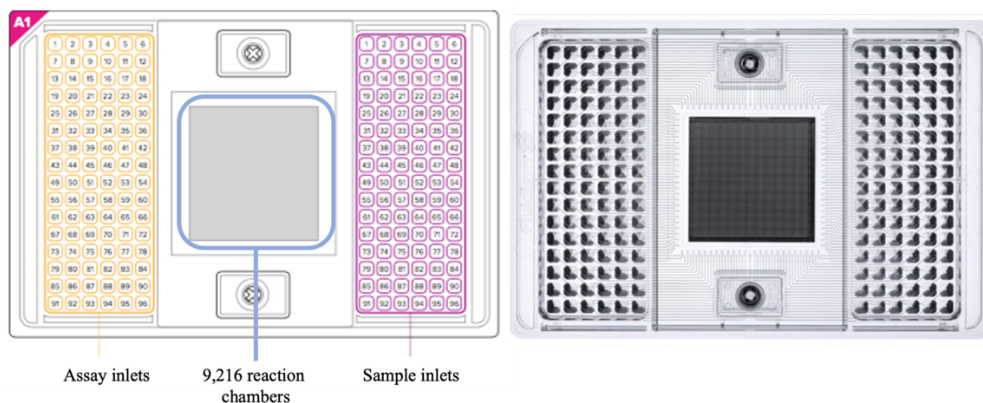


Figure 8.4: Schematic representation of a 96x96 IFC qPCR card developed by Fluidigm.

8.4. Gene expression analysis on mice tissues

To investigate the possible implication in RTT pathogenesis of *Haus7* and *Nsdhl* from the RNASeq and 96x96 qPCR, the longitudinal expression of the genes was evaluated at different timepoints in the cerebral cortex and hippocampus of *Mecp2*-mutant male mice vs their WT littermates of two different strains: the *Mecp2*-null and the *Mecp2* Y120D mouse lines, deeply characterized in section 4.2.

Primers for the genes are reported in Table 8.5.

Genes	Forward primer	Reverse primer
<i>Haus7</i>	5'-AGTACCCAGCCTGCACCCAAGT-3'	5'-GGCTCTCCTTCCTGCTTCCTTGC-3'
<i>Nsdhl</i>	5'-TCATTGGCACCAAGACTGTCA-3'	5'-AACACTGGCACTGCTGGTTA-3'

Table 8.5: Primers for Haus7 and Nsdhl designed and used for the qPCR experiments.

8.4.1. RNA purification, quality control, cDNA synthesis and quantitative RT-PCR

Mutant mice and WT littermates at the established post-natal day were sacrificed by dislocation and brains were rapidly removed. Selected tissues were dissected and immediately frozen on dry-ice and stored at -80°C until analysis. Tissues were lysed and total RNA was extracted using Purezol and a Potter-ELV glass grinder was used to mechanically triturate selected tissues. As for RNA extraction from primary cultures, samples were incubated for 5 minutes at RT and 100% chloroform was added 1:5 (200 μ L/1 mL Purezol) and centrifugated (13,000g, 20 minutes, 4°C) to separate the aqueous and the organic phases. The aqueous solution containing the RNA was isolated and added with 100% isopropanol to induce RNA precipitation. Samples were stored at -20°C until the following day. Then, after a centrifugation (13,000g, 20 minutes, 4°C) and a wash with 70% EtOH, RNA was further purified by adding 80 μ L Purezol/sample, following the exact protocol and proportions of the volumes mentioned above. Pellets were then

precipitated in 100% isopropanol and stored for one hour at -80°C and then washed in 70% EtOH. Finally, RNA was completely dried at RT, resuspended in 15µL and 30 µL of H₂O RNase-free, respectively for hippocampus and cerebral cortex. RNA was quantified using a spectrophotometer (NanoDrop 1000) and RNA integrity was verified by agarose electrophoresis. Good quality RNA samples exhibiting the 28S and 18S bands with a relative intensity of 2:1 were selected for the subsequent analysis. First strand cDNA was synthesized using the RT² First StrandKit (Qiagen, 330404) following manufacturer instructions and used as a template for qPCR performed with SYBR Green Master Mix (Applied Biosystems, 4472908).

The gene expression analysis was performed in triplicates for each sample and Ct values were normalized to the expression of the housekeeping genes:

- *CicloA* (forward primer 5'-GGCAAATGCTGGACCAAACACAA-3', reverse primer 5'-GTAAAATGCCCGCAAGTCAAAG-3');
- *Rpl13* (forward primer 5'-TGGCTGGCATCCACAAGAAA-3', reverse primer 5'-TTCTTCAGCAGAACTGTCTC-3').

Excel (Microsoft) and Prism were used to analyze the transcriptional data. The relative changes in gene expression in KO compared to WT samples were calculated using the 2^(-ΔΔCt) method (Livak & Schmittgen, 2001).

8.5. Protein extraction and Western Blot

8.5.1. Protein extraction and quantification

Mutant mice and WT littermates at the established post-natal day were sacrificed by dislocation and brains were rapidly removed. Selected tissues were dissected and immediately frozen on dry-ice and stored at -80°C until analysis. At the time of the analysis, tissues were sonicated for 10 seconds (30 amplitudes) in ice-cold RIPA buffer (100 mM Tris HCl pH 7.5, 300mM NaCl, 10 mM EDTA, 2% NP-40, 0.2% SDS, 1% sodium deoxycholate) containing Protein Inhibitor Complex 1X (Sigma Merck, #P8340) and PhosSTOP 1X (Sigma Merck, #4906845001). The process was repeated for two

cycles in case of the hippocampus and 4 times for the cerebral cortex. Tissues were then left on ice for 30 minutes and centrifuged at 13,000g for 30 min at 4°C. Supernatants were then collected and stored at -80°C until analysis. Protein concentrations were calculated using bicinchoninic acid (BCA) assay kit (Thermo Scientific, #23228) following manufacturer's procedure.

8.5.2. Western Blot

TGX Stain-Free gels prepared by FastCast Acrylamide Kit (Bio-Rad, 10%: #1610183) were loaded with 30 µg of protein lysates. At the end of electrophoretic separation and before transfer, a Stain-Free gel image was acquired by ChemiDoc Touch Imaging System (Bio-Rad) to normalize protein expression results. Proteins were blotted on a nitrocellulose membrane (Trans-blot Turbo Nitrocellulose Transfer Packs, Bio-Rad Mini #1704159) using the Trans-blot SD (Bio-Rad) semidry apparatus. Membranes were incubated at room temperature for 1 h in blocking solution (Tris-buffered saline containing 0.1% Tween-20 (TBS-T) and 5% nonfat milk) and then incubated O/N with Nsdhl primary antibody diluted in 5% nonfat milk TBS-T (4°C) (anti-Nsdhl D-11, Santa-Cruz sc-390871 1:1000). After 3 washes in TBS-T (10 minutes each), blots were incubated with the appropriate HRP-conjugated secondary antibody (Peroxidase-conjugated AffiniPure Goat anti-mouse IgG (H+L), mouse #115-035-003, Jackson ImmunoResearch) diluted in blocking solution. Visualization of immunocomplexes was performed using the ECL substrates kits from Cyanagen and the Bio-Rad ChemiDoc™ System. Bands were quantified using the Image Lab 5.2.1 Software.

9. BIBLIOGRAPHY

- Absinta M, Maric D, Gharagozloo M, Garton T, Smith MD, Jin J, Fitzgerald KC, Song A, Liu P, Lin JP et al (2021) A lymphocyte-microglia-astrocyte axis in chronic active multiple sclerosis. *Nature* 597: 709-714
- Abuhatzira, L., Makedonski, K., Kaufman, Y., Razin, A., & Shemer, R. (2007). MeCP2 deficiency in the brain decreases BDNF levels by REST/CoREST-mediated repression and increases TRKB production. *Epigenetics*, 2(4), 214-222. <https://doi.org/10.4161/epi.2.4.5212>
- Adams, V. H., McBryant, S. J., Wade, P. A., Woodcock, C. L., & Hansen, J. C. (2007). Intrinsic disorder and autonomous domain function in the multifunctional nuclear protein, MeCP2. *J Biol Chem*, 282(20), 15057-15064. <https://doi.org/10.1074/jbc.M700855200>
- Adkins, N. L., & Georgel, P. T. (2011). MeCP2: structure and function. *Biochem Cell Biol*, 89(1), 1-11. <https://doi.org/10.1139/o10-112>
- Albizzati, E., Florio, E., Miramondi, F., Sormonta, I., Landsberger, N., & Frasca, A. (2022). Identification of Region-Specific Cytoskeletal and Molecular Alterations in Astrocytes of Mecp2 Deficient Animals. *Front Neurosci*, 16, 823060. <https://doi.org/10.3389/fnins.2022.823060>
- Allen, J. A., Halverson-Tamboli, R. A., & Rasenick, M. M. (2007). Lipid raft microdomains and neurotransmitter signalling. *Nat Rev Neurosci*, 8(2), 128-140. <https://doi.org/10.1038/nrn2059>
- Amir, R. E., Van den Veyver, I. B., Wan, M., Tran, C. Q., Francke, U., & Zoghbi, H. Y. (1999). Rett syndrome is caused by mutations in X-linked MECP2, encoding methyl-CpG-binding protein 2. *Nat Genet*, 23(2), 185-188. <https://doi.org/10.1038/13810>
- Andoh-Noda, T., Akamatsu, W., Miyake, K., Matsumoto, T., Yamaguchi, R., Sanosaka, T., Okada, Y., Kobayashi, T., Ohyama, M., Nakashima, K., Kurosawa, H., Kubota, T., & Okano, H. (2015). Differentiation of multipotent neural stem cells derived from Rett syndrome patients is biased toward the astrocytic lineage. *Mol Brain*, 8, 31. <https://doi.org/10.1186/s13041-015-0121-2>
- Ariani, F., Hayek, G., Rondinella, D., Artuso, R., Mencarelli, M. A., Spanhol-Rosseto, A., Pollazzon, M., Buoni, S., Spiga, O., Ricciardi, S., Meloni, I., Longo, I., Mari, F., Broccoli, V., Zappella, M., & Renieri, A. (2008). FOXP1 is responsible for the congenital variant of Rett syndrome. *Am J Hum Genet*, 83(1), 89-93. <https://doi.org/10.1016/j.ajhg.2008.05.015>
- Armstrong, D., Dunn, J. K., Antalffy, B., & Trivedi, R. (1995). Selective dendritic alterations in the cortex of Rett syndrome. *J Neuropathol Exp Neurol*, 54(2), 195-201. <https://doi.org/10.1097/00005072-199503000-00006>
- Armstrong, D. D. (2005). Neuropathology of Rett syndrome. *J Child Neurol*, 20(9), 747-753. <https://doi.org/10.1177/08830738050200090901>
- Baj, G., Patrizio, A., Montalbano, A., Sciancalepore, M., & Tongiorgi, E. (2014). Developmental and maintenance defects in Rett syndrome neurons identified by a new mouse staging system in vitro. *Front Cell Neurosci*, 8, 18. <https://doi.org/10.3389/fncel.2014.00018>

- Ballas, N., Liroy, D. T., Grunseich, C., & Mandel, G. (2009). Non-cell autonomous influence of MeCP2-deficient glia on neuronal dendritic morphology. *Nat Neurosci*, *12*(3), 311-317. <https://doi.org/10.1038/nn.2275>
- Barres, B. A. (2008). The mystery and magic of glia: a perspective on their roles in health and disease. *Neuron*, *60*(3), 430-440. <https://doi.org/10.1016/j.neuron.2008.10.013>
- Bauman, M. L., Kemper, T. L., & Arin, D. M. (1995). Pervasive neuroanatomic abnormalities of the brain in three cases of Rett's syndrome. *Neurology*, *45*(8), 1581-1586. <https://doi.org/10.1212/wnl.45.8.1581>
- Bebensee, D. F., Can, K., & Müller, M. (2017). Increased Mitochondrial Mass and Cytosolic Redox Imbalance in Hippocampal Astrocytes of a Mouse Model of Rett Syndrome: Subcellular Changes Revealed by Ratiometric Imaging of JC-1 and roGFP1 Fluorescence. *Oxid Med Cell Longev*, *2017*, 3064016. <https://doi.org/10.1155/2017/3064016>
- Bedogni, F., Cobolli Gigli, C., Pozzi, D., Rossi, R. L., Scaramuzza, L., Rossetti, G., Pagani, M., Kilstrup-Nielsen, C., Matteoli, M., & Landsberger, N. (2016). Defects During Mecp2 Null Embryonic Cortex Development Precede the Onset of Overt Neurological Symptoms. *Cereb Cortex*, *26*(6), 2517-2529. <https://doi.org/10.1093/cercor/bhv078>
- Bedogni, F., Rossi, R. L., Galli, F., Cobolli Gigli, C., Gandaglia, A., Kilstrup-Nielsen, C., & Landsberger, N. (2014). Rett syndrome and the urge of novel approaches to study MeCP2 functions and mechanisms of action. *Neurosci Biobehav Rev*, *46 Pt 2*, 187-201. <https://doi.org/10.1016/j.neubiorev.2014.01.011>
- Belichenko, P. V., Wright, E. E., Belichenko, N. P., Masliah, E., Li, H. H., Mobley, W. C., & Francke, U. (2009). Widespread changes in dendritic and axonal morphology in Mecp2-mutant mouse models of Rett syndrome: evidence for disruption of neuronal networks. *J Comp Neurol*, *514*(3), 240-258. <https://doi.org/10.1002/cne.22009>
- Ben-Shachar, S., Chahrour, M., Thaller, C., Shaw, C. A., & Zoghbi, H. Y. (2009). Mouse models of MeCP2 disorders share gene expression changes in the cerebellum and hypothalamus. *Hum Mol Genet*, *18*(13), 2431-2442. <https://doi.org/10.1093/hmg/ddp181>
- Bergo, A., Strollo, M., Gai, M., Barbiero, I., Stefanelli, G., Sertic, S., Cobolli Gigli, C., Di Cunto, F., Kilstrup-Nielsen, C., & Landsberger, N. (2015). Methyl-CpG binding protein 2 (MeCP2) localizes at the centrosome and is required for proper mitotic spindle organization. *J Biol Chem*, *290*(6), 3223-3237. <https://doi.org/10.1074/jbc.M114.608125>
- Bhatnagar, S., Zhu, X., Ou, J., Lin, L., Chamberlain, L., Zhu, L. J., Wajapeyee, N., & Green, M. R. (2014). Genetic and pharmacological reactivation of the mammalian inactive X chromosome. *Proc Natl Acad Sci U S A*, *111*(35), 12591-12598. <https://doi.org/10.1073/pnas.1413620111>
- Bittolo, T., Raminelli, C. A., Deiana, C., Baj, G., Vaghi, V., Ferrazzo, S., Bernareggi, A., & Tongiorgi, E. (2016). Pharmacological treatment with mirtazapine rescues cortical atrophy and respiratory deficits in MeCP2 null mice. *Sci Rep*, *6*, 19796. <https://doi.org/10.1038/srep19796>
- Björkhem, I., Leoni, V., & Meaney, S. (2010). Genetic connections between neurological disorders and cholesterol metabolism. *J Lipid Res*, *51*(9), 2489-2503. <https://doi.org/10.1194/jlr.R006338>

- Brendel, C., Belakhov, V., Werner, H., Wegener, E., Gärtner, J., Nudelman, I., Baasov, T., & Huppke, P. (2011). Readthrough of nonsense mutations in Rett syndrome: evaluation of novel aminoglycosides and generation of a new mouse model. *J Mol Med (Berl)*, *89*(4), 389-398. <https://doi.org/10.1007/s00109-010-0704-4>
- Brown, K., Selfridge, J., Lagger, S., Connelly, J., De Sousa, D., Kerr, A., Webb, S., Guy, J., Merusi, C., Koerner, M. V., & Bird, A. (2016). The molecular basis of variable phenotypic severity among common missense mutations causing Rett syndrome. *Hum Mol Genet*, *25*(3), 558-570. <https://doi.org/10.1093/hmg/ddv496>
- Buchovecky, C. M., Turley, S. D., Brown, H. M., Kyle, S. M., McDonald, J. G., Liu, B., Pieper, A. A., Huang, W., Katz, D. M., Russell, D. W., Shendure, J., & Justice, M. J. (2013). A suppressor screen in Mecp2 mutant mice implicates cholesterol metabolism in Rett syndrome. *Nat Genet*, *45*(9), 1013-1020. <https://doi.org/10.1038/ng.2714>
- Bulcha, J. T., Wang, Y., Ma, H., Tai, P. W. L., & Gao, G. (2021). Viral vector platforms within the gene therapy landscape. *Signal Transduct Target Ther*, *6*(1), 53. <https://doi.org/10.1038/s41392-021-00487-6>
- Caldas, H., & Herman, G. E. (2003). NSDHL, an enzyme involved in cholesterol biosynthesis, traffics through the Golgi and accumulates on ER membranes and on the surface of lipid droplets. *Hum Mol Genet*, *12*(22), 2981-2991. <https://doi.org/10.1093/hmg/ddg321>
- Calfa, G., Li, W., Rutherford, J. M., & Pozzo-Miller, L. (2015). Excitation/inhibition imbalance and impaired synaptic inhibition in hippocampal area CA3 of Mecp2 knockout mice. *Hippocampus*, *25*(2), 159-168. <https://doi.org/10.1002/hipo.22360>
- Carrette, L. L. G., Wang, C. Y., Wei, C., Press, W., Ma, W., Kelleher, R. J., 3rd, & Lee, J. T. (2018). A mixed modality approach towards Xi reactivation for Rett syndrome and other X-linked disorders. *Proc Natl Acad Sci U S A*, *115*(4), E668-e675. <https://doi.org/10.1073/pnas.1715124115>
- Castro, J., Garcia, R. I., Kwok, S., Banerjee, A., Petravicz, J., Woodson, J., Mellios, N., Tropea, D., & Sur, M. (2014). Functional recovery with recombinant human IGF1 treatment in a mouse model of Rett Syndrome. *Proc Natl Acad Sci U S A*, *111*(27), 9941-9946. <https://doi.org/10.1073/pnas.1311685111>
- Chahrour, M., Jung, S. Y., Shaw, C., Zhou, X., Wong, S. T., Qin, J., & Zoghbi, H. Y. (2008). MeCP2, a key contributor to neurological disease, activates and represses transcription. *Science*, *320*(5880), 1224-1229. <https://doi.org/10.1126/science.1153252>
- Chahrour, M., & Zoghbi, H. Y. (2007). The story of Rett syndrome: from clinic to neurobiology. *Neuron*, *56*(3), 422-437. <https://doi.org/10.1016/j.neuron.2007.10.001>
- Chandler, S. P., Guschin, D., Landsberger, N., & Wolffe, A. P. (1999). The methyl-CpG binding transcriptional repressor MeCP2 stably associates with nucleosomal DNA. *Biochemistry*, *38*(22), 7008-7018. <https://doi.org/10.1021/bi990224y>
- Chang, Q., Khare, G., Dani, V., Nelson, S., & Jaenisch, R. (2006). The disease progression of Mecp2 mutant mice is affected by the level of BDNF expression. *Neuron*, *49*(3), 341-348. <https://doi.org/10.1016/j.neuron.2005.12.027>
- Chao, H. T., Zoghbi, H. Y., & Rosenmund, C. (2007). MeCP2 controls excitatory synaptic strength by regulating glutamatergic synapse number. *Neuron*, *56*(1), 58-65. <https://doi.org/10.1016/j.neuron.2007.08.018>

- Chapleau, C. A., Calfa, G. D., Lane, M. C., Albertson, A. J., Larimore, J. L., Kudo, S., Armstrong, D. L., Percy, A. K., & Pozzo-Miller, L. (2009). Dendritic spine pathologies in hippocampal pyramidal neurons from Rett syndrome brain and after expression of Rett-associated MECP2 mutations. *Neurobiol Dis*, *35*(2), 219-233. <https://doi.org/10.1016/j.nbd.2009.05.001>
- Chen, R. Z., Akbarian, S., Tudor, M., & Jaenisch, R. (2001). Deficiency of methyl-CpG binding protein-2 in CNS neurons results in a Rett-like phenotype in mice. *Nat Genet*, *27*(3), 327-331. <https://doi.org/10.1038/85906>
- Cheng, T. L., Chen, J., Wan, H., Tang, B., Tian, W., Liao, L., & Qiu, Z. (2017). Regulation of mRNA splicing by MeCP2 via epigenetic modifications in the brain. *Sci Rep*, *7*, 42790. <https://doi.org/10.1038/srep42790>
- Chhatbar, K., Cholewa-Waclaw, J., Shah, R., Bird, A., & Sanguinetti, G. (2020). Quantitative analysis questions the role of MeCP2 as a global regulator of alternative splicing. *PLoS Genet*, *16*(10), e1009087. <https://doi.org/10.1371/journal.pgen.1009087>
- Chhatbar, K., Connelly, J., Webb, S., Kriaucionis, S., & Bird, A. (2022). A critique of the hypothesis that CA repeats are primary targets of neuronal MeCP2. *Life Sci Alliance*, *5*(12). <https://doi.org/10.26508/lsa.202201522>
- Claveria-Gimeno, R., Lanuza, P. M., Morales-Chueca, I., Jorge-Torres, O. C., Vega, S., Abian, O., Esteller, M., & Velazquez-Campoy, A. (2017). The intervening domain from MeCP2 enhances the DNA affinity of the methyl binding domain and provides an independent DNA interaction site. *Sci Rep*, *7*, 41635. <https://doi.org/10.1038/srep41635>
- Cobolli Gigli, C., Scaramuzza, L., De Simone, M., Rossi, R. L., Pozzi, D., Pagani, M., Landsberger, N., & Bedogni, F. (2018). Lack of Methyl-CpG Binding Protein 2 (MeCP2) Affects Cell Fate Refinement During Embryonic Cortical Development. *Cereb Cortex*, *28*(5), 1846-1856. <https://doi.org/10.1093/cercor/bhx360>
- Cobolli Gigli, C., Scaramuzza, L., Gandaglia, A., Bellini, E., Gabaglio, M., Parolaro, D., Kilstrop-Nielsen, C., Landsberger, N., & Bedogni, F. (2016). MeCP2 Related Studies Benefit from the Use of CD1 as Genetic Background. *PLoS One*, *11*(4), e0153473. <https://doi.org/10.1371/journal.pone.0153473>
- Connelly, J. C., Cholewa-Waclaw, J., Webb, S., Steccanella, V., Waclaw, B., & Bird, A. (2020). Absence of MeCP2 binding to non-methylated GT-rich sequences in vivo. *Nucleic Acids Res*, *48*(7), 3542-3552. <https://doi.org/10.1093/nar/gkaa102>
- Croci, S., Carriero, M. L., Capitani, K., Daga, S., Donati, F., Frullanti, E., Lamacchia, V., Tita, R., Giliberti, A., Valentino, F., Benetti, E., Ciabattini, A., Furini, S., Lo Rizzo, C., Pinto, A. M., Conticello, S. G., Renieri, A., & Meloni, I. (2020). High rate of HDR in gene editing of p.(Thr158Met) MECP2 mutational hotspot. *Eur J Hum Genet*, *28*(9), 1231-1242. <https://doi.org/10.1038/s41431-020-0624-x>
- Cronk, J. C., Derecki, N. C., Ji, E., Xu, Y., Lampano, A. E., Smirnov, I., Baker, W., Norris, G. T., Marin, I., Coddington, N., Wolf, Y., Turner, S. D., Aderem, A., Klibanov, A. L., Harris, T. H., Jung, S., Litvak, V., & Kipnis, J. (2015). Methyl-CpG Binding Protein 2 Regulates Microglia and Macrophage Gene Expression in Response to Inflammatory Stimuli. *Immunity*, *42*(4), 679-691. <https://doi.org/10.1016/j.immuni.2015.03.013>
- Cuddapah, V. A., Pillai, R. B., Shekar, K. V., Lane, J. B., Motil, K. J., Skinner, S. A., Tarquinio, D. C., Glaze, D. G., McGwin, G., Kaufmann, W. E., Percy, A. K., Neul, J. L., & Olsen, M. L. (2014). Methyl-CpG-binding protein 2 (MECP2)

- mutation type is associated with disease severity in Rett syndrome. *J Med Genet*, 51(3), 152-158. <https://doi.org/10.1136/jmedgenet-2013-102113>
- Cunha-Ferreira, I., Chazeau, A., Buijs, R. R., Stucchi, R., Will, L., Pan, X., Adolfs, Y., van der Meer, C., Wolthuis, J. C., Kahn, O. I., Schätzle, P., Altelaar, M., Pasterkamp, R. J., Kapitein, L. C., & Hoogenraad, C. C. (2018). The HAUS Complex Is a Key Regulator of Non-centrosomal Microtubule Organization during Neuronal Development. *Cell Rep*, 24(4), 791-800. <https://doi.org/10.1016/j.celrep.2018.06.093>
- Cunningham, D., Spsychala, K., McLarren, K. W., Garza, L. A., Boerkoel, C. F., & Herman, G. E. (2009). Developmental expression pattern of the cholesterologenic enzyme NSDHL and negative selection of NSDHL-deficient cells in the heterozygous Bpa(1H)/+ mouse. *Mol Genet Metab*, 98(4), 356-366. <https://doi.org/10.1016/j.ymgme.2009.06.016>
- D'Ercole, A. J., Ye, P., Calikoglu, A. S., & Gutierrez-Ospina, G. (1996). The role of the insulin-like growth factors in the central nervous system. *Mol Neurobiol*, 13(3), 227-255. <https://doi.org/10.1007/bf02740625>
- Dani, V. S., Chang, Q., Maffei, A., Turrigiano, G. G., Jaenisch, R., & Nelson, S. B. (2005). Reduced cortical activity due to a shift in the balance between excitation and inhibition in a mouse model of Rett syndrome. *Proc Natl Acad Sci U S A*, 102(35), 12560-12565. <https://doi.org/10.1073/pnas.0506071102>
- Dave, A., Shukla, F., Wala, H., & Pillai, P. (2019). Mitochondrial Electron Transport Chain Complex Dysfunction in MeCP2 Knock-Down Astrocytes: Protective Effects of Quercetin Hydrate. *J Mol Neurosci*, 67(1), 16-27. <https://doi.org/10.1007/s12031-018-1197-9>
- De Felice, C., Signorini, C., Leoncini, S., Pecorelli, A., Durand, T., Valacchi, G., Ciccoli, L., & Hayek, J. (2012). The role of oxidative stress in Rett syndrome: an overview. *Ann N Y Acad Sci*, 1259, 121-135. <https://doi.org/10.1111/j.1749-6632.2012.06611.x>
- de Leeuw, C. N., Dyka, F. M., Boye, S. L., Laprise, S., Zhou, M., Chou, A. Y., Borretta, L., McInerney, S. C., Banks, K. G., Portales-Casamar, E., Swanson, M. I., D'Souza, C. A., Boye, S. E., Jones, S. J., Holt, R. A., Goldowitz, D., Hauswirth, W. W., Wasserman, W. W., & Simpson, E. M. (2014). Targeted CNS Delivery Using Human MiniPromoters and Demonstrated Compatibility with Adeno-Associated Viral Vectors. *Mol Ther Methods Clin Dev*, 1, 5. <https://doi.org/10.1038/mtm.2013.5>
- Delépine, C., Nectoux, J., Letourneur, F., Baud, V., Chelly, J., Billuart, P., & Bienvenu, T. (2015). Astrocyte Transcriptome from the Mecp2(308)-Truncated Mouse Model of Rett Syndrome. *Neuromolecular Med*, 17(4), 353-363. <https://doi.org/10.1007/s12017-015-8363-9>
- Deng, V., Matagne, V., Banine, F., Frerking, M., Ohliger, P., Budden, S., Pevsner, J., Dissen, G. A., Sherman, L. S., & Ojeda, S. R. (2007). FXYP1 is an MeCP2 target gene overexpressed in the brains of Rett syndrome patients and Mecp2-null mice. *Hum Mol Genet*, 16(6), 640-650. <https://doi.org/10.1093/hmg/ddm007>
- Deogracias, R., Yazdani, M., Dekkers, M. P., Guy, J., Ionescu, M. C., Vogt, K. E., & Barde, Y. A. (2012). Fingolimod, a sphingosine-1 phosphate receptor modulator, increases BDNF levels and improves symptoms of a mouse model of Rett syndrome. *Proc Natl Acad Sci U S A*, 109(35), 14230-14235. <https://doi.org/10.1073/pnas.1206093109>

- Dolce, A., Ben-Zeev, B., Naidu, S., & Kossoff, E. H. (2013). Rett syndrome and epilepsy: an update for child neurologists. *Pediatr Neurol*, 48(5), 337-345. <https://doi.org/10.1016/j.pediatrneurol.2012.11.001>
- du Souich, C., Chou, A., Yin, J., Oh, T., Nelson, T. N., Hurlburt, J., Arbour, L., Friedlander, R., McGillivray, B. C., Tyshchenko, N., Rump, A., Poskitt, K. J., Demos, M. K., Van Allen, M. I., & Boerkoel, C. F. (2009). Characterization of a new X-linked mental retardation syndrome with microcephaly, cortical malformation, and thin habitus. *Am J Med Genet A*, 149a(11), 2469-2478. <https://doi.org/10.1002/ajmg.a.33071>
- du Souich, C., Raymond, F. L., Grzeschik, K. H., & Boerkoel, C. F. (1993). NSDHL-Related Disorders. In M. P. Adam, D. B. Everman, G. M. Mirzaa, R. A. Pagon, S. E. Wallace, L. J. H. Bean, K. W. Gripp, & A. Amemiya (Eds.), *GeneReviews*(®). University of Washington, Seattle
- Copyright © 1993-2022, University of Washington, Seattle. GeneReviews is a registered trademark of the University of Washington, Seattle. All rights reserved.
- Ehinger, Y., Bruyère, J., Panayotis, N., Abada, Y. S., Borloz, E., Matagne, V., Scaramuzzino, C., Vitet, H., Delatour, B., Saidi, L., Villard, L., Saudou, F., & Roux, J. C. (2020). Huntingtin phosphorylation governs BDNF homeostasis and improves the phenotype of Mecp2 knockout mice. *EMBO Mol Med*, 12(2), e10889. <https://doi.org/10.15252/emmm.201910889>
- Ehrhart, F., Coort, S. L., Cirillo, E., Smeets, E., Evelo, C. T., & Curfs, L. (2016). New insights in Rett syndrome using pathway analysis for transcriptomics data. *Wien Med Wochenschr*, 166(11-12), 346-352. <https://doi.org/10.1007/s10354-016-0488-4> (Neue Erkenntnisse zum Rett-Syndrom mit der Signalweganalyse von Transkriptomdaten.)
- Ehrhart, F., Coort, S. L., Eijssen, L., Cirillo, E., Smeets, E. E., Bahram Sangani, N., Evelo, C. T., & Curfs, L. M. G. (2019). Integrated analysis of human transcriptome data for Rett syndrome finds a network of involved genes. *World J Biol Psychiatry*, 1-14. <https://doi.org/10.1080/15622975.2019.1593501>
- Einspieler, C., Kerr, A. M., & Prechtel, H. F. (2005). Is the early development of girls with Rett disorder really normal? *Pediatr Res*, 57(5 Pt 1), 696-700. <https://doi.org/10.1203/01.Pdr.0000155945.94249.0a>
- Fehr, S., Bebbington, A., Ellaway, C., Rowe, P., Leonard, H., & Downs, J. (2011). Altered attainment of developmental milestones influences the age of diagnosis of rett syndrome. *J Child Neurol*, 26(8), 980-987. <https://doi.org/10.1177/0883073811401396>
- Fehr, S., Wilson, M., Downs, J., Williams, S., Murgia, A., Sartori, S., Vecchi, M., Ho, G., Polli, R., Psoni, S., Bao, X., de Klerk, N., Leonard, H., & Christodoulou, J. (2013). The CDKL5 disorder is an independent clinical entity associated with early-onset encephalopathy. *Eur J Hum Genet*, 21(3), 266-273. <https://doi.org/10.1038/ejhg.2012.156>
- Filosa, S., Pecorelli, A., D'Esposito, M., Valacchi, G., & Hajek, J. (2015). Exploring the possible link between MeCP2 and oxidative stress in Rett syndrome. *Free Radic Biol Med*, 88(Pt A), 81-90. <https://doi.org/10.1016/j.freeradbiomed.2015.04.019>
- Frasca, A., Spiombi, E., Palmieri, M., Albizzati, E., Valente, M. M., Bergo, A., Leva, B., Kilstrup-Nielsen, C., Bianchi, F., Di Carlo, V., Di Cunto, F., & Landsberger, N. (2020). MECP2 mutations affect ciliogenesis: a novel perspective for Rett

- syndrome and related disorders. *EMBO Mol Med*, 12(6), e10270. <https://doi.org/10.15252/emmm.201910270>
- Fuks, F., Hurd, P. J., Deplus, R., & Kouzarides, T. (2003). The DNA methyltransferases associate with HP1 and the SUV39H1 histone methyltransferase. *Nucleic Acids Res*, 31(9), 2305-2312. <https://doi.org/10.1093/nar/gkg332>
- Fukuda, T., Itoh, M., Ichikawa, T., Washiyama, K., & Goto, Y. (2005). Delayed maturation of neuronal architecture and synaptogenesis in cerebral cortex of Mecp2-deficient mice. *J Neuropathol Exp Neurol*, 64(6), 537-544. <https://doi.org/10.1093/jnen/64.6.537>
- Gabel, C. A., Li, Z., DeMarco, A. G., Zhang, Z., Yang, J., Hall, M. C., Barford, D., & Chang, L. (2022). Molecular architecture of the augmin complex. *Nat Commun*, 13(1), 5449. <https://doi.org/10.1038/s41467-022-33227-7>
- Gabel, H. W., Kinde, B., Stroud, H., Gilbert, C. S., Harmin, D. A., Kastan, N. R., Hemberg, M., Ebert, D. H., & Greenberg, M. E. (2015). Disruption of DNA-methylation-dependent long gene repression in Rett syndrome. *Nature*, 522(7554), 89-93. <https://doi.org/10.1038/nature14319>
- Gadalla, K. K., Bailey, M. E., Spike, R. C., Ross, P. D., Woodard, K. T., Kalburgi, S. N., Bachaboina, L., Deng, J. V., West, A. E., Samulski, R. J., Gray, S. J., & Cobb, S. R. (2013). Improved survival and reduced phenotypic severity following AAV9/MECP2 gene transfer to neonatal and juvenile male Mecp2 knockout mice. *Mol Ther*, 21(1), 18-30. <https://doi.org/10.1038/mt.2012.200>
- Gadalla, K. K. E., Vudhironarit, T., Hector, R. D., Sinnott, S., Bahey, N. G., Bailey, M. E. S., Gray, S. J., & Cobb, S. R. (2017). Development of a Novel AAV Gene Therapy Cassette with Improved Safety Features and Efficacy in a Mouse Model of Rett Syndrome. *Mol Ther Methods Clin Dev*, 5, 180-190. <https://doi.org/10.1016/j.omtm.2017.04.007>
- Gandaglia, A., Brivio, E., Carli, S., Palmieri, M., Bedogni, F., Stefanelli, G., Bergo, A., Leva, B., Cattaneo, C., Pizzamiglio, L., Cicerone, M., Bianchi, V., Kilstrup-Nielsen, C., D'Annessa, I., Di Marino, D., D'Adamo, P., Antonucci, F., Frasca, A., & Landsberger, N. (2019). A Novel Mecp2(Y120D) Knock-in Model Displays Similar Behavioral Traits But Distinct Molecular Features Compared to the Mecp2-Null Mouse Implying Precision Medicine for the Treatment of Rett Syndrome. *Mol Neurobiol*, 56(7), 4838-4854. <https://doi.org/10.1007/s12035-018-1412-2>
- Gao, Y., Su, J., Guo, W., Polich, E. D., Magyar, D. P., Xing, Y., Li, H., Smrt, R. D., Chang, Q., & Zhao, X. (2015). Inhibition of miR-15a Promotes BDNF Expression and Rescues Dendritic Maturation Deficits in MeCP2-Deficient Neurons. *Stem Cells*, 33(5), 1618-1629. <https://doi.org/10.1002/stem.1950>
- Garg, S. K., Liroy, D. T., Cheval, H., McGann, J. C., Bissonnette, J. M., Murtha, M. J., Foust, K. D., Kaspar, B. K., Bird, A., & Mandel, G. (2013). Systemic delivery of MeCP2 rescues behavioral and cellular deficits in female mouse models of Rett syndrome. *J Neurosci*, 33(34), 13612-13620. <https://doi.org/10.1523/jneurosci.1854-13.2013>
- Genaro-Mattos, T. C., Anderson, A., Allen, L. B., Korade, Z., & Mirnics, K. (2019). Cholesterol Biosynthesis and Uptake in Developing Neurons. *ACS Chem Neurosci*, 10(8), 3671-3681. <https://doi.org/10.1021/acscchemneuro.9b00248>
- Gibson, J. H., Slobedman, B., K, N. H., Williamson, S. L., Minchenko, D., El-Osta, A., Stern, J. L., & Christodoulou, J. (2010). Downstream targets of methyl CpG

- binding protein 2 and their abnormal expression in the frontal cortex of the human Rett syndrome brain. *BMC Neurosci*, 11, 53. <https://doi.org/10.1186/1471-2202-11-53>
- Glaze, D. G. (2005). Neurophysiology of Rett syndrome. *J Child Neurol*, 20(9), 740-746. <https://doi.org/10.1177/08830738050200090801>
- Glaze, D. G., Neul, J. L., Kaufmann, W. E., Berry-Kravis, E., Condon, S., Stoms, G., Oosterholt, S., Della Pasqua, O., Glass, L., Jones, N. E., & Percy, A. K. (2019). Double-blind, randomized, placebo-controlled study of trofinetide in pediatric Rett syndrome. *Neurology*, 92(16), e1912-e1925. <https://doi.org/10.1212/wnl.00000000000007316>
- Glaze, D. G., Neul, J. L., Percy, A., Feyma, T., Beisang, A., Yaroshinsky, A., Stoms, G., Zuchero, D., Horrigan, J., Glass, L., & Jones, N. E. (2017). A Double-Blind, Randomized, Placebo-Controlled Clinical Study of Trofinetide in the Treatment of Rett Syndrome. *Pediatr Neurol*, 76, 37-46. <https://doi.org/10.1016/j.pediatrneurol.2017.07.002>
- Goffredo D, Conti L, Di Febo F, Biella G, Tosoni A, Vago G, Biunno I, Moiana A, Bolognini D, Toselli M et al (2008) Setting the conditions for efficient, robust and reproducible generation of functionally active neurons from adult subventricular zone-derived neural stem cells. *Cell Death Differ* 15: 1847-1856
- Gold WA, Lacina TA, Cantrill LC, Christodoulou J (2015) MeCP2 deficiency is associated with reduced levels of tubulin acetylation and can be restored using HDAC6 inhibitors. *J Mol Med (Berl)* 93: 63-72
- Gold, W. A., Krishnaraj, R., Ellaway, C., & Christodoulou, J. (2018). Rett Syndrome: A Genetic Update and Clinical Review Focusing on Comorbidities. *ACS Chem Neurosci*, 9(2), 167-176. <https://doi.org/10.1021/acschemneuro.7b00346>
- Gogliotti RG, Fisher NM, Stansley BJ, Jones CK, Lindsley CW, Conn PJ, Niswender CM (2018) Total RNA Sequencing of Rett Syndrome Autopsy Samples Identifies the M(4) Muscarinic Receptor as a Novel Therapeutic Target. *J Pharmacol Exp Ther* 365: 291-300
- Gomathi, M., Padmapriya, S., & Balachandar, V. (2020). Drug Studies on Rett Syndrome: From Bench to Bedside. *J Autism Dev Disord.* <https://doi.org/10.1007/s10803-020-04381-y>
- Gorba, T., & Conti, L. (2013). Neural stem cells as tools for drug discovery: novel platforms and approaches. *Expert Opin Drug Discov*, 8(9), 1083-1094. <https://doi.org/10.1517/17460441.2013.805199>
- Goshima, G., Mayer, M., Zhang, N., Stuurman, N., & Vale, R. D. (2008). Augmin: a protein complex required for centrosome-independent microtubule generation within the spindle. *J Cell Biol*, 181(3), 421-429. <https://doi.org/10.1083/jcb.200711053>
- Gray, S. J., Foti, S. B., Schwartz, J. W., Bachaboina, L., Taylor-Blake, B., Coleman, J., Ehlers, M. D., Zylka, M. J., McCown, T. J., & Samulski, R. J. (2011). Optimizing promoters for recombinant adeno-associated virus-mediated gene expression in the peripheral and central nervous system using self-complementary vectors. *Hum Gene Ther*, 22(9), 1143-1153. <https://doi.org/10.1089/hum.2010.245>
- Gritti, A., Parati, E. A., Cova, L., Frolichsthal, P., Galli, R., Wanke, E., Faravelli, L., Morassutti, D. J., Roisen, F., Nickel, D. D., & Vescovi, A. L. (1996). Multipotential stem cells from the adult mouse brain proliferate and self-renew in response to basic fibroblast growth factor. *J Neurosci*, 16(3), 1091-1100.

- Grosser, E., Hirt, U., Janc, O. A., Menzfeld, C., Fischer, M., Kempkes, B., Vogelgesang, S., Manzke, T. U., Opitz, L., Salinas-Riester, G., & Müller, M. (2012). Oxidative burden and mitochondrial dysfunction in a mouse model of Rett syndrome. *Neurobiol Dis*, 48(1), 102-114. <https://doi.org/10.1016/j.nbd.2012.06.007>
- Gulmez Karaca, K., Brito, D. V. C., & Oliveira, A. M. M. (2019). MeCP2: A Critical Regulator of Chromatin in Neurodevelopment and Adult Brain Function. *Int J Mol Sci*, 20(18). <https://doi.org/10.3390/ijms20184577>
- Guo, J. U., Su, Y., Shin, J. H., Shin, J., Li, H., Xie, B., Zhong, C., Hu, S., Le, T., Fan, G., Zhu, H., Chang, Q., Gao, Y., Ming, G. L., & Song, H. (2014). Distribution, recognition and regulation of non-CpG methylation in the adult mammalian brain. *Nat Neurosci*, 17(2), 215-222. <https://doi.org/10.1038/nn.3607>
- Gutierrez, H., & Davies, A. M. (2011). Regulation of neural process growth, elaboration and structural plasticity by NF- κ B. *Trends Neurosci*, 34(6), 316-325. <https://doi.org/10.1016/j.tins.2011.03.001>
- Guy, J., Cheval, H., Selfridge, J., & Bird, A. (2011). The role of MeCP2 in the brain. *Annu Rev Cell Dev Biol*, 27, 631-652. <https://doi.org/10.1146/annurev-cellbio-092910-154121>
- Guy, J., Gan, J., Selfridge, J., Cobb, S., & Bird, A. (2007). Reversal of neurological defects in a mouse model of Rett syndrome. *Science*, 315(5815), 1143-1147. <https://doi.org/10.1126/science.1138389>
- Guy, J., Hendrich, B., Holmes, M., Martin, J. E., & Bird, A. (2001). A mouse Mecp2-null mutation causes neurological symptoms that mimic Rett syndrome. *Nat Genet*, 27(3), 322-326. <https://doi.org/10.1038/85899>
- Haase FD, Coorey B, Riley L, Cantrill LC, Tam PPL, Gold WA (2021) Pre-clinical Investigation of Rett Syndrome Using Human Stem Cell-Based Disease Models. *Front Neurosci* 15: 698812
- Hacein-Bey-Abina, S., Garrigue, A., Wang, G. P., Soulier, J., Lim, A., Morillon, E., Clappier, E., Caccavelli, L., Delabesse, E., Beldjord, K., Asnafi, V., MacIntyre, E., Dal Cortivo, L., Radford, I., Brousse, N., Sigaux, F., Moshous, D., Hauer, J., Borkhardt, A., . . . Cavazzana-Calvo, M. (2008). Insertional oncogenesis in 4 patients after retrovirus-mediated gene therapy of SCID-X1. *J Clin Invest*, 118(9), 3132-3142. <https://doi.org/10.1172/jci35700>
- Hagberg, B., Aicardi, J., Dias, K., & Ramos, O. (1983). A progressive syndrome of autism, dementia, ataxia, and loss of purposeful hand use in girls: Rett's syndrome: report of 35 cases. *Ann Neurol*, 14(4), 471-479. <https://doi.org/10.1002/ana.410140412>
- Hagberg, B., & Witt-Engerström, I. (1986). Rett syndrome: a suggested staging system for describing impairment profile with increasing age towards adolescence. *Am J Med Genet Suppl*, 1, 47-59. <https://doi.org/10.1002/ajmg.1320250506>
- Haggarty SJ, Silva MC, Cross A, Brandon NJ, Perlis RH (2016) Advancing drug discovery for neuropsychiatric disorders using patient-specific stem cell models. *Mol Cell Neurosci* 73: 104-115
- Ho, C. M., Hotta, T., Kong, Z., Zeng, C. J., Sun, J., Lee, Y. R., & Liu, B. (2011). Augmin plays a critical role in organizing the spindle and phragmoplast microtubule arrays in Arabidopsis. *Plant Cell*, 23(7), 2606-2618. <https://doi.org/10.1105/tpc.111.086892>
- Hordeaux, J., Buza, E. L., Jeffrey, B., Song, C., Jahan, T., Yuan, Y., Zhu, Y., Bell, P., Li, M., Chichester, J. A., Calcedo, R., & Wilson, J. M. (2020). MicroRNA-mediated

- inhibition of transgene expression reduces dorsal root ganglion toxicity by AAV vectors in primates. *Sci Transl Med*, 12(569). <https://doi.org/10.1126/scitranslmed.aba9188>
- Hordeaux, J., Wang, Q., Katz, N., Buza, E. L., Bell, P., & Wilson, J. M. (2018). The Neurotropic Properties of AAV-PHP.B Are Limited to C57BL/6J Mice. *Mol Ther*, 26(3), 664-668. <https://doi.org/10.1016/j.ymthe.2018.01.018>
- Hotta, T., Kong, Z., Ho, C. M., Zeng, C. J., Horio, T., Fong, S., Vuong, T., Lee, Y. R., & Liu, B. (2012). Characterization of the Arabidopsis augmin complex uncovers its critical function in the assembly of the acentrosomal spindle and phragmoplast microtubule arrays. *Plant Cell*, 24(4), 1494-1509. <https://doi.org/10.1105/tpc.112.096610>
- Hsia, K. C., Wilson-Kubalek, E. M., Dottore, A., Hao, Q., Tsai, K. L., Forth, S., Shimamoto, Y., Milligan, R. A., & Kapoor, T. M. (2014). Reconstitution of the augmin complex provides insights into its architecture and function. *Nat Cell Biol*, 16(9), 852-863. <https://doi.org/10.1038/ncb3030>
- Hussain, G., Wang, J., Rasul, A., Anwar, H., Imran, A., Qasim, M., Zafar, S., Kamran, S. K. S., Razzaq, A., Aziz, N., Ahmad, W., Shabbir, A., Iqbal, J., Baig, S. M., & Sun, T. (2019). Role of cholesterol and sphingolipids in brain development and neurological diseases. *Lipids Health Dis*, 18(1), 26. <https://doi.org/10.1186/s12944-019-0965-z>
- Hutchins, J. R., Toyoda, Y., Hegemann, B., Poser, I., Hériché, J. K., Sykora, M. M., Augsburg, M., Hudecz, O., Buschhorn, B. A., Bulkescher, J., Conrad, C., Comartin, D., Schleiffer, A., Sarov, M., Pozniakovsky, A., Slabicki, M. M., Schloissnig, S., Steinmacher, I., Leuschner, M., . . . Peters, J. M. (2010). Systematic analysis of human protein complexes identifies chromosome segregation proteins. *Science*, 328(5978), 593-599. <https://doi.org/10.1126/science.1181348>
- Ip, J. P. K., Mellios, N., & Sur, M. (2018). Rett syndrome: insights into genetic, molecular and circuit mechanisms. *Nat Rev Neurosci*, 19(6), 368-382. <https://doi.org/10.1038/s41583-018-0006-3>
- Itoh, M., Ide, S., Takashima, S., Kudo, S., Nomura, Y., Segawa, M., Kubota, T., Mori, H., Tanaka, S., Horie, H., Tanabe, Y., & Goto, Y. (2007). Methyl CpG-binding protein 2 (a mutation of which causes Rett syndrome) directly regulates insulin-like growth factor binding protein 3 in mouse and human brains. *J Neuropathol Exp Neurol*, 66(2), 117-123. <https://doi.org/10.1097/nen.0b013e3180302078>
- Itoh, M., Tahimic, C. G., Ide, S., Otsuki, A., Sasaoka, T., Noguchi, S., Oshimura, M., Goto, Y., & Kurimasa, A. (2012). Methyl CpG-binding protein isoform MeCP2_e2 is dispensable for Rett syndrome phenotypes but essential for embryo viability and placenta development. *J Biol Chem*, 287(17), 13859-13867. <https://doi.org/10.1074/jbc.M111.309864>
- Jeffery, L., & Nakielnny, S. (2004). Components of the DNA methylation system of chromatin control are RNA-binding proteins. *J Biol Chem*, 279(47), 49479-49487. <https://doi.org/10.1074/jbc.M409070200>
- Johnson, B. S., Zhao, Y. T., Fasolino, M., Lamonica, J. M., Kim, Y. J., Georgakilas, G., Wood, K. H., Bu, D., Cui, Y., Goffin, D., Vahedi, G., Kim, T. H., & Zhou, Z. (2017). Biotin tagging of MeCP2 in mice reveals contextual insights into the Rett syndrome transcriptome. *Nat Med*, 23(10), 1203-1214. <https://doi.org/10.1038/nm.4406>

- Jordan, C., Li, H. H., Kwan, H. C., & Francke, U. (2007). Cerebellar gene expression profiles of mouse models for Rett syndrome reveal novel MeCP2 targets. *BMC Med Genet*, *8*, 36. <https://doi.org/10.1186/1471-2350-8-36>
- Kamasaki, T., O'Toole, E., Kita, S., Osumi, M., Usukura, J., McIntosh, J. R., & Goshima, G. (2013). Augmin-dependent microtubule nucleation at microtubule walls in the spindle. *J Cell Biol*, *202*(1), 25-33. <https://doi.org/10.1083/jcb.201304031>
- Kaufmann, W. E., Sprouse, J., Rebowe, N., Hanania, T., Klamer, D., & Missling, C. U. (2019). ANAVEX®2-73 (blarcamesine), a Sigma-1 receptor agonist, ameliorates neurologic impairments in a mouse model of Rett syndrome. *Pharmacol Biochem Behav*, *187*, 172796. <https://doi.org/10.1016/j.pbb.2019.172796>
- Khwaja, O. S., Ho, E., Barnes, K. V., O'Leary, H. M., Pereira, L. M., Finkelstein, Y., Nelson, C. A., 3rd, Vogel-Farley, V., DeGregorio, G., Holm, I. A., Khatwa, U., Kapur, K., Alexander, M. E., Finnegan, D. M., Cantwell, N. G., Walco, A. C., Rappaport, L., Gregas, M., Fichorova, R. N., . . . Kaufmann, W. E. (2014). Safety, pharmacokinetics, and preliminary assessment of efficacy of mecasermin (recombinant human IGF-1) for the treatment of Rett syndrome. *Proc Natl Acad Sci U S A*, *111*(12), 4596-4601. <https://doi.org/10.1073/pnas.1311141111>
- Kim, D. G., Cho, S., Lee, K. Y., Cheon, S. H., Yoon, H. J., Lee, J. Y., Kim, D., Shin, K. S., Koh, C. H., Koo, J. S., Choi, Y., Lee, H. H., Oh, Y. K., Jeong, Y. S., Chung, S. J., Baek, M., Jung, K. Y., Lim, H. J., Kim, H. S., . . . Lee, B. J. (2021). Crystal structures of human NSDHL and development of its novel inhibitor with the potential to suppress EGFR activity. *Cell Mol Life Sci*, *78*(1), 207-225. <https://doi.org/10.1007/s00018-020-03490-2>
- Kim, K. Y., Hysolli, E., & Park, I. H. (2011). Neuronal maturation defect in induced pluripotent stem cells from patients with Rett syndrome. *Proc Natl Acad Sci U S A*, *108*(34), 14169-14174. <https://doi.org/10.1073/pnas.1018979108>
- Kinde, B., Gabel, H. W., Gilbert, C. S., Griffith, E. C., & Greenberg, M. E. (2015). Reading the unique DNA methylation landscape of the brain: Non-CpG methylation, hydroxymethylation, and MeCP2. *Proc Natl Acad Sci U S A*, *112*(22), 6800-6806. <https://doi.org/10.1073/pnas.1411269112>
- Kishi, N., MacDonald, J. L., Ye, J., Molyneaux, B. J., Azim, E., & Macklis, J. D. (2016). Reduction of aberrant NF-κB signalling ameliorates Rett syndrome phenotypes in Mecp2-null mice. *Nat Commun*, *7*, 10520. <https://doi.org/10.1038/ncomms10520>
- Klein, M. E., Liroy, D. T., Ma, L., Impey, S., Mandel, G., & Goodman, R. H. (2007). Homeostatic regulation of MeCP2 expression by a CREB-induced microRNA. *Nat Neurosci*, *10*(12), 1513-1514. <https://doi.org/10.1038/nn2010>
- Kokura, K., Kaul, S. C., Wadhwa, R., Nomura, T., Khan, M. M., Shinagawa, T., Yasukawa, T., Colmenares, C., & Ishii, S. (2001). The Ski protein family is required for MeCP2-mediated transcriptional repression. *J Biol Chem*, *276*(36), 34115-34121. <https://doi.org/10.1074/jbc.M105747200>
- Kriaucionis, S., Paterson, A., Curtis, J., Guy, J., Macleod, N., & Bird, A. (2006). Gene expression analysis exposes mitochondrial abnormalities in a mouse model of Rett syndrome. *Mol Cell Biol*, *26*(13), 5033-5042. <https://doi.org/10.1128/mcb.01665-05>
- Krishnaraj, R., Haase, F., Coorey, B., Luca, E. J., Wong, I., Boyling, A., Ellaway, C., Christodoulou, J., & Gold, W. A. (2019). Genome-wide transcriptomic and proteomic studies of Rett syndrome mouse models identify common signaling

- pathways and cellular functions as potential therapeutic targets. *Hum Mutat*, 40(12), 2184-2196. <https://doi.org/10.1002/humu.23887>
- Krishnaraj, R., Ho, G., & Christodoulou, J. (2017). RettBASE: Rett syndrome database update. *Hum Mutat*, 38(8), 922-931. <https://doi.org/10.1002/humu.23263>
- Krol, J., Loedige, I., & Filipowicz, W. (2010). The widespread regulation of microRNA biogenesis, function and decay. *Nat Rev Genet*, 11(9), 597-610. <https://doi.org/10.1038/nrg2843>
- Kron, M., Howell, C. J., Adams, I. T., Ransbottom, M., Christian, D., Ogier, M., & Katz, D. M. (2012). Brain activity mapping in Mecp2 mutant mice reveals functional deficits in forebrain circuits, including key nodes in the default mode network, that are reversed with ketamine treatment. *J Neurosci*, 32(40), 13860-13872. <https://doi.org/10.1523/jneurosci.2159-12.2012>
- Landucci E, Brindisi M, Bianciardi L, Catania LM, Daga S, Croci S, Frullanti E, Fallerini C, Butini S, Brogi S et al (2018) iPSC-derived neurons profiling reveals GABAergic circuit disruption and acetylated α -tubulin defect which improves after iHDAC6 treatment in Rett syndrome. *Exp Cell Res* 368: 225-235
- Laubner, D., Breitling, R., & Adamski, J. (2003). Embryonic expression of cholesterologenic genes is restricted to distinct domains and colocalizes with apoptotic regions in mice. *Brain Res Mol Brain Res*, 115(1), 87-92. [https://doi.org/10.1016/s0169-328x\(03\)00094-9](https://doi.org/10.1016/s0169-328x(03)00094-9)
- Lawo, S., Bashkurov, M., Mullin, M., Ferreria, M. G., Kittler, R., Habermann, B., Tagliaferro, A., Poser, I., Hutchins, J. R., Hegemann, B., Pinchev, D., Buchholz, F., Peters, J. M., Hyman, A. A., Gingras, A. C., & Pelletier, L. (2009). HAUS, the 8-subunit human Augmin complex, regulates centrosome and spindle integrity. *Curr Biol*, 19(10), 816-826. <https://doi.org/10.1016/j.cub.2009.04.033>
- Le, T. T. H., Tran, N. T., Dao, T. M. L., Nguyen, D. D., Do, H. D., Ha, T. L., Kühn, R., Nguyen, T. L., Rajewsky, K., & Chu, V. T. (2019). Efficient and Precise CRISPR/Cas9-Mediated MECP2 Modifications in Human-Induced Pluripotent Stem Cells. *Front Genet*, 10, 625. <https://doi.org/10.3389/fgene.2019.00625>
- Lee, H. M., Kuijjer, M. B., Ruiz Blanes, N., Clark, E. P., Aita, M., Galiano Arjona, L., Kokot, A., Sciaky, N., Simon, J. M., Bhatnagar, S., Philpot, B. D., & Cerase, A. (2020). A small-molecule screen reveals novel modulators of MeCP2 and X-chromosome inactivation maintenance. *J Neurodev Disord*, 12(1), 29. <https://doi.org/10.1186/s11689-020-09332-3>
- Lekman, A. Y., Hagberg, B. A., & Svennerholm, L. T. (1991). Membrane cerebral lipids in Rett syndrome. *Pediatr Neurol*, 7(3), 186-190. [https://doi.org/10.1016/0887-8994\(91\)90082-v](https://doi.org/10.1016/0887-8994(91)90082-v)
- Lekman, A. Y., Hagberg, B. A., & Svennerholm, L. T. (1999). Cerebrospinal fluid gangliosides in patients with Rett syndrome and infantile neuronal ceroid lipofuscinosis. *Eur J Paediatr Neurol*, 3(3), 119-123. [https://doi.org/10.1016/s1090-3798\(99\)90099-5](https://doi.org/10.1016/s1090-3798(99)90099-5)
- Leonard, H., Gold, W., Samaco, R., Sahin, M., Benke, T., & Downs, J. (2022). Improving clinical trial readiness to accelerate development of new therapeutics for Rett syndrome. *Orphanet J Rare Dis*, 17(1), 108. <https://doi.org/10.1186/s13023-022-02240-w>
- Lewis, J. D., Meehan, R. R., Henzel, W. J., Maurer-Fogy, I., Jeppesen, P., Klein, F., & Bird, A. (1992). Purification, sequence, and cellular localization of a novel

- chromosomal protein that binds to methylated DNA. *Cell*, 69(6), 905-914. [https://doi.org/10.1016/0092-8674\(92\)90610-o](https://doi.org/10.1016/0092-8674(92)90610-o)
- Li, C., & Samulski, R. J. (2020). Engineering adeno-associated virus vectors for gene therapy. *Nat Rev Genet*, 21(4), 255-272. <https://doi.org/10.1038/s41576-019-0205-4>
- Li, Y., Wang, H., Muffat, J., Cheng, A. W., Orlando, D. A., Lovén, J., Kwok, S. M., Feldman, D. A., Bateup, H. S., Gao, Q., Hockemeyer, D., Mitalipova, M., Lewis, C. A., Vander Heiden, M. G., Sur, M., Young, R. A., & Jaenisch, R. (2013). Global transcriptional and translational repression in human-embryonic-stem-cell-derived Rett syndrome neurons. *Cell Stem Cell*, 13(4), 446-458. <https://doi.org/10.1016/j.stem.2013.09.001>
- Lioy, D. T., Garg, S. K., Monaghan, C. E., Raber, J., Foust, K. D., Kaspar, B. K., Hirrlinger, P. G., Kirchhoff, F., Bissonnette, J. M., Ballas, N., & Mandel, G. (2011). A role for glia in the progression of Rett's syndrome. *Nature*, 475(7357), 497-500. <https://doi.org/10.1038/nature10214>
- Liu, X. Y., Dangel, A. W., Kelley, R. I., Zhao, W., Denny, P., Botcherby, M., Cattanach, B., Peters, J., Hunsicker, P. R., Mallon, A. M., Strivens, M. A., Bate, R., Miller, W., Rhodes, M., Brown, S. D., & Herman, G. E. (1999). The gene mutated in bare patches and striated mice encodes a novel 3beta-hydroxysteroid dehydrogenase. *Nat Genet*, 22(2), 182-187. <https://doi.org/10.1038/9700>
- Livak, K. J., & Schmittgen, T. D. (2001). Analysis of relative gene expression data using real-time quantitative PCR and the 2(-Delta Delta C(T)) Method. *Methods*, 25(4), 402-408. <https://doi.org/10.1006/meth.2001.1262>
- Lombardi, L. M., Baker, S. A., & Zoghbi, H. Y. (2015). MECP2 disorders: from the clinic to mice and back. *J Clin Invest*, 125(8), 2914-2923. <https://doi.org/10.1172/jci78167>
- Long, S. W., Ooi, J. Y., Yau, P. M., & Jones, P. L. (2011). A brain-derived MeCP2 complex supports a role for MeCP2 in RNA processing. *Biosci Rep*, 31(5), 333-343. <https://doi.org/10.1042/bsr20100124>
- Lopez, A. M., Chuang, J. C., Posey, K. S., & Turley, S. D. (2017). Suppression of brain cholesterol synthesis in male Mecp2-deficient mice is age dependent and not accompanied by a concurrent change in the rate of fatty acid synthesis. *Brain Res*, 1654(Pt A), 77-84. <https://doi.org/10.1016/j.brainres.2016.10.021>
- Lund, E. G., Xie, C., Kotti, T., Turley, S. D., Dietschy, J. M., & Russell, D. W. (2003). Knockout of the cholesterol 24-hydroxylase gene in mice reveals a brain-specific mechanism of cholesterol turnover. *J Biol Chem*, 278(25), 22980-22988. <https://doi.org/10.1074/jbc.M303415200>
- Luoni, M., Giannelli, S., Indrigo, M. T., Niro, A., Massimino, L., Iannielli, A., Passeri, L., Russo, F., Morabito, G., Calamita, P., Gregori, S., Deverman, B., & Broccoli, V. (2020). Whole brain delivery of an instability-prone Mecp2 transgene improves behavioral and molecular pathological defects in mouse models of Rett syndrome. *Elife*, 9. <https://doi.org/10.7554/eLife.52629>
- Lykken, E. A., Shyng, C., Edwards, R. J., Rozenberg, A., & Gray, S. J. (2018). Recent progress and considerations for AAV gene therapies targeting the central nervous system. *J Neurodev Disord*, 10(1), 16. <https://doi.org/10.1186/s11689-018-9234-0>
- Lyst, M. J., & Bird, A. (2015). Rett syndrome: a complex disorder with simple roots. *Nat Rev Genet*, 16(5), 261-275. <https://doi.org/10.1038/nrg3897>

- Lyst, M. J., Ekiert, R., Ebert, D. H., Merusi, C., Nowak, J., Selfridge, J., Guy, J., Kastan, N. R., Robinson, N. D., de Lima Alves, F., Rappsilber, J., Greenberg, M. E., & Bird, A. (2013). Rett syndrome mutations abolish the interaction of MeCP2 with the NCoR/SMRT co-repressor. *Nat Neurosci*, *16*(7), 898-902. <https://doi.org/10.1038/nn.3434>
- Maezawa, I., & Jin, L. W. (2010). Rett syndrome microglia damage dendrites and synapses by the elevated release of glutamate. *J Neurosci*, *30*(15), 5346-5356. <https://doi.org/10.1523/jneurosci.5966-09.2010>
- Maezawa, I., Swanberg, S., Harvey, D., LaSalle, J. M., & Jin, L. W. (2009). Rett syndrome astrocytes are abnormal and spread MeCP2 deficiency through gap junctions. *J Neurosci*, *29*(16), 5051-5061. <https://doi.org/10.1523/jneurosci.0324-09.2009>
- Mancini, J., Dubus, J. C., Jouve, E., Roux, J. C., Franco, P., Lagrue, E., Castelnaud, P., Cances, C., Chaix, Y., Rougeot-Jung, C., Cornu, C., Desportes, V., Vallée, L., Bahi-Buisson, N., Truillet, R., Attolini, L., Villard, L., Blin, O., & Micallef, J. (2018). Effect of desipramine on patients with breathing disorders in RETT syndrome. *Ann Clin Transl Neurol*, *5*(2), 118-127. <https://doi.org/10.1002/acn3.468>
- Marano, D., Fioriniello, S., D'Esposito, M., & Della Ragione, F. (2021). Transcriptomic and Epigenomic Landscape in Rett Syndrome. *Biomolecules*, *11*(7). <https://doi.org/10.3390/biom11070967>
- Marballi, K., & MacDonald, J. L. (2021). Proteomic and transcriptional changes associated with MeCP2 dysfunction reveal nodes for therapeutic intervention in Rett syndrome. *Neurochem Int*, *148*, 105076. <https://doi.org/10.1016/j.neuint.2021.105076>
- Marchetto, M. C., Carromeu, C., Acab, A., Yu, D., Yeo, G. W., Mu, Y., Chen, G., Gage, F. H., & Muotri, A. R. (2010). A model for neural development and treatment of Rett syndrome using human induced pluripotent stem cells. *Cell*, *143*(4), 527-539. <https://doi.org/10.1016/j.cell.2010.10.016>
- Marschik, P. B., Kaufmann, W. E., Sigafos, J., Wolin, T., Zhang, D., Bartl-Pokorny, K. D., Pini, G., Zappella, M., Tager-Flusberg, H., Einspieler, C., & Johnston, M. V. (2013). Changing the perspective on early development of Rett syndrome. *Res Dev Disabil*, *34*(4), 1236-1239. <https://doi.org/10.1016/j.ridd.2013.01.014>
- Matagne, V., Ehinger, Y., Saidi, L., Borges-Correia, A., Barkats, M., Bartoli, M., Villard, L., & Roux, J. C. (2017). A codon-optimized Mecp2 transgene corrects breathing deficits and improves survival in a mouse model of Rett syndrome. *Neurobiol Dis*, *99*, 1-11. <https://doi.org/10.1016/j.nbd.2016.12.009>
- McCormack, M. P., & Rabbitts, T. H. (2004). Activation of the T-cell oncogene LMO2 after gene therapy for X-linked severe combined immunodeficiency. *N Engl J Med*, *350*(9), 913-922. <https://doi.org/10.1056/NEJMra032207>
- McGraw, C. M., Samaco, R. C., & Zoghbi, H. Y. (2011). Adult neural function requires MeCP2. *Science*, *333*(6039), 186. <https://doi.org/10.1126/science.1206593>
- McKinley, K. L., & Cheeseman, I. M. (2017). Large-Scale Analysis of CRISPR/Cas9 Cell-Cycle Knockouts Reveals the Diversity of p53-Dependent Responses to Cell-Cycle Defects. *Dev Cell*, *40*(4), 405-420.e402. <https://doi.org/10.1016/j.devcel.2017.01.012>
- McLarren, K. W., Severson, T. M., du Souich, C., Stockton, D. W., Kratz, L. E., Cunningham, D., Henderson, G., Morin, R. D., Wu, D., Paul, J. E., An, J., Nelson,

- T. N., Chou, A., DeBarber, A. E., Merkens, L. S., Michaud, J. L., Waters, P. J., Yin, J., McGillivray, B., . . . Boerkoel, C. F. (2010). Hypomorphic temperature-sensitive alleles of NSDHL cause CK syndrome. *Am J Hum Genet*, *87*(6), 905-914. <https://doi.org/10.1016/j.ajhg.2010.11.004>
- Meaney, S., Bodin, K., Diczfalusy, U., & Björkhem, I. (2002). On the rate of translocation in vitro and kinetics in vivo of the major oxysterols in human circulation: critical importance of the position of the oxygen function. *J Lipid Res*, *43*(12), 2130-2135. <https://doi.org/10.1194/jlr.m200293-jlr200>
- Medrihan, L., Tantalaki, E., Aramuni, G., Sargsyan, V., Dudanova, I., Missler, M., & Zhang, W. (2008). Early defects of GABAergic synapses in the brain stem of a MeCP2 mouse model of Rett syndrome. *J Neurophysiol*, *99*(1), 112-121. <https://doi.org/10.1152/jn.00826.2007>
- Mellén, M., Ayata, P., Dewell, S., Kriaucionis, S., & Heintz, N. (2012). MeCP2 binds to 5hmC enriched within active genes and accessible chromatin in the nervous system. *Cell*, *151*(7), 1417-1430. <https://doi.org/10.1016/j.cell.2012.11.022>
- Mnatzakanian, G. N., Lohi, H., Munteanu, I., Alfred, S. E., Yamada, T., MacLeod, P. J., Jones, J. R., Scherer, S. W., Schanen, N. C., Friez, M. J., Vincent, J. B., & Minassian, B. A. (2004). A previously unidentified MECP2 open reading frame defines a new protein isoform relevant to Rett syndrome. *Nat Genet*, *36*(4), 339-341. <https://doi.org/10.1038/ng1327>
- Mo, C., Valachovic, M., Randall, S. K., Nickels, J. T., & Bard, M. (2002). Protein-protein interactions among C-4 demethylation enzymes involved in yeast sterol biosynthesis. *Proc Natl Acad Sci U S A*, *99*(15), 9739-9744. <https://doi.org/10.1073/pnas.112202799>
- Morabito, G., Giannelli, S. G., Ordazzo, G., Bido, S., Castoldi, V., Indrigo, M., Cabassi, T., Cattaneo, S., Luoni, M., Cancellieri, C., Sessa, A., Bacigaluppi, M., Taverna, S., Leocani, L., Lanciego, J. L., & Broccoli, V. (2017). AAV-PHP.B-Mediated Global-Scale Expression in the Mouse Nervous System Enables GBA1 Gene Therapy for Wide Protection from Synucleinopathy. *Mol Ther*, *25*(12), 2727-2742. <https://doi.org/10.1016/j.ymthe.2017.08.004>
- Moroto, M., Nishimura, A., Morimoto, M., Isoda, K., Morita, T., Yoshida, M., Morioka, S., Tozawa, T., Hasegawa, T., Chiyonobu, T., Yoshimoto, K., & Hosoi, H. (2013). Altered somatosensory barrel cortex refinement in the developing brain of Mecp2-null mice. *Brain Res*, *1537*, 319-326. <https://doi.org/10.1016/j.brainres.2013.09.017>
- Moser, S. J., Weber, P., & Lütschg, J. (2007). Rett syndrome: clinical and electrophysiologic aspects. *Pediatr Neurol*, *36*(2), 95-100. <https://doi.org/10.1016/j.pediatrneurol.2006.10.003>
- Müller, M. (2019). Disturbed redox homeostasis and oxidative stress: Potential players in the developmental regression in Rett syndrome. *Neurosci Biobehav Rev*, *98*, 154-163. <https://doi.org/10.1016/j.neubiorev.2018.12.009>
- Naegelin, Y., Kuhle, J., Schädelin, S., Datta, A. N., Magon, S., Amann, M., Barro, C., Ramelli, G. P., Heesom, K., Barde, Y. A., Weber, P., & Kappos, L. (2021). Fingolimod in children with Rett syndrome: the FINGORETT study. *Orphanet J Rare Dis*, *16*(1), 19. <https://doi.org/10.1186/s13023-020-01655-7>
- Nagarajan, N., Quast, C., Boxall, A. R., Shahid, M., & Rosenmund, C. (2001). Mechanism and impact of allosteric AMPA receptor modulation by the ampakine

- CX546. *Neuropharmacology*, 41(6), 650-663. [https://doi.org/10.1016/s0028-3908\(01\)00133-2](https://doi.org/10.1016/s0028-3908(01)00133-2)
- Nageshappa, S., Carromeu, C., Trujillo, C. A., Mesci, P., Espuny-Camacho, I., Pasciuto, E., Vanderhaeghen, P., Verfaillie, C. M., Raitano, S., Kumar, A., Carvalho, C. M., Bagni, C., Ramocki, M. B., Araujo, B. H., Torres, L. B., Lupski, J. R., Van Esch, H., & Muotri, A. R. (2016). Altered neuronal network and rescue in a human MECP2 duplication model. *Mol Psychiatry*, 21(2), 178-188. <https://doi.org/10.1038/mp.2015.128>
- Nan, X., Campoy, F. J., & Bird, A. (1997). MeCP2 is a transcriptional repressor with abundant binding sites in genomic chromatin. *Cell*, 88(4), 471-481. [https://doi.org/10.1016/s0092-8674\(00\)81887-5](https://doi.org/10.1016/s0092-8674(00)81887-5)
- Nan, X., Ng, H. H., Johnson, C. A., Laherty, C. D., Turner, B. M., Eisenman, R. N., & Bird, A. (1998). Transcriptional repression by the methyl-CpG-binding protein MeCP2 involves a histone deacetylase complex. *Nature*, 393(6683), 386-389. <https://doi.org/10.1038/30764>
- Nan, X., Tate, P., Li, E., & Bird, A. (1996). DNA methylation specifies chromosomal localization of MeCP2. *Mol Cell Biol*, 16(1), 414-421. <https://doi.org/10.1128/mcb.16.1.414>
- Nectoux, J., Fichou, Y., Rosas-Vargas, H., Cagnard, N., Bahi-Buisson, N., Nusbaum, P., Letourneur, F., Chelly, J., & Bienvenu, T. (2010). Cell cloning-based transcriptome analysis in Rett patients: relevance to the pathogenesis of Rett syndrome of new human MeCP2 target genes. *J Cell Mol Med*, 14(7), 1962-1974. <https://doi.org/10.1111/j.1582-4934.2010.01107.x>
- Nerli, E., Roggero, O. M., Baj, G., & Tongiorgi, E. (2020). In vitro modeling of dendritic atrophy in Rett syndrome: determinants for phenotypic drug screening in neurodevelopmental disorders. *Sci Rep*, 10(1), 2491. <https://doi.org/10.1038/s41598-020-59268-w>
- Neul, J. L., Fang, P., Barrish, J., Lane, J., Caeg, E. B., Smith, E. O., Zoghbi, H., Percy, A., & Glaze, D. G. (2008). Specific mutations in methyl-CpG-binding protein 2 confer different severity in Rett syndrome. *Neurology*, 70(16), 1313-1321. <https://doi.org/10.1212/01.wnl.0000291011.54508.aa>
- Neul, J. L., Kaufmann, W. E., Glaze, D. G., Christodoulou, J., Clarke, A. J., Bahi-Buisson, N., Leonard, H., Bailey, M. E., Schanen, N. C., Zappella, M., Renieri, A., Huppke, P., & Percy, A. K. (2010). Rett syndrome: revised diagnostic criteria and nomenclature. *Ann Neurol*, 68(6), 944-950. <https://doi.org/10.1002/ana.22124>
- Neul, J. L., Percy, A. K., Benke, T. A., Berry-Kravis, E. M., Glaze, D. G., Peters, S. U., Jones, N. E., & Youakim, J. M. (2022). Design and outcome measures of LAVENDER, a phase 3 study of trofinetide for Rett syndrome. *Contemp Clin Trials*, 114, 106704. <https://doi.org/10.1016/j.cct.2022.106704>
- Neul, J. L., Skinner, S. A., Annese, F., Lane, J., Heydemann, P., Jones, M., Kaufmann, W. E., Glaze, D. G., & Percy, A. K. (2020). Metabolic Signatures Differentiate Rett Syndrome From Unaffected Siblings. *Front Integr Neurosci*, 14, 7. <https://doi.org/10.3389/fnint.2020.00007>
- Nomura, Y. (2005). Early behavior characteristics and sleep disturbance in Rett syndrome. *Brain Dev*, 27 Suppl 1, S35-s42. <https://doi.org/10.1016/j.braindev.2005.03.017>

- Nomura, Y., & Segawa, M. (2005). Natural history of Rett syndrome. *J Child Neurol*, 20(9), 764-768. <https://doi.org/10.1177/08830738050200091201>
- Nuber, U. A., Kriaucionis, S., Roloff, T. C., Guy, J., Selfridge, J., Steinhoff, C., Schulz, R., Lipkowitz, B., Ropers, H. H., Holmes, M. C., & Bird, A. (2005). Up-regulation of glucocorticoid-regulated genes in a mouse model of Rett syndrome. *Hum Mol Genet*, 14(15), 2247-2256. <https://doi.org/10.1093/hmg/ddi229>
- O'Driscoll, C. M., Lima, M. P., Kaufmann, W. E., & Bressler, J. P. (2015). Methyl CpG binding protein 2 deficiency enhances expression of inflammatory cytokines by sustaining NF- κ B signaling in myeloid derived cells. *J Neuroimmunol*, 283, 23-29. <https://doi.org/10.1016/j.jneuroim.2015.04.005>
- O'Kusky, J. R., Ye, P., & D'Ercole, A. J. (2000). Insulin-like growth factor-I promotes neurogenesis and synaptogenesis in the hippocampal dentate gyrus during postnatal development. *J Neurosci*, 20(22), 8435-8442. <https://doi.org/10.1523/jneurosci.20-22-08435.2000>
- O'Leary, H. M., Kaufmann, W. E., Barnes, K. V., Rakesh, K., Kapur, K., Tarquinio, D. C., Cantwell, N. G., Roche, K. J., Rose, S. A., Walco, A. C., Bruck, N. M., Bazin, G. A., Holm, I. A., Alexander, M. E., Swanson, L. C., Baczewski, L. M., Poon, C., Mayor Torres, J. M., Nelson, C. A., 3rd, & Sahin, M. (2018). Placebo-controlled crossover assessment of mecamermin for the treatment of Rett syndrome. *Ann Clin Transl Neurol*, 5(3), 323-332. <https://doi.org/10.1002/acn3.533>
- Ogier, M., Wang, H., Hong, E., Wang, Q., Greenberg, M. E., & Katz, D. M. (2007). Brain-derived neurotrophic factor expression and respiratory function improve after ampakine treatment in a mouse model of Rett syndrome. *J Neurosci*, 27(40), 10912-10917. <https://doi.org/10.1523/jneurosci.1869-07.2007>
- Okabe, Y., Kusaga, A., Takahashi, T., Mitsumasu, C., Murai, Y., Tanaka, E., Higashi, H., Matsuishi, T., & Kosai, K. (2010). Neural development of methyl-CpG-binding protein 2 null embryonic stem cells: a system for studying Rett syndrome. *Brain Res*, 1360, 17-27. <https://doi.org/10.1016/j.brainres.2010.08.090>
- Osenberg, S., Karten, A., Sun, J., Li, J., Charkowick, S., Felice, C. A., Kritzer, M., Nguyen, M. V. C., Yu, P., & Ballas, N. (2018). Activity-dependent aberrations in gene expression and alternative splicing in a mouse model of Rett syndrome. *Proc Natl Acad Sci U S A*, 115(23), E5363-e5372. <https://doi.org/10.1073/pnas.1722546115>
- Pacheco, N. L., Heaven, M. R., Holt, L. M., Crossman, D. K., Boggio, K. J., Shaffer, S. A., Flint, D. L., & Olsen, M. L. (2017). RNA sequencing and proteomics approaches reveal novel deficits in the cortex of Mecp2-deficient mice, a model for Rett syndrome. *Mol Autism*, 8, 56. <https://doi.org/10.1186/s13229-017-0174-4>
- Panayotis, N., Ehinger, Y., Felix, M. S., & Roux, J. C. (2022). State-of-the-art therapies for Rett syndrome. *Dev Med Child Neurol*. <https://doi.org/10.1111/dmcn.15383>
- Patnaik, A., Spiombi, E., Frasca, A., Landsberger, N., Zagrebelsky, M., & Korte, M. (2020). Fingolimod Modulates Dendritic Architecture in a BDNF-Dependent Manner. *Int J Mol Sci*, 21(9). <https://doi.org/10.3390/ijms21093079>
- Patrizi, A., Picard, N., Simon, A. J., Gunner, G., Centofante, E., Andrews, N. A., & Fagiolini, M. (2016). Chronic Administration of the N-Methyl-D-Aspartate Receptor Antagonist Ketamine Improves Rett Syndrome Phenotype. *Biol Psychiatry*, 79(9), 755-764. <https://doi.org/10.1016/j.biopsych.2015.08.018>

- Pecorelli, A., Leoni, G., Cervellati, F., Canali, R., Signorini, C., Leoncini, S., Cortelazzo, A., De Felice, C., Ciccoli, L., Hayek, J., & Valacchi, G. (2013). Genes related to mitochondrial functions, protein degradation, and chromatin folding are differentially expressed in lymphomonocytes of Rett syndrome patients. *Mediators Inflamm*, 2013, 137629. <https://doi.org/10.1155/2013/137629>
- Penning, T. M. (1997). Molecular endocrinology of hydroxysteroid dehydrogenases. *Endocr Rev*, 18(3), 281-305. <https://doi.org/10.1210/edrv.18.3.0302>
- Petrov, A. M., Kasimov, M. R., & Zefirov, A. L. (2016). Brain Cholesterol Metabolism and Its Defects: Linkage to Neurodegenerative Diseases and Synaptic Dysfunction. *Acta Naturae*, 8(1), 58-73.
- Petry, S., Groen, A. C., Ishihara, K., Mitchison, T. J., & Vale, R. D. (2013). Branching microtubule nucleation in *Xenopus* egg extracts mediated by augmin and TPX2. *Cell*, 152(4), 768-777. <https://doi.org/10.1016/j.cell.2012.12.044>
- Picker, J. D., Yang, R., Ricceri, L., & Berger-Sweeney, J. (2006). An altered neonatal behavioral phenotype in *Mecp2* mutant mice. *Neuroreport*, 17(5), 541-544. <https://doi.org/10.1097/01.wnr.0000208995.38695.2f>
- Pini, G., Congiu, L., Benincasa, A., DiMarco, P., Bigoni, S., Dyer, A. H., Mortimer, N., Della-Chiesa, A., O'Leary, S., McNamara, R., Mitchell, K. J., Gill, M., & Tropea, D. (2016). Illness Severity, Social and Cognitive Ability, and EEG Analysis of Ten Patients with Rett Syndrome Treated with Mecasermin (Recombinant Human IGF-1). *Autism Res Treat*, 2016, 5073078. <https://doi.org/10.1155/2016/5073078>
- Przanowski, P., Wasko, U., Zheng, Z., Yu, J., Sherman, R., Zhu, L. J., McConnell, M. J., Tushir-Singh, J., Green, M. R., & Bhatnagar, S. (2018). Pharmacological reactivation of inactive X-linked *Mecp2* in cerebral cortical neurons of living mice. *Proc Natl Acad Sci U S A*, 115(31), 7991-7996. <https://doi.org/10.1073/pnas.1803792115>
- Qu, X., Kumar, A., Blockus, H., Waites, C., & Bartolini, F. (2019). Activity-Dependent Nucleation of Dynamic Microtubules at Presynaptic Boutons Controls Neurotransmission. *Curr Biol*, 29(24), 4231-4240.e4235. <https://doi.org/10.1016/j.cub.2019.10.049>
- Rett, A. (1966). [On a unusual brain atrophy syndrome in hyperammonemia in childhood]. *Wien Med Wochenschr*, 116(37), 723-726. (Uber ein eigenartiges hirnatrophisches Syndrom bei Hyperammonämie im Kindersalter.)
- Ricciardi, S., Boggio, E. M., Grosso, S., Lonetti, G., Forlani, G., Stefanelli, G., Calcagno, E., Morello, N., Landsberger, N., Biffo, S., Pizzorusso, T., Giustetto, M., & Broccoli, V. (2011). Reduced AKT/mTOR signaling and protein synthesis dysregulation in a Rett syndrome animal model. *Hum Mol Genet*, 20(6), 1182-1196. <https://doi.org/10.1093/hmg/ddq563>
- Riedmann, C., & Fondufe-Mittendorf, Y. N. (2016). Comparative analysis of linker histone H1, MeCP2, and HMGD1 on nucleosome stability and target site accessibility. *Sci Rep*, 6, 33186. <https://doi.org/10.1038/srep33186>
- Ross, P. D., Guy, J., Selfridge, J., Kamal, B., Bahey, N., Tanner, K. E., Gillingwater, T. H., Jones, R. A., Loughrey, C. M., McCarroll, C. S., Bailey, M. E., Bird, A., & Cobb, S. (2016). Exclusive expression of MeCP2 in the nervous system distinguishes between brain and peripheral Rett syndrome-like phenotypes. *Hum Mol Genet*, 25(20), 4389-4404. <https://doi.org/10.1093/hmg/ddw269>
- Roux, J. C., Zala, D., Panayotis, N., Borges-Correia, A., Saudou, F., & Villard, L. (2012a). Modification of *Mecp2* dosage alters axonal transport through the

- Huntingtin/Hap1 pathway. *Neurobiol Dis*, 45(2), 786-795. <https://doi.org/10.1016/j.nbd.2011.11.002>
- Roux, J. C., Zala, D., Panayotis, N., Borges-Correia, A., Saudou, F., & Villard, L. (2012b). [Unexpected link between Huntington disease and Rett syndrome]. *Med Sci (Paris)*, 28(1), 44-46. <https://doi.org/10.1051/medsci/2012281016> (Un lien inattendu entre maladie de Huntington et syndrome de Rett.)
- Sánchez-Huertas, C., & Lüders, J. (2015). The augmin connection in the geometry of microtubule networks. *Curr Biol*, 25(7), R294-299. <https://doi.org/10.1016/j.cub.2015.02.006>
- Sanfeliu, A., Kaufmann, W. E., Gill, M., Guasoni, P., & Tropea, D. (2019). Transcriptomic Studies in Mouse Models of Rett Syndrome: A Review. *Neuroscience*, 413, 183-205. <https://doi.org/10.1016/j.neuroscience.2019.06.013>
- Scaramuzza, L., De Rocco, G., Desiato, G., Cobolli Gigli, C., Chiacchiarretta, M., Mirabella, F., Pozzi, D., De Simone, M., Conforti, P., Pagani, M., Benfenati, F., Cesca, F., Bedogni, F., & Landsberger, N. (2021). The enhancement of activity rescues the establishment of Mecp2 null neuronal phenotypes. *EMBO Mol Med*, 13(4), e12433. <https://doi.org/10.15252/emmm.202012433>
- Schitine, C., Xapelli, S., Agasse, F., Sardà-Arroyo, L., Silva, A. P., De Melo Reis, R. A., de Mello, F. G., & Malva, J. O. (2012). Ampakine CX546 increases proliferation and neuronal differentiation in subventricular zone stem/progenitor cell cultures. *Eur J Neurosci*, 35(11), 1672-1683. <https://doi.org/10.1111/j.1460-9568.2012.08072.x>
- Segatto, M., Trapani, L., Di Tunno, I., Sticozzi, C., Valacchi, G., Hayek, J., & Pallottini, V. (2014). Cholesterol metabolism is altered in Rett syndrome: a study on plasma and primary cultured fibroblasts derived from patients. *PLoS One*, 9(8), e104834. <https://doi.org/10.1371/journal.pone.0104834>
- Shahbazian, M., Young, J., Yuva-Paylor, L., Spencer, C., Antalffy, B., Noebels, J., Armstrong, D., Paylor, R., & Zoghbi, H. (2002). Mice with truncated MeCP2 recapitulate many Rett syndrome features and display hyperacetylation of histone H3. *Neuron*, 35(2), 243-254. [https://doi.org/10.1016/s0896-6273\(02\)00768-7](https://doi.org/10.1016/s0896-6273(02)00768-7)
- Shahbazian, M. D., Antalffy, B., Armstrong, D. L., & Zoghbi, H. Y. (2002). Insight into Rett syndrome: MeCP2 levels display tissue- and cell-specific differences and correlate with neuronal maturation. *Hum Mol Genet*, 11(2), 115-124. <https://doi.org/10.1093/hmg/11.2.115>
- Sharma, A., & Mehan, S. (2021). Targeting PI3K-AKT/mTOR signaling in the prevention of autism. *Neurochem Int*, 147, 105067. <https://doi.org/10.1016/j.neuint.2021.105067>
- Shovlin, S., Delepine, C., Swanson, L., Bach, S., Sahin, M., Sur, M., Kaufmann, W. E., & Tropea, D. (2022). Molecular Signatures of Response to Mecasermin in Children With Rett Syndrome. *Front Neurosci*, 16, 868008. <https://doi.org/10.3389/fnins.2022.868008>
- Shovlin, S., & Tropea, D. (2018). Transcriptome level analysis in Rett syndrome using human samples from different tissues. *Orphanet J Rare Dis*, 13(1), 113. <https://doi.org/10.1186/s13023-018-0857-8>
- Signorini, C., De Felice, C., Leoncini, S., Giardini, A., D'Esposito, M., Filosa, S., Della Ragione, F., Rossi, M., Pecorelli, A., Valacchi, G., Ciccoli, L., & Hayek, J. (2011). F₄-neuroprostanes mediate neurological severity in Rett syndrome. *Clin Chim Acta*, 412(15-16), 1399-1406. <https://doi.org/10.1016/j.cca.2011.04.016>

- Sinnett, S. E., Boyle, E., Lyons, C., & Gray, S. J. (2021). Engineered microRNA-based regulatory element permits safe high-dose miniMECP2 gene therapy in Rett mice. *Brain*, *144*(10), 3005-3019. <https://doi.org/10.1093/brain/awab182>
- Sinnett, S. E., Hector, R. D., Gadalla, K. K. E., Heindel, C., Chen, D., Zaric, V., Bailey, M. E. S., Cobb, S. R., & Gray, S. J. (2017). Improved MECP2 Gene Therapy Extends the Survival of MeCP2-Null Mice without Apparent Toxicity after Intracisternal Delivery. *Mol Ther Methods Clin Dev*, *5*, 106-115. <https://doi.org/10.1016/j.omtm.2017.04.006>
- Skene, P. J., Illingworth, R. S., Webb, S., Kerr, A. R., James, K. D., Turner, D. J., Andrews, R., & Bird, A. P. (2010). Neuronal MeCP2 is expressed at near histone-octamer levels and globally alters the chromatin state. *Mol Cell*, *37*(4), 457-468. <https://doi.org/10.1016/j.molcel.2010.01.030>
- Smrt, R. D., Szulwach, K. E., Pfeiffer, R. L., Li, X., Guo, W., Pathania, M., Teng, Z. Q., Luo, Y., Peng, J., Bordey, A., Jin, P., & Zhao, X. (2010). MicroRNA miR-137 regulates neuronal maturation by targeting ubiquitin ligase mind bomb-1. *Stem Cells*, *28*(6), 1060-1070. <https://doi.org/10.1002/stem.431>
- Spitzer, N. C. (2006). Electrical activity in early neuronal development. *Nature*, *444*(7120), 707-712. <https://doi.org/10.1038/nature05300>
- Squillaro, T., Alessio, N., Cipollaro, M., Melone, M. A., Hayek, G., Renieri, A., Giordano, A., & Galderisi, U. (2012). Reduced expression of MECP2 affects cell commitment and maintenance in neurons by triggering senescence: new perspective for Rett syndrome. *Mol Biol Cell*, *23*(8), 1435-1445. <https://doi.org/10.1091/mbc.E11-09-0784>
- Sugino, K., Hempel, C. M., Okaty, B. W., Arnson, H. A., Kato, S., Dani, V. S., & Nelson, S. B. (2014). Cell-type-specific repression by methyl-CpG-binding protein 2 is biased toward long genes. *J Neurosci*, *34*(38), 12877-12883. <https://doi.org/10.1523/jneurosci.2674-14.2014>
- Tang, X., Drotar, J., Li, K., Clairmont, C. D., Brumm, A. S., Sullins, A. J., Wu, H., Liu, X. S., Wang, J., Gray, N. S., Sur, M., & Jaenisch, R. (2019). Pharmacological enhancement of KCC2 gene expression exerts therapeutic effects on human Rett syndrome neurons and Mecp2 mutant mice. *Sci Transl Med*, *11*(503). <https://doi.org/10.1126/scitranslmed.aau0164>
- Tarquinio, D. C., Motil, K. J., Hou, W., Lee, H. S., Glaze, D. G., Skinner, S. A., Neul, J. L., Annese, F., McNair, L., Barrish, J. O., Geerts, S. P., Lane, J. B., & Percy, A. K. (2012). Growth failure and outcome in Rett syndrome: specific growth references. *Neurology*, *79*(16), 1653-1661. <https://doi.org/10.1212/WNL.0b013e31826e9a70>
- Tierney, E., Bukelis, I., Thompson, R. E., Ahmed, K., Aneja, A., Kratz, L., & Kelley, R. I. (2006). Abnormalities of cholesterol metabolism in autism spectrum disorders. *Am J Med Genet B Neuropsychiatr Genet*, *141b*(6), 666-668. <https://doi.org/10.1002/ajmg.b.30368>
- Tillotson, R., & Bird, A. (2019). The Molecular Basis of MeCP2 Function in the Brain. *J Mol Biol*. <https://doi.org/10.1016/j.jmb.2019.10.004>
- Tillotson, R., Cholewa-Waclaw, J., Chhatbar, K., Connelly, J. C., Kirschner, S. A., Webb, S., Koerner, M. V., Selfridge, J., Kelly, D. A., De Sousa, D., Brown, K., Lyst, M. J., Kriaucionis, S., & Bird, A. (2021). Neuronal non-CG methylation is an essential target for MeCP2 function. *Mol Cell*, *81*(6), 1260-1275.e1212. <https://doi.org/10.1016/j.molcel.2021.01.011>

- Tillotson, R., Selfridge, J., Koerner, M. V., Gadalla, K. K. E., Guy, J., De Sousa, D., Hector, R. D., Cobb, S. R., & Bird, A. (2017). Radically truncated MeCP2 rescues Rett syndrome-like neurological defects. *Nature*, *550*(7676), 398-401. <https://doi.org/10.1038/nature24058>
- Tracey, T. J., Steyn, F. J., Wolvetang, E. J., & Ngo, S. T. (2018). Neuronal Lipid Metabolism: Multiple Pathways Driving Functional Outcomes in Health and Disease. *Front Mol Neurosci*, *11*, 10. <https://doi.org/10.3389/fnmol.2018.00010>
- Trappe, R., Laccone, F., Cobilanschi, J., Meins, M., Huppke, P., Hanefeld, F., & Engel, W. (2001). MECP2 mutations in sporadic cases of Rett syndrome are almost exclusively of paternal origin. *Am J Hum Genet*, *68*(5), 1093-1101. <https://doi.org/10.1086/320109>
- Tropea, D., Giacometti, E., Wilson, N. R., Beard, C., McCurry, C., Fu, D. D., Flannery, R., Jaenisch, R., & Sur, M. (2009). Partial reversal of Rett Syndrome-like symptoms in MeCP2 mutant mice. *Proc Natl Acad Sci U S A*, *106*(6), 2029-2034. <https://doi.org/10.1073/pnas.0812394106>
- Tropea, D., Kreiman, G., Lyckman, A., Mukherjee, S., Yu, H., Horng, S., & Sur, M. (2006). Gene expression changes and molecular pathways mediating activity-dependent plasticity in visual cortex. *Nat Neurosci*, *9*(5), 660-668. <https://doi.org/10.1038/nn1689>
- Trujillo, C. A., Adams, J. W., Negraes, P. D., Carromeu, C., Tejwani, L., Acab, A., Tsuda, B., Thomas, C. A., Sodhi, N., Fichter, K. M., Romero, S., Zanella, F., Sejnowski, T. J., Ulrich, H., & Muotri, A. R. (2021). Pharmacological reversal of synaptic and network pathology in human MECP2-KO neurons and cortical organoids. *EMBO Mol Med*, *13*(1), e12523. <https://doi.org/10.15252/emmm.202012523>
- Tsujimura, K., Abematsu, M., Kohyama, J., Namihira, M., & Nakashima, K. (2009). Neuronal differentiation of neural precursor cells is promoted by the methyl-CpG-binding protein MeCP2. *Exp Neurol*, *219*(1), 104-111. <https://doi.org/10.1016/j.expneurol.2009.05.001>
- Tudor, M., Akbarian, S., Chen, R. Z., & Jaenisch, R. (2002). Transcriptional profiling of a mouse model for Rett syndrome reveals subtle transcriptional changes in the brain. *Proc Natl Acad Sci U S A*, *99*(24), 15536-15541. <https://doi.org/10.1073/pnas.242566899>
- Uehara, R., Nozawa, R. S., Tomioka, A., Petry, S., Vale, R. D., Obuse, C., & Goshima, G. (2009). The augmin complex plays a critical role in spindle microtubule generation for mitotic progression and cytokinesis in human cells. *Proc Natl Acad Sci U S A*, *106*(17), 6998-7003. <https://doi.org/10.1073/pnas.0901587106>
- Urduinguio, R. G., Lopez-Serra, L., Lopez-Nieva, P., Alaminos, M., Diaz-Uriarte, R., Fernandez, A. F., & Esteller, M. (2008). Mecp2-null mice provide new neuronal targets for Rett syndrome. *PLoS One*, *3*(11), e3669. <https://doi.org/10.1371/journal.pone.0003669>
- Vacca, M., Tripathi, K. P., Speranza, L., Aiese Cigliano, R., Scalabrì, F., Marracino, F., Madonna, M., Sanseverino, W., Perrone-Capano, C., Guarracino, M. R., & D'Esposito, M. (2016). Effects of Mecp2 loss of function in embryonic cortical neurons: a bioinformatics strategy to sort out non-neuronal cells variability from transcriptome profiling. *BMC Bioinformatics*, *17*(2), S14. <https://doi.org/10.1186/s12859-015-0859-7>
- van Deijk, A. F., Camargo, N., Timmerman, J., Heistek, T., Brouwers, J. F., Mogavero, F., Mansvelder, H. D., Smit, A. B., & Verheijen, M. H. (2017). Astrocyte lipid

- metabolism is critical for synapse development and function in vivo. *Glia*, 65(4), 670-682. <https://doi.org/10.1002/glia.23120>
- Vashi, N., & Justice, M. J. (2019). Treating Rett syndrome: from mouse models to human therapies. *Mamm Genome*, 30(5-6), 90-110. <https://doi.org/10.1007/s00335-019-09793-5>
- Villani C, Sacchetti G, Bagnati R, Passoni A, Fusco F, Carli M, Invernizzi RW (2016) Lovastatin fails to improve motor performance and survival in methyl-CpG-binding protein2-null mice. *Elife* 5
- Wang, I. T., Reyes, A. R., & Zhou, Z. (2013). Neuronal morphology in MeCP2 mouse models is intrinsically variable and depends on age, cell type, and Mecp2 mutation. *Neurobiol Dis*, 58, 3-12. <https://doi.org/10.1016/j.nbd.2013.04.020>
- Wang, Y. P., Qi, S. T., Wei, Y., Ge, Z. J., Chen, L., Hou, Y., Ouyang, Y. C., Schatten, H., Zhao, J. G., & Sun, Q. Y. (2013). Knockdown of UCHL5IP causes abnormalities in γ -tubulin localisation, spindle organisation and chromosome alignment in mouse oocyte meiotic maturation. *Reprod Fertil Dev*, 25(3), 495-502. <https://doi.org/10.1071/rd12300>
- Williams, E. C., Zhong, X., Mohamed, A., Li, R., Liu, Y., Dong, Q., Ananiev, G. E., Mok, J. C., Lin, B. R., Lu, J., Chiao, C., Cherney, R., Li, H., Zhang, S. C., & Chang, Q. (2014). Mutant astrocytes differentiated from Rett syndrome patients-specific iPSCs have adverse effects on wild-type neurons. *Hum Mol Genet*, 23(11), 2968-2980. <https://doi.org/10.1093/hmg/ddu008>
- Wood, K. H., Johnson, B. S., Welsh, S. A., Lee, J. Y., Cui, Y., Krizman, E., Brodtkin, E. S., Blendy, J. A., Robinson, M. B., Bartolomei, M. S., & Zhou, Z. (2016). Tagging methyl-CpG-binding domain proteins reveals different spatiotemporal expression and supports distinct functions. *Epigenomics*, 8(4), 455-473. <https://doi.org/10.2217/epi-2015-0004>
- Xu X, Kozikowski AP, Pozzo-Miller L (2014) A selective histone deacetylase-6 inhibitor improves BDNF trafficking in hippocampal neurons from Mecp2 knockout mice: implications for Rett syndrome. *Frontiers in cellular neuroscience* 8: 68
- Yuan ZF, Mao SS, Shen J, Jiang LH, Xu L, Xu JL, Gao F (2020) Insulin-Like Growth Factor-1 Down-Regulates the Phosphorylation of FXYP1 and Rescues Behavioral Deficits in a Mouse Model of Rett Syndrome. *Front Neurosci* 14: 20
- Yasui, D. H., Gonzales, M. L., Aflatooni, J. O., Crary, F. K., Hu, D. J., Gavino, B. J., Golub, M. S., Vincent, J. B., Carolyn Schanen, N., Olson, C. O., Rastegar, M., & Lasalle, J. M. (2014). Mice with an isoform-ablating Mecp2 exon 1 mutation recapitulate the neurologic deficits of Rett syndrome. *Hum Mol Genet*, 23(9), 2447-2458. <https://doi.org/10.1093/hmg/ddt640>
- Yasui, D. H., Xu, H., Dunaway, K. W., Lasalle, J. M., Jin, L. W., & Maezawa, I. (2013). MeCP2 modulates gene expression pathways in astrocytes. *Mol Autism*, 4(1), 3. <https://doi.org/10.1186/2040-2392-4-3>
- Young, J. I., Hong, E. P., Castle, J. C., Crespo-Barreto, J., Bowman, A. B., Rose, M. F., Kang, D., Richman, R., Johnson, J. M., Berget, S., & Zoghbi, H. Y. (2005). Regulation of RNA splicing by the methylation-dependent transcriptional repressor methyl-CpG binding protein 2. *Proc Natl Acad Sci U S A*, 102(49), 17551-17558. <https://doi.org/10.1073/pnas.0507856102>
- Zachariah, R. M., Olson, C. O., Ezeonwuka, C., & Rastegar, M. (2012). Novel MeCP2 isoform-specific antibody reveals the endogenous MeCP2E1 expression in

- murine brain, primary neurons and astrocytes. *PLoS One*, 7(11), e49763. <https://doi.org/10.1371/journal.pone.0049763>
- Zachariah, R. M., & Rastegar, M. (2012). Linking epigenetics to human disease and Rett syndrome: the emerging novel and challenging concepts in MeCP2 research. *Neural Plast*, 2012, 415825. <https://doi.org/10.1155/2012/415825>
- Zandl-Lang, M., Züllig, T., Trötz Müller, M., Naegelin, Y., Abela, L., Wilken, B., Scholl-Buergi, S., Karall, D., Kappos, L., Köfeler, H., & Plecko, B. (2022). Changes in the Cerebrospinal Fluid and Plasma Lipidome in Patients with Rett Syndrome. *Metabolites*, 12(4). <https://doi.org/10.3390/metabo12040291>
- Zanella, S., Mebarek, S., Lajard, A. M., Picard, N., Dutschmann, M., & Hilaire, G. (2008). Oral treatment with desipramine improves breathing and life span in Rett syndrome mouse model. *Respir Physiol Neurobiol*, 160(1), 116-121. <https://doi.org/10.1016/j.resp.2007.08.009>
- Zhang, J., & Liu, Q. (2015). Cholesterol metabolism and homeostasis in the brain. *Protein Cell*, 6(4), 254-264. <https://doi.org/10.1007/s13238-014-0131-3>
- Zhao, Y. T., Goffin, D., Johnson, B. S., & Zhou, Z. (2013). Loss of MeCP2 function is associated with distinct gene expression changes in the striatum. *Neurobiol Dis*, 59, 257-266. <https://doi.org/10.1016/j.nbd.2013.08.001>
- Zheng, W. H., & Quirion, R. (2004). Comparative signaling pathways of insulin-like growth factor-1 and brain-derived neurotrophic factor in hippocampal neurons and the role of the PI3 kinase pathway in cell survival. *J Neurochem*, 89(4), 844-852. <https://doi.org/10.1111/j.1471-4159.2004.02350.x>
- Zupa, E., Würtz, M., Neuner, A., Hoffmann, T., Rettel, M., Böhler, A., Vermeulen, B. J. A., Eustermann, S., Schiebel, E., & Pfeffer, S. (2022). The augmin complex architecture reveals structural insights into microtubule branching. *Nat Commun*, 13(1), 5635. <https://doi.org/10.1038/s41467-022-33228-6>

Gene Forrester

10. Appendices

10.1. Appendix I

ID	DESCRIPTION	P-VALUE	P-ADJ	Q-VALUE
GO:0099003	vesicle-mediated transport in synapse	5.11186E-11	1.33777E-07	1.18003E-07
GO:0098693	regulation of synaptic vesicle cycle	6.75513E-09	5.89273E-06	5.1979E-06
GO:0007611	learning or memory	1.35959E-07	8.79376E-05	7.75686E-05
GO:0042391	regulation of membrane potential	3.80135E-07	0.000131	0.000116
GO:0048167	regulation of synaptic plasticity	3.90272E-07	0.000131	0.000116
GO:0016082	synaptic vesicle priming	4.01565E-07	0.000131	0.000116
GO:0006836	neurotransmitter transport	4.68246E-07	0.000136	0.000120
GO:0071805	potassium ion transmembrane transport	1.78682E-06	0.000334	0.000295
GO:0035249	synaptic transmission, glutamatergic	2.75899E-06	0.000425	0.000375
GO:1901214	regulation of neuron death	2.99198E-06	0.000435	0.000384
GO:0007409	axonogenesis	4.49168E-06	0.000573	0.000506
GO:0006887	exocytosis	4.74794E-06	0.000573	0.000506
GO:0015672	monovalent inorganic cation transport	5.62304E-06	0.000640	0.000564
GO:0099637	neurotransmitter receptor transport	6.10634E-06	0.000666	0.000587
GO:0099643	signal release from synapse	7.21268E-06	0.000726	0.000640
GO:0070997	neuron death	1.12389E-05	0.001016	0.000896
GO:1990778	protein localization to cell periphery	1.16619E-05	0.001016	0.000896
GO:0009914	hormone transport	1.20342E-05	0.001016	0.000896
GO:0010976	positive regulation of neuron projection development	1.32152E-05	0.001081	0.000953
GO:0001505	regulation of neurotransmitter levels	2.38809E-05	0.001838	0.001621
GO:0043524	negative regulation of neuron apoptotic process	2.59506E-05	0.001886	0.001664
GO:0048268	clathrin coat assembly	3.29279E-05	0.002210	0.001949
GO:0046879	hormone secretion	3.96358E-05	0.002530	0.002232
GO:0016050	vesicle organization	4.25965E-05	0.002654	0.002341
GO:0019933	cAMP-mediated signaling	4.85907E-05	0.002957	0.002609
GO:0031346	positive regulation of cell projection organization	6.50788E-05	0.003725	0.003285
GO:0050803	regulation of synapse structure or activity	6.61072E-05	0.003725	0.003285
GO:0007215	glutamate receptor signaling pathway	6.68911E-05	0.003725	0.003285
GO:1903532	positive regulation of secretion by cell	8.01926E-05	0.004219	0.003721
GO:0034765	regulation of ion transmembrane transport	8.06034E-05	0.004219	0.003721
GO:0051402	neuron apoptotic process	9.40347E-05	0.004474	0.003947
GO:0098657	import into cell	9.9135E-05	0.004633	0.004087
GO:0060478	acrosomal vesicle exocytosis	0.000132	0.005557	0.004901
GO:0035418	protein localization to synapse	0.000134	0.005557	0.004901

GO:0099500	vesicle fusion to plasma membrane	0.000151	0.006017	0.005307
GO:0048489	synaptic vesicle transport	0.000198	0.007493	0.006609
GO:0010038	response to metal ion	0.000203	0.007493	0.006609
GO:0050808	synapse organization	0.000203	0.007493	0.006609
GO:1903305	regulation of regulated secretory pathway	0.000246	0.008827	0.007787
GO:0006898	receptor-mediated endocytosis	0.000263	0.009316	0.008218
GO:0060079	excitatory postsynaptic potential	0.000363	0.012011	0.010595
GO:0015711	organic anion transport	0.000511	0.015555	0.013721
GO:0051260	protein homooligomerization	0.000538	0.016185	0.014276
GO:0051961	negative regulation of nervous system development	0.000558	0.016599	0.014642
GO:0007188	adenylate cyclase-modulating G protein-coupled receptor signaling pathway	0.000572	0.016748	0.014774
GO:0097479	synaptic vesicle localization	0.000576	0.016748	0.014774
GO:0099072	regulation of postsynaptic membrane neurotransmitter receptor levels	0.000641	0.017629	0.015550
GO:0034329	cell junction assembly	0.000647	0.017629	0.015550
GO:0050807	regulation of synapse organization	0.000800	0.020335	0.017937
GO:0021700	developmental maturation	0.000826	0.020792	0.018341
GO:1904377	positive regulation of protein localization to cell periphery	0.000927	0.022877	0.020180
GO:0099590	neurotransmitter receptor internalization	0.000988	0.023609	0.020825
GO:0014072	response to isoquinoline alkaloid	0.000992	0.023609	0.020825
GO:0050768	negative regulation of neurogenesis	0.001003	0.023643	0.020855
GO:0098969	neurotransmitter receptor transport to postsynaptic membrane	0.001158	0.026540	0.023411
GO:0061025	membrane fusion	0.001180	0.026556	0.023424
GO:0051588	regulation of neurotransmitter transport	0.001322	0.028822	0.025423
GO:0071248	cellular response to metal ion	0.001530	0.032782	0.028916
GO:1903540	establishment of protein localization to postsynaptic membrane	0.001541	0.032782	0.028916
GO:0002791	regulation of peptide secretion	0.001572	0.033171	0.029260
GO:0051952	regulation of amine transport	0.001597	0.033171	0.029260
GO:0032535	regulation of cellular component size	0.001704	0.034300	0.030256
GO:0035592	establishment of protein localization to extracellular region	0.001889	0.036620	0.032302
GO:0031503	protein-containing complex localization	0.002041	0.038285	0.033771
GO:0008038	neuron recognition	0.002048	0.038285	0.033771
GO:0071692	protein localization to extracellular region	0.002143	0.039767	0.035078
GO:0098739	import across plasma membrane	0.002238	0.040950	0.036121
GO:0008277	regulation of G protein-coupled receptor signaling pathway	0.002317	0.042112	0.037146
GO:0048639	positive regulation of developmental growth	0.002344	0.042313	0.037324
GO:1902476	chloride transmembrane transport	0.002529	0.044718	0.039445
GO:0098656	anion transmembrane transport	0.002768	0.047981	0.042323
GO:0010721	negative regulation of cell development	0.002892	0.049175	0.043376

Table 10.1: GO enrichment analysis for biological processes of NPC-derived KO vs WT at DIV7, ranked by p -adj (p -adj cut-off < 0.1). The function simplify was used to remove redundancy of enriched GO terms.

10.2. Appendix II

ID	DESCRIPTION	P-VALUE	P-ADJ	Q-VALUE
GO:0050808	synapse organization	2.81E-15	1.53E-11	1.35E-11
GO:0099003	vesicle-mediated transport in synapse	7.07E-12	1.93E-08	1.69E-08
GO:0042391	regulation of membrane potential	1.63E-11	2.97E-08	2.61E-08
GO:0007215	glutamate receptor signaling pathway	5.58E-11	7.61E-08	6.69E-08
GO:0007611	learning or memory	9.17E-11	8.87E-08	7.80E-08
GO:0050803	regulation of synapse structure or activity	9.76E-11	8.87E-08	7.80E-08
GO:0034765	regulation of ion transmembrane transport	1.33E-10	1.03E-07	9.08E-08
GO:0050807	regulation of synapse organization	2.32E-10	1.58E-07	1.39E-07
GO:0007416	synapse assembly	1.32E-09	7.22E-07	6.34E-07
GO:0001505	regulation of neurotransmitter levels	9.47E-09	3.69E-06	3.24E-06
GO:0006836	neurotransmitter transport	2.24E-08	8.15E-06	7.16E-06
GO:0006887	exocytosis	5.31E-08	1.70E-05	1.50E-05
GO:0046434	organophosphate catabolic process	6.19E-08	1.88E-05	1.65E-05
GO:0007409	axonogenesis	7.65E-08	2.00E-05	1.76E-05
GO:0072511	divalent inorganic cation transport	7.80E-08	2.00E-05	1.76E-05
GO:0007269	neurotransmitter secretion	8.54E-08	2.00E-05	1.76E-05
GO:0099643	signal release from synapse	8.54E-08	2.00E-05	1.76E-05
GO:0010959	regulation of metal ion transport	8.81E-08	2.00E-05	1.76E-05
GO:1903532	positive regulation of secretion by cell	1.31E-07	2.56E-05	2.25E-05
GO:0099601	regulation of neurotransmitter receptor activity	1.42E-07	2.62E-05	2.30E-05
GO:0035249	synaptic transmission, glutamatergic	2.08E-07	3.67E-05	3.22E-05
GO:0032409	regulation of transporter activity	2.75E-07	4.68E-05	4.11E-05
GO:0051963	regulation of synapse assembly	4.34E-07	6.96E-05	6.11E-05
GO:0099072	regulation of postsynaptic membrane neurotransmitter receptor levels	4.62E-07	7.19E-05	6.32E-05
GO:0098693	regulation of synaptic vesicle cycle	1.18E-06	1.58E-04	1.38E-04
GO:0097120	receptor localization to synapse	2.14E-06	2.67E-04	2.35E-04
GO:0043087	regulation of GTPase activity	2.16E-06	2.67E-04	2.35E-04
GO:0007626	locomotor behavior	2.45E-06	2.97E-04	2.61E-04
GO:0045666	positive regulation of neuron differentiation	2.52E-06	2.99E-04	2.63E-04
GO:0048588	developmental cell growth	3.97E-06	0.00044	3.88E-04
GO:0070588	calcium ion transmembrane transport	5.21E-06	0.00056	0.00049
GO:0099565	chemical synaptic transmission, postsynaptic	7.66E-06	0.00076	0.00067
GO:0099637	neurotransmitter receptor transport	8.13E-06	0.00078	0.00068
GO:0030048	actin filament-based movement	8.67E-06	0.00081	0.00071
GO:1903522	regulation of blood circulation	8.80E-06	0.00081	0.00071
GO:0060402	calcium ion transport into cytosol	1.02E-05	0.00091	0.00080
GO:0035637	multicellular organismal signaling	1.11E-05	0.00095	0.00083
GO:0051648	vesicle localization	1.15E-05	0.00097	0.00085

GO:0051592	response to calcium ion	1.27E-05	0.00104	0.00091
GO:0051650	establishment of vesicle localization	1.28E-05	0.00104	0.00091
GO:0098742	cell-cell adhesion via plasma-membrane adhesion molecules	1.57E-05	0.00124	0.00109
GO:0034329	cell junction assembly	1.73E-05	0.00131	0.00115
GO:0060560	developmental growth involved in morphogenesis	1.89E-05	0.00141	0.00124
GO:0007264	small GTPase mediated signal transduction	1.97E-05	0.00146	0.00128
GO:0098657	import into cell	2.05E-05	0.00147	0.00129
GO:0048168	regulation of neuronal synaptic plasticity	2.08E-05	0.00147	0.00129
GO:0014812	muscle cell migration	2.44E-05	0.00166	0.00146
GO:1990778	protein localization to cell periphery	2.67E-05	0.00180	0.00158
GO:0003012	muscle system process	2.79E-05	0.00183	0.00161
GO:0031644	regulation of nervous system process	3.14E-05	0.00204	0.00179
GO:0009154	purine ribonucleotide catabolic process	4.12E-05	0.00250	0.00220
GO:0009261	ribonucleotide catabolic process	4.12E-05	0.00250	0.00220
GO:0043547	positive regulation of GTPase activity	4.94E-05	0.00293	0.00257
GO:0043254	regulation of protein-containing complex assembly	5.35E-05	0.00314	0.00276
GO:0007213	G protein-coupled acetylcholine receptor signaling pathway	6.13E-05	0.00356	0.00313
GO:0048638	regulation of developmental growth	6.45E-05	0.00370	0.00325
GO:0031346	positive regulation of cell projection organization	6.79E-05	0.00385	0.00339
GO:1901214	regulation of neuron death	7.23E-05	0.00402	0.00353
GO:0071277	cellular response to calcium ion	7.73E-05	0.00421	0.00370
GO:0032970	regulation of actin filament-based process	8.13E-05	0.00427	0.00375
GO:0046887	positive regulation of hormone secretion	8.36E-05	0.00430	0.00378
GO:0006813	potassium ion transport	8.66E-05	0.00441	0.00388
GO:1902903	regulation of supramolecular fiber organization	1.16E-04	0.00588	0.00516
GO:0045669	positive regulation of osteoblast differentiation	1.19E-04	0.00593	0.00521
GO:0071805	potassium ion transmembrane transport	1.20E-04	0.00595	0.00523
GO:0048284	organelle fusion	1.23E-04	0.00601	0.00528
GO:0051480	regulation of cytosolic calcium ion concentration	1.24E-04	0.00601	0.00528
GO:0014049	positive regulation of glutamate secretion	1.61E-04	0.00750	0.00659
GO:0099590	neurotransmitter receptor internalization	1.73E-04	0.00788	0.00692
GO:0044282	small molecule catabolic process	1.73E-04	0.00788	0.00692
GO:0086003	cardiac muscle cell contraction	1.82E-04	0.00814	0.00715
GO:0031338	regulation of vesicle fusion	1.94E-04	0.00848	0.00745
GO:0051588	regulation of neurotransmitter transport	1.95E-04	0.00848	0.00745
GO:0070997	neuron death	1.99E-04	0.00848	0.00745
GO:0045778	positive regulation of ossification	2.63E-04	0.01061	0.00932
GO:0001764	neuron migration	2.94E-04	0.01167	0.01025
GO:0051961	negative regulation of nervous system development	2.95E-04	0.01167	0.01025
GO:1901888	regulation of cell junction assembly	3.11E-04	0.01210	0.01063
GO:1903539	protein localization to postsynaptic membrane	3.27E-04	0.01242	0.01091

GO:0042476	odontogenesis	3.28E-04	0.01242	0.01091
GO:0001558	regulation of cell growth	3.61E-04	0.01342	0.01179
GO:0048659	smooth muscle cell proliferation	3.73E-04	0.01374	0.01207
GO:0051494	negative regulation of cytoskeleton organization	4.05E-04	0.01451	0.01275
GO:0098659	inorganic cation import across plasma membrane	4.07E-04	0.01451	0.01275
GO:0099587	inorganic ion import across plasma membrane	4.07E-04	0.01451	0.01275
GO:0035176	social behavior	4.27E-04	0.01505	0.01323
GO:0110148	biomineralization	4.37E-04	0.01516	0.01332
GO:0072176	nephric duct development	4.69E-04	0.01590	0.01397
GO:0010721	negative regulation of cell development	4.73E-04	0.01592	0.01399
GO:0009914	hormone transport	4.82E-04	0.01613	0.01417
GO:0001503	ossification	4.88E-04	0.01621	0.01425
GO:0031345	negative regulation of cell projection organization	4.96E-04	0.01638	0.01439
GO:0072523	purine-containing compound catabolic process	5.70E-04	0.01815	0.01595
GO:0043523	regulation of neuron apoptotic process	6.44E-04	0.01985	0.01744
GO:0045646	regulation of erythrocyte differentiation	0.00065	0.02002	0.01758
GO:0055074	calcium ion homeostasis	0.00066	0.02012	0.01768
GO:1905144	response to acetylcholine	0.00068	0.02012	0.01768
GO:0051703	intraspecies interaction between organisms	0.00069	0.02026	0.01780
GO:0043542	endothelial cell migration	0.00076	0.02193	0.01927
GO:0031503	protein-containing complex localization	0.00082	0.02314	0.02033
GO:0050905	neuromuscular process	0.00083	0.02325	0.02043
GO:0051952	regulation of amine transport	0.00084	0.02346	0.02061
GO:0046785	microtubule polymerization	0.00085	0.02357	0.02071
GO:0090132	epithelium migration	0.00087	0.02396	0.02105
GO:0051402	neuron apoptotic process	0.00092	0.02460	0.02161
GO:0040013	negative regulation of locomotion	0.00100	0.02615	0.02298
GO:0051271	negative regulation of cellular component movement	0.00100	0.02615	0.02298
GO:0014047	glutamate secretion	0.00103	0.02653	0.02330
GO:0010769	regulation of cell morphogenesis involved in differentiation	0.00106	0.02710	0.02381
GO:0097011	cellular response to granulocyte macrophage colony-stimulating factor stimulus	0.00107	0.02710	0.02381
GO:0032956	regulation of actin cytoskeleton organization	0.00109	0.02731	0.02399
GO:0060047	heart contraction	0.00114	0.02827	0.02483
GO:1905475	regulation of protein localization to membrane	0.00116	0.02852	0.02505
GO:2000310	regulation of NMDA receptor activity	0.00120	0.02922	0.02567
GO:2000311	regulation of AMPA receptor activity	0.00120	0.02922	0.02567
GO:0031109	microtubule polymerization or depolymerization	0.00123	0.02956	0.02597
GO:0031110	regulation of microtubule polymerization or depolymerization	0.00123	0.02956	0.02597
GO:0001662	behavioral fear response	0.00124	0.02956	0.02597
GO:0031113	regulation of microtubule polymerization	0.00124	0.02956	0.02597
GO:0032232	negative regulation of actin filament bundle assembly	0.00125	0.02963	0.02603

GO:0014075	response to amine	0.00127	0.02985	0.02622
GO:0098877	neurotransmitter receptor transport to plasma membrane	0.00127	0.02985	0.02622
GO:0007193	adenylate cyclase-inhibiting G protein-coupled receptor signaling pathway	0.00132	0.03059	0.02687
GO:0019226	transmission of nerve impulse	0.00137	0.03123	0.02744
GO:2001222	regulation of neuron migration	0.00144	0.03221	0.02830
GO:0010594	regulation of endothelial cell migration	0.00146	0.03237	0.02843
GO:0048660	regulation of smooth muscle cell proliferation	0.00146	0.03237	0.02843
GO:0097012	response to granulocyte macrophage colony-stimulating factor	0.00152	0.03340	0.02934
GO:0016042	lipid catabolic process	0.00155	0.03384	0.02973
GO:0051258	protein polymerization	0.00161	0.03464	0.03044
GO:0033555	multicellular organismal response to stress	0.00164	0.03497	0.03072
GO:0051017	actin filament bundle assembly	0.00182	0.03803	0.03341
GO:0071868	cellular response to monoamine stimulus	0.00183	0.03803	0.03341
GO:0071870	cellular response to catecholamine stimulus	0.00183	0.03803	0.03341
GO:0006898	receptor-mediated endocytosis	0.00190	0.03899	0.03425
GO:0008217	regulation of blood pressure	0.00198	0.04034	0.03544
GO:0043084	penile erection	0.00211	0.04159	0.03654
GO:0014910	regulation of smooth muscle cell migration	0.00213	0.04159	0.03654
GO:0051937	catecholamine transport	0.00213	0.04159	0.03654
GO:0030534	adult behavior	0.00217	0.04184	0.03676
GO:0090257	regulation of muscle system process	0.00227	0.04289	0.03768
GO:0019693	ribose phosphate metabolic process	0.00248	0.04679	0.04111
GO:0086004	regulation of cardiac muscle cell contraction	0.00256	0.04773	0.04193
GO:0030100	regulation of endocytosis	0.00256	0.04773	0.04193
GO:1903115	regulation of actin filament-based movement	0.00261	0.04792	0.04210
GO:0097756	negative regulation of blood vessel diameter	0.00262	0.04792	0.04210
GO:0070498	interleukin-1-mediated signaling pathway	0.00269	0.04857	0.04267
GO:0006506	GPI anchor biosynthetic process	0.00275	0.04957	0.04355

Table 10.2: GO enrichment analysis for biological processes of NPC-derived KO vs WT at DIV14, ranked by *p*-adj (*p*-adj cut-off < 0.1). The function *simplify* was used to remove redundancy of enriched GO terms.

10.3. Appendix III

ID	DESCRIPTION	P-VALUE	P-ADJ	Q-VALUE
GO:0042391	regulation of membrane potential	3.79E-12	2.10E-08	1.80E-08
GO:0099003	vesicle-mediated transport in synapse	1.60E-11	4.24E-08	3.65E-08
GO:0007611	learning or memory	2.30E-11	4.24E-08	3.65E-08
GO:0034765	regulation of ion transmembrane transport	3.89E-09	3.07E-06	2.64E-06
GO:0045666	positive regulation of neuron differentiation	1.29E-08	7.91E-06	6.80E-06

GO:0050808	synapse organization	1.78E-08	9.86E-06	8.48E-06
GO:0007215	glutamate receptor signaling pathway	2.84E-08	1.43E-05	1.23E-05
GO:0035249	synaptic transmission, glutamatergic	3.40E-08	1.57E-05	1.35E-05
GO:0007409	axonogenesis	5.23E-08	2.23E-05	1.91E-05
GO:0007626	locomotor behavior	6.60E-08	2.61E-05	2.25E-05
GO:0008016	regulation of heart contraction	8.01E-08	2.96E-05	2.54E-05
GO:0001505	regulation of neurotransmitter levels	1.42E-07	4.43E-05	3.81E-05
GO:0006887	exocytosis	1.44E-07	4.43E-05	3.81E-05
GO:0046434	organophosphate catabolic process	1.96E-07	5.72E-05	4.92E-05
GO:0007213	G protein-coupled acetylcholine receptor signaling pathway	2.96E-07	8.11E-05	6.98E-05
GO:0006836	neurotransmitter transport	3.08E-07	8.11E-05	6.98E-05
GO:0060047	heart contraction	3.32E-07	8.35E-05	7.18E-05
GO:0048168	regulation of neuronal synaptic plasticity	4.29E-07	9.88E-05	8.50E-05
GO:0007264	small GTPase mediated signal transduction	5.19E-07	1.15E-04	9.87E-05
GO:0007416	synapse assembly	7.02E-07	1.44E-04	1.24E-04
GO:0050803	regulation of synapse structure or activity	9.39E-07	1.79E-04	1.54E-04
GO:0098693	regulation of synaptic vesicle cycle	1.07E-06	1.97E-04	1.70E-04
GO:0051961	negative regulation of nervous system development	1.26E-06	2.18E-04	1.88E-04
GO:0050807	regulation of synapse organization	2.01E-06	3.17E-04	2.73E-04
GO:0043647	inositol phosphate metabolic process	2.34E-06	3.50E-04	3.01E-04
GO:0031346	positive regulation of cell projection organization	2.78E-06	3.76E-04	3.23E-04
GO:0010959	regulation of metal ion transport	2.87E-06	3.76E-04	3.23E-04
GO:0007269	neurotransmitter secretion	2.92E-06	3.76E-04	3.23E-04
GO:0099643	signal release from synapse	2.92E-06	3.76E-04	3.23E-04
GO:0003012	muscle system process	3.06E-06	0.00038	3.23E-04
GO:0035637	multicellular organismal signaling	3.07E-06	0.00038	0.00032
GO:1901214	regulation of neuron death	3.18E-06	0.00038	0.00032
GO:0051648	vesicle localization	4.08E-06	0.00044	0.00038
GO:1905144	response to acetylcholine	4.23E-06	0.00044	0.00038
GO:0099072	regulation of postsynaptic membrane neurotransmitter receptor levels	4.72E-06	0.00046	0.00040
GO:0099565	chemical synaptic transmission, postsynaptic	4.72E-06	0.00046	0.00040
GO:0043279	response to alkaloid	4.73E-06	0.00046	0.00040
GO:1902903	regulation of supramolecular fiber organization	5.27E-06	0.00049	0.00043
GO:2001222	regulation of neuron migration	6.13E-06	0.00055	0.00047
GO:0010721	negative regulation of cell development	6.15E-06	0.00055	0.00047
GO:0030048	actin filament-based movement	6.63E-06	0.00058	0.00050
GO:0051494	negative regulation of cytoskeleton organization	7.56E-06	0.00062	0.00054
GO:0032409	regulation of transporter activity	7.65E-06	0.00062	0.00054
GO:0006813	potassium ion transport	7.72E-06	0.00062	0.00054
GO:0099601	regulation of neurotransmitter receptor activity	7.98E-06	0.00062	0.00054
GO:1903532	positive regulation of secretion by cell	8.74E-06	0.00066	0.00057

GO:0050768	negative regulation of neurogenesis	9.01E-06	0.00067	0.00058
GO:0051650	establishment of vesicle localization	1.18E-05	0.00084	0.00072
GO:0098657	import into cell	1.18E-05	0.00084	0.00072
GO:0010769	regulation of cell morphogenesis involved in differentiation	1.23E-05	0.00086	0.00074
GO:0070997	neuron death	1.29E-05	0.00087	0.00075
GO:0019098	reproductive behavior	1.60E-05	0.00107	0.00092
GO:0001764	neuron migration	1.83E-05	0.00118	0.00101
GO:0071805	potassium ion transmembrane transport	2.03E-05	0.00128	0.00110
GO:0098926	postsynaptic signal transduction	2.62E-05	0.00160	0.00137
GO:0051258	protein polymerization	2.75E-05	0.00165	0.00142
GO:1902414	protein localization to cell junction	2.78E-05	0.00165	0.00142
GO:0010038	response to metal ion	3.06E-05	0.00176	0.00152
GO:0051271	negative regulation of cellular component movement	4.34E-05	0.00231	0.00199
GO:0072511	divalent inorganic cation transport	4.34E-05	0.00231	0.00199
GO:0032271	regulation of protein polymerization	4.45E-05	0.00232	0.00200
GO:0032535	regulation of cellular component size	4.46E-05	0.00232	0.00200
GO:0070588	calcium ion transmembrane transport	4.49E-05	0.00232	0.00200
GO:0043087	regulation of GTPase activity	4.61E-05	0.00236	0.00203
GO:0051963	regulation of synapse assembly	4.66E-05	0.00236	0.00203
GO:0007193	adenylate cyclase-inhibiting G protein-coupled receptor signaling pathway	4.89E-05	0.00239	0.00206
GO:0014812	muscle cell migration	5.42E-05	0.00257	0.00221
GO:0051480	regulation of cytosolic calcium ion concentration	5.48E-05	0.00257	0.00221
GO:0009154	purine ribonucleotide catabolic process	6.27E-05	0.00287	0.00247
GO:0009261	ribonucleotide catabolic process	6.27E-05	0.00287	0.00247
GO:0097553	calcium ion transmembrane import into cytosol	6.37E-05	0.00288	0.00248
GO:0032232	negative regulation of actin filament bundle assembly	6.87E-05	0.00302	0.00260
GO:0051952	regulation of amine transport	6.92E-05	0.00302	0.00260
GO:0099637	neurotransmitter receptor transport	7.03E-05	0.00303	0.00261
GO:0048588	developmental cell growth	7.93E-05	0.00330	0.00283
GO:0032970	regulation of actin filament-based process	8.35E-05	0.00337	0.00290
GO:0031644	regulation of nervous system process	8.53E-05	0.00342	0.00294
GO:0050905	neuromuscular process	8.90E-05	0.00352	0.00303
GO:0040013	negative regulation of locomotion	9.24E-05	0.00360	0.00310
GO:0031109	microtubule polymerization or depolymerization	1.12E-04	0.00423	0.00364
GO:0098742	cell-cell adhesion via plasma-membrane adhesion molecules	1.15E-04	0.00427	0.00367
GO:0051937	catecholamine transport	1.16E-04	0.00427	0.00367
GO:0046785	microtubule polymerization	1.28E-04	0.00463	0.00398
GO:0048638	regulation of developmental growth	1.29E-04	0.00465	0.00400
GO:0043112	receptor metabolic process	1.36E-04	0.00485	0.00417
GO:0034329	cell junction assembly	1.48E-04	0.00518	0.00446
GO:0017157	regulation of exocytosis	1.51E-04	0.00524	0.00451

GO:0035176	social behavior	1.72E-04	0.00592	0.00509
GO:0072523	purine-containing compound catabolic process	1.81E-04	0.00616	0.00530
GO:0043523	regulation of neuron apoptotic process	1.88E-04	0.00631	0.00542
GO:0019233	sensory perception of pain	2.05E-04	0.00672	0.00578
GO:0032886	regulation of microtubule-based process	2.32E-04	0.00738	0.00635
GO:0030072	peptide hormone secretion	2.81E-04	0.00875	0.00752
GO:0051703	intraspecies interaction between organisms	2.92E-04	0.00902	0.00776
GO:2000310	regulation of NMDA receptor activity	0.00030	0.00914	0.00786
GO:0035641	locomotory exploration behavior	0.00034	0.01003	0.00862
GO:0008038	neuron recognition	0.00035	0.01036	0.00891
GO:0033555	multicellular organismal response to stress	0.00037	0.01066	0.00916
GO:0042220	response to cocaine	0.00038	0.01091	0.00939
GO:0009896	positive regulation of catabolic process	0.00039	0.01105	0.00950
GO:0030534	adult behavior	0.00040	0.01124	0.00967
GO:1990778	protein localization to cell periphery	0.00040	0.01124	0.00967
GO:0033002	muscle cell proliferation	0.00041	0.01124	0.00967
GO:0009914	hormone transport	0.00043	0.01172	0.01008
GO:0019751	polyol metabolic process	0.00043	0.01172	0.01008
GO:0048259	regulation of receptor-mediated endocytosis	0.00043	0.01172	0.01008
GO:0051588	regulation of neurotransmitter transport	0.00044	0.01173	0.01009
GO:0055074	calcium ion homeostasis	0.00045	0.01185	0.01019
GO:0046838	phosphorylated carbohydrate dephosphorylation	0.00049	0.01258	0.01082
GO:0046488	phosphatidylinositol metabolic process	0.00054	0.01356	0.01167
GO:1903539	protein localization to postsynaptic membrane	0.00056	0.01398	0.01203
GO:0110053	regulation of actin filament organization	0.00059	0.01463	0.01258
GO:0007019	microtubule depolymerization	0.00059	0.01463	0.01258
GO:0007618	mating	0.00059	0.01463	0.01258
GO:0043405	regulation of MAP kinase activity	0.00060	0.01472	0.01266
GO:0090257	regulation of muscle system process	0.00062	0.01493	0.01284
GO:0071248	cellular response to metal ion	0.00063	0.01498	0.01288
GO:0035640	exploration behavior	0.00063	0.01505	0.01294
GO:0051402	neuron apoptotic process	0.00064	0.01506	0.01295
GO:0051017	actin filament bundle assembly	0.00071	0.01630	0.01402
GO:0002090	regulation of receptor internalization	0.00077	0.01723	0.01482
GO:1901888	regulation of cell junction assembly	0.00077	0.01723	0.01482
GO:0014048	regulation of glutamate secretion	0.00081	0.01816	0.01562
GO:0060760	positive regulation of response to cytokine stimulus	0.00082	0.01825	0.01570
GO:0140115	export across plasma membrane	0.00096	0.02056	0.01768
GO:0001975	response to amphetamine	0.00096	0.02056	0.01768
GO:0098962	regulation of postsynaptic neurotransmitter receptor activity	0.00096	0.02056	0.01768
GO:0051261	protein depolymerization	0.00098	0.02074	0.01783

GO:0030900	forebrain development	0.00099	0.02082	0.01791
GO:0098884	postsynaptic neurotransmitter receptor internalization	0.00099	0.02082	0.01791
GO:0032386	regulation of intracellular transport	0.00100	0.02088	0.01796
GO:0045646	regulation of erythrocyte differentiation	0.00103	0.02128	0.01830
GO:0014910	regulation of smooth muscle cell migration	0.00122	0.02483	0.02135
GO:0042551	neuron maturation	0.00129	0.02569	0.02210
GO:0014074	response to purine-containing compound	0.00145	0.02787	0.02396
GO:0051222	positive regulation of protein transport	0.00146	0.02802	0.02410
GO:0033627	cell adhesion mediated by integrin	0.00149	0.02847	0.02449
GO:0007026	negative regulation of microtubule depolymerization	0.00150	0.02852	0.02453
GO:0050795	regulation of behavior	0.00176	0.03227	0.02775
GO:1901880	negative regulation of protein depolymerization	0.00184	0.03331	0.02864
GO:0034620	cellular response to unfolded protein	0.00192	0.03452	0.02969
GO:0001662	behavioral fear response	0.00193	0.03452	0.02969
GO:0031113	regulation of microtubule polymerization	0.00193	0.03452	0.02969
GO:0044282	small molecule catabolic process	0.00196	0.03493	0.03004
GO:0031000	response to caffeine	0.00198	0.03505	0.03014
GO:0007631	feeding behavior	0.00203	0.03572	0.03072
GO:0060384	innervation	0.00210	0.03650	0.03139
GO:0006898	receptor-mediated endocytosis	0.00216	0.03732	0.03209
GO:0043271	negative regulation of ion transport	0.00222	0.03798	0.03266
GO:1901136	carbohydrate derivative catabolic process	0.00229	0.03876	0.03333
GO:0019226	transmission of nerve impulse	0.00237	0.03996	0.03437
GO:0031623	receptor internalization	0.00240	0.04029	0.03464
GO:0060560	developmental growth involved in morphogenesis	0.00246	0.04103	0.03528
GO:0003254	regulation of membrane depolarization	0.00247	0.04103	0.03528
GO:0031345	negative regulation of cell projection organization	0.00248	0.04103	0.03528
GO:0061082	myeloid leukocyte cytokine production	0.00259	0.04271	0.03673
GO:0071692	protein localization to extracellular region	0.00272	0.04393	0.03778
GO:0043084	penile erection	0.00273	0.04393	0.03778
GO:0031331	positive regulation of cellular catabolic process	0.00282	0.04505	0.03874
GO:1900101	regulation of endoplasmic reticulum unfolded protein response	0.00286	0.04553	0.03915
GO:0071868	cellular response to monoamine stimulus	0.00289	0.04576	0.03935
GO:0071870	cellular response to catecholamine stimulus	0.00289	0.04576	0.03935
GO:0045777	positive regulation of blood pressure	0.00295	0.04639	0.03990
GO:0022411	cellular component disassembly	0.00298	0.04675	0.04020
GO:0030308	negative regulation of cell growth	0.00306	0.04776	0.04107
GO:1990138	neuron projection extension	0.00306	0.04776	0.04107
GO:0034109	homotypic cell-cell adhesion	0.00309	0.04796	0.04125
GO:0021700	developmental maturation	0.00309	0.04796	0.04125
GO:0010613	positive regulation of cardiac muscle hypertrophy	0.00311	0.04813	0.04139

GO:0016311	dephosphorylation	0.00315	0.04849	0.04170
GO:0045742	positive regulation of epidermal growth factor receptor signaling pathway	0.00316	0.04849	0.04170
GO:1904951	positive regulation of establishment of protein localization	0.00319	0.04849	0.04170
GO:0035264	multicellular organism growth	0.00319	0.04849	0.04170

Table 10.3: GO enrichment analysis for biological processes of NPC-derived KO vs WT in the analysis overtime, ranked by *p*-adj (*p*-adj cut-off < 0.05). The function simplify was used to remove redundancy of enriched GO terms.

10.4. Appendix IV

DIV 7-14-18 P-ADJ < 0.1	
GENE NAME	Gene description
<i>SGCA</i>	sarcoglycan, alpha (dystrophin-associated glycoprotein)
<i>LGR5</i>	leucine rich repeat containing G protein coupled receptor 5
<i>WNT7B</i>	wingless-type MMTV integration site family, member 7B
<i>SLCO1C1</i>	solute carrier organic anion transporter family, member 1c1
<i>NSDHL</i>	NAD(P) dependent steroid dehydrogenase-like
<i>HAUS7</i>	HAUS augmin-like complex, subunit 7
<i>MECP2</i>	methyl CpG binding protein 2
<i>COBLL1</i>	Cobl-like 1
<i>MITF</i>	melanogenesis associated transcription factor
<i>LPAR3</i>	lysophosphatidic acid receptor 3
<i>MARCHF4</i>	membrane associated ring-CH-type finger 4
<i>DSC3</i>	desmocollin 3
<i>GRM4</i>	glutamate receptor, metabotropic 4
<i>GPR27</i>	G protein-coupled receptor 27
<i>XIST</i>	inactive X specific transcripts
<i>OTOGL</i>	otogelin-like
DIV 14-18 P-ADJ < 0.1	
GENE NAME	Gene description
<i>CDCP3</i>	CUB domain containing protein 3
<i>STARD13</i>	StAR-related lipid transfer (START) domain containing 13
<i>VIP</i>	vasoactive intestinal polypeptide
<i>FGD6</i>	FYVE, RhoGEF and PH domain containing 6
<i>AVPR1A</i>	arginine vasopressin receptor 1A
<i>FRS2</i>	fibroblast growth factor receptor substrate 2
<i>MYH3</i>	myosin, heavy polypeptide 3, skeletal muscle, embryonic
<i>DSCC1</i>	DNA replication and sister chromatid cohesion 1
<i>BCL6</i>	B cell leukemia/lymphoma 6

<i>BBX</i>	bobby sox HMG box containing
<i>TYMS</i>	thymidylate synthase
<i>ST8SIA2</i>	ST8 alpha-N-acetyl-neuraminide alpha-2,8-sialyltransferase 2
<i>CYP27A1</i>	cytochrome P450, family 27, subfamily a, polypeptide 1
<i>ZFP106</i>	zinc finger protein 106
<i>RBBP9</i>	retinoblastoma binding protein 9, serine hydrolase
<i>NECAB3</i>	N-terminal EF-hand calcium binding protein 3
<i>TRPC3</i>	transient receptor potential cation channel, subfamily C, member 3
<i>CAR9</i>	carbonic anhydrase 9
<i>TINAGL1</i>	tubulointerstitial nephritis antigen-like 1
<i>SEPSECS</i>	Sep (O-phosphoserine) tRNA:Sec (selenocysteine) tRNA synthase
<i>TEX26</i>	testis expressed 26
<i>NR2F2</i>	nuclear receptor subfamily 2, group F, member 2
<i>FUNDC2</i>	FUN14 domain containing 2
<i>DPP8</i>	dipeptidylpeptidase 8
<i>ATP1A1</i>	ATPase, Na ⁺ /K ⁺ transporting, alpha 1 polypeptide
<i>MYH2</i>	myosin, heavy polypeptide 2, skeletal muscle, adult
<i>ARHGEF5</i>	Rho guanine nucleotide exchange factor (GEF) 5
<i>RFC3</i>	replication factor C (activator 1) 3
<i>HROB</i>	homologous recombination factor with OB-fold
<i>SYNRG</i>	synergyn, gamma
<i>TBCEL</i>	tubulin folding cofactor E-like
<i>EGR1</i>	early growth response 1
<i>MAN2A2</i>	mannosidase 2, alpha 2
<i>CDH26</i>	cadherin-like 26
<i>AJAP1</i>	adherens junction associated protein 1
<i>FMO1</i>	flavin containing monooxygenase 1
<i>DAAM2</i>	dishevelled associated activator of morphogenesis 2
<i>RASL12</i>	RAS-like, family 12
<i>ABCB4</i>	ATP-binding cassette, sub-family B (MDR/TAP), member 4
<i>TTC9</i>	tetratricopeptide repeat domain 9
<i>SERPINB6B</i>	serine (or cysteine) peptidase inhibitor, clade B, member 6b
<i>ZFP36</i>	zinc finger protein 36
<i>PRSS22</i>	protease, serine 22
<i>ARHGEF37</i>	Rho guanine nucleotide exchange factor (GEF) 37
<i>POFUT1</i>	protein O-fucosyltransferase 1
<i>NXPH3</i>	neurexophilin 3
<i>ASB8</i>	ankyrin repeat and SOCS box-containing 8
<i>BCL11B</i>	B cell leukemia/lymphoma 11B
<i>PDP2</i>	pyruvate dehydrogenase phosphatase catalytic subunit 2
<i>RTL5</i>	retrotransposon Gag like 5

<i>SERPIN1B</i>	serine (or cysteine) peptidase inhibitor, clade B, member 1b
<i>TCHH</i>	trichohyalin
<i>MAF</i>	avian musculoaponeurotic fibrosarcoma oncogene homolog
<i>IPCEF1</i>	interaction protein for cytohesin exchange factors 1
<i>PLAC9B</i>	placenta specific 9b
<i>H2BC3</i>	H2B clustered histone 3
<i>FIRRE</i>	functional intergenic repeating RNA element
<i>4930458D05RIK</i>	RIKEN cDNA 4930458D05 gene
<i>KCNE1L</i>	potassium voltage-gated channel, Isk-related family, member 1-like, pseudogene
<i>SMIM17</i>	small integral membrane protein 17
<i>LDLRAD2</i>	low density lipoprotein receptor class A domain containing 2
<i>GM37019</i>	predicted gene, 37019

DIV 7-14 P-ADJ < 0.1

GENE NAME	Gene description
<i>ACVR1B</i>	activin A receptor, type 1B
<i>PDZD4</i>	PDZ domain containing 4
<i>PNCK</i>	pregnancy upregulated non-ubiquitously expressed CaM kinase
<i>SNX9</i>	sorting nexin 9
<i>SRI</i>	sorcin
<i>KIFC2</i>	kinesin family member C2
<i>HIF3A</i>	hypoxia inducible factor 3, alpha subunit
<i>RBFOX1</i>	RNA binding protein, fox-1 homolog (C. elegans) 1
<i>FAM163B</i>	family with sequence similarity 163, member B
<i>TRPM2</i>	transient receptor potential cation channel, subfamily M, member 2
<i>KCNQ2</i>	potassium voltage-gated channel, subfamily Q, member 2
<i>EEF1A2</i>	eukaryotic translation elongation factor 1 alpha 2
<i>H3F3B</i>	H3.3 histone B
<i>SLC12A5</i>	solute carrier family 12, member 5
<i>GLRA2</i>	glycine receptor, alpha 2 subunit
<i>SULT4A1</i>	sulfotransferase family 4A, member 1
<i>RAB32</i>	RAB32, member RAS oncogene family
<i>PTPRK</i>	protein tyrosine phosphatase, receptor type, K
<i>MGAT1</i>	mannoside acetylglucosaminyltransferase 1
<i>KLHL29</i>	kelch-like 29
<i>CACNA1G</i>	calcium channel, voltage-dependent, T type, alpha 1G subunit
<i>CHGA</i>	chromogranin A
<i>HCN1</i>	hyperpolarization activated cyclic nucleotide gated potassium channel 1
<i>ATP8A2</i>	ATPase, aminophospholipid transporter-like, class I, type 8A, member 2
<i>JPH4</i>	junctophilin 4
<i>LY6H</i>	lymphocyte antigen 6 complex, locus H
<i>ITSN1</i>	intersectin 1 (SH3 domain protein 1A)

VWA5A	von Willebrand factor A domain containing 5A
ATP6V1G2	ATPase, H ⁺ transporting, lysosomal V1 subunit G2
CNIH2	cornichon family AMPA receptor auxiliary protein 2
VLDLR	very low-density lipoprotein receptor
AGAP2	ArfGAP with GTPase domain, ankyrin repeat and PH domain 2
RBFOX3	RNA binding protein, fox-1 homolog (C. elegans) 3
HPRT	hypoxanthine guanine phosphoribosyl transferase
GDAP1	ganglioside-induced differentiation-associated-protein 1
PDIA4	protein disulfide isomerase associated 4
PRKAR1B	protein kinase, cAMP dependent regulatory, type I beta
ICA1L	islet cell autoantigen 1-like
STXBP1	syntaxin binding protein 1
DNM1	dynamain 1
SLC4A10	solute carrier family 4, sodium bicarbonate cotransporter-like, member 10
NMI	N-myc (and STAT) interactor
SNAP25	synaptosomal-associated protein 25
NAPB	N-ethylmaleimide sensitive fusion protein attachment protein beta
SLC16A4	solute carrier family 16 (monocarboxylic acid transporters), member 4
DYRK2	dual-specificity tyrosine-(Y)-phosphorylation regulated kinase 2
HPCA	hippocalcin
NSG1	neuron specific gene family member 1
DYNC1H1	dynein cytoplasmic 1 intermediate chain 1
GIPR	gastric inhibitory polypeptide receptor
CCDC90B	coiled-coil domain containing 90B
PGM2L1	phosphoglucomutase 2-like 1
ATP2B3	ATPase, Ca ⁺⁺ transporting, plasma membrane 3
RAB3A	RAB3A, member RAS oncogene family
CELF6	CUGBP, Elav-like family member 6
RASGRF1	RAS protein-specific guanine nucleotide-releasing factor 1
ARPP21	cyclic AMP-regulated phosphoprotein, 21
ABLIM3	actin binding LIM protein family, member 3
INHA	inhibin alpha
SNAP91	synaptosomal-associated protein 91
CPLX1	complexin 1
STON1	stonin 1
CPNE7	copine VII
NRIP3	nuclear receptor interacting protein 3
DPP10	dipeptidylpeptidase 10
SETD7	SET domain containing (lysine methyltransferase) 7
PSD	pleckstrin and Sec7 domain containing
CCN3	cellular communication network factor 3

<i>VSTM2L</i>	V-set and transmembrane domain containing 2-like
<i>KCNJ9</i>	potassium inwardly-rectifying channel, subfamily J, member 9
<i>KCNH2</i>	potassium voltage-gated channel, subfamily H (eag-related), member 2
<i>SHANK1</i>	SH3 and multiple ankyrin repeat domains 1
<i>RAP1GAP2</i>	RAP1 GTPase activating protein 2
<i>HEXDC</i>	hexosaminidase (glycosyl hydrolase family 20, catalytic domain) containing
<i>RALYL</i>	RALY RNA binding protein-like
<i>PITPNC1</i>	phosphatidylinositol transfer protein, cytoplasmic 1
<i>DOK4</i>	docking protein 4
<i>SH3BGR</i>	SH3-binding domain glutamic acid-rich protein
<i>ATPIA3</i>	ATPase, Na ⁺ /K ⁺ transporting, alpha 3 polypeptide
<i>KLF8</i>	Kruppel-like factor 8
<i>MYRIP</i>	myosin VIIA and Rab interacting protein
<i>GOLGA7B</i>	golgi autoantigen, golgin subfamily a, 7B
<i>MAP3K9</i>	mitogen-activated protein kinase kinase kinase 9
<i>LHFPL4</i>	lipoma HMGIC fusion partner-like protein 4
<i>MDGA1</i>	MAM domain containing glycosylphosphatidylinositol anchor 1
<i>TMEM145</i>	transmembrane protein 145
<i>PTX4</i>	pentraxin 4
<i>KCNJ4</i>	potassium inwardly-rectifying channel, subfamily J, member 4
<i>CAMSAP3</i>	calmodulin regulated spectrin-associated protein family, member 3
<i>NYAPI</i>	neuronal tyrosine-phosphorylated phosphoinositide 3-kinase adaptor 1
<i>BASPI</i>	brain abundant, membrane attached signal protein 1
<i>PNMA2</i>	paraneoplastic antigen MA2
<i>GOLPH3L</i>	golgi phosphoprotein 3-like
<i>HRK</i>	harakiri, BCL2 interacting protein (contains only BH3 domain)
<i>ZFP474</i>	zinc finger protein 474
<i>1110032F04RIK</i>	RIKEN cDNA 1110032F04 gene
<i>FOXO3</i>	forkhead box O3
<i>PGBD5</i>	piggyBac transposable element derived 5
<i>CAMK2N2</i>	calcium/calmodulin-dependent protein kinase II inhibitor 2
<i>SLC6A7</i>	solute carrier family 6 (neurotransmitter transporter, L-proline), member 7
<i>EPHA3</i>	Eph receptor A3
<i>KCNIP1</i>	Kv channel-interacting protein 1
<i>SHISA7</i>	shisa family member 7
<i>SPOCK3</i>	sparc/osteonectin, cwcv and kazal-like domains proteoglycan 3
<i>TMEM74</i>	transmembrane protein 74
<i>GABRA5</i>	gamma-aminobutyric acid (GABA) A receptor, subunit alpha 5
<i>SPOCK1</i>	sparc/osteonectin, cwcv and kazal-like domains proteoglycan 1
<i>BC051142</i>	cDNA sequence BC051142
<i>GNAI1</i>	guanine nucleotide binding protein (G protein), alpha inhibiting 1

GDA	guanine deaminase
IL1RAPL2	interleukin 1 receptor accessory protein-like 2
DPP6	dipeptidylpeptidase 6
TRANK1	tetratricopeptide repeat and ankyrin repeat containing 1
UNC5D	unc-5 netrin receptor D
FCHO1	FCH domain only 1
GM13889	predicted gene 13889
KCNB2	potassium voltage gated channel, Shab-related subfamily, member 2
GM10605	predicted gene 10605
KCTD12	potassium channel tetramerisation domain containing 12
PCDHGB8	protocadherin gamma subfamily B, 8
GM43398	predicted gene 43398
9330121K16RIK	RIKEN cDNA 9330121K16 gene
GM49654	predicted gene, 49654
PDXP	pyridoxal (pyridoxine, vitamin B6) phosphatase

Table 10.4: Intersection of genes among the timepoints of the time-specific analysis. 16 genes are in common among the three timepoints, 124 are significantly deregulated both at DIV7 and 14, while 62 are in common between DIV14 and 18.

10.5. Appendix V

Cluster	Gene name	Gene description	Log2FoldChange	P-value	P-adj
1	Nalcn	sodium leak channel, non-selective	-0.39004	0.00054	0.01359
1	Csfl	colony stimulating factor 1 (macrophage)	-0.44011	0.00247	0.03819
1	Zfpn2	zinc finger protein, multitype 2	-0.15640	0.00151	0.02709
1	Parp9	poly (ADP-ribose) polymerase family, member 9	-0.44640	0.00099	0.02039
1	Map3k8	mitogen-activated protein kinase kinase kinase 8	-0.73552	0.00161	0.02822
1	Myoz2	myozenin 2	-1.30430	0.00318	0.04484
1	Fam53b	family with sequence similarity 53, member B	-0.16709	0.00358	0.04829
1	Sytl4	synaptotagmin-like 4	-0.42994	0.00046	0.01211
1	Maml2	mastermind like transcriptional coactivator 2	-0.29206	0.00050	0.01281
1	Parp14	poly (ADP-ribose) polymerase family, member 14	-0.32251	0.00000	0.00015
1	Hykk	hydroxylysine kinase 1	-0.07712	0.00087	0.01880
1	Tmem255a	transmembrane protein 255A	-0.41393	0.00056	0.01387
1	Fgf2	fibroblast growth factor 2	-0.40764	0.00234	0.03671
1	Parp12	poly (ADP-ribose) polymerase family, member 12	-0.11127	0.00296	0.04297
1	Card6	caspase recruitment domain family, member 6	-0.17219	0.00061	0.01481
1	Trim56	tripartite motif-containing 56	-0.29149	0.00053	0.01341
1	Crebrf	CREB3 regulatory factor	-0.05432	0.00053	0.01337
1	Dtx3l	deltex 3-like, E3 ubiquitin ligase	-0.27247	0.00000	0.00034

1	Klk6	kallikrein related-peptidase 6	1.45485	0.00086	0.01851
1	Zfp809	zinc finger protein 809	-0.17393	0.00266	0.03979
1	Gm12843	predicted gene 12843	-0.87593	0.00080	0.01783
1	Gm6548	predicted gene 6548	-0.41509	0.00074	0.01691
1	6430584L05 Rik	RIKEN cDNA 6430584L05 gene	2.97118	0.00008	0.00371
2	Itgb2	integrin beta 2	0.82529	0.00120	0.02330
2	Jag2	jagged 2	-0.14267	0.00222	0.03520
2	Cd244a	CD244 molecule A	1.63916	0.00025	0.00807
2	Rarres2	retinoic acid receptor responder (tazarotene induced) 2	-0.27846	0.00226	0.03560
2	Spire2	spire type actin nucleation factor 2	-0.19304	0.00159	0.02793
2	Vtn	vitronectin	1.90076	0.00257	0.03904
2	Hkdc1	hexokinase domain containing 1	0.78115	0.00184	0.03081
2	Glipr111	GLI pathogenesis-related 1 like 1	-0.30949	0.00279	0.04124
2	Efcab10	EF-hand calcium binding domain 10	0.66462	0.00182	0.03070
2	Gas2l2	growth arrest-specific 2 like 2	-0.11313	0.00335	0.04644
2	Asb14	ankyrin repeat and SOCS box-containing 14	1.19693	0.00070	0.01634
2	Ribc2	RIB43A domain with coiled-coils 2	-0.26543	0.00296	0.04300
2	Ece2	endothelin converting enzyme 2	0.14983	0.00036	0.01042
2	Qpct	glutaminy-peptide cyclotransferase (glutaminy cyclase)	0.04657	0.00347	0.04732
2	Pmaip1	phorbol-12-myristate-13-acetate-induced protein 1	-0.50968	0.00097	0.02012
2	Lox	lysyl oxidase	-0.67469	0.00239	0.03720
2	Anxa1	annexin A1	-0.02159	0.00160	0.02814
2	Rin1	Ras and Rab interactor 1	0.19246	0.00040	0.01108
2	Ribc1	RIB43A domain with coiled-coils 1	-0.04284	0.00302	0.04339
2	Iqca	IQ motif containing with AAA domain	-0.42672	0.00185	0.03094
2	Stoml3	stomatin (Epb7.2)-like 3	1.59753	0.00008	0.00379
2	Uox	urate oxidase	0.26812	0.00137	0.02540
2	Aqp7	aquaporin 7	0.52136	0.00016	0.00607
2	Vwa5b1	von Willebrand factor A domain containing 5B1	-0.81655	0.00158	0.02783
2	Cda	cytidine deaminase	-0.26241	0.00267	0.03987
2	Arhgef19	Rho guanine nucleotide exchange factor (GEF) 19	0.04725	0.00376	0.04985
2	B3gnt4	UDP-GlcNAc:betaGal beta-1,3-N-acetylglucosaminyltransferase 4	-0.56108	0.00172	0.02957
2	Medag	mesenteric estrogen dependent adipogenesis	0.97287	0.00005	0.00270
2	Igsf1	immunoglobulin superfamily, member 1	-0.27152	0.00355	0.04799
2	Mtcp1	mature T cell proliferation 1	0.21992	0.00045	0.01210
2	Irx3	Iroquois related homeobox 3	-0.21413	0.00076	0.01717
2	Mpzl2	myelin protein zero-like 2	0.16104	0.00031	0.00936
2	Cdhr4	cadherin-related family member 4	-0.31882	0.00077	0.01724
2	Cryz12	crystallin zeta like 2	-0.26530	0.00221	0.03512
2	Arhgef5	Rho guanine nucleotide exchange factor (GEF) 5	-0.07816	0.00005	0.00255
2	Fancd2os	Fancd2 opposite strand	-0.13749	0.00193	0.03172

2	Dnaic2	dynein, axonemal, intermediate chain 2	-0.15208	0.00359	0.04829
2	Mfrp	membrane frizzled-related protein	0.53424	0.00069	0.01611
2	Cdhr3	cadherin-related family member 3	1.30710	0.00017	0.00615
2	Igfbp7	insulin-like growth factor binding protein 7	-0.65823	0.00017	0.00609
2	Lpar3	lysophosphatidic acid receptor 3	0.03923	0.00000	0.00004
2	Kirrel2	kirre like nephrin family adhesion molecule 2	1.92643	0.00025	0.00788
2	Atg9b	autophagy related 9B	1.28877	0.00000	0.00020
2	Ttc16	tetratricopeptide repeat domain 16	-0.21663	0.00024	0.00765
2	Cdh26	cadherin-like 26	0.58921	0.00009	0.00401
2	Ccdc81	coiled-coil domain containing 81	0.16625	0.00116	0.02278
2	Capsl	calcyphosine-like	-0.40873	0.00261	0.03937
2	Aipl1	aryl hydrocarbon receptor-interacting protein-like 1	0.94881	0.00201	0.03268
2	Slc16a11	solute carrier family 16 (monocarboxylic acid transporters), member 11	0.47601	0.00044	0.01192
2	Lrrc18	leucine rich repeat containing 18	0.14373	0.00046	0.01229
2	Tmem212	transmembrane protein 212	1.21427	0.00019	0.00666
2	Gpr75	G protein-coupled receptor 75	0.17521	0.00086	0.01854
2	Sntn	sentan, cilia apical structure protein	1.08177	0.00005	0.00286
2	Oxgr1	oxoglutarate (alpha-ketoglutarate) receptor 1	2.62044	0.00051	0.01306
2	Ankrd45	ankyrin repeat domain 45	-0.21014	0.00135	0.02513
2	Irx3os	iroquois homeobox 3, opposite strand	0.68850	0.00084	0.01836
2	Zfp474	zinc finger protein 474	1.01872	0.00002	0.00142
2	Cd24a	CD24a antigen	-0.10623	0.00181	0.03063
2	Odf3b	outer dense fiber of sperm tails 3B	0.39803	0.00088	0.01880
2	Tctex1d4	Tctex1 domain containing 4	0.82349	0.00097	0.02011
2	Rtl5	retrotransposon Gag like 5	-0.12007	0.00000	0.00003
2	Serp1nb1b	serine (or cysteine) peptidase inhibitor, clade B, member 1b	-1.04387	0.00059	0.01442
2	2010001K21Rik	RIKEN cDNA 2010001K21 gene	0.18675	0.00026	0.00829
2	Mme11	membrane metallo-endopeptidase-like 1	0.07669	0.00327	0.04559
2	Eda	ectodysplasin-A	-0.18414	0.00315	0.04451
2	Armc4	armadillo repeat containing 4	-0.21672	0.00118	0.02308
2	Chia1	chitinase, acidic 1	0.38075	0.00023	0.00761
2	Dhrs3	dehydrogenase/reductase (SDR family) member 3	-0.35632	0.00164	0.02862
2	Efcab1	EF-hand calcium binding domain 1	-0.12495	0.00005	0.00261
2	Ccdc78	coiled-coil domain containing 78	0.36557	0.00104	0.02103
2	1700024G13Rik	RIKEN cDNA 1700024G13 gene	0.90746	0.00111	0.02205
2	Trpc5os	transient receptor potential cation channel, subfamily C, member 5, opposite strand	-0.90960	0.00011	0.00449
2	Nup62cl	nucleoporin 62 C-terminal like	0.17437	0.00121	0.02344
2	Zfp990	zinc finger protein 990	-0.20665	0.00009	0.00413
2	Dcdc2b	doublecortin domain containing 2b	0.49855	0.00101	0.02050
2	Ifi2712a	interferon, alpha-inducible protein 27 like 2A	1.13074	0.00214	0.03424
2	4930458D05Rik	RIKEN cDNA 4930458D05 gene	-0.36107	0.00000	0.00003

2	Gm45351	predicted gene 45351	-1.25923	0.00021	0.00710
2	2810047C21 Rik1	RIKEN cDNA 2810047C21 gene 1	-1.16885	0.00052	0.01321
2	Ldlrad2	low density lipoprotein receptor class A domain containing 2	-0.61707	0.00010	0.00421
2	4933406C10 Rik	RIKEN cDNA 4933406C10 gene	0.16259	0.00371	0.04940
2	1700064M1 5Rik	RIKEN cDNA 1700064M15 gene	-0.99886	0.00248	0.03823
2	Pcdhgc5	protocadherin gamma subfamily C, 5	-0.05235	0.00002	0.00136
2	Gm10636	predicted gene 10636	-0.07525	0.00006	0.00313
2	Frmpd2	FERM and PDZ domain containing 2	0.30730	0.00357	0.04811
2	Gm49417	predicted gene, 49417	0.67500	0.00176	0.03002
3	Grm3	glutamate receptor, metabotropic 3	-0.55469	0.00330	0.04592
3	Rnase4	ribonuclease, RNase A family 4	-0.81737	0.00006	0.00319
3	Tekt2	tektin 2	-0.67926	0.00260	0.03933
3	Zfp185	zinc finger protein 185	-0.83202	0.00080	0.01777
3	Irx5	Iroquois homeobox 5	-0.47401	0.00083	0.01814
3	Hrob	homologous recombination factor with OB-fold	-0.50395	0.00035	0.01011
3	Dpp4	dipeptidylpeptidase 4	-2.36582	0.00186	0.03100
3	Syng4	synaptogyrin 4	0.57194	0.00119	0.02314
3	Abcb4	ATP-binding cassette, sub-family B (MDR/TAP), member 4	-0.24542	0.00009	0.00391
3	Fam25c	family with sequence similarity 25, member C	-2.33597	0.00070	0.01635
3	Lurap11	leucine rich adaptor protein 1-like	-0.13583	0.00236	0.03688
3	Gm14964	predicted gene 14964	-0.29901	0.00149	0.02696
3	Tchh	trichohyalin	-0.87350	0.00000	0.00007
3	Xlr3c	X-linked lymphocyte-regulated 3C	-1.30202	0.00000	0.00000
3	Dsc3	desmocollin 3	-1.39984	0.00000	0.00001
3	Nnat	neuronatin	-0.80087	0.00010	0.00435
3	Plac9b	placenta specific 9b	-2.82009	0.00114	0.02247
3	Has2os	hyaluronan synthase 2, opposite strand	-2.49626	0.00179	0.03040
3	Gm45444	predicted gene 45444	-2.37191	0.00327	0.04559

Table 10.5: DEGs belonging to cluster 1, 2, 3 of the overtime analysis (p -adj cut-off < 0.05).

10.6. Appendix VI

First 96 selected DEGs	Biological function	Forward primer (5'-3')	Reverse primer (5'-3')
<i>Bhlhe22</i>	Nervous system development	GCTCCTCGCCAAGAACTACA	CTTGGTTGAGGTAGGCGACTAA
<i>Ccn3</i>	Nervous system development	CATCGTTCGGCCTTGTAAC	GATTTCTTGGTGCGGAGACAC
<i>Daam2</i>	Nervous system development	AGAGGAACCAAGTTGTAGAAGACC	ATCGATGAAGCGGGTCACAA

<i>Dok4</i>	Nervous system development	CTCGCACCTTCACTTGTGAC	CCGTGATCCCAGACATTCCA
<i>Fgf14</i>	Nervous system development	TCGATGGAACCAAGGATGACA	ACTCCCTGGATGGCAACAA
<i>Fgf2</i>	nervous system development	TCTTCCTGCGCATCCATCC	GCACACACTCCCTTGATAGACA
<i>Gap43</i>	Nervous system development	TCCAACGGAGACTGCAGAAA	TCCTGTCGGGCACCTTCC
<i>Junb</i>	Nervous system development	TTTTCGGGTCAGGGATCAGAC	TTGCTGTTGGGGACGATCAA
<i>Mif</i>	Nervous system development	CCAGCCAACCTTCCCAACATA	GCCAATGCTCTTGCTTCAGAC
<i>Nkd2</i>	Nervous system development	GGGTCCACTGAGACTTAGCAA	TGGCGGTTGTCTTCTTCCA
<i>Prtg</i>	nervous system development	ATAGAACAGCCCTGCCTACA	ACGTCGTAGATCTGCAACAC
<i>Rasgrp1</i>	nervous system development	TCAGCCGAGCTGCTACAAAA	CTTCAGGCCAAACTCCTGGAGAA
<i>Rbfox3</i>	Nervous system development	ACCAATAAGAAGCCTGGGAACC	TCAGGCCCATAGACTGTTCTTA
<i>Slitr1</i>	nervous system development	ATCCAGGCTCAGGCTTAAA	CGTTGGAAAGCTTAGGCTTCA
<i>Wif1</i>	Nervous system development	AGTGTCCGGATGGGTTCTAC	CACACAGACCACCGTTCATAC
<i>Wnt7b</i>	nervous system development	CGCCTCATGAACCTTCAAA	CTGACACACCGTGACACTTAC
<i>Arhgap4</i>	microtubule cytoskeleton organization	GGGCTACAACCTGAGTATGAC	CTGAAGCTCCAGGCAATGAA
<i>Epha3</i>	microtubule cytoskeleton organization	AAGGAGTTGGATGCCACCAATA	CCGCTGCAAACCTTCTCCAAA
<i>Fgd6</i>	microtubule cytoskeleton organization	TGAAGCTGTCTCGAAAAGTCA	ACTGCATGGGTGTGGTGTGA
<i>Hap1</i>	microtubule cytoskeleton organization	CAGATGCTGGCCTCAGAGAA	TGCTCCATAATCCTGCATGTA
<i>Kifc2</i>	microtubule cytoskeleton organization	CTGGACTGGGTCTTCTCTCAA	CTGGAGGCAGGACAACACA
<i>Klhl1</i>	microtubule cytoskeleton organization	AAGGTGGCACACAGCTACA	GCTCTTCAGCTGGAAGGAGTA
<i>Pdcp</i>	microtubule cytoskeleton organization	CGCTCAGCGACGGAAG	ATGCACTGGAACATGTAAGGG
<i>Stard13</i>	microtubule cytoskeleton organization	TGCCTCAGAGCATCCAACAA	TCACTCCTGACTTGC GGAAAA
<i>Tbcel</i>	microtubule cytoskeleton organization	TCTGTGCTCACGTGTCAGAA	CTCCAGCTGAGGAACATTTGAC
<i>Tubb3</i>	microtubule cytoskeleton organization	GCGCATCAGCGTATACTACA	AGGTTCCAAGTCCACCAGAA
<i>Zmym6</i>	microtubule cytoskeleton organization	GCGGTTCTCAGGGATTGACA	GCTTCCCCATCTTCCCCAAA
<i>Atp8a2</i>	neuron projection morphogenesis	GAACAGACATTCGGGATCTCA	ATGGCAGTCGGACAATGACA
<i>Camk2b</i>	neuron projection morphogenesis	GCCTGCTGAAGCATTCCAA	GATCGAAGACCAGGTAGTGAA
<i>Haus7</i>	neuron projection morphogenesis	CCCCATCATCCAAGCTGTCTA	GGTGTCTGCAATCTCCATGAC
<i>Psd</i>	neuron projection morphogenesis	CTATACCGACTCGATGGCTTCA	CCAGCCACCAATTTGCTGAA
<i>Shank1</i>	neuron projection morphogenesis	AGTGCCAGCATGGAGAAAA	CTGCAGCCAAGATCTCATCCA
<i>Vstm2l</i>	neuron projection morphogenesis	GACTGGACTGACAAGCAGAC	TATTTTGGTGGCGTCTTCC

<i>Atp1a1</i>	Ion transmembrane transport	AAGCTGACACCACGGAGAA	ATTCTGGACAGAGCGAACCA
<i>Dpp10</i>	Ion transmembrane transport	CTCGGTTTACTGGAGCACTGTA	CACTGATGGGTTTCGCTTGAC
<i>Dpp6</i>	Ion transmembrane transport	GTGCATAAACACCACGGACAA	GGTCGTTGATAGCCTTCTGAAC
<i>Kenh2</i>	Ion transmembrane transport	GTCTCTCCCAACACCAACTCA	TGCCGAAGATGCTGGCATA
<i>Kcni1</i>	Ion transmembrane transport	ACCCAGACAGGCTCTGTAAA	TTCATGGACTGTCCCTCTCA
<i>Kcnq2</i>	Ion transmembrane transport	ACTTTGAGAAACGGCGGAAC	CGGTGCGTGAGAGGTTAGTA
<i>Slco1c1</i>	Ion transmembrane transport	TCTAGGTGGCATACTGGATA	GGTGTAGATACCCAGAGCAAA
<i>Trpc3</i>	Ion transmembrane transport	GTGAAGACCACCCAGTTCAC	CTTGCACTCAGACCACATCA
<i>Trpm2</i>	Ion transmembrane transport	TGAGAAGGATGTGGCTCTCA	TCCATCCACGACGTTGTAAC
<i>Vip</i>	Ion transmembrane transport	GCAGAAAATGGCACACCCTA	CTGCTGTAATCGCTGGTGAA
<i>Cbln1</i>	synapse assembly and organization	CGTGGTGAAAGTCTACAACAGAC	CGGCGAAGGCTGAAATCAC
<i>Lhfp14</i>	synapse assembly and organization	GGAGGAGCTCAAACAGGAGAA	TGAGCAACAGGGCATGGTA
<i>Pnck</i>	synapse assembly and organization	AAGAAACAGACGGAGGACATCA	GCCAGCATCACCTCAGAGAA
<i>Syndig1</i>	synapse assembly and organization	CTGTCTATGACGTGGAGGAA	CTGTGTCGCTGGAGTAGTCA
<i>Cabyr</i>	synaptic transmission and plasticity	GGGGCAAAGAGGAAGCTCTA	GTACAACAAGTCTGGGCTTTGAA
<i>Cnih2</i>	synaptic transmission and plasticity	CCTGGGCCTCAACATCCC	ACATGACCTCAGAGCCATCC
<i>Fos</i>	synaptic transmission and plasticity	ATGGGCTCTCCTGTCAACAC	GCTGTACCCTGGGGATAAA
<i>Gabra3</i>	synaptic transmission and plasticity	AACAAGCTGCTCAGACTGGTA	ATGGGGCATTACAGCGTGTA
<i>Grm4</i>	synaptic transmission and plasticity	TCAAGAAGGGAAGCCACATCAA	ACCTCCCCTCCTGTTTCGTA
<i>Gsg11</i>	synaptic transmission and plasticity	ATAGACGGGCTGAAGCTCAA	ATCATGTGTGCGACCATTCC
<i>Jph4</i>	synaptic transmission and plasticity	GCTGATAGCCCAGGATCTACA	TGTCAGAACCTCCTGAGTCC
<i>Lgr5</i>	synaptic transmission and plasticity	CTCCAACCTCAGCGTCTTCA	ATGTAGGAGACTGGCGGGTA
<i>Ly6h</i>	synaptic transmission and plasticity	TGCCAGCCCACCGATAC	TAACGAAGTCGCAGGAGGAA
<i>Neur1a</i>	synaptic transmission and plasticity	AGCTGCACCTGAGTCACAA	GCCACCCCGTTCAGTCA
<i>Shisa7</i>	synaptic transmission and plasticity	GTCTATGAGGCTGCTGTGAA	GCTTCAGGTAGGCTTCATCCA
<i>Slc12a5</i>	synaptic transmission and plasticity	ACCTTTGCTGGGGCTATGTA	AAGATGGCCATAGCTGGGAA
<i>Sores1</i>	synaptic transmission and plasticity	TCCATCCGAAGCAAGAAGAC	CCAAACTCAGCAGAGCTGTA
<i>Sv2c</i>	synaptic transmission and plasticity	TGGATGATTGGCGGCATCTA	TAGGCTGAACCCATGCTGAA
<i>Cplx1</i>	synaptic vesicle-mediated transport, exo- and endocytosis	GGTCATGCGGCAGGGTATAA	CTCCGAGTTGGCCTCCA
<i>Itsn1</i>	synaptic vesicle-mediated transport, exo- and endocytosis	CCCTGTCATGAAACAGCAACC	GCATGCTAGCAATCCCTCCTA
<i>Napb</i>	synaptic vesicle-mediated transport, exo- and endocytosis	GGAACAGAACAGTGAAGCGTAC	AGCCACTGATCCAAACGTGATA
<i>Nsg1</i>	synaptic vesicle-mediated transport, exo- and endocytosis	GAGTTCACCGTCAGCATCAC	AAGACGACACAGGTGAGGAA
<i>Snap25</i>	synaptic vesicle-mediated transport, exo- and endocytosis	CGCCAGATCGACAGGATCA	CACGTTGGTTGGCTTCATCA

<i>Ston1</i>	synaptic vesicle-mediated transport, exo- and endocytosis	AGACCGGCTTCCGGATAAAA	CCTGGTCTGACCCAAGTTCTA
<i>Arhgdig</i>	signal transduction	GCTCCAGGGCCTATCATCA	ATGCCCTCCTCAGGACAAA
<i>Rgs10</i>	signal transduction	CCACACCCCTGTGATGTTCCA	AGACTTCAAGAAGCGGCTGTA
<i>Cyp27a1</i>	Metabolic processes	GCCACATGCCCTGTCTAA	ATCCGGGAGTTTGTGGGAAC
<i>Necab3</i>	Metabolic processes	CTCACTGCCATGGACACTACA	GCAGCAGAAATCGTGTGACAA
<i>Nsdhl</i>	Metabolic processes	TCATTGGCACCAAGACTGTCA	AACACTGGCACTGCTGGTTA
<i>Pgm2l1</i>	Metabolic processes	GCTTTGTTGTGGGCTATGACA	CTGCAGCTGTGAGTTTAGCAA
<i>Pitpnc1</i>	Metabolic processes	CTGCCGAAATTCTCCATCCA	GGTCTTTGGCTTCACTGTCA
<i>Fundc2</i>	Mitochondria	GTTGGAAAATTGGCTGCAACA	ACTGCTCTTTGGCTTCTTCA
<i>Gdap1</i>	Mitochondria	CTGTGAGGCCACTCAGATCA	CTTCCTTCATCGGGCATTAAACC
<i>Pdp2</i>	Mitochondria	TTCGGGGATGTCCAGCTAAA	TTGAGGGCCTCCGTATCAAAA
<i>Ajap1</i>	Extracellular matrix and cell-cell adhesion	GACCGGGGAGTACAAGTCC	CCACAGGGATGAGATGCCTA
<i>Cobll1</i>	Extracellular matrix and cell-cell adhesion	CCCTGGCTCAGACTGATGAA	CATGCTGTCTGGAGCAATCC
<i>Nxph3</i>	Extracellular matrix and cell-cell adhesion	TAGTGCAGGGCAGCCTCTA	CCCTCATGGTCATCGTGTTC
<i>Spock3</i>	Extracellular matrix and cell-cell adhesion	GCACTTGAATCCAGGAAAACC	GCGGCTGCATTTTCGTCTTTA
<i>Baspl</i>	Transcription regulation	CGCCACAGGCACCCAAA	TTGGCCTTCTCGTCGTTTAC
<i>Bcl6</i>	Transcription regulation	GGGAAACCCAGTCAGAGTA	CTCAGAGAAAACGGCAGTCAC
<i>Epas1</i>	Transcription regulation	AAGCTTTTCGCCATGGACAC	CAAGGTCTCCAAATCCAGTTTAC
<i>Klf8</i>	Transcription regulation	AAAGCTCACCGCAGAATCCA	TCCGAGCGAGCAAATTTCCA
<i>Raly1</i>	Transcription regulation	TGGTTACGTATTTGACTACGATTACTACA	GAGGTACACGGCCATGGTAA
<i>Arhgef37</i>	Other	TCCAGGATGTGAACGGCAATA	TCAGCTGCTCCACTTTGGTA
<i>Ica11</i>	Other	ATCAAAGCGACGGGAAAGAA	TGTCTCCTGGATGGAGTGAA
<i>Pcdhgb8</i>	Other	GTGAGTGTGCTGAGGAGAA	GGTCTCTGGGCTTGAGAGAAA
<i>Pnma2</i>	Other	CTTGGCTCCTTGGTTCTTGAAA	CAACTCTGGGGAGTCACACA
<i>Sepsecs</i>	Other	AGGCTTAGCCTCTTGAACAAA	GCAACTGGCCACTGAATGAA
<i>Mecp2</i>	–	GGCCGATCTGCTGAAAAGTA	GGTCCAAGGAGGTGTCTCC
<i>Actb</i>	Housekeeping	CCCTAAGGCCAACCGTGAAA	AGCCTGGATGGCTACGTACA
<i>Gapdh</i>	Housekeeping	CAAGGTCATCCAGAGCTGAA	CAGATCCACGACGGACACA
<i>Rpl13</i>	Housekeeping	TGAGATTGGCCGGACTCCCTA	AGAACGGCCGAGCGGAAA

Table 10.6: List of the first 96 DEGs tested in the 96x96 IFC qRT-PCR and their respective primers.